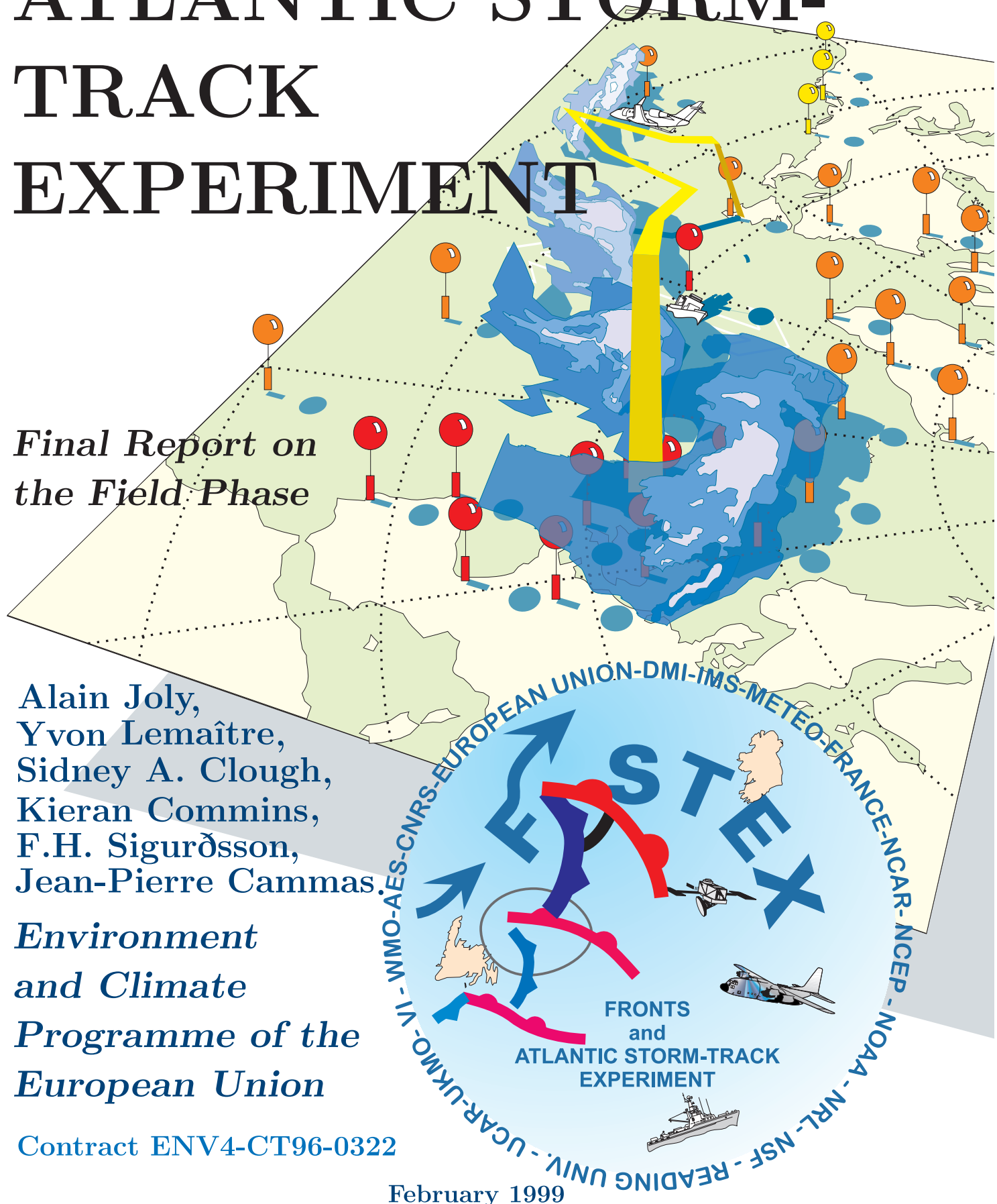# THE FRONTS and ATLANTIC STORM-TRACK EXPERIMENT

Final Report on the Field Phase

Alain Joly,
Yvon Lemaître,
Sidney A. Clough,
Kieran Commins,
F.H. Sigurðsson,
Jean-Pierre Cammas.

Environment and Climate Programme of the European Union

February 1999

The Fronts and Atlantic Storm-Track Experiment

Final Report on the Field Phase

Edited by Alain Joly, Météo-France

Production Note

This amateurish typesetting realization shows what can be achieved on a small and outdated computing system (it takes a week to outdate a computing system, these days) by combining two languages, PostScript® and LaTeX 2_ε.

This combination has been pushed very far in some parts of the document, where layers of LaTeX lay out are sandwiched between layers of PostScript graphics (and vice-versa elsewhere). This has been achieved thanks to an extremely efficient implementation of LaTeX that includes (vector) Type 1 fonts and the most remarkable PostScript driver DVIPSONE developed for PC-based systems by Y&Y. Most graphics have had to be redrawn and this has been done with Corel DRAW®. The use of vector graphics has been favoured as much as possible, so that, with the Type 1 fonts for text, the final PostScript file is practically resolution-independent and ready for the best (and alas worse) printing devices. In this version, however, and for lack of room on the disk, the resolution of some photographs has probably been somewhat too much reduced. This needs to be revised if any proper printing appears to be possible.

LaTeX 2_ε is the only language directly manipulated in this work, since it features a powerful interface with PostScript, in the form of the package `graphicx` developed by D. Carlisle. LaTeX has originally been developed in the USA by L. Lamport, it rests on D. Knuth's TeX, but it might be of interest in this particular instance to note that it is now mostly developed by European computer scientists (led by F. Mittelbach). LaTeX has a built-in system of cross-reference that the package `hyperref` turns into hyperlinks in the on-line version of the document. The other package employed is `multicols`, for the Short-Notes. Based on the language and these extensions, about a thousand lines of new LaTeX 2_ε code has been written in order to produce the various components of the present layout. It should be noted that the level of flexibility and complexity reached in the lay-out of this document by an amateur shows that this LaTeX 2_ε-PostScript combination can only be compared directly to Xpress® (see the General Summary for example), and provides a full Computer Aided Typesetting and Publishing system for a twentieth or less of the cost. Actually, there is a close equivalent implementation of LaTeX that is disseminated as a freeware.

The document has been built from contributions provided in plain ASCII or `html` files for text and Encapsulated PostScript files for most figures, although some came on paper. Redrawing was motivated by either the need to add color to black and white originals or by the size of the original `eps` file, which had to be reduced. At the cost of some time, a severe size vs. content compromise has been seeked in order to limit the storage of the basic files of the document and also in order to limit the size of the future on-line `pdf` file. The basic files are 0,8 Mo of text and LaTeX commands, 26,3 Mo of `eps` vector graphics and 8,9 Mo of bitmaps graphics and photographs in uncompressed `tif` format. On the Pentium I system employed, a LaTeX 2_ε compilation of the full document takes 78 s, it is turned into a single 82.9 Mo PostScript file by DVIPSONE in 107 s. Then, Adobe's Acrobat® Distiller turns it into a 9,5 Mo `pdf` file in 510 s and this file is optimized by Acrobat Exchange in 75 s, leading to a final size of 8.8 Mo. The original printing has been done on a part by part basis on the CANON Colorlaser printer of the Centre National de Recherches Météorologiques.

The fonts in text and some figures are the Type 1 version of the 10pt Computer Modern family developed by Y&Y, while most figures are labelled using the standard PostScript fonts.

The Short Notes are based on work or material done or provided by their authors, the text is by the Editor, who takes the blame for any error he may have introduced.

Lay-out design and implementation by A. Joly, between early december 1998 and 24 march 1999.

Executive Summary

The Fronts and Atlantic Storm Track (FASTEX) project addresses several open scientific questions relating to atmospheric cyclone depressions forming in the North-Atlantic ocean and reaching the west coast of Europe. They bring there most of the water and soften the seasonal contrasts, but they are also the cause of numerous costly damages when they take the shape of storms.

The role of the clouds associated with these cyclones in the radiative and water budget of the climate system is one such questions. Others are the influence of various processes such as ocean-atmosphere interaction on their evolution, the predictability of the development of such cyclones and, more generally, the proper theoretical framework that explains these weather systems.

This report gives an account of the first years of the FASTEX project. It concentrates on the key event of this phase, the occurrence of a major field experiment in January and February 1997.

The specific objectives of the field operations were to gather data on the cloud systems by combining dropsondes and airborne Doppler radars and, above all, to perform these flights on a system previously sampled at earlier stages. In other words, FASTEX as a field programme aimed at collecting data on cyclone full life-cycles. Both these goals have been reached.

The data obtained in this way has been organized into a Data Base and scientists from anywhere can access it at *http://www.cnrm.meteo.fr/fastex/.*

The detailed organization of the core of the cyclones is accessible. It is shown that they are extremelly inhomogeneous and the consequences of this fact are now being assessed. The project has also produced a new climatology of cyclones, the first real time implementation of adaptive observation and its assessment as a mean of making certain the forecast of damageable cyclogenesis. The study of the objectives relating to clouds is continued under the project FASTEX Cloud System Study.

General Summary and Overview

The Fronts and Atlantic Storm-Track Experiment is an atmospheric science project that focuses on the mid-latitude cyclones that form and develop over the North-Atlantic ocean and eventually hit the West Coast of Europe (as illustrated by Fig. A). These cyclones provide most of northern Europe's resources in water. They are also, however, responsible for the most damaging weather over large areas, such as floods and strong winds.

On the long time scales, the Atlantic mid-latitude cyclones play a key role in shaping the climate of Western Europe. They are the main rainmakers in this area, and, in close relationship, they also are the main cloudmakers. Cyclones act within the climate system both individually and as a population. As the latter, they strongly interact with the very large scale flow: they contribute to maintening, for periods of several days to several weeks, the same large scale pattern and as a result, they travel along the same track: this observational fact has led to coin the name "storm-track".

These periods of continuing weather pattern are called weather regimes. The storm-tracks are the zones of most active energy and water exchange in mid-latitudes, hence their importance in the global climate balance. The activity of storm-tracks embodies essentially the collective impact of cyclones. However, cyclones can reach such extreme values in wind and rain generation that they can, individually, also influence the longer term evolution: individual events are, for example, suspected of causing regime transitions. For the same reason, namely their ability to generate large winds and rainfalls over large areas for relatively long times, mid-latitude cyclones are critical to the economy.

On both the time scales of climate and of daily weather, mid-latitude cyclones offer open scientific questions. The Fronts and Atlantic Storm-Track Experiment (FASTEX) has been set-up to bring useful contributions to several of them. The areas of particular interest to FASTEX are:
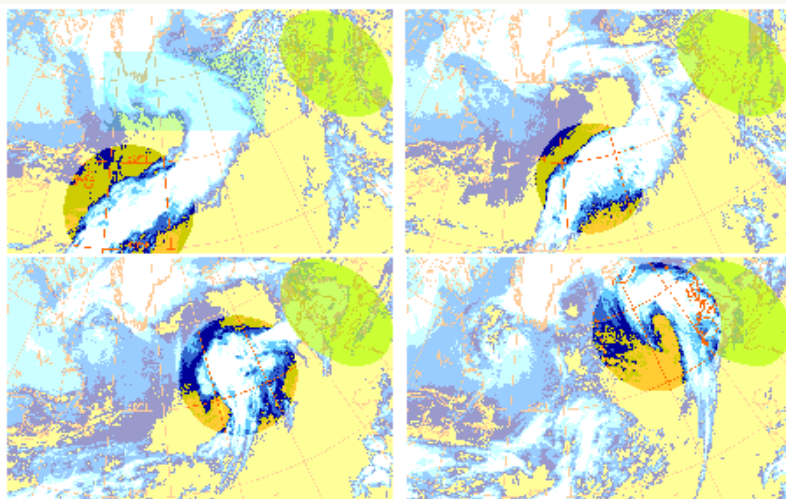
Figure A: 36h of weather evolution in the Atlantic during a period of zonal weather regime (one image every 12 h). A "second generation" low forms along the front of its parent (blue shading, top left panel) and reaches Europe (green shading) while developing rapidly, and its characteristic cloud system takes shape and expands. This phenomena is the main character of FASTEX. The original GOES and METEOSAT images have been retrieved on line from the FASTEX Data Base. The dates are 7 and 8 February 1997.

Figure B: Some of the observing facilities that took part to the field phase of FASTEX. From top to bottom: the 3 aircraft based in Shannon, Ireland, the Icelandic Coast-Guard Ægir, the launch of a radiosonde from the Bugaev in mid-ocean. (Photos: N. Raynal, P. Bessemoulin and T. Douffet.)

- the cyclones influence climate partly through the impact on the radiative budget of the large cloud systems that they generate; the internal structure of these cloud systems is quite rich, involving organizations on many scales and a number of two-way interactions with dynamical processes; the details of these organizations, the way they bear on the average properties of the system as a whole (as a climate model should see them, in short), the mechanisms involved in these cloud-dynamics interaction are, to a large extent, unknown;

- the interaction between the underlying ocean and the storm-track is also an area where better data and better understanding are required; very little is known, for example, about turbulent fluxes in the presence of extreme winds at sea;

- a remarkable, if somewhat worrying, property of mid-latitude cyclones is that, on the daily weather time scale, they successfully challenge the state-of-the-art forecasting techniques of the moment, and this has been going on for more than a hundred years; in other words, in the presence of the risk of rapid cyclogenesis, the predictability of the atmosphere drops dramatically, we are nearly completely blind even to its immediate future, and progress in this particular domain is very, very slow; scientists are, however, beginning to understand why this is so;
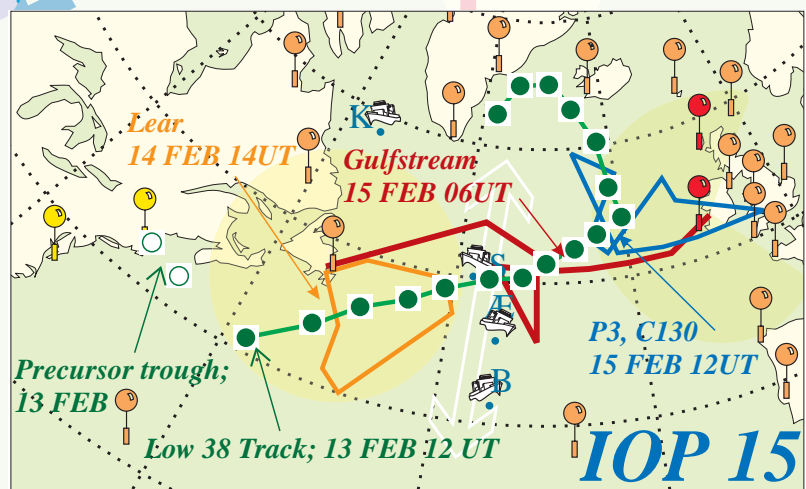

Figure C: One example of a FASTEX Intensive Observing Period: the facilities are employed in succession along the track of the cyclone of interest. All cases are presented in this framework in Part 3.
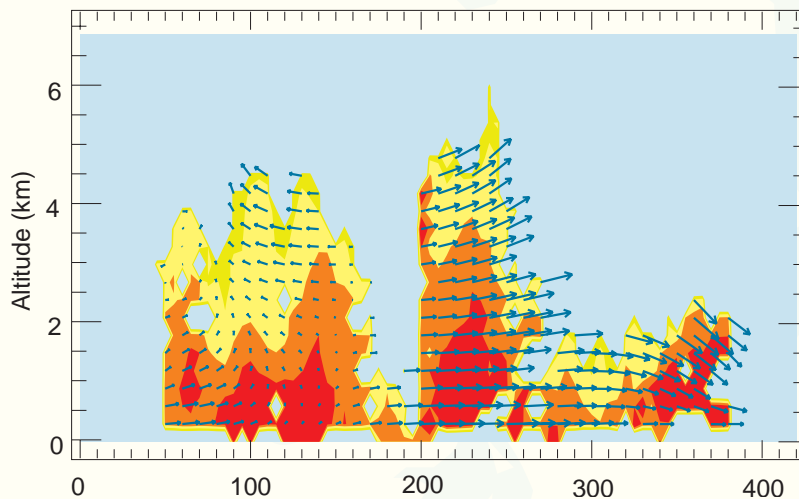
Figure D: Vertical cross-section of the flow within a cloud system. Wind vectors obtained from airborne Doppler radar data. Shading: reflectivity showing the precipitating areas. Result from the CNRS/CETP group.

an enterely new approach of observation combined to the most recent data assimilation techniques may allow a decisive breakthrough and this has been actually tested as part of FASTEX; however, one may have to face the fact that this short predictability limit is an intrinsic property of nature. In this case, only a statistical approach is available to us: this situation would put an end to the dream of a deterministic forecast, a unique and certain future fully determined by observing today's weather;

- a common meeting point of these topics are the dynamical processes operating within cyclones and between the cyclones

and their environment, so that any aspect of the cyclone problem has to, at some stage, deal with available cyclone theories; it turns out that important changes have taken place in this area in the past decade and the idea that cyclones result from the spontaneous release of the instability of its environment (in the sense of fluid dynamics) now appears to be a bit short sighted.

There are new observational requirements attached to each of these topics. There are also new observational facilities that become available, such as airborne Doppler radars that can give access to the internal structure of cloud systems. For these reasons, one of the first significant step of the FASTEX

project has been to set-up and run a major two months field project (Fig. B). Its specific objectives were to document the life-cycle of North-Atlantic cyclones, in order to deliver the data needed to address the topics listed above.

The project and its basic plans emerged from French and British groups in 1993. They attracted scientists from the United States of America, Canada, Ireland and a number of other countries and organizations, including the European Commission and the World Meteorological Organization. This was needed by the scale of the observational challenge: tracking about 10 cyclones from their birth in the western or middle ocean to their mature stage close to the European coasts (Fig. C). The field phase of FASTEX thus took place in January and February 1997. Beside a significant overhaul of the operational observing network, up to 4 ships had been positioned in the middle of the Atlantic, up to 7 instrumented aircraft were available on air fields on both sides of the ocean. This observing system was coordinated by a special Operations Centre located at Shannon, Ireland.
The observing period has reached the following goals:

- about ten mature and developing cloud systems and related cylones have been sampled by airborne Doppler radars (Fig. D) and dropsondes;
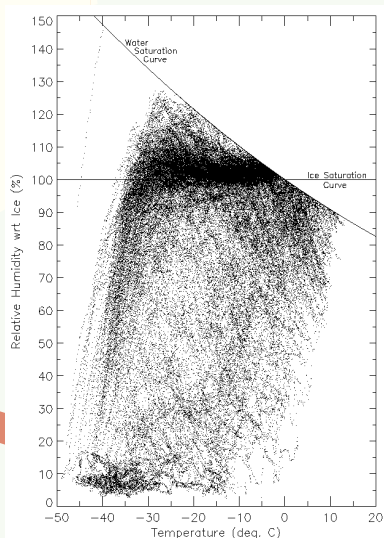
Figure E: *Relative humidity measurements from the UK C-130 dropsondes were able, in FASTEX, to discriminate between saturation with respect to ice (dominating) and to water. Result from the JCMM group.*

for about half these cases, the structure of the system has been observed on scales unheard of so far with in-situ data; this was the data required to make some progress on the internal organization of large stratiform cloud systems (Fig. E);

- about ten cyclones have been observed at several key stages of their life-cycle with radiosondes and dropsondes, thus enabling the documentation of life-cycles, which is central in modern cyclone theory and impacts all other topics;

- the new approach to observation suggested by recent work on the predictability of cyclones has been tested for the first time in real time and with real facilities on real cases;

- unique datasets have been obtained by the ships on turbulent fluxes under strong winds and high seas, but also on oceanography-related topics.

The data collected during this field experiment has been gathered into a Data Base. This critical task has been coordinated by the Toulouse Météo-France GAME group, but has involved all participants. This Data Base has been opened *three-weeks* after the end of operations to the scientific community *at large* (it is not restricted to FASTEX participants) on the INTERNET at http://www.cnrm.meteo.fr/fastex/. This Data Base has many assets to offer to any person interested

in mid-latitude cyclones: more than 10,000 high-resolution, checked, in situ soundings spread all along the storm-track (not just on its beginning or end), a remarkable collection of remotely sensed data and a full series of analyzed fields combining the obervations into a coherent set (Fig. F) are three examples. The first scientific results will be published at the end of 1999 in a special issue of the *Quarterly Journal of the Royal Meteorological Society.* However, the scientific work on the data is currently going on and will so for a few years.

The present report is meant to provide some reference information on the field phase and to show some of the first results, especially those relating to the organization of the cloud systems.
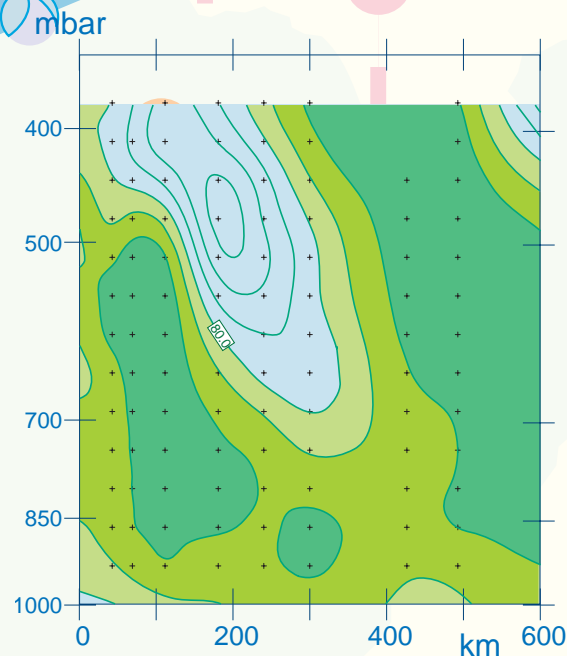

Figure F: *Vertical cross-section of the structure of a cloud system derived from the 4D-VAR data assimilation of dropsondes: a dry intrusion that is not in the initial guess field but in the measurements only is reasonably described. Result from the Météo-France group.*

The Editor's Note

*T*his report is primarily the document requested by Article 6 and Article 10 of Annex II of the contract ENV4-CT96-0322 between the European Commission and the five partners of the EC-FASTEX project, one of the components of FASTEX. Following the terms of Article 10, this report couvre tous les travaux, les objectifs, les résultats et les conclusions and it begins with a general summary of the project.

It offers a good opportunity, in fact, to gather in a single document the most significant features of our project. This is what I have tried to do with the help of the contributors of the various parts.
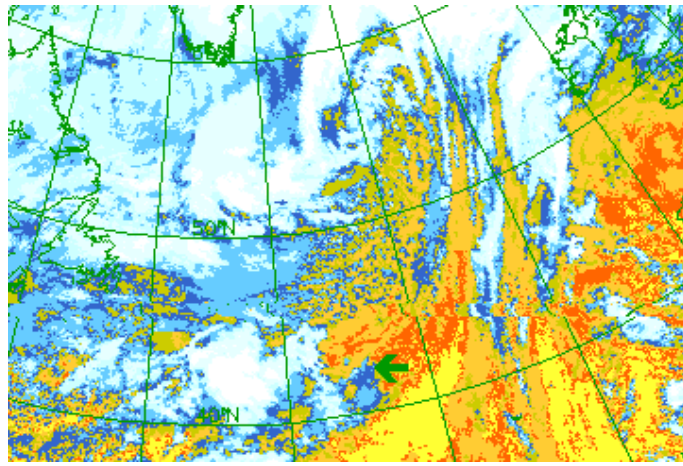
The main line of the report deals with the objectives and deliverables as they were accepted as part of the Environment and Climate Programme: an event, the field phase of FASTEX (Parts 2 and 3), the resulting Data Base (Part 4) and the first results on cloud system structure (Parts 5 to 8). This information is given in the main text.

In order to try to make this useful to people getting acquainted with FASTEX and the available data or currently working on FASTEX, the report contains a graphical summary of each case (Part 3), which was built early in 1997, prepared in french, but remained essentially unpublished.

However, this is only one part of FASTEX. Although a significant delay has been introduced, I have added, in the form of short-notes, information on the other aspects of FASTEX, in the hope to turn this document into a reference about the first years of this 10 years or so project.

I would like to thank the European Commission, and in particular, Drs Ghazi and Brüning, for supporting FASTEX. The Commission has always been aware of the full extent of FASTEX, and in particular, its implications for weather forecasting have never been ignored. The readers should know that, for example, the Commission asked me to help them prepare a press release at the end of the field phase, and they insisted that this should be focused on adaptive observation, which is, indeed, a "hot" scientific topic. I am grateful to them for this openness.

I also deeply thank Alain Protat, Yvon Lemaître, Geneviève Jaubert, Georges Scialom, Sid Clough and Gerald Desroziers who gave me essential contributions to this report.

This document has been prepared enterely numerically, so that it is available in the form of one or several files in (protected) `pdf` *format as part of the documentation in the Data Base. This probably is its best chance to get one reader.*

This report is, finally, a tribute to all those who have given time, ideas and sometimes taken risks in the course of FASTEX. I hope that it will ultimately find its way to them.

If I can include all the information that I would like to put in it, my only remaining regret about this report will be that, following Article 6, it is written in "english" (although probably only Part 7 is truly in english). It is certain that the english literature will not get any better thanks to us, and furthermore, I must say that I am not convinced that this will help reading it.

FASTEX seen from a distance of 36 000 km from the surface, with a new weather system forming (top) and going to meet a ship (arrow), all a nice and picturesque scene, and FASTEX seen from the ship, the research and weather ship Victor Bugaev (bottom), picturesque but less nice. The ship was painted afresh (white) about three weeks before. Photo by Emmanuel Gizard, Météo-France.

Contents

Part 1

Scientific objectives, observing strategy

by
Alain Joly*, Alan J. Thorpe**,
Yvon Lemaître•, Dave Jorgensen⋆,
Melvyn A. Shapiro⋆, Keith A. Browning**,
Jean-Pierre Cammas•, Chris Snyder◇,
François Lalaurette*, Peter Lynch♣.

*Météo-France, URA CNRS 1357, Groupe d'Etude de l'Atmosphère Météorologique, Toulouse, France,
**University of Reading, Reading, United Kingdom,
⋆National Oceanic and Atmospheric Administration, Boulder and Washington, United States of America,
•Centre National de la Recherche Scientifique, France,
◇National Center for Atmospheric Research,
♣Met Éireann, Dublin, Ireland.

January 1997

February 1997

-20 -17 -14 -11 -8 -5 -2 1 4 7 10 13 16 19
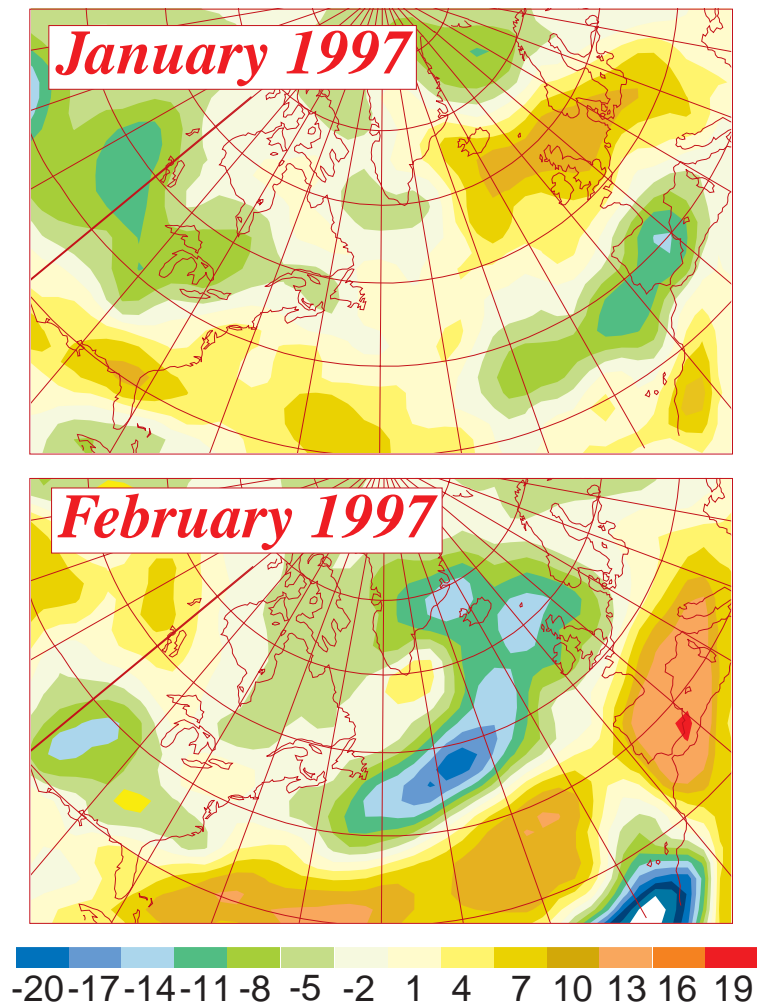
Figure 1.1: *Outgoing Longwave Radiation anomaly for January 1997 (top) and February 1997 (bottom). This figure is to be compared with the North-Atlantic Storm-Track at the same time: this comparison reveals that, in the presence of a well established Storm-Track, as was the case in February, the radiative anomaly results directly from the mid-latitude storms. Figure prepared by C. Piriou, from Météo-France, with data from NOAA/NESDIS.*

1.1 FASTEX : an experiment on Atlantic cyclones and cloud systems

Mid-latitude cyclonic storms, which occur predominantly in oceanic storm-tracks, are recognized as playing a crucial role in the climate system. Figure 1.1, compared to the actual tracks of storms (Figure SN1.2.2), shows, as an example, the impact of February's 1997 Storm-Track on the radiative budget of the atmosphere. Current and foreseeable global climate models inadequately resolve these storms ; it is critical that pro-

cesses such as heat (radiative, sensible and latent), moisture, and momentum fluxes associated with these storms be properly understood and included in climate models (Browning, 1994b). Being essentially oceanic, these storms are poorly observed routinely and have been subject to only a few major observational campaigns (see Subsection 1.2.3 below). These have focused mainly on the western entrance of the North Atlantic storm-track where important but special conditions dominate, such as extremely strong ocean-air fluxes. The majority of cyclones are less dependent on such fluxes. A particular problem in the North-Atlantic is the secondary generation of storms along fronts towards the eastern end of the storm-track, on its european side (Ayrault et al., 1995).

The unique feature of the Fronts and Atlantic Storm-Track Experiment is the desire to provide a bridge, for the first time, between the large-scale dynamics of cyclogenesis and the consequent mesoscale and cloud-scale processes within the storms. This holistic approach is very demanding in requiring a description of features such as the upper jet stream on synoptic scales at the same time as detailed radiative, dynamical and cloud structures. This has not been attempted before but it is crucial if the phenomenon is to be described in a complete enough way for inclusion in, and verification of predictions from, large-scale numerical models.

A major issue is the two way interaction between the large-scale flow and the Atlantic storms. The latter have to be fairly precisely handled by climate models as the translation of climate evolution into changes in the frequency and intensity of storms must be established.

An especially important aspect of these storms which requires this holistic approach is the cloud systems. Cloud systems are to some extent the slaves of the large-scale forcing but they themselves alter the energy fluxes in the storms. The linkages between cloud microphysical, radiative, latent heating and dynamical processes must be established if meaningful parameterizations are to be established for climate and numerical weather prediction models. An example of such coupling on the mesoscale organization is discussed in Part 7.

These ideas leads to a long-term (typically 10 years) programme. This Report presents an overview of the first part of this programme, covering preliminary work and the large scale field phase. It is focused on the cloud-related results, but the other components of the programme are also outlined. The programme, and in particular the detailed analysis of the data collected during the field phase, two years ago, is undergoing. Part of this work is covered by the FASTEX Cloud System Study (FASTEX-CSS) project.

1.1.1 Goals of FASTEX

The ultimate aim of FASTEX is to provide the scientific understanding necessary to enable detailed diagnostic and predictive analyses of the *life-cycles* of Atlantic storms and cloud-systems. This involves study of the coupling between the cloud systems and their dynamics, the phases of development of the clouds, the embedded mesoscale substructures, microphysics and their modelling on a range of scales. These topics form the core of the FASTEX CSS project.

The present Report is concerned with the field experiment itself, the delivery of the FASTEX data base and the derivation of the first results. The measurable objectives of this project were:

- to conduct a field experiment concerning cloud systems within extra-tropical cyclones. This has provided a unique data set :

Short Note 1.1:
North-Atlantic weather regimes

by F. Ayrault, F. Lalaurette and C. Loo

Figure SN1.1.1: *The climatological definition of the North-Atlantic weather regimes. Dark-red lines: 700 mbar geopotential height (interval: 50mgp). White lines and shading: 300 mbar zonal wind (interval: $10m.s^{-1}$).*

ZONAL

BLOCKING

GREENLAND RIDGE

ATLANTIC RIDGE
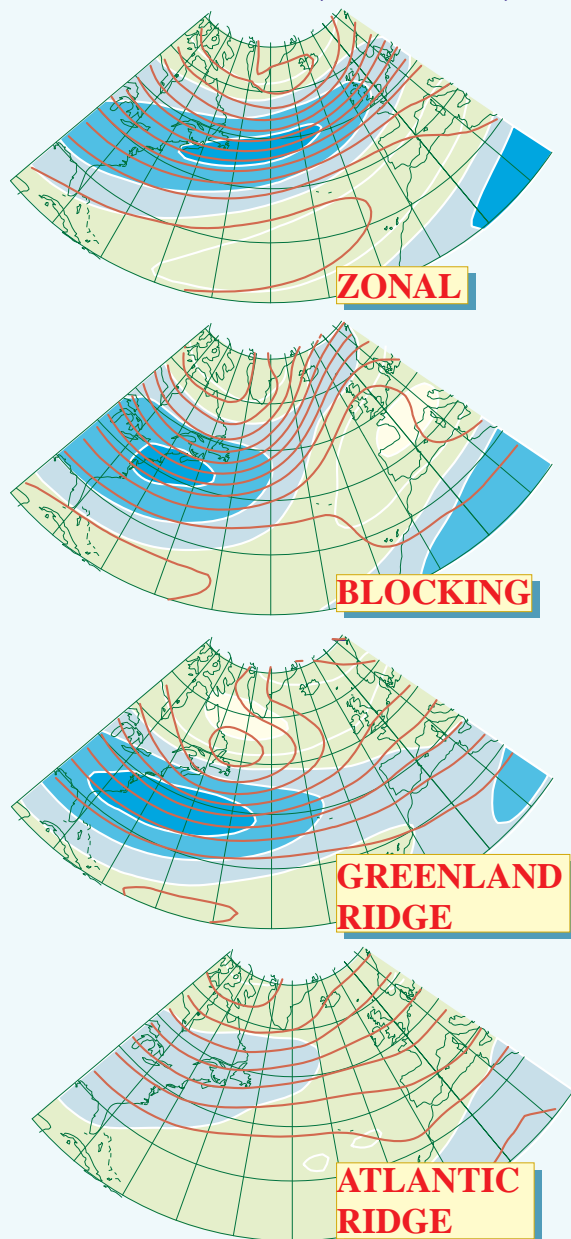
How to characterize the very large-scale, slow evolution of the weather, the environment within which cyclones form and evolve ?

Traditionally, this scale, which is a characteristic of the climate, is described on the basis of monthly averages. At mid-latitudes, the january average is contrasted with the july one. It turns out that such maps are not representative of the actual weather pattern because the variability on the same, large scale remains quite large. This variability is a critical parameter of actual weather and has to be described (Hoskins et al., 1983).

A different concept that accounts for this intraseasonal variability is therefore needed: the weather regimes.

The definition of weather regimes that appears to be both useful and dynamically relevant is the one proposed by Vautard et al. (1988). A weather regime is a 3D field pattern that is quasi-steady and therefore relatively persistent. Low depressions and cyclones account for the variability of the weather on the time scale of a day or so. Weather regimes account for the variability on time scales of a week or so. They have been defined originally by using the long time series of analysis from the National Weather Service. Fig. SN1.1.1 shows the approximation that has been derived in the course of FASTEX from the shorter by finer analyses from ECMWF between 1984 and 1994. They have been defined by combining a principal component analysis on a coarse grid (3°of resolution) and automatic clustering (Ayrault et al., 1995).

The large scale weather over the Atlantic evolves between the 4 patterns shown by the figure. The most characteristic features of the regimes are reasonably robust with respect to the base dataset and the construction technique. The regimes are shown through the 700 mbar geopotential height and the upper-level zonal velocity. The latter easily highlight the presence of a baroclinic zone, which is the environment needed by cyclone, their fuel reservoir, in a sense.

The first two regimes, respectively called "zonal" and "blocking", are the two most frequent. The zonal regime, with its long east-west baroclinic area is the one that brings Europe most of its cyclones, and therefore, rain. In this case, western Europe is influenced by oceanic conditions. The blocking regime, on the other hand, has a quickly interrupted baroclinic zone: the continental influence over Europe often dominates, while most cyclones are diverted towards Greenland and Iceland.

The link between regimes and the occurrence of cyclones over Europe is shown by Fig. 1.4.

The statistical distribution of the regimes (derived from the same sample) is given by Fig. 1.3. Variations about this statistical distribution generally translates into actual problems: a larger persistence of blocking leads to drought in the following summer. A larger persistence of zonal regime means floods at the end of the same winter or in the spring. A change of the climate that will impact Europe will most likely do so through a change of the regime patterns or time frequency distributions. Vautard (1990) presents a statistical analysis of regimes transitions, using a much larger sample. Vautard and Legras (1988) has confirmed the original work of Hoskins et al. (1983) about regime maintenance: the high frequency variability (namely the cyclones) plays the most important role. Weather regimes and cyclones seen as a population are one among many examples of two-way interaction, here on the seasonal scale. The relevant way to describe cyclone in this instance is by referring to the "storm-track" (see Short Note 1.2). It is also interesting to compare these averaged conditions with the actual weather in January and February 1997, described in section 2.2 (Part 2 , see Fig. 2.2). The forecast of weather regimes during the field phase is presented in Short Note 2.6.

> —relating to the initiation of storms in the mid-Atlantic storm-track,
>
> —relating to the structure of the developing cloud-cyclone system near western Europe.

- to organize the data into an open and accessible Data Base.

- to provide both raw and processed data, including analyzed fields obtained with both the operational and special data collected during the field phase.

1.1.2   FASTEX, the Environment and Climate Programme and the international context

The FASTEX project, considering the field phase and the subsequent analysis phase, is built to address the following tasks of the Programme :

- Theme 1, Area 1.1, 1.1.1 Basic processes in the climate system, task 4 : *studies of radiative coupling in the (…) troposphere, including the role of (…) clouds and cloud systems and their dynamics (…).* See Parts 5, 6 and 7 for examples of preliminary results in this area. See also Short Note 2.2 for the contribution of a FASTEX-related programme (called CATCH) to Task 2, on the dynamics of air-sea fluxes.

- Theme 1, Area 1.1, 1.1.3 Climate variability, simulation of climate and prediction of climate change, task 2 : (…) ; *dynamic assimilation of data and new methodologies (…).* (See Part 8 for some results.) Task 6 : *Development of improved forecasts of change in the type, distribution and frequency of meteorological extremes.* (The first part of this work has been to established a new climatology of cyclogenesis: derived results are shown in the present Part and the next one. See Short Note 1.5 for a summary or Ayrault (1998) for full results. See also the Short Notes 1.1, 1.2 and 2.6 on weather regimes, their strong link with the storm-track and their medium-range forecast.)

At the international level, FASTEX is an integral component of the World Climate Research Programme (WCRP) through its Global Energy and Water Cycle Experiment (GEWEX). Recognising the importance of the large-scale effects of clouds as one of the largest sources of uncertainty in climate prediction models, WCRP/GEWEX has established the GEWEX Cloud System Study (GCSS). The primary aim of GCSS
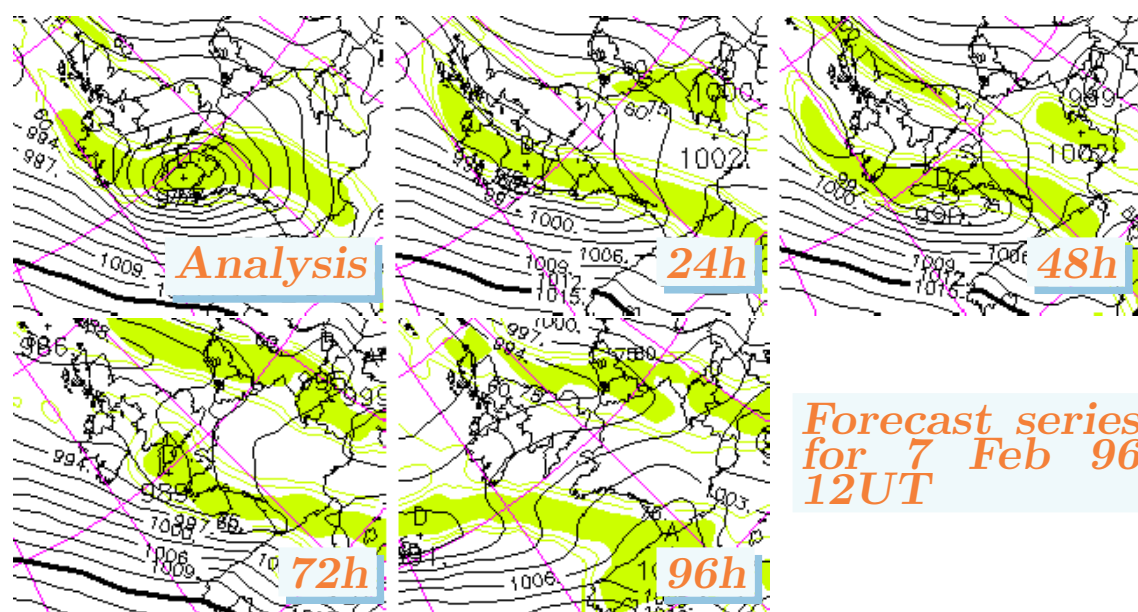
Figure 1.2: *A series of forecast for the 7/2/96 12UT together with the verifying analysis, taken from the ECMWF operational dissemination. Contours: mean sea level pressure every 3 mbar. Shaded areas: 700 mbar relative humidity larger than 80 %.*

is to develop better understanding of cloud systems leading to improved parameterization of cloud processes within climate models (Browning, 1994). GCSS is subdivided into four components, each of them being dedicated to a class of cloud system. FASTEX is a key observational component of the GCSS group on Extratropical Layer Cloud Systems.

Through GEWEX/GCSS and COMPARE, FASTEX is a collaboration with Canadian groups. Because of its scale and universal scope, FASTEX involve a cooperation with US scientists.

In France, FASTEX is the priority project of the national programme Programme Atmosphère et Océan à Mésoéchelle (PATOM) coordinated by the Institut National des Sciences de l'Univers for the period 96–98 and sponsored by several institutions (Météo-France, IFREMER, etc). In the UK, FASTEX is a priority project of the Joint Centre for Mesoscale Meteorology (JCMM) ; the JCMM is supported by the UK Met Office, NERC and the University of Reading.

1.2   Cyclogenesis: a short review

During the last few years, the theoretical study of cyclogenesis has experienced a remarkable renewal of interest. This is due to the simultaneous emergence of new problems in dynamical meteorology and of new approaches to solve them. The result is a drastic change of perspective in the way cyclogenesis is understood conceptually by most meteorologists. This in turn impacts the way this phenomena should be observed or predicted.

Short Note 1.2:
Storm-Track and tracks of storms

by Ch. Baehr and F. Ayrault
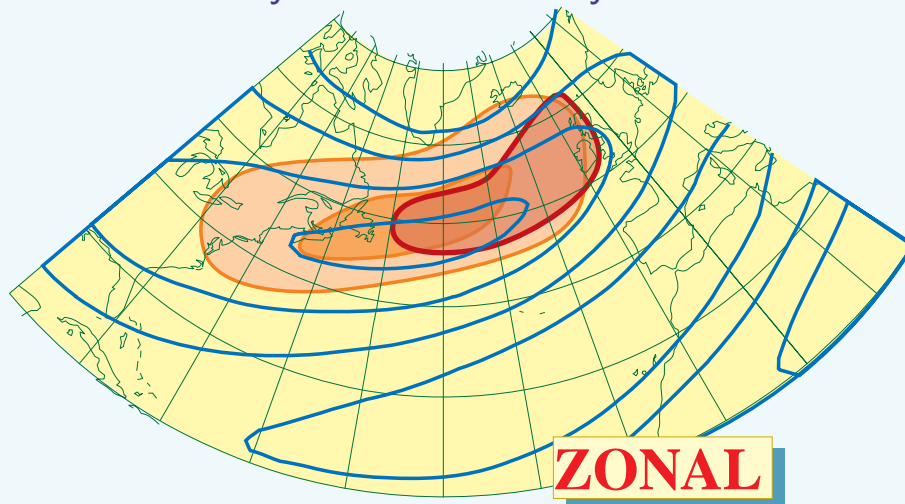
Figure SN1.2.1: *The classical (orange shading) and improved classical (red shading) definition of the storm-track during the zonal regime. The fields are the high frequency variability (2–6 days) and ultra-high frequency variability (0.5–2 days). From Ayrault et al., 1995.*

What is the North-Atlantic storm-track ? As the name suggests, it represents the preferred location of evolving cyclones and storms. Like the weather regimes (Short Note 1.1), storm-tracks are concepts that stemmed from the new approach to the description of the climate started by Blackmon et al. (1977) and based on time series of analysed fields. This approach separates the components of the climate and weather into categories according to the time-scale of their variability. The weather regime are quasi-steady persistent patterns that account for the low frequency variability. The latter results from applying a low-pass filter to the time-series at each grid-point.

The storm-tracks are originally defined as maxima in the so-called "high-frequency" variability (with eigenperiods of 2–6 days). For the Atlantic, using the same ECMWF analyses as in the construction of Fig. SN1.1.1 , this classical definition of a storm-track is shown by Fig. SN1.2.1. It is shown in relationship with the upper-level wind, highlighting its stronger orientation towards the north-east.

This definition is not satisfactory since it gives the strong impression that cyclones are mostly present in the western part of the North-Atlantic basin: Europe appears to be marginally reached by storms. This is not exactly what the synoptic experience suggests.

When Ayrault et al. (1995) take into account the "ultra-high" frequency variability (with eigenperiods in the range 0.5–2 days), a more realistic distribution emerges. The map then suggests that it is useful to distinguish between the main storm-track cyclones that are closely tied to the regime baroclinic zone and the end-of-stormtrack cyclones, that evolve more rapidly and depend on transient features of the main cyclones such as their fronts. FASTEX has been started as a project studying end-of-stormtrack systems, since they appear to be the ones that reach Europe.

Although this separation is sometimes useful, a more direct definition of the storm-track is possible, and indeed, necessary since the cut-off at 2 days between high and ultra-high frequency is somewhat arbitrary, perhaps artificial. Following Ayrault et al. (1995), a cyclone of practically any amplitude can be defined using its vorticity signature. Ayrault (1995) has devised an automatic algorithm that enables to track a cyclone from one analysis to the next: as a result, large sets of trajectories and life-cycles can be extracted. The storm-track is revealed by computing the density of trajectories: the number of cyclone tracks that moves over a given grid-point, each system being counted once at that point.

This technique has been applied to the analyses of the FASTEX period included in the Data Base (see Part 4). The results are presented in two sets (Fig. SN1.2.2) in order to highlight the dependence of the storm-track on the weather regime. In periods of blocking and weak Greenland Ridge regime, as in January 1997, cyclones form at their usual location but then fork, a branch moving towards Iceland, another towards Spain. During a long spell of zonal regime, such as in February 1997, cyclone cross the ocean zonally. Note that the largest density is reached near Europe, not near the East-Coast of America, clearly showing the importance of this phenomena for our continent.

Figure SN1.2.2: *Map of density of trajectories computed from the analyses in the FASTEX Data Base using the automatic tracking algorithm of Ayrault (1995) that follows the 850 mbar vorticity maxima. These maps provide a direct picture of the cyclone tracks as well as their number.*
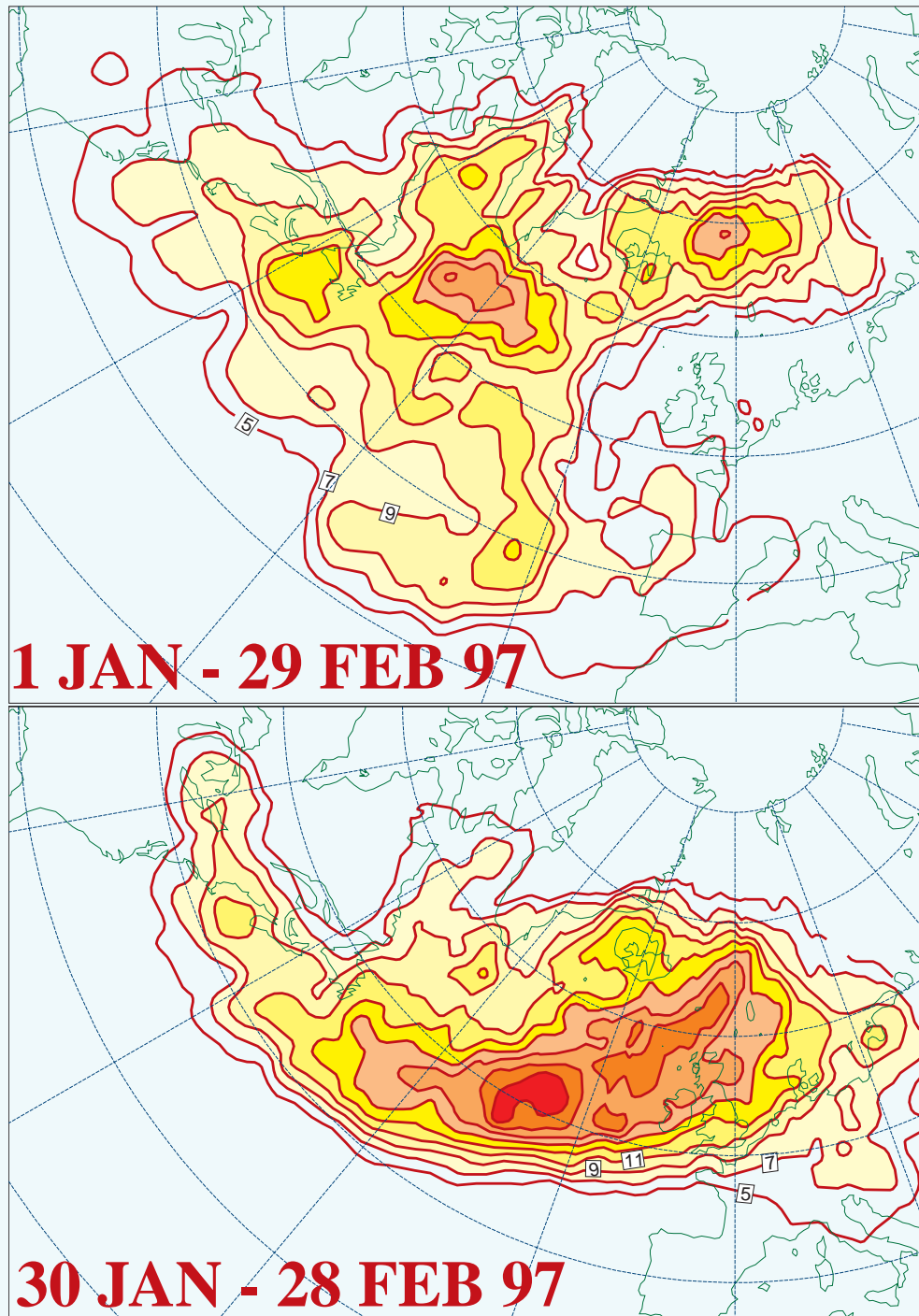
1.2.1   Theoretical perspective

The new problems are the studies of cyclogenesis on the 1000 km horizontal scale. This scale is the only one that is explicitly mentioned in the founding paper on the life cycles of cyclones by Bjerknes and Solberg (1922): it is not new. The semi-geostrophic theory of frontogenesis of Hoskins and Bretherton (1972) provides a simple but realistic description of an atmospheric front: here lies the novelty. With respect to the classical cyclogenesis model of baroclinic instability (Charney, 1947, Eady, 1949), the fronts have a richer organization of the wind field than the simple baroclinic zone. This can lead to different instabilities. Schär and Davies (1990) or Joly and Thorpe (1990) show, for example, under which conditions normal mode instability can happen along a front within the context of semi-geostrophic theory.

The new approaches, on the other hand, result from the parallel questioning of the relevance of the normal mode stability analysis as a theoretical explanation of cyclogenesis. This is mostly the work of Farrell (1984, 1985, 1989) and it applied originally to the explosive growth of large scale waves. The general idea is that the same physical mechanisms present in the normal modes can be triggered much more efficiently by initial conditions involving organized precursors. This work provides a theoretical support to ideas that had been voiced for a long time (*e.g.* Sutcliffe, 1947 Kleinschmidt, 1950). Some details of the evolution of the theoretical framework are given by Short Note 1.3. The framework proposed by Farrell (1988) is also more suitable to address some of the difficulties noticed in the new work on frontal stability. For example, the time scale of frontogenesis is not different from that of frontal cyclogenesis, so the two mechanisms cannot be separated as neatly as the normal analysis requires it. In the same spirit, it appears that time-dependent basic flows, not amenable to normal mode analysis in the strict sense (in spite of attempts such as Joly and Thorpe, 1991), can lead to new mechanisms for the development — or the absence of development — of cyclone-like features.

The combination of these new problems and approaches led to a series of new theoretical results about cyclogenesis. Thorncroft and Hoskins (1990) exhibited the non-linear development of a cyclone along the cold front of a baroclinic wave triggered by an upper-level feature. This anomaly overcomes the stabilizing effect of frontogenesis clearly shown by Bishop and Thorpe (1994a, 1994b). The latter studied the effect of stretching deformation on moist frontal cyclogenesis the effectiveness of the deformation to hinder cyclone formation is quantified. Another series of results address the relationship between pressure deepening, cyclone activity and the mechanisms for cyclogenesis. Malardel *et al.* (1993) pointed out that, on its own, the additional conversion mechanism that a frontal environment provides (due to the presence of wind shear) leads to short-lived systems with very little deepening. Joly (1995) fully generalizes this result to a wide variety of initial conditions as well as to transient development: the baroclinic interaction appears to be the only mechanism that allows deepening larger 10 mbar. That does not imply that the non-baroclinic systems are weak during their short life-cycle: just the reverse, it shows that looking only at the pressure field can be misleading.

It appears, therefore, that a whole new set of ideas and hypotheses are now available for testing against observations. The meteorological subjects of interest are not the explosive large-scale waves but a wider spectrum of cyclones more or less modest that form where fronts are present: in the wake of these large waves, in the middle or eastern part of oceanic basins such as the Pacific or the Atlantic one. These cyclones strongly depend on many properties of their environment: the baroclinicity, the presence of low level frontal jets but also that of frontogenetic forcing, the existence of moving, organised features, etc.

Short Note 1.3:
A cloud of physics in the Report: linear theories of mid-latitude cyclones

by A. Joly

1.3.1 From necessary conditions for instability...

Up to the mid-eighties, the "standard model" for providing an explanation of mid-latitude cyclones was built along the lines proposed by Bjerknes (1927). It is called *linear normal mode stability analysis* and is imported from fluid mechanics. One seeks to identify the newly developing cyclones with a spontaneously growing perturbation of a "basic flow".

This basic flow represents the large scale context within which cyclones are thought to form. It is assumed to be steady and it also is low-dimensional (1D or 2D). Bjerknes had in mind, originally, the Polar Front, an extreme steady separation between two air masses. None of the solutions can convincingly be associated with actual cyclones (Orlanski, 1968). Following the same method, but using a simple *jet-stream flow*, a smooth transition from warm to cold air, Eady (1949) and Charney (1947) obtained very convincing results.

A fundamental concept was, furthermore, introduced by both papers: the troposphere, on the scale of cyclones, is close to some *balance*. The state of the atmosphere can be described with few variables (one, with boundary conditions, is enough). This idea has many consequences (see Short Note 1.6) and remains an essential, reliable, reference up to this day.

Returning to the stability analysis and in order to be specific, let X be a meridional axis pointing towards warm air at the equator, Z be the vertical and Y the zonal direction. The basic flow is in strict balance, since it is steady. It comprises a zonal wind flow $\overline{V}(X, Z)$ in *geostrophic* equilibrium with a thermal field $\overline{\theta}(X, Z)$ (Fig. SN1.3.1). These fields can equivalently be represented through a distribution of *potential vorticity* (the single summary field appropriate here, see again Short Note 1.6) $\overline{P}(X, Z)$ and boundary conditions provided by $\overline{\theta}(X, Z = 0)$ at the "surface" (ac-

tually, the top of the boundary layer) and $\overline{\theta}(X, Z = H)$ at the top of the domain considered (the tropopause or sometimes, higher).

The question is *can a perturbation Φ' to the basic flow grow spontaneously,* and if so, what does it look like ? The potential perturbation Φ' is the single variable needed to represent the state of the balanced perturbation. Using once more the idea of balance, it is possible to recover the dominant wind and temperature perturbations from equations like $u' \sim -f^{-1}\partial_Y \Phi'$, $v' \sim f^{-1}\partial_X \Phi'$ and $\theta' \sim (g/\theta_0) \ \partial_Z \Phi'$. A linear normal mode is a solution of the form:

$$\Phi' \;=\; \widehat{\Phi}(X, Z) \, e^{i \, \ell Y} \, e^{\sigma \, t}, \qquad \text{(SN1.3.1)}$$

where ℓ is the zonal wavenumber or scale of the perturbation and σ its complex growth rate $\sigma = \sigma_r + i \, \sigma_i$. A spontaneously growing solution exists as soon as one can find a function $\sigma_r(\ell, \overline{P}) > 0$.

Certainly the most powerful and elegant result of this body of work is the *Charney and Stern (1962) theorem*. The ambition of this theorem is to predict which basic flows will support unstable waves and will, therefore, be conducive to cyclogenesis. It is a kind of existence theorem for solutions of the form of Eq. (SN1.3.1). It takes the form of integral constraints, such as:

$$\sigma_r \left[\int_0^{L_x}\!\!\int_0^H \frac{f}{\overline{PJ}} \left(\frac{\partial \overline{P}}{\partial X}\right)_{\overline{\theta}} A^2(X, Z) \ r dX dZ \right.$$

$$\text{(SN1.3.2)}$$

$$\left. + \int_0^{L_x} \left[\frac{f^2}{\overline{P}} \left(\frac{\partial \overline{\theta}}{\partial X}\right) A^2(X, .) \right]_0^H dX \right] \;=\; 0$$

where the positive real number

$$A^2(X, Z) \;=\; \frac{\left|\widehat{\Phi}(X, Z)\right|^2}{\sigma_r^2 + \left(\ell \overline{V_g}(X, Z) + \sigma_i\right)^2}$$

Figure SN1.3.1: *Example of geometry and notations employed to study the origin of mid-latitude cyclones in a baroclinic zone. The latter is represented by the combination of the jet-stream (blue tube) in balance with a moderate horizontal gradient of potential temperature θ.*
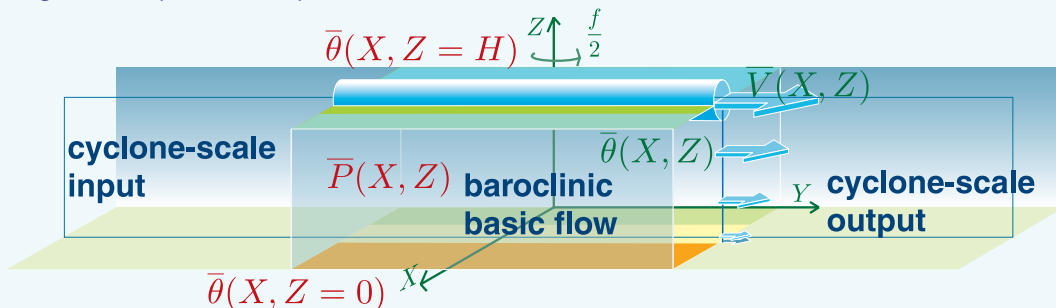
is a measure of the unstable wave amplitude. Eq. (SN1.3.2) is an example of a *necessary condition for instability*. Since for non zero σ_r to exist, the integrals must be zero, $\left(\partial \overline{P}/\partial X\right)_{\overline{\theta}}$ must change sign in the interior (there must be an extremum of $\overline{P}$) or $\left(\partial \overline{\theta}/\partial X\right)$ at $Z = 0$ and $Z = H$ must have different signs. There are also constraints on the phase speed and scale of the perturbation.

The interpretation of normal mode analysis is plainly stated for example by Eady (1949). It can be stated as follows Let E_G be an overall measure of the wave amplitude, for example its energy (but many others can be named and employed):

$$E_G \left\langle \Phi', \Phi' \right\rangle \quad = \quad \text{(SN1.3.3)}$$
$$\frac{1}{2} \frac{1}{L_x L_y} \int_0^{L_x} \int_0^{L_y} \int_0^H f^{-2} \left[(\partial_Y \Phi')^2 + (\partial_X \Phi')^2 \right]$$
$$+ \frac{\theta_0}{g} \frac{f \overline{J}}{\rho_0 \overline{P}} (\partial_Z \Phi')^2 \ \rho_0 dX dY dZ.$$

The normal modes form a basis onto which any perturbation can be projected. Let $\{\Phi_k\}_{k=1,K}$ be the normal modes. All kinds of small amplitude, unorganized perturbations enter the basic flow. Any such perturbation can be expanded in the normal mode basis as: $\Phi' = \sum_{k=1}^K b_k \Phi_k$, with a flat series of b_k. Consider now that the energy can be said to change between an initial time t_0 and a final time t_1 as:

$$E_G \left\langle \Phi', \Phi' \right\rangle \ = \ \sum_{k=1}^K |b_k|^2 \ e^{2\sigma_{kr}(t_1-t_0)}. \quad \text{(SN1.3.4)}$$

In the presence of a large dominant instability characterized by σ_{xr} this expansion reduces to:

$$E_G \left\langle \Phi', \Phi' \right\rangle \ \sim \ |b_x|^2 \ e^{2\sigma_{xr}(t_1-t_0)} :$$

any arbitrary perturbation tends to behaves and to look like the most unstable normal mode. The other solutions seem not to be useful. *The basic flow kind of generates perturbations that look like the most unstable normal mode (Fig. SN1.3.2).*

1.3.2 ...to sufficient conditions for linear development

An important assumption is made, more or less implicitely, in order to write Eq. (SN1.3.4): the normal modes have to be orthogonal to one another in the sense of energy.

The change of energy for an arbitrary perturbation between times t_0 and t_1 is, in fact:

$$E_G \left\langle \Phi', \Phi' \right\rangle \ = \quad \text{(SN1.3.5)}$$
$$\sum_{k=1}^K \sum_{j=1}^K b_k \overline{b_j} \ e^{(\sigma_k + \overline{\sigma_j})(t_1-t_0)} \ E_G \left\langle \Phi_k, \Phi_j \right\rangle,$$

where $E_G \left\langle \Phi_k, \Phi_j \right\rangle$ is the scalar product of the two normal modes Φ_k and Φ_j that can be constructed from the norm E_G, energy. In other words, $E_G \left\langle \Phi_k, \Phi_j \right\rangle$ says how two normal modes are energetically correlated in a given basic flow. The classical interpretation of normal mode theory, and indeed its usefulness, crucially depends on the fact that normal modes are energetically independent. In this case, only unstable modes in the sense of Eq. (SN1.3.1) can grow.

Eq. (SN1.3.5) suggests that this is *not required* any more when normal modes are not energetically independent. For the sake of example, consider a set of *neutral* modes: $\forall k \in \{1, \ldots, K\}$, $\sigma_{kr} = 0$, but such that two modes are correlated in the sense of energy, modes 1 and 2, say: $E_G \left\langle \Phi_1, \Phi_2 \right\rangle > 0$. Then, let Φ' be the perturbation which is the sum of these two modes. Eq. (SN1.3.5) reads:

$$E_G \left\langle \Phi', \Phi' \right\rangle = 2 \cos \left[(\sigma_{1i} - \sigma_{2i})(t_1 - t_0) \right] E_G \left\langle \Phi_1, \Phi_2 \right\rangle.$$

This perturbation amplifies and then decays: *transient growth* becomes possible, *even in the absence of instability*. However, it can also decay and then perhaps grow, if not destroyed by turbulence: *the initial phase, more generally the initial conditions become essential*, while they did not matter in the normal mode analysis. In reference to the description of cyclogenesis made by synopticians (Sutcliffe, 1947, for example), this kind of evolution that depends more on initial conditions than on the presence of an instability can be called *linear development*.

It appears, then, that if two normal modes or more, with close phase speeds, can easily be correlated in the sense of energy, linear development and the related solutions cannot be ruled out as a possible explanation for systems like cyclones. In the presence of unstable normal modes, this process provides additional transfers that will boost the effective growth rate of certain combinations of normal modes. These facts were pointed out essentially by Farrel (1984, 1985).

Figure SN1.3.2: *The classical perspective: the baroclinic zone in the atmosphere acts as a generator of phase-locked cyclones. The equation represents the eigenvalue problem that defines the normal modes.*
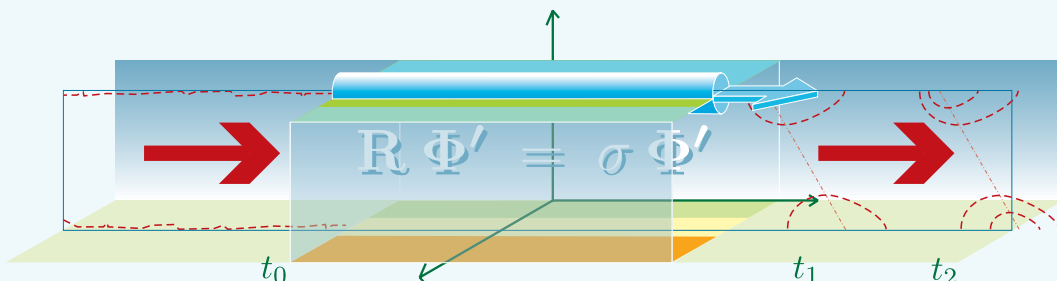
In this new perspective, the question addressed by Charney and Stern has to be restated. They asked "which basic flows support unstable waves". Today's question is "which basic flows support non-orthogonal normal modes", unstable or not. In the present case of energy as defined by Eq. (SN1.3.4), the correlation between two modes can be written:

$$
\begin{aligned}
E_G \langle \mathbf{\Phi}_k, \mathbf{\Phi}_j \rangle \;=\; & -\int_0^{L_x}\!\!\int_0^{H} \frac{i\,\ell}{\overline{PJ}} \left(\frac{\partial \overline{P}}{\partial X}\right)_{\overline{\theta}} \left(\frac{\overline{\widehat{\Phi}_j \widehat{\Phi}_k}}{s_k}\right. \\
& \left. + \frac{\overline{\widehat{\Phi}_k \widehat{\Phi}_j}}{s_j}\right)\; \rho_0\, dX\, dZ \qquad (\mathrm{SN1.3.6}) \\
& + \int_0^{L_x} i\,\ell \left[\frac{\partial \overline{\theta}/\partial X}{\overline{P}} \left(\frac{\overline{\widehat{\Phi}_j \widehat{\Phi}_k}}{s_k} + \frac{\overline{\widehat{\Phi}_i \widehat{\Phi}_j}}{s_j}\right) \right]_0^{H}\, dX,
\end{aligned}
$$

where $s_k = \sigma_{kr} + i\,(\sigma_{ki} + \ell V_g)$. As long as $(\overline{PJ})^{-1}\,(\partial \overline{P}/\partial X)_{\overline{\theta}}$ and $\overline{P}^{-1}\,(\partial \overline{\theta}/\partial X)\,(Z=0,H)$ are constants, this scalar product reduces to the canonical form and nothing unexpected happens.

However, as soon as these are functions of space, even trivial ones, canonical orthogonality will be lost. The non-separability that results from this prevents, in general, the integrals to be trivially zero. Such is the *very weak sufficient condition for allowing transient linear development* (Joly, 1995).

In other words, one can expect linear development even in basic states that are stable in the sense of Charney and Stern.

As Farrell (1989) as shown for classical baroclinic instability problems, or Joly (1995) for fronts, this mechanism is, in fact, *extremely efficient* in the atmosphere. A new "standard model" is emerging, as a result. It consists of looking for the *initial conditions* that will get the largest energy $E_G \langle \Phi', \Phi' \rangle$ (or any other measure of growth) in a given time. In this perspective, *the basic flow kind of amplifies some of the initial perturbations that enter it* (Fig. SN1.3.3), while others decay (Farrell, 1994).

1.3.3 Some consequences

The normal mode analysis has provided a very clear depiction of the physical mechanism that enables the growth of large scale mid-latitude cyclones: it is called *baroclinic instability*. The same mechanism operates in the new solutions, but more efficiently and at different scales and in different basic flows: it can be called *baroclinic interaction*. The normal mode analysis predicts likely time and space scale for the cyclones as well as a space scale below which cyclones should not exist. It strongly suggests, as well, that the growing systems should have a fixed shape in space (represented by $\widehat{\Phi}(X,Z)$): this is called *phase-locking*. The shape amplifies and propagates, but it is not deformed. Unlike the mechanism for growth, these other features do not match observations well, as is the case for a number of necessary conditions for instability. As a consequence (or a symptom of its limitations), this theory had very little influence on practical forecasting, synopticians finding many of its features hard to swallow.

Consider the time scale: the normal mode theory predicts a time scale of about 2 days for conditions close to the climatological jet-stream. Some say that, indeed, this is the order of magnitude of the evolution of a cyclone. However, it means literally, according to (SN1.3.1), that the initial amplitude, assumed to be barely measurable, is about trebled in 2 days. Starting from 1 mbar (but in principle, even less), it takes 2 days to reach 3 mbar, 4 days to get to 9 mbar. Now, according to, for example Ayrault (1998), the typical deepening of cyclones is between 10 and 20 mbar in *1 day*. There is a confusion between the time scale of a full life-cycle (2 days indeed) and the meaning of the growth rate σ_r, which needs to be very large to allow the most unstable mode to emerge and reach finite amplitude in a matter of *hours*. The new, finite-time analysis provides much more realistic answers.

The most rapidly growing initial conditions are combinations of normal modes. As a result, the separability of the time dependence built in a single normal mode is lost: *the most rapidly growing solutions undergo significant changes of shape: this also fits observations better.*

Figure SN1.3.3: *The current perspective: the baroclinic zone in the atmosphere acts as an amplifier of pre-existing precursors of cyclones, which yeields shape-changing systems. The equation represents the eigenvalue problem that defines the modes that have a maximum amplification of energy in a given time, the singular vectors of* $\mathbf{R}^*\mathbf{R}$.
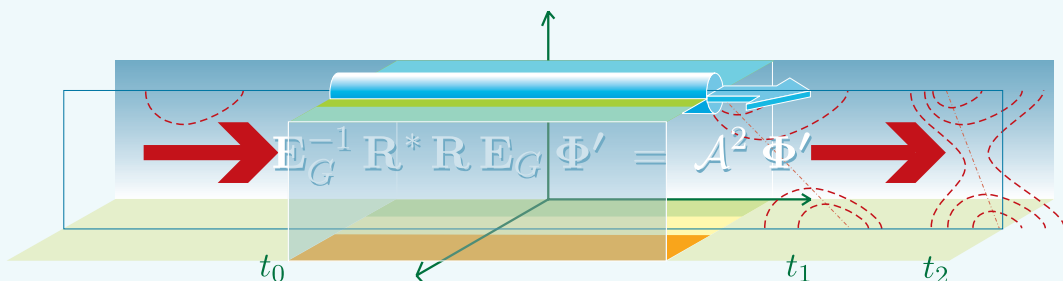
This evolution of the theoretical framework for understanding cyclogenesis has consequences that reach beyond the history of ideas. Observation, for example. Normal mode instability analysis supports the idea that the cyclone scale evolution is enterely determined by the basic flow: it is sufficient, therefore, to set up an observational network that concentrates on the large scale basic flow, the rest being deduced. The new perspective insists on the importance of initial conditions, that is the motion on the cyclone scale itself. The observational network has to address both the basic flow scale *and* the pre-existing subtle features on the cyclone scale itself.

Furthermore, Eady (1949) also interpreted the existence of time scales provided by such linear models in terms of predictability, and this remains true, normal mode or not. The time scale of the largest amplification defines the predictability: beyond this time scale, small errors will have grown enough so as to reach amplitudes of the same magnitude as the real solution and the forecast becomes highly uncertain. The time scale suggested by the transient development perspective is reduced to 0.5 to 1 day. The consequences of this rather bad news on the prediction of cyclone events are discussed in Short Note 1.4.

1.2.2   Practical forecast perspective

At the same time, the objective, numerical forecast of these frontal or more generally, these "end-of-storm-track" cyclones remains a serious practical difficulty in spite of the continuous progress of numerical weather prediction. This was noted in the report by the french forecasters Beugin and Rochard (1991) after the numerous trying cases they had to face during the winter 1989–1990. A new generation of models is now available, and yet the difficulty is still there.

This is illustrated by Fig. 1.2 showing the successive forecasts of a 1996 case of interest from the ECMWF operational suite. Although the general characteristics are well predicted, an accurate forecast of precipitations over Ireland and, most important, of the wind over the Channel appears to be impossible, because they are different at every new run. Clearly, however, the problem is not simply in the ability of these models to represent cyclones properly: some of the forecast for a given event are excellent. The solution calls for a different approach than, for example, trying to improve parameterizations. The problem is related to the sensitivity of these developments to initial conditions.

In spite of undisputable progress in Numerical Weather Prediction, that improve forecast on average, this particular but economically important problem still arises (recall the Christmas day 1997 storms). This situation encourages the in-depth study of the parallel approaches put forward in FASTEX.

Beside the need to check the new theoretical ideas on cyclogenesis, there is also a demand for improved, validated, conceptual models of cyclogenesis that can help assessing real forecasts and a demand for exploring possible solutions to stabilize forecasts in the range 24h–96h. These questions asked by the forecasters and users of weather forecast to the meteorological scientific community have motivated the launch of the Fronts and Atlantic Storm-Track Experiment (FASTEX).

1.2.3   Observational perspective

The continuing progress in observational technology is a further motivation. From this point of view, FASTEX is the offspring of two streams of field studies focused on cyclogenesis and frontal dynamics. The first one is the series of field experiments conducted along the East-Coast of North-America in the eighties: the Genesis of Atlantic Lows Experiment (GALE; Dirks *et al.*, 1988), the Experiment on Rapidly

Intensifying Cyclones over the Atlantic (ERICA; Hadlock and Kreitzberg, 1988) and the two successive field phases of the Canadian Atlantic Storms Program (CASP; Stewart *et al.*, 1987, Stewart, 1991). These experiments were meant to provide an understanding of the process of rapid or even explosive cyclogenesis taking place along the western boundaries of oceanic basins, a category of cyclones that is not the focus of FASTEX. The second stream of field projects is European: the FRONTS-87 (Clough and Testud, 1988) was organized by the UK and France to collect data to validate the semi-geostrophic theory of frontogenesis and study frontal precipitations. More recently, the UK conducted the FRONTS-92 project (Browning *et al.*, 1995) as a pilot experiment preparing the grounds for FASTEX.

1.2.4 Short history of FASTEX

The first papers outlining the main objectives as well as the characteristic set-up of the observing system that are the hallmark of FASTEX were written at Météo-France in 1991 (Joly and Lalaurette, 1991). Very soon, however, because of its strong links with ongoing theoretical co-operation and with FRONTS 92, FASTEX became a French and UK initiative (the name has been coined by Keith Browning). The preparatory work begun in 1993 in both countries, after the first drafts describing the project had been evaluated by a panel including a number of US scientists. A first meeting of the Core Steering Group, including US representatives, took place at the end of 1993 in Toulouse. The US participation took shape at the first meeting of the Scientific Steering Group in Washington in March 1995. It included the key addition to the scientific objectives of the testing of the adaptive observation strategy as a practical method to tackle the forecast problem.

Since then, FASTEX is a large, joint project strongly supported by both American and European scientists and organizations, with regular planning meetings and production of documents, most notably the FASTEX Science Plan (Thorpe and Shapiro, 1995), the FASTEX Operations Overview (Jorgensen and Joly, 1995) and the FASTEX Operations Plan (Jorgensen *et al.*, 1996). Table 1.4 presents an overall time-table of the project. This Part summarizes these plans, beginning by defining the cyclones of interest (section 1.3) and formally presenting the scientific objectives (section 1.4). Section 1.5 presents the observational objectives of the field phase. They are followed by a summary of the observing system and sampling strategies (section 1.6), with details of the options available to gather data on the cloud system in the Multiscale Sampling Area (section 1.7). The outcome of the field phase is presented in Part 2. The sample of cases observed is summarized in Part 3.

1.3 Climatology of FASTEX cyclones

The aim of a climatological study of Atlantic cyclogenesis are *(i)* to characterize the existence of the specific properties of the cyclones hitting the west coast of Europe *(ii)* to determine the time of year when they are most frequent *(iii)* to derive some picture of their life cycle. The detailed results of the first part of this work is to be found in Ayrault *et al.* (1995). It has evolved into building a new, quantitative classification of North-Atlantic cyclones (Short Note 1.5). The results, derived from an automatic tracking algorithm (Ayrault, 1995) employed here to tackle item *(iii)*, will be published in due course.

The starting point is the classical work of Sanders and Gyakum (1980) and of Roebber (1984). Both studies cover the Pacific and Atlantic oceans. They concentrate

Short Note 1.4:
Why is the forecast of cyclogenesis difficult ?

by F. Lalaurette and A. Joly

Assuming that nowadays weather forecast rely on numerical models, possible causes of forecast errors are *(i)* model errors, *(ii)* uncertainties in the initial conditions and *(iii)* an intrinsically low predictability of the atmosphere. The first generations of models, in the sixties and seventies, met some serious difficulties when simulating after the fact cyclogenesis cases, so that possibility *(i)* remained important. However, since the early eighties, it can be said that models have reached an extremely reasonable level of realism. Although model errors, specifically, simplifications with respect to the actual atmospheric dynamics, still exist, they do not appear to be the major source of forecast error. The effort was then brought to bear on item *(ii)* by improving the observational network on one hand, mostly with remote sensing (the surface based in-situ observations are not really on the upside) and, on the other hand, by making a better use of observations in the process of analysis, namely the preparation of initial conditions for a forecast (see Part 8 for details). Yet, the hope that, eventually, deterministic forecast were possible until 10 to 15 days or so remained widely accepted: very few people had really realized that such a thing as *(iii)* could exist. It is a limitation that is out of our control, that will still be there even if we can get precise data from all over the Earth and put in into a perfect model.

Figure SN1.4.1: *Six of the 51 solutions proposed by ECMWF ensemble forecast in the presence of a well established zonal regime, all showing possible solutions valid at the same time. The field shown is mean sea level pressure over the Atlantic. Even on this very small subsample, the diversity is striking.*
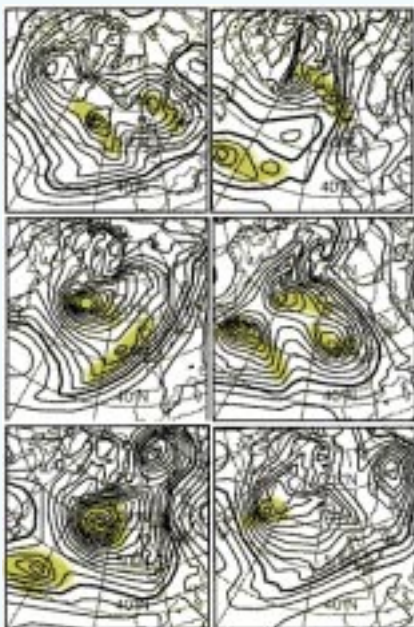
Figure SN1.4.2: *The natural growth of uncertainty in the course of a numerical weather forecast is shown in an idealized simulation. Black contours: surface geopotential. Dark-red contours: surface potential temperature. Shading: variance of surface potential temperature forecast error, a direct measure of uncertainty. It is small (yellow) and uniform at initial time.*
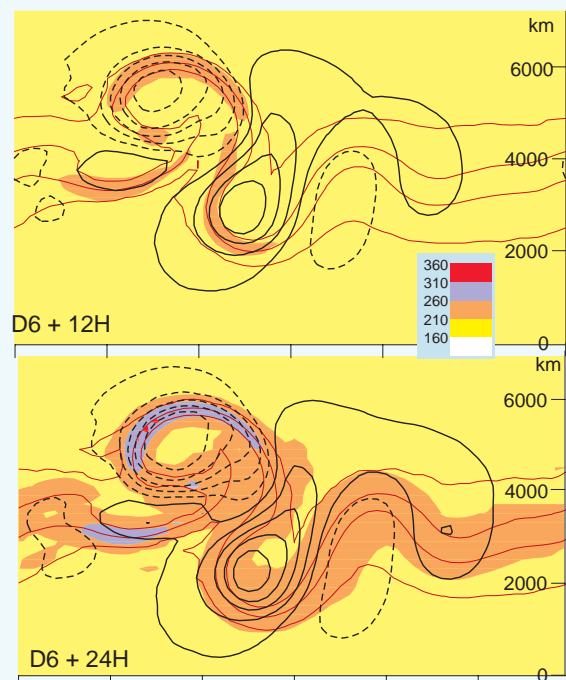
Following striking examples of misforecast of rapid cyclogenesis events with fine models, it became apparent that there was room for a stochastic approach to weather forecast. Ensemble forecast systems were developed (see e.g. Molteni et al., 1996). Their existence allows, among other things, to get a direct impression of *(iii)*. Figure SN1.4.1 is an example of the dispersion of possible solutions that result from the small uncertainties in the initial conditions in the presence of a well established zonal regime. A whole range of possibilities are shown for western Europe: from fair weather in the right corners to very nasty storms, as in the middle right panel. There are 45 other solutions available. It is important to realize the following facts: *(a)* the model employed here is a state of the art one, with the resolution that was employed operationnally in the eighties, when one and only one run was performed, *(b)* the initial conditions are perturbed, but the amplitude of the changes remains within the bounds of analysis error and *(c)* such a wide dispersion of possibilities does not occur every day, in spite of *(b)*. This is the fact that reveals that a source of forecast error of kind *(iii)* exists independently of *(ii)*.

The presence of a strong baroclinic zone is, by itself, a source of forecast uncertainty, the main reason why the deterministic forecast of cyclogenesis remains a major difficulty. The Ensemble Prediction illustrates this at medium but also at short ranges, since a dispersion such as in Fig. SN1.4.1 can sometimes be seen as soon as two or three days. In the short range, an even better grasp of this intrinsic predictability can be achieved. One can make the assumption that errors evolve linearly. It is then possible to compute explicitly the evolution of second order statistical moments, without being limited by the size of an ensemble sample and the unavoidable representativeness problems. This explicit calculation is, however, very expensive: it can be done either locally with a sophisticated model or globally, but with a simplified model.

The second approach is meaningfull to outline the link between predictability and the essential dynamics of cyclogenesis. The results are illustrated by Figure SN1.4.2. A generic large scale cyclone development event in a baroclinic zone is simulated and this reference solution is shown by the contours. The important information is contained in the shading. It shows a direct measure of uncertainty, the field of the variance of forecast error of the low level potential temperature. In this experiment, it is assumed that, initially, the uncertainty is small and is the same everywhere. It turns out that uncertainty does *not* remain uniform: very quickly, areas of large uncertainty develop. Within 24 h, it appears to embody the whole of the baroclinic zone itself, with large peaks in the frontal areas. The scale and amplitude of the variance reached within 24 h are large enough so that it is impossible to know whether waves will be present or not along the fronts. This is why the forecast of mid-latitude cyclones is difficult.

A slightly different view of the same thing is shown by Figure SN1.4.3. This time, the impact of more observations somewhere in the baroclinic zone has been simulated by including an area of reduced initial variance. The area has been chosen arbitrarily, as happens with an observational system that depends on ships or aircraft of opportunity. Is this of any benefit ? The example shown says "no" (except where the observation was made): very quickly, the baroclinic zone supresses the benefit of the better knowledge of the weather, and the extra data has no impact far downstream, beyond the trough, for example.

These fundamental numerical experiments indicate that it may well happen that the predictability of rapid cyclogenesis may be as low as half a day or one day. The objectives of FASTEX dealing with the theories of cyclogenesis are meant to help understanding the fundamental reasons for the rapid build up of error variance in a baroclinic area, much more rapid than anticipated by linear normal mode approaches: see subsection 1.2.1 and the Short Note 1.3 on this topic. The arbitrary addition of observations does not seem to help. Yet, these experiments heavily underline the fact that predictability is flow dependent. It might be possible, therefore, to perform a deterministic cyclogenesis forecast in the short range by having a flow dependent observation system. Its purpose will be to reduce to a minimum the initial forecast error variance *where* it is going to grow most rapidly. The predictability objectives of FASTEX have been set up to study this last "chance": see subsection 1.4.3 and Short Notes 1.7 and 1.8.

Figure SN1.4.3: *In another similar situation, two runs with locally different initial variance are compared. The contours are the upper-level geopotential (blue lines) and potential temperature (dark-red lines). The shading shows the area of lesser uncertainty that can result from having, for example, more observations: precisely, it shows the percentage of variance reduction in the reference and "improved" runs. The result is that the benefit of a better knowledge of the flow dissipates extremelly rapidly.*
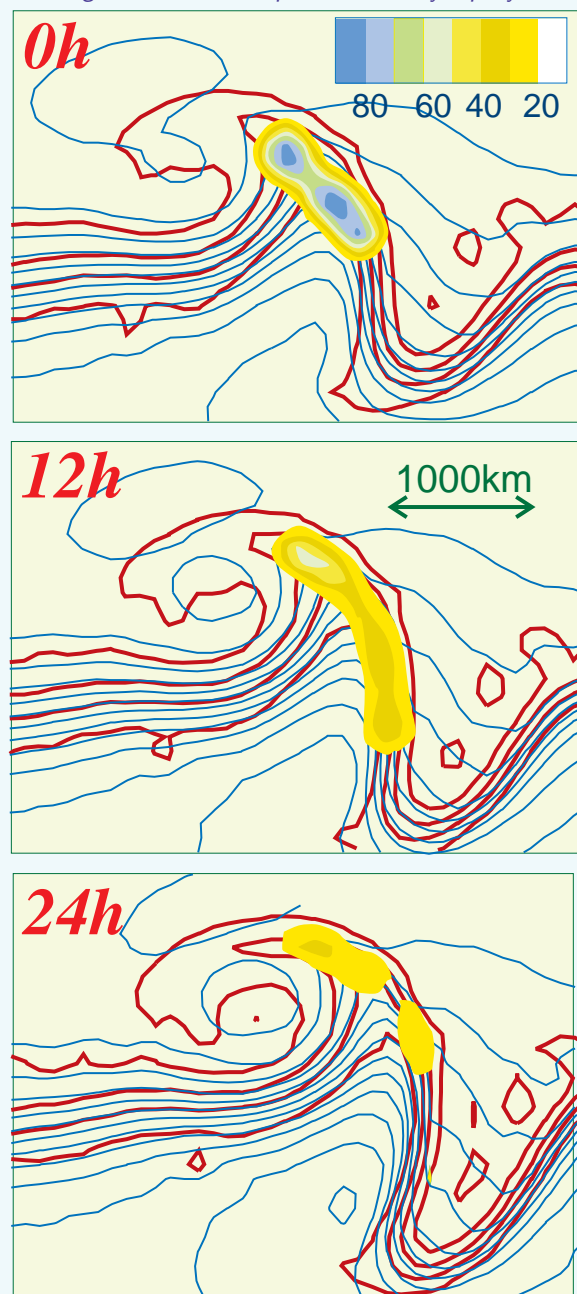
on explosively deepening cylones, and, from that point of view, find very little activity off the European coasts. This does not fit with the feeling of the European people, who find that cyclones are reasonably frequent. The reason, of course, is that these cyclones turn into "bombs" (as defined in the above references) very unfrequently and their spectral properties are significantly different. This is clearly shown by Ayrault *et al.* (1995) based on an extraction from ECMWF operational analyses between 1984 and 1994 at full time resolution, namely every 6 hours. (Only the winter season has been included.) It becomes possible to analyse the "ultra-high" frequency variability, with a period in the range 0.5–1.5 days.

A first distinctive property of the Eastern end of an oceanic basin like the Atlantic is its low frequency variability (characteristic period > 10 days): it is maximum. This means that the large scale flow pattern, or the environment in which the cyclones evolve, undergoes large changes. In order to study cyclones in relatively homogenous large-scale environments, it is necessary to separate the large-scale flow into different weather regimes (see Short Note 1.1). Following the definition of Vautard *et al.*

Figure 1.3: *Climatological frequency of weather regimes over the North-Atlantic during the winter months. Derived from ECMWF analyses from 1986 to 1994. The onset of the zonal or of the Greenland Ridge regimes implies cyclogenesis events for FASTEX, unlike the blocking regime. The statistical distribution of regimes roughly estimated here is a critical characteristic of climate. (Figure after F. Ayrault, Météo-France.)*
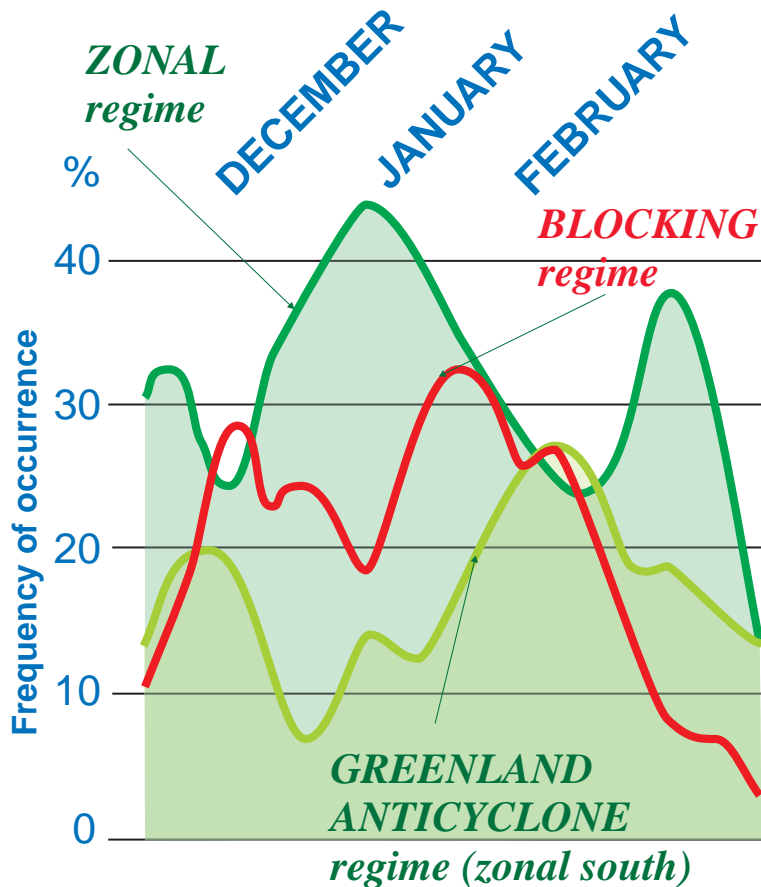
(1988), weather regimes are defined as persistent patterns of the large scale flow. Various techniques lead to the definition of four regimes over the Atlantic. The Zonal regime and the "Greenland Ridge" regime correspond to a zonally extended baroclinic zone, more to the south in the second case (see Fig. SN1.1.1). The Blocking and Atlantic Ridge regimes conversely correspond to a jet-flow deviated to the north as soon as 40°W. As a result, cyclones reaching Europe from the west occur during spells of the first two regimes. The empirical frequency of occurrence of these regimes is shown by Fig. 1.3. It appears that the most favourable period for a zonal-like regime is the first half of January, with about 60 %.

The second distinctive property of Eastern oceanic basin cyclogenesis is their characteristic time scale. The maximum of variability in the 2–6 days range is, during Zonal regime, centered on 50°N and 45°W. The maximum of variability in the 0.5–1.5 days range is centered on 55°N and 25°W, that is at the eastern end of the high-frequency variability maxima that is often used to define the "Storm-Track". It has an amplitude in that range and area that is comparable to that in the 2–6 days range. This means that the FASTEX cyclones can be expected to be an equal mixture of rather well known baroclinic systems and of a different kind that evolves more rapidly. The latter category indeed appears to be impossible to separate spectrally from fronts and so the successful techniques introduced by Blackmon *et al.* (1984) cannot be employed to outline the properties of these cyclones. Instead, an event-oriented technique must be employed.

A whole new set of cyclone prototypes has thus been obtained by Ayrault (1998). These results confirm two important ideas outlined in the introductory section: the reduced scale (in time and space) of the cyclones to be met at the end of the classical storm-tracks, the existence of new types that depend on environmental properties differing from the baroclinicity (Short Note 1.5). Similar remarks can be derived from a case study approach and conceptualization: see Browning and Roberts (1994) and Rivals *et al.* (1998).

Some of Ayrault's (1995) results were very useful to plan FASTEX. The events of interest are defined using vorticity at 850 mbar (as pressure deepening is not a relevant criterion): the cyclone must be reachable from Ireland (the reasons for this are given in section 1.7 below), must have a large enough amplitude ($\zeta_{\max} \geq 10^{-4}$ s^{-1}, where ζ is the relative vorticity) and must have developed somehow in the previous 12 h. Figure 1.4 shows the time distribution of these events for the past januaries and februaries for which ECMWF analysis is homogenous enough in a statistical sense. Over this period, there are, on average, 11 cyclones within these two months. However, the interannual variability is very large, with very active winters like 1990 — that motivated a programme like FASTEX in France — and very, very dull ones like 1989. This, of course, introduces an element of risk in FASTEX.

An important conclusion to be drawn from Fig. 1.4 is the fact that cyclones rarely comes as isolated individual events. On the contrary, they happen in surges, with very close chaining of two, three or even more events. This is reminiscent of the Norwegian idea of "families" of cyclones. This fact has borne on the logistics of FASTEX (see section 2.4).

This collection of events can then be back-tracked, so that a rough idea of their life-cycle can be obtained. The result is shown by Fig. 1.5. The large black dots suggest the most frequent low level path followed by these cyclones. The dashed contours define areas that enclose 60 % of the trajectories of the cyclones. The change in shape and, even more so, of area, conveys an idea of the dispersion of

Short Note 1.5:
New climatological types of cyclones

by F. Ayrault

1.5.1   Classification methodology

The new semi-automatic classification of North--Atlantic cyclones is fully described in Ayrault (1998). The data is provided by the first ECMWF re-analysis of the period 1979–1993 (Gibson *et al.*, 1993). From the global T106L31 set of re-analysed fields, 14 "winter" seasons extending from 16 october to 15 april have been extracted over the north-american continent, the north-Atlantic ocean and western Europe. The automatic tracking technique of Ayrault (1995), much employed, has been primarily applied to these 14 years of data, yielding part or all of the life-cycle of 24514 events at 850 mbar and 30926 at 300 mbar.

Figure SN1.5.2: *Example of life-cycle retrieved from the tracking algorithm. The two stages that have been isolated and ordered into classes are defined on this figure: the initiation and maturation stages.*
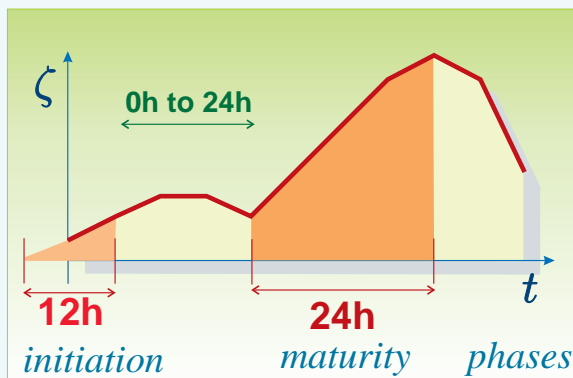
The classification is based on partial time-series of fields extracted in square boxes with 2500 km side and centered

on the event. Looking at the trajectories revealed such a wide range of possibilities that it seemed impossible to classify entire life-cycles. Based on the 850 mbar trajectories, two independent classifications have been undertaken (and the process has been repeated using the 300 mbar trajectories): a classification of the *initiation stage*, during which new events are created. It extends over 12h (−6h, 0h, +6h). Then, independently, a classification of the *maturation stage* is performed. It covers the 24h preceding the time of maximum amplitude (Fig. SN1.5.2). The fact that the two classifications are very different, leads to conclude that the genesis of a low is a process quite independent from its subsequent development.

Consider the classification of the maturation period: each trajectory having a maturation period contained within 2500 km of the domain boundary (reducing the available set to 1648 trajectories) becomes a set of $15 \times 15 \times 4 \times 5 = 4500$ values. No automatic classification algorithm can deal with such an amount of data. A reduction is performed, first. The temperature fields are turned into anomalies, all the fields are normalised and a principal component analysis is performed on the resulting grids. The number of components retained for the classification is obtained after many sensitivity tests (this is why the method is "semi" automatic).

The reduced trajectories are organized into classes using hierarchical clustering. At each iteration, each set is splitted into 2 subsets obtained by minimizing the resulting intra-class variance. The process is initiated by simply assuming that all the events are in one set. The main advantage of this technique is that the number of classes is determined from the results rather than imposed. A useful classification emerges when, roughly speaking, the variances are about half the initial variance.

Figure SN1.5.1: *The structure of the 7 maturation classes at the beginning of their 24 h development phase. The top-left one corresponds to rapidly deepening systems. The number of cases in the composite and its frequency in shown in boxes. Purple contours: 850 mbar vorticity; brown contours: 850 mbar θ_e; orange contours: 300 mbar vorticity.*
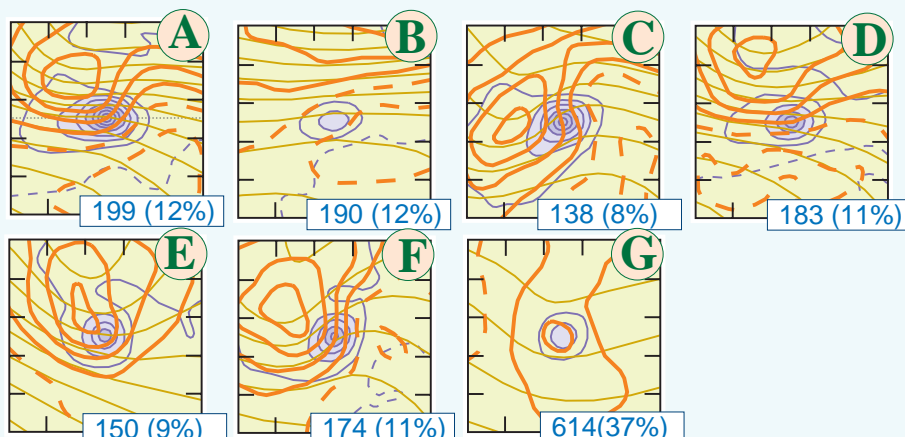
Figure SN1.5.3: *There are 12 classes that describe the various ways in which a new cyclone forms. One way of trying to condense the information is to gather them into larger "families", as done here. Purple contours: 850 mbar vorticity. Brown contours: 850 mbar θ_e. Green contour: large 700 mbar relative humidity. Orange contours: 300 mbar vorticity. Blue arrows: 300 mbar wind. From top to bottom: cold air cyclogenesis; cyclogenesis initiated by an upper-level maximum; cyclogenesis in a complex jet-entrance/front system; splitting of an older system.*

112 (27%)

172 (42%)

104 (25%)

22 (6%)
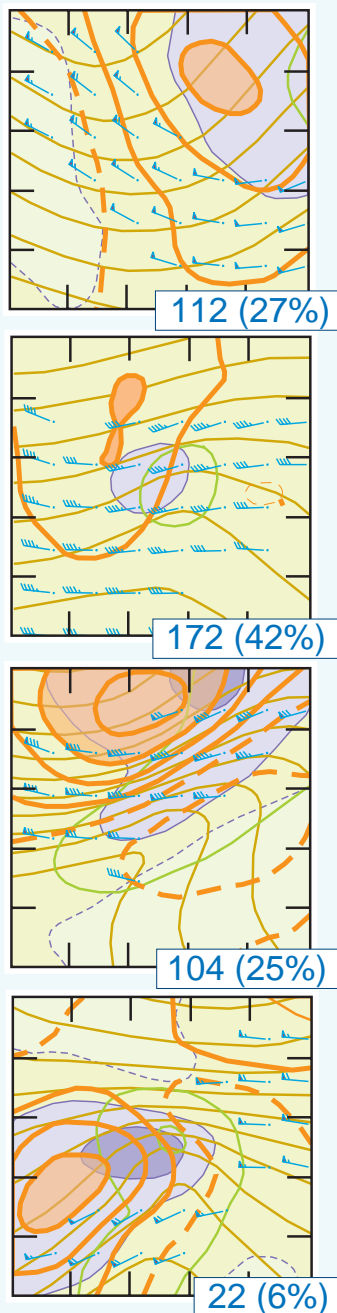
Now the key idea to recover geophysically meaningful "paradigmatic" events is to forget about the principal component reduction. Instead, once events are classified in this way, the composite event is built from averaging the *original* fields themselves.

1.5.2 Maturation and initiation classes

The maturation stage based on 850 mbar trajectories can be described by 7 classes (Fig. SN1.5.1). Most of them (5 out of 7) involve some form of baroclinic interaction. The initiation stage, on the other hand, reveals 12 classes. For the sake of brevity, they can (roughly) be divided into 4 super-classes or families: lows initiated by a pre-existing upper-level precursor, lows forming in the cold air, lows created in a complex jet-inflow/front-like environment and lows resulting from the breakdown or splitting of entire older, pre-existing systems (Fig. SN1.5.3).

The most important characteristic of this classification is that all the features it reveals are quantitative: the frequency of the classes, the transitions giving the initiation classes of a given maturation class, the amplifications and many other parameters since each type is a series of gridded fields.

The most dangerous cyclones belong to Maturation Class A: they are the rapid deepeners. Fig. SN1.5.4 shows this clearly. It appears, however, that a large baroclinicity does not, on its own, imply that such an extreme event will occur: the figure shows that Class B also occurs in a strongly baroclinic environment, but does not deepen. Looking back at Fig. SN1.5.1, it appears that the other necessary ingredient is the presence of a significant upper-level precursor that the classifications show to be independent from the initial surface cyclone.

Figure SN1.5.4: *The maturation classes (shown by Fig. SN1.5.1) are plotted in a 24h pressure fall/background baroclinicity space. This shows that large baroclinicity is necessary but not sufficient to lead to rapid deepening.*
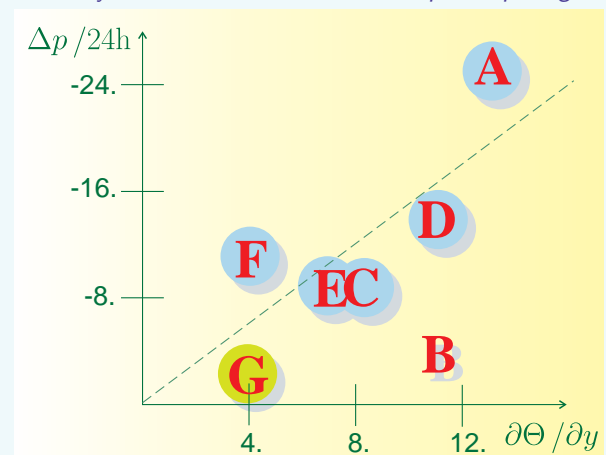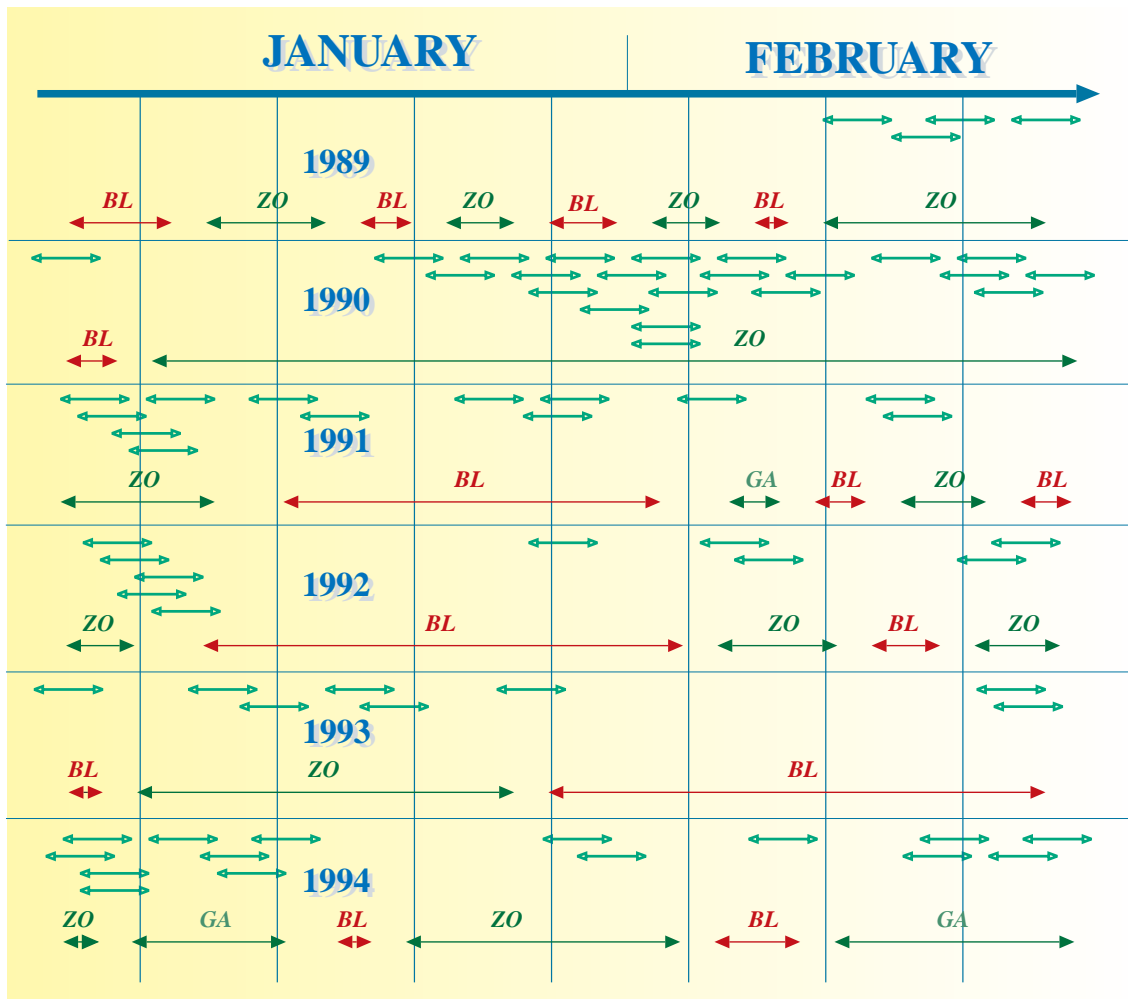
Figure 1.4: *An automatic tracking algorithm has been applied to 6 pairs of January and February months of ECMWF analyses. Cyclones having moved within a range of 800 km from western Ireland, with a maximum vorticity at 850 mbar larger than $10^{-4}s^{-1}$ having increased in the previous 12h define a suitable event (a developing cyclone of significant amplitude). Each event is shown by a thick arrow at the time it occurred. The arrows of variable length correspond to the weather regime: ZO for zonal, GA for Greenland Ridge and BL for Blocking. This figure shows the link between regimes and cyclogenesis as well as the large year to year variability. (Figure prepared by F. Ayrault, Météo-France.)*

the trajectories at low levels. The fact that a drastic reduction can be seen between -48 h and -60 h is not due to a sudden concentration of trajectories, but to a sudden reduction of the total number. In other words, quite a few new cyclones form within the -48 h area. The upper-level components (at 300 mbar) can be followed as well: see the white dots on the figure. Their motion is significantly (and not surprisingly) more rapid. The dispersion is also much more important. This diagram helps picturing the time scale and locations that have to be sampled by a field experiment such as FASTEX that is focused on entire life-cycles rather than a particular time of them. This will become apparent in the presentation of the scientific objectives.

Figure 1.5: *Another result from the automatic tracking algorithm. Cyclones reaching the easternmost circle have been backtracked at two levels. Circles show the most frequent location: black circles at 850 mbar, white ones at 300 mbar. The areas enclosed by the dashed lines contain 60% of all trajectories at 850 mbar, their areas convey an idea of the dispersion. (Figure prepared by F. Ayrault, Météo-France.)*
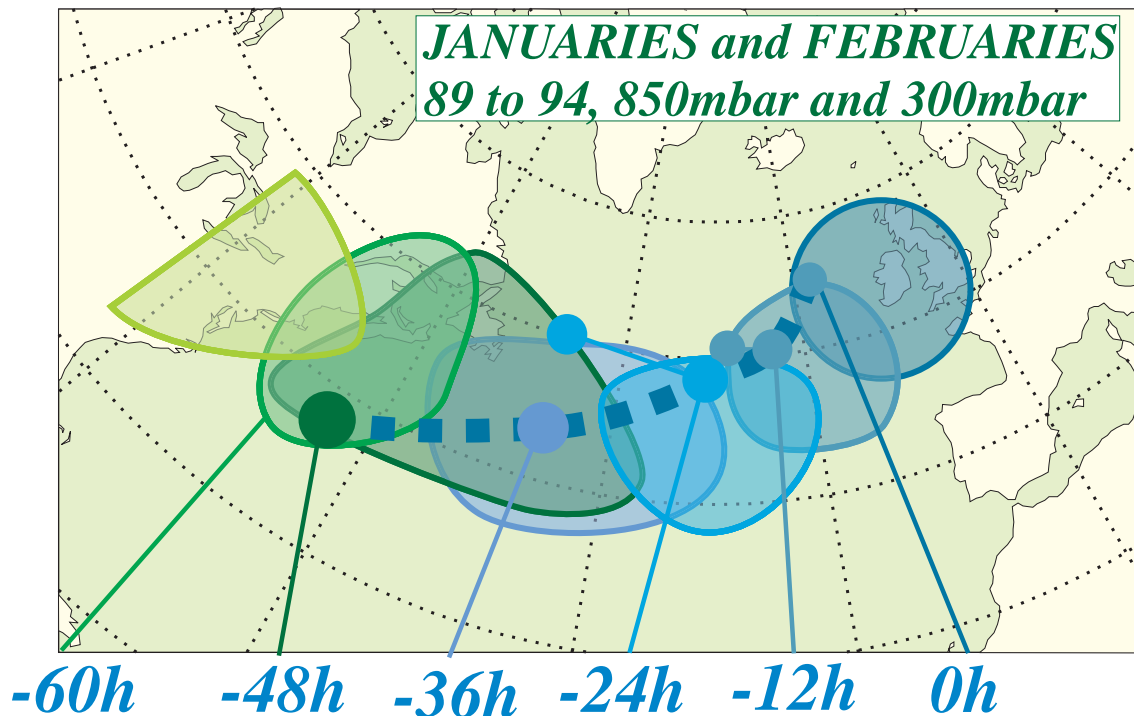
1.4 Scientific objectives

Section 1.2 explains the reasons that led to prepare FASTEX. To a large extent, these reasons determine the scientific objectives.

1.4.1 Cyclone cloud systems

There are two important issues that call for detailed measurements, using new technologies, of the cloud systems associated with FASTEX cyclones.

Internal structure of layer clouds

The first one is to improve the understanding of the internal organization and properties of the clouds themselves. The characteristic feature of these clouds is their arrangement into layers. A recent review of the current knowledge as well as of the gaps in this knowledge is offered by Ryan (1996).

There are several critical aspects of the vertical structure of the cyclone clouds.

- •The first one is the vertical distribution of the microphysical composition, especially at cloud top, and cloud base as well as in the melting layer. The radiative properties of the cloud system will, for example, primarily depend on the optical properties of the cloud top and bottom boundaries. The presence of a melting

layer implies a region of enhanced liquid water that is important both radiatively and for precipitation rate control.

•Another critical aspect of layered clouds is the distribution of latent heating, an essential part of the dynamical and microphysical feedback.

•A property has been noted and is gathering interest as it could have a strong influence on other aspects: the multiple layering of these clouds.

•Within a storm, the horizontal distribution of these vertical profiles is inhomogeneous and a better knowledge of their mapping is required. The water budget and precipitation efficiency of these cloud systems is not well known either.

Deficiencies or uncertainties in the knowledge and treatment within models of these properties impacts on the long term effect of these systems seen as a population (the role of these cloud systems in the climate) as well as on the use of radiative measurements such as in remote sensing inversion. The latter is an often downplayed issue but yet essential if satellite based measurements of temperature and water distribution are to be used more thoroughly.

The impact of layer clouds on climate and the need for documenting the related processes are defined by Stewart *et al.* (1994). One further gap in the present datasets identified in this and the previous review is a series of measurements performed well off the coasts, above the open ocean.

It is apparent that the cloud system associated with a FASTEX storm must be observed on two scales at least. In order to understand the coupling with the dynamics on the scale of the cyclone, an overall knowledge of the ascent zones and clouds is required. At the same time, the internal distribution of vertical layering, water distribution and heating is needed. An airborne Doppler radar such as ASTRAIA/ELDORA (Hildebrand *et al.*, 1996), aided by some in situ microphysical measurements, can provide this multiple scale information. In vertical mode, it can also describe cloud layering.

Cloud-embedded mesoscale dynamics

The second issue related to the cyclone cloud system is that its organization is conducive to all kinds of mesoscale activity. One of its aspect is the presence of rainbands: an example that is relevant to the kind of systems observed on the European West Coast can be found in Lemaître and Scialom (1992). Beside the re-organization of the synoptic scale ascent, there is also the breakup of frontal zones or precipitating bands into mesoscale vorticies. An example of such evolution within a (strong) mid-latitude low is studied by Neiman *et al.* (1993). The processes involve complex interactions between diabatic processes (moist processes, surface fluxes) and dynamical ones. Many unsolved questions relating to the formation and structure of these features require, very much as on the larger scale, the documentation of their life-cycle. Because they occur within cloudy air, the same new airborne Doppler radar technology can provide the required data.

1.4.2   Air-Sea interaction objectives

Very little is known of the behaviour of both atmospheric and oceanic boundary layer in areas combining large fetch and strong winds. It is doubtful that the dramatic change in the shape of the interface that results from these forcings have no effect on the fluxes. See Short Note 2.2 for a few details.
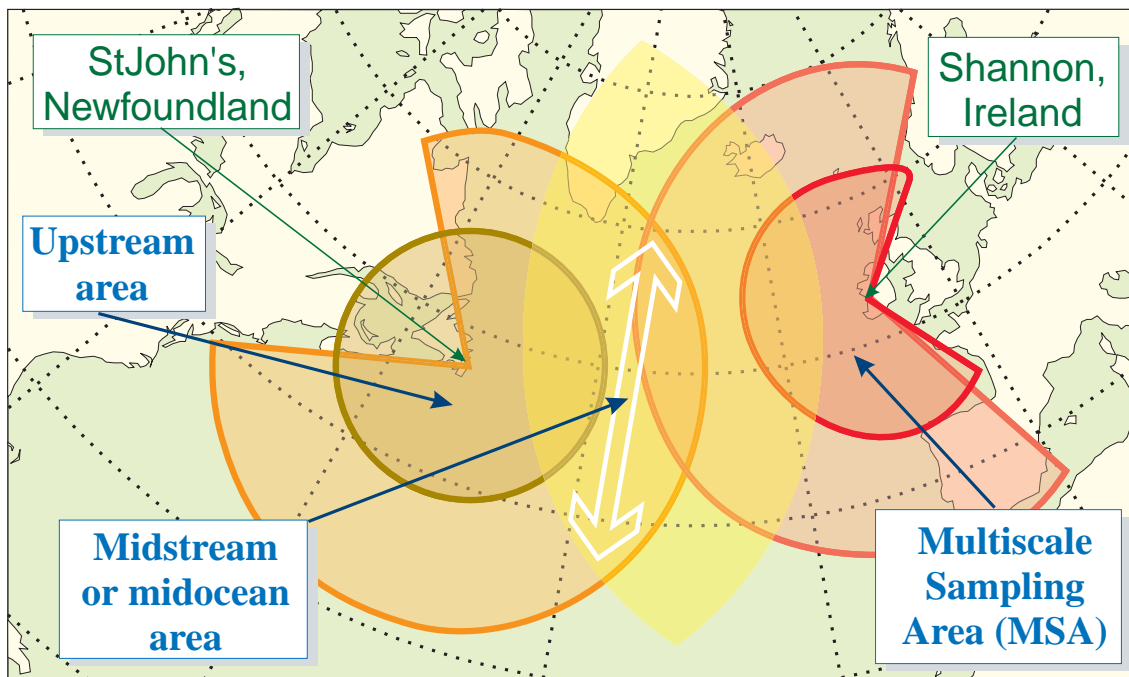
Figure 1.6: *The areas of operations of FASTEX. The heavy solid line is centered over Shannon, Ireland. It defines the inner boundary of the Multiscale Sampling Area (MSA) and corresponds to the maximum ferry time of a C-130 like aircraft in the absence of wind (∼ 1500 km). The heavy long-dashed line is centered over St John's, Newfoundland. It defines the inner boundary of the Upstream Area and is the maximum ferry time of a Learjet-like aircraft (∼ 980 km). The heavy dashed lines and dash-dotted lines correspond respectively to ∼ 1820 km and ∼ 2720 km. They correspond to the maximum ferry time of the Gulfstream (flying at high level) and two thirds of its maximum range. The intersection loosely defines the Midstream Area. The elongated arrow marks the area within which the ships, the main component in this area, will evolve, moving along it following the evolution of regimes.*

At the same time, the effects of these exchanges are suspected to be of influence in the genesis of cyclones (Davis and Emanuel, 1988, Langland *et al.*, 1995). The purely marine cyclones that ultimately hit the west border of the ocean form in the area where the Gulfstream is disrupted into several branches and vorticies. It also looses heat in the same location. This heat most likely goes into the atmosphere. It could favour cyclogenesis by reducing the tropospheric static stability (the pre-conditioning mechanism).

1.4.3 Cyclone predictability

FASTEX is also motivated by the practical forecast problem continuously posed by these cyclones. Part of the answer is to obtain, as a result of the dynamical objectives, a new set of theoretically and observationally validated conceptual models. These will point out the key properties of the flow to observe and analyze properly.

There is another approach, though, that is complementary to the previous one. Indeed, it may not be enough to get the generating mechanisms right to obtain a good forecast. It is also necessary to keep the error level in other parts of the flow

Short Note 1.6:
Cyclogenesis as a finite amplitude interaction between pre-organized structures

by A. Joly after B.J. Hoskins, A.J. Thorpe and C. Bishop

Figure SN1.6.1: *Schematic representation of a developing weather system within a simple baroclinic zone. The tube is the jet-stream, blue arrows show the wind associated with the forming cyclone. The large arrows stand for the vertical motion, the ascending part of which yields precipitation.*

Another important theoretical model of cyclogenesis that has taken much more flesh in recent years is related to properties and concepts associated to the *potential vorticity* field. Potential vorticity has been introduced by Rossby (1940) and Ertel (1942) as a conserved variable representative of vorticity, very much like potential temperature is the conserved version of temperature. The perspective summarized in this note, however, stems from original ideas from Kleinschmidt (1950). The existence of detailed consistent global analyses and the development of powerful numerical techniques have led Hoskins, McIntyre and Robertson (1985) to revisit the various properties of potential vorticity.

They outline an "explanatory" framework that can handle the finite amplitude characteristics that seem to be present in most cyclogenesis events(see Short Note 1.5 for observation-based cyclone types). This framework is derived from the existence of an overall balance between the wind field on one hand and the thermal field on the other. As a result, the usual state parameters of the atmosphere are not independent: the distribution of potential vorticity and boundary conditions contain all the information needed to describe the balanced part of the flow. The process of recovering wind and temperature from potential vorticity is called potential vorticity inversion.

A further step is needed to build cause and effects relationships that can be used to express *and check* an understanding of a given cyclogenesis: it is called *attribution*. The potential vorticity field and related boundary conditions are not uniform: they can be viewed as the superposition of a background, reference component and of a number of *anomalies*. Although close to the framework of linear the-

ory, the linear assumption is not required here. That part of the flow that results from inverting a given anomaly (coupled wind and temperature anomalies) can be attributed to this anomaly. This is very much like decomposing an electric field into the sum of individual fields, each of them resulting from given, local electric charges: the charges are replaced, here, by a potential vorticity anomalies. The classical and powerful idea of action at a distance, often employed in physics, can then be adapted, in a proper way, to understanding a weather situation (Bishop and Thorpe, 1994, Thorpe and Bishop, 1995).

Figure SN1.6.1 shows an idealized developing system. At first sight, there is a single feature, the developing cyclone, with its many aspects, namely wind, clouds, temperature changes. It is possible to understand how this system works by decomposing it into three components (Fig. SN1.6.2), a baroclinic background and two anomalies that can be summarized by their potential vorticity signature, their "charge". The vertical motion that generates the clouds but is also responsible for converting the energy that accompanies the development results from the interactions between these component. The idea here is that each elementary components threatens the balance of the other structures and the vertical motion is the response that will maintain the overall balance.

FASTEX is to provide a series a well documented cases that can be employed as testbeds for this and other theoretical perspectives, such as the one presented in Short Note 1.3. See Short Note 2.3 for an application of inversion and attribution to find the precursor structures that have led to the development of FASTEX Low 41.
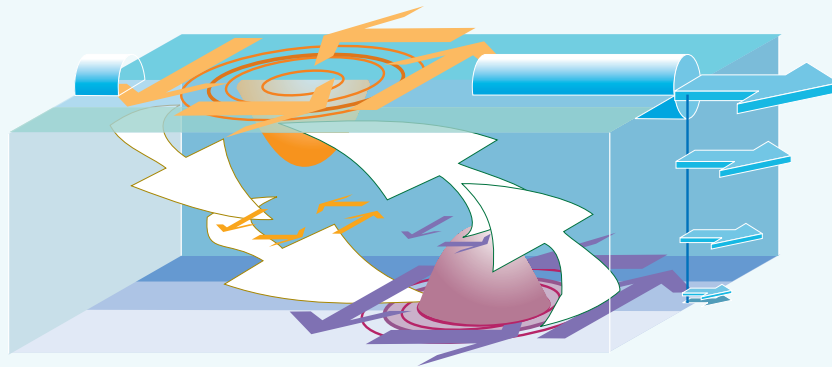
Figure SN1.6.2: *The system of Fig. SN1.6.2 can be understood as the result of the interactions between the three elementary "objects" represented by symbols with similar colours: the baroclinic zone (bluish), an upper-level anomaly (orangish) and a low level anomaly (purplish). The vertical circulation results from the interactions of two such objects at least.*

as low as possible. FASTEX cyclones may form, as has been said above, in several different ways. This also means that small initial errors in the analysis have just as many different ways to grow, sometimes very rapidly, and wreck the forecast. The predictability of cyclogenesis depends therefore on improved control of analysis and forecast error growth.

A possible practical solution is to concentrate measurements in the areas where small uncertainties may cause the greatest threat to the forecast quality. These areas, assumed to be few in numbers and relatively local in space, will obviously depend on the current flow. Hence the idea of an *adaptive observing system.*

The basic concept is to concentrate measurements on areas that are dynamically critical for a proper prediction of cyclogenesis downstream of these zones in the next 24 to 36 hours. Another key idea is that these areas should be objectively determined or predicted. At least part, and perhaps all of the anwser can indeed be provided by adjoint models. Short Note 1.8 illustrates the principle of targeting in the idealized framework of observing system simulations of Short Note 1.7.

FASTEX is designed to allow the first full scale test of one or several adaptive observation strategies. This relates FASTEX to the US Weather Research Program. A more detailed discussion of this new approach to observation can be found in Snyder (1996) or Bergot et al. (1999). See Short Note 2.4 for some results.

1.4.4 Dynamics of wave cyclones

The recent theoretical results presented above (subsection 1.2.1, Short Note 1.3, Short Note 1.6), supported by new case studies (*e.g.* Rivals *et al.*, 1996), suggest that new important issues are:

• the appearance or creation of a new cyclone at low level involves a variety of mechanisms while its subsequent development, that may or may not happen, involve one and only one such mechanism, a form of baroclinic interaction with the

Table 1.1: *FASTEX Scientific Steering Group*

A.J. Thorpe, chairperson	Univ. of Reading (UK)	R. Langland	NRL (USA)
P. Bessemoulin	Météo-France (F)	Y. Lemaître	CETP (F)
K.A. Browning	Univ. of Reading (UK)	A. Lorenc	UKMO (UK)
D. Cadet, CSG chair (93–96)	CNRS (F)	P. Lynch	Met Éireann (IRL)
J.P. Cammas	Labo. d'Aérologie (F)	B. Martner	NOAA (USA)
J.P. Chalon, CSG chair (96–)	Météo-France (F)	P. Mascart	Labo. d'Aérologie (F)
S.A. Clough	UKMO (UK)	S. Nelson	NSF (USA)
Ph. Courtier	CNES (F)	T.E. Nordeng	DNMI (N)
P. Dubreuil	AES (CA)	H. Olafsson	VI (ICL)
K.A. Emanuel	MIT (USA)	J. Pailleux	WMO/COSNA
L. Eymard	CETP (F)	P.O.G. Persson	NOAA (USA)
C. Fairall	NOAA (USA)	J. Rasmussen	NOAA (USA)
R. Gall	NCAR (USA)	F. Roux	Labo. d'Aérologie (F)
T. Hewson	UKMO (UK)	M.A. Shapiro	NOAA (USA)
P. Hildebrand	NCAR (USA)	C. Snyder	NCAR (USA)
P.V. Hobbs	Univ. of Washington (USA)	A. Staniforth	AES (CA)
A. Joly	Météo-France (F)	G. Stephens	NASA (USA)
D. Jorgensen	NOAA (USA)	R. Stewart	AES (CA)
T. Johannesson	VI (ICL)	J. Testud	CETP (F)
K. Katsaros	IFREMER (F)	C. Velden	Univ. of Wisconsin (USA)
D. Keyser	SUNY (USA)	R. Wakimoto	UCLA (USA)

upper-levels, and these two steps may be separated by a few days of quasi-neutral behaviour,

• the creation mechanisms include the presence of an unstable quasi-steady environment (in the sense of Charney and Stern, 1962) or the triggering of the same conversion mechanisms as in the instability theory by a pre-existing, quasi-passive structure in an environment that then does not need to be unstable or also the active participation of the environmental flow, through, for example, its induced deformation field,

• the development mechanism, the baroclinic interaction, primarily result from upper-level incoming, independent vorticies rather than from the upscale growth of the new, low level cyclone generating its own upper-level component: this results from the small initial scale of the new wave. A consequence is that a cyclone can go through several stages of baroclinic development with transient upper-level coupling.

In order to address these issues, thermal and dynamical observations have to be collected when a low level cyclone forms, possibly prior to this on occasion as well as when it develops or reaches its mature stage. Also, not only the cyclone should be measured, but a fair portion of its environment as well.

1.4.5   Other objectives

A further objective of FASTEX is Data Assimilation. A reference analysis is planned as part of the project, beyond the one already provided in the Data Base (see Parts 4 and 8). It will be a test the ability of the variational approach (in 4D mode) to use concentrated arrays of dropsondes.

Once this is achieved, it will be possible, through observing system experiments, to determine the data requirements in terms of precision and resolution that are needed

to properly reconstruct the structure and evolution of synoptic and sub-synoptic cyclones. The importance of a good knowledge of the distribution of water vapour and of condensed water will be studied as well as the ability of satellite data to replace or not in-situ data.

This broad set of objectives has been constructed and will be studied by the scientists meeting in the FASTEX Scientific Steering Group shown by Table 1.1. Figure 1.7 shows how the FASTEX project has been organized to prepare and implement these ideas and the plans described below, while Table 1.2 shows the institutions and agencies supporting FASTEX.
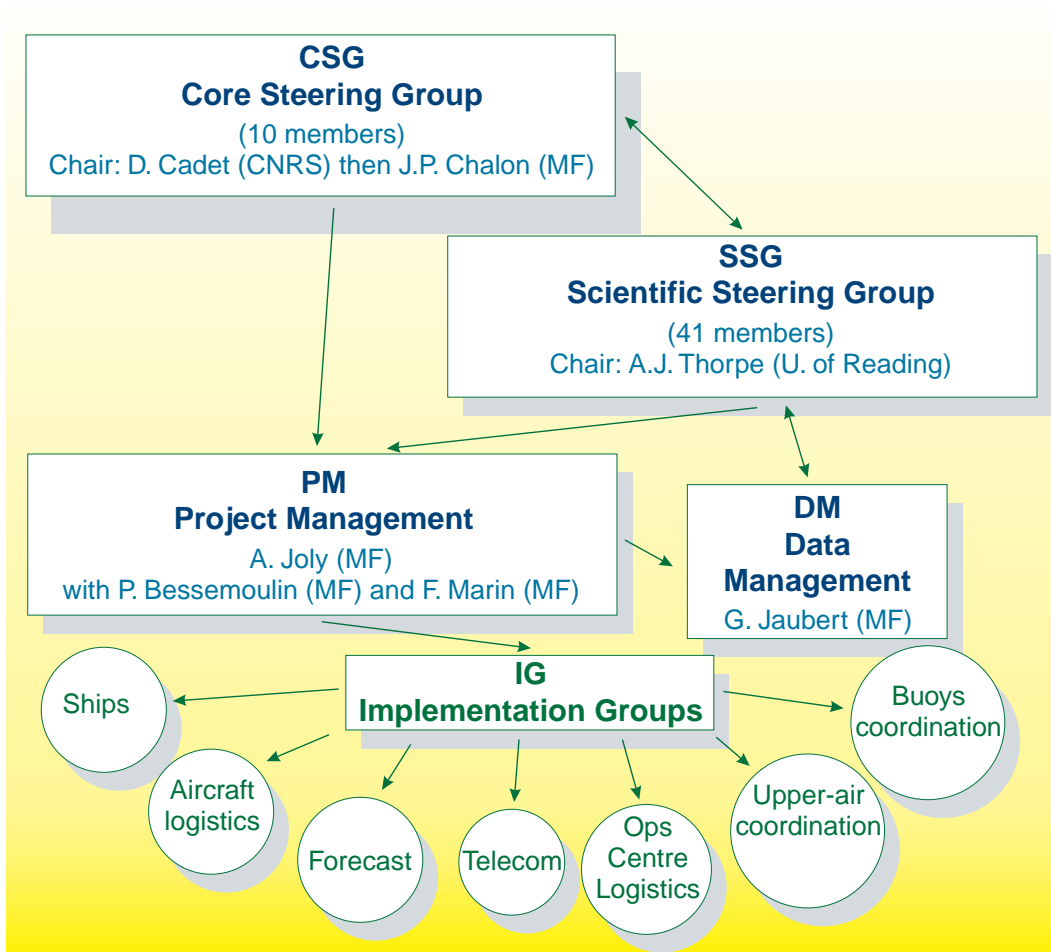
Figure 1.7: *A short schematic overview of the project organization. Decisions are ultimately taken by the Core Steering Group, where representatives of the funding agencies meet representatives of the scientists. The participating agencies are listed in Table 1.2. Objectives and plans where drafted and discussed by the Scientific Steering Group, which had a number of sub-planning groups not shown here. The work of the SSG is best illustrated by the FASTEX Operations Plans document, edited by D. Jorgensen from NOAA. These plans and decisions are implemented by the Project Management and the Implementation Groups.*

Table 1.2: *Organizations supporting FASTEX*

Support of the use of large facilities	
CNRS/INSU	France
European Commission	
Météo-France	France
NOAA	USA
NRL, ONR	USA
National Science Foundation	USA
UK Meteorological Office	UK
Other sources of support	
Atmospheric Environment Service	Canada
Danish Meteorological Institute	Denmark
EGOS	
Icelandic Met. Service	Iceland
Joint Centre for Meso. Met.	UK
Met Éireann	Ireland
NCAR/MMM	USA
WMO/COSNA	

1.5   Specific objectives of the field phase

Essential components of these objectives are difficult to address with existing datasets. The key to FASTEX as a field project is contained in the idea that the evolution of cylones is likely to be more complex than the continuous growth of some kind of instability followed by a non-linear saturation process. This statement immediately leads to the requirement that entire *life-cycles* have to be documented. Most if not all past field projects dealing with mid-latitude cyclones have actually observed weather systems at one stage. The resulting studies are directed towards the structures of these systems. Important (and not so recent) ideas on cyclogenesis involve the existence of precursor systems and the possibility of transient interactions between such systems or other flow organizations such as fronts. In order to check these ideas on real cases as directly as possible, cyclones have to be tracked across the ocean throughout their life-history.

It follows that the primary experimental objective of the field phase of FASTEX is to perform numerous direct observations of the structure of the *same* cyclones at several key stages of their life-cycle. The data should, ideally, take the form of precise vertical profiles of the key dynamical quantities (wind, temperature, humidity) covering the whole depth of the troposphere and the lower stratosphere.

Another goal of the field phase is to perform the first real-time implementation of an adaptive observing system for reducing forecast errors for selected cyclones. This requirement is *a priori* quite independent from the one of adapting the observing system in order to capture the growth of an actual cyclone. Since forecast-error control involves the use of well defined numerical algorithms in order to determine the key areas, the FASTEX scientists tended to call this component of FASTEX "objective targeting". The task of observing different stages in the cyclone life-cycle, on the other hand, depends on reading synoptic charts and looking at satellite images with concepts in mind, and in this case the method of selecting critical features was commonly referred to as "subjective targeting". The numerical products needed for "objective targeting" were exploited in two different places: the NCEP products were analysed in Washington (USA) while the NRL, Météo-France and ECMWF products were interpreted in Shannon. Coordination was made possible by the presence of a

representative of the Washington group at Shannon, Dr. Snyder. See e.g. Bishop and Toth (1998), Gelaro *et al.* (1999), Bergot *et al.* (1999), Langland *et al.* (1999) or Buizza and Montani (1999) for more details.

The primary objective concerning the organisation of mature cyclones was to describe their three-dimensional precipitation and wind structure over a 1000 by 1000 km domain using a combination of dropsondes and airborne Doppler radar. These sensors were deployed in a manner that systematically covered as much of the cyclone with a regular grid of data assimilation and validation of numerical simulations.

Finally, another objective deriving directly from the scientific objectives mentioned previously is to document turbulent fluxes in high winds in mid-ocean.

Figure 1.8: *The observing system planned for FASTEX. The special facilities are explicitly listed in the schematic as well as in Table 1.3. The "environment" of the cyclogenesis area is monitored by an increase of upper-air measurements: this increase is indicated by the color code of radiosonde-like symbols: yellow, 6 h on alert; orange, 6 h all the time; red, 3 h on alert.*
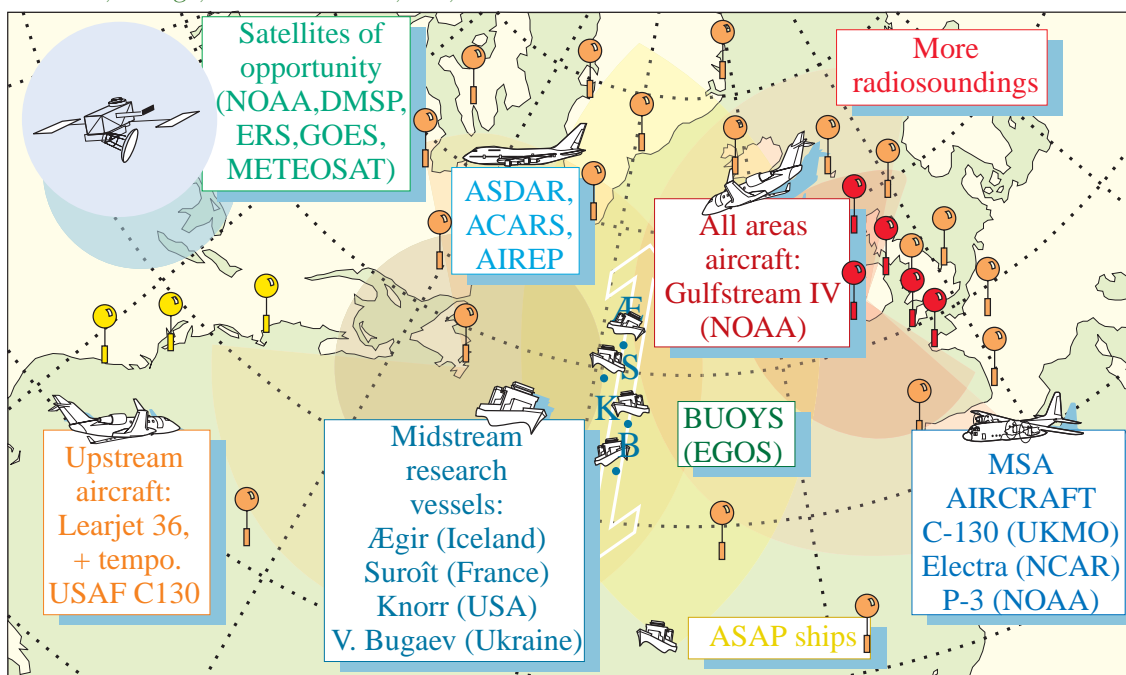
1.6 Observing strategy and platforms

In order to achieve the primary experimental objective of FASTEX, namely to follow a number of cyclones throughout their life-cycle, a special distribution of observing facilities had to be devised. The North-Atlantic area has been divided into three adjacent areas: the "Far Upstream Area", centered on the airport of St John's in Newfoundland, the mid-stream area, centered about the longitute 35°W and the Multiscale Sampling Area (often termed MSA). The Multiscale Sampling Area was focused on Shannon airport in Ireland (Fig. 1.6).

The purpose of enhancing observations in the Far Upstream Area is to observe the early stages of the formation of a new cyclone, possibly its genesis. The Far Upstream

Table 1.3: *Major facilities and participating institutions*

Facility	instruments, functions	owner, crew's home institution	Funding agency
CC ÆGIR	radiosoundings	Icelandic Coast Guard (IS)	EC
RV KNORR	radiosoundings, profilers, fluxes	Woods Hole (USA)	NOAA
RV LE SUROÎT	radiosoundings, profilers, fluxes	IFREMER (F)	CNRS, EC
RV V. BUGAEV	radiosoundings	UkrSCES (Ukraine)	Météo-France
C-130 (UK)	dropsoundings	UK Met Office	UK Met Office
C-130 (USA)	dropsoundings	US Air Force	US Air Force
ELECTRA	Doppler radar	NCAR (USA)	CNRS, NSF
GULFSTREAM-IV	dropsoundings	NOAA (USA)	NOAA, Météo-France, CNRS, NRL
LEARJET	dropsoundings	FIC (USA)	NSF
WP-3D (P3)	radars (1 Doppler), dropsoundings	NOAA(USA)	NOAA, CNRS, Météo-France
Increased soundings on a regular basis	6h soundings	CAN, Greenland, IS, IE, UK, F, SP, Azores (P), Bermuda, DK	Countries, WMO, EC
Increased soundings on alert	6h soundings 3h soundings	USA IE, F, UK	NCAR, NOAA Countries
Buoys	surface obs.	EGOS	EGOS
Operations Centre at Shannon	monitoring, forecast	Aer Rianta (IE)	EC
Staff of Shannon Ops Centre and Scientific crews	forecasters, scientists	CNRS(F), CMC(CAN), JCMM(UK), Met Eireann(IE), Météo-France(F), NCAR(USA), NOAA(USA), NRL(USA), UCAR(USA), UCLA(USA), UK Met Office(UK)	Institutions, NSF, EC
Staff of US targeting operations	forecasters, scientists	MIT(USA), NCEP(USA), NCAR(USA), Penn State U.(USA), U. of Wisconsin(USA)	NOAA, NSF
Agencies without direct participation:	European Commission (EC), European Group on Ocean Station (EGOS), National Science Foundation (USA), World Meteorological Organisation (WMO).		
see Appendix A for other acronyms.			
Selected Country Codes:	CAN: Canada, DK: Denmark, F: France, IE: Ireland, IS: Iceland, P: Portugal, SP:Spain.		

Area is also the primary area for collecting the observations for the predictability (targeting) objectives.

The purpose of enhancing observations in the midstream area is to fill, as well as possible, the well known "data void" in the middle of the oceanic basin. It is located at the end of the most persistent (or least variable) part of the storm-track, a very good place to catch the developing phase of many cyclones. More to the west, they are still forming with a small amplitude. More to the east, it may be difficult to cope with the large low-frequency variability that causes big changes in the location of the storm-track. It is also a good location for frequent encounts of the strong winds and high seas required for the measurements of air-sea fluxes, as well as for making oceanographic observations: it coinicides with the eastern part of the zone where the Gulf Stream current splits into several "drifts".

Finally, the Multiscale Sampling Area is where the mature cyclones and their cloud system are to be observed with, as the name suggests, the possibility to collect data on their structure at several different scales. How this is achieved is told in Section 1.7.

Table 1.3 and Figure 1.8 summarizes the observing platforms and instruments available for FASTEX. It also provides the list of institutes, agencies and organizations that have supported the project. A much more detailed table can be found in Joly *et al.* (1997). The present table has been updated with the actual facilities available.

Figure 1.9 shows how these platforms should have been employed, under ideal circumstances, in the course of a FASTEX Intensive Observations Period (IOP). The first thing to note is the long duration of an IOP: activities related to an individual cyclone event occur over 48h to 60h. A lead time of 30h to 42h is needed, for logistical reasons, to analyse the situation and to plan the activities. The "constitutive" decision to launch an IOP has to be taken, therefore, on the basis of 84h or 96h forecast products. It depends on the strong expectation of a significant cyclone moving into the Multiscale Sampling Area: the estimated time for this to happen sets the reference date, denoted 0h in Fig. 1.5. This decision-taking problem can be called the "FASTEX dilemma": FASTEX is motivated by the difficulty of making reliable cyclogenesis forecasts at practically any range but for FASTEX to collect the data required to understand this problem, reliable medium-range forecasts are required. One practical step that was taken to help solve what was, indeed, the main difficulty of the operation was to transmit in real time via the Global Telecommunication System as many extra observations as possible so as to improve the performance of the operational numerical weather prediction systems. Several forecast centres made the necessary changes for this data to be included in their assimilation suite.

The diagram in Fig. 1.9 also shows the main facilities and the way they were employed in FASTEX. The scenario for an ideal IOP are exposed in the Short Note 1.9. The first thing to note is a significant uplift with respect to the background observations made from the conventional World Weather Watch upper-air stations: from Canada to Bermuda, including Greenland, Iceland, the Faroes, Ireland, the Azores and the European west coast, about 30 stations performed 6-hourly soundings during the whole two months of the FASTEX field phase. A number of commercial ships equipped for launching sondes more or less automatically also contributed to this improvement. The USA similarly re-inforced 4 of their stations but on an alert basis. Furthermore, the number of drifting buoys in the Central Atlantic has also been significantly increased. In these ways, practically *all* cyclogenesis events that took place within the two months are better documented than usual.

Short Note 1.7:
Simulating FASTEX on the computer

by C. Fischer and A. Joly

The most original component of the observing system proposed for FASTEX is the midstream one (Fig. 1.6): it consists of vertical profiles from the low stratosphere to the surface in the middle of the North Atlantic ocean, where only a few ships and occasional aircraft data provide some coverage at one or the other level, and low resolution remote sensing. This midstream part is, furthermore, essential to all FASTEX objectives. This is obvious for the documentation of life-cycles. The midstream data is to provide also well defined western boundary conditions to the studies on the mature system, a reliable information on a significant part of their input budget.
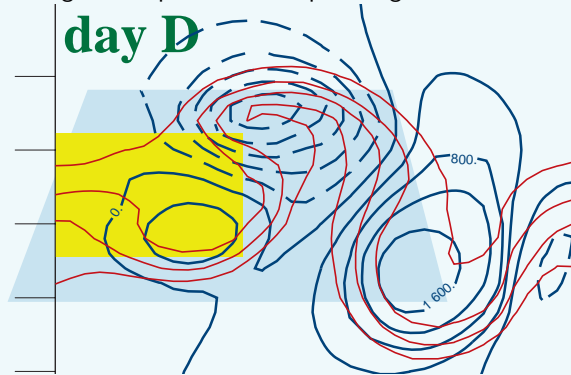
Figure SN1.7.1: *The generic, idealized situation employed in the simulations of upstream observing system for FASTEX: a large scale baroclinic storm that generates a front over the "Atlantic" area (blue shaded zone), where cyclones may or may not develop. A period of two days, shown here, has been employed. Top: initial conditions and upstream area (green-yellow shading). Bottom: solution 2 days later. The shaded boxes are the verification areas. Dark-red lines: surface potential temperature, interval 4K. This field will be used as the reference background in subsequent figures. Blue lines: surface geopotential, negative values dashed. Interval: 400 J/kg.*
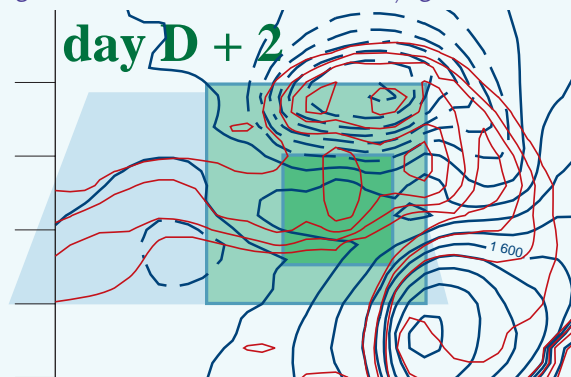
How to turn the idea of in-situ observations midstream into something real ? One possibility is to dedicate one aircraft

at least to quasi-regular missions, for example 1 or 2 days ahead of a system of interest reaching Europe. This aircraft would cross the main baroclinic zone meridionally, providing a detailed, north-south vertical cross-section: this is the solution proposed in the earliest project documents, with the possibility of using remotely controlled aircraft. Another possibility is to station ships in the area. This is costly and, given that most cyclones travel through this zone while developing, it can also be dangerous. There are also questions relating to the location of these ships and their possible displacements. In order to ground the decisions on a minimum of scientific basis, it was decided quite early to try to address these questions through computer simulations.
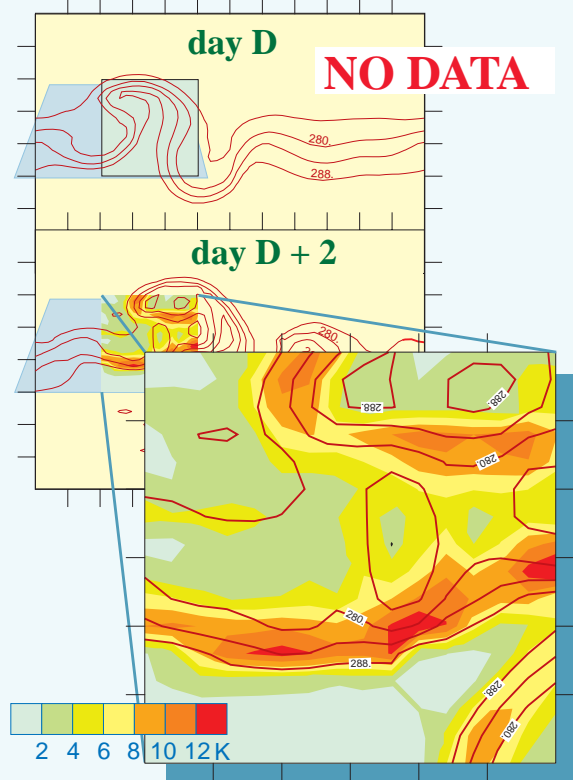
Figure SN1.7.2: *The various possible observing systems are evaluated through their impact on the uncertainty, represented here by the variance of forecast error of the surface potential temperature (shading), not on the solution itself, which is not changed. Results are compared to the variance generated in the absence of data, shown on the present figure. The initial variance (top) is uniform. After 2 days (bottom and blow up), as shown in Short Note 1.4, the variance is a complex function of space, with several maxima of large uncertainty along the frontal areas.*

The approach chosen is to study the behaviour of the *second order* moments, representing the statistics of forecast error, rather than gathering a collection of "typical" cases and to influence the solution itself. There are too many possible transitions, as the climatology of cyclones indicate. It is hoped that the dynamics of the variance and covariance embodies all the possible sources of cyclogenesis. This is strictly correct only as far as the evolution is linear. A single non-linear trajectory has been, therefore, employed. Figure SN1.7.1 shows its main features as well as the relevant domains. This trajectory is the final phase of growth of a large scale cyclone. It sets up a cold front in its wake out of which waves may develop.

The mechanism from which waves could grow generate variance, that is uncertainty in the forecast, as explained in Short Note 1.4. Figure SN1.7.2 gives the maximum variance generation assuming a small uniform uncertainty at the beginning of the period of interest: it is a pure dynamical evolution of the initial variance/covariance matrix.

This is an idealized context simulated with a simplified model that allows for explicit calculation of the evolution of the full error statistics matrix. The impact of observations is studied only through their effect on the variance: a piece of data reduces the variance where it has been taken and around it, the projection being made essentially according to the local covariance function between the data point and its neighbours. This area of reduced variance is then propagated or advected by the flow and influenced by the sources of variance in the course of time (see Fig. SN1.4.3 for an example of evolution). The impact is judged after 2 days. The time evolution and assimilation are performed together, following a Kalman filter algorithm (Fischer et al., 1998).

Figure SN1.7.3 illustrates two configurations of the observing system. One represents the "ships" solution: a regular and constant source of data at fixed locations. Provided the ships are within the baroclinic area, this turned out to be the best solution tested. The best that can be obtained from aircraft, employed in the spirit of "adaptive observation" explained in Short Note 1.8 is also shown. The initial idea of making a straight cross-section, based on common sense, has been ruled out by this study: it has a weak impact only. Similarly, these simple experiments have shown that ships away from the baroclinic area are useless. For this reason, it is important that the ship keep with the (slow) meridional displacements of the jet-stream.

These experiments are representative of what current assimilation systems can do (3D-VAR and non-cycling, short period 4D-VAR), starting with isotropic covariance functions. Since assimilating tools of that kind were to be employed during FASTEX and for some time afterwards, the experiments led us to insist on having ships involved.

But the Kalman filter developed for this study allows for a little anticipation on future evolution, as shown in Short Note 1.8.
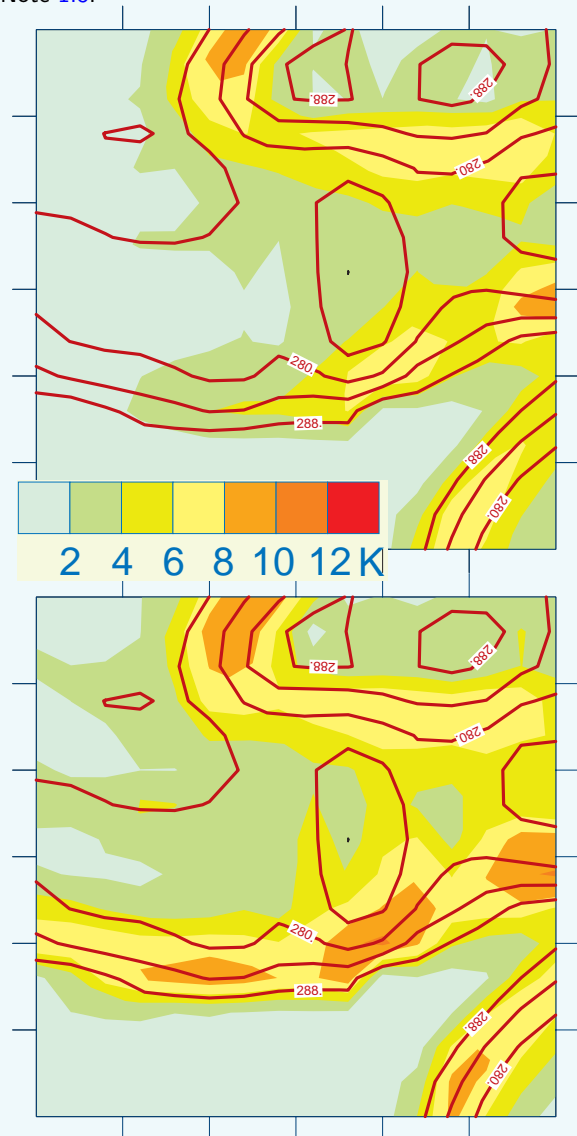
Figure SN1.7.3: *Two examples of impact of simulated observing system on the variance of forecast error of surface potential temperature. Top panel: impact of two fixed sources sending new data continuously every 6 h ("ships"). The ships are in the middle of the surface baroclinic zone and upper-level baroclinic zone respectively, and this is very important. Bottom panel: impact of multiple sources upstream assimilated during the first 6h only, using isotropic covariances ("aircraft dropsondes").*

Short Note 1.8:
The principle of adaptive observation and its potential

by C. Fischer and A. Joly
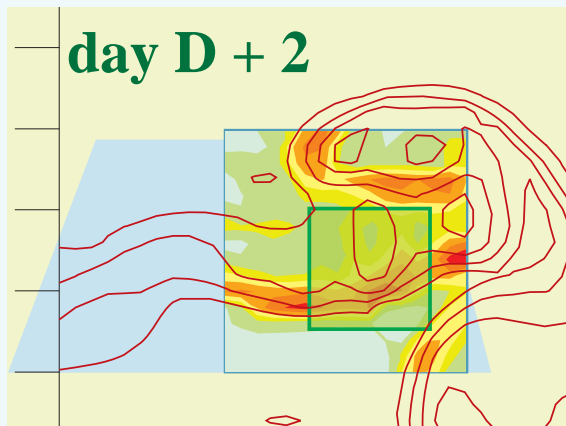
Figure SN1.8.1: *Assume that this is time $D - 1$ or $D - 2$. Adaptive observation addresses the following question: given a forecast to time $D + 2$, where to put observations at time D in order to minimize the growth of uncertainty within a selected area between D and $D + 2$? The top panel shows the expected uncertainty that will result from the growth of a cyclone over the Atlantic in the absence of data (see Short Notes 1.7 and 1.4). The area where the uncertainty must be minimized is shown by the green square. One possible answer is to compute in advance the singular vectors that will generate the most variance between D and $D + 2$ on the verification domain. Observing facilities can then be directed (adapted) towards the critical area pointed out in this way and sample the flow there. The bottom panel shows the structure of the most unstable of these singular vectors. The field shown is the temperature anomaly at the surface (red and dark blue shading) and at the model top (tropopause, light blue and orange shading). Blueish dashed contours are for negative values, the amplitude is arbitrary. The dark-red contours on both panels are the background, large scale cyclone used as the reference solution. The arrows show the track of a simulated flight sampling this structure at time D.*
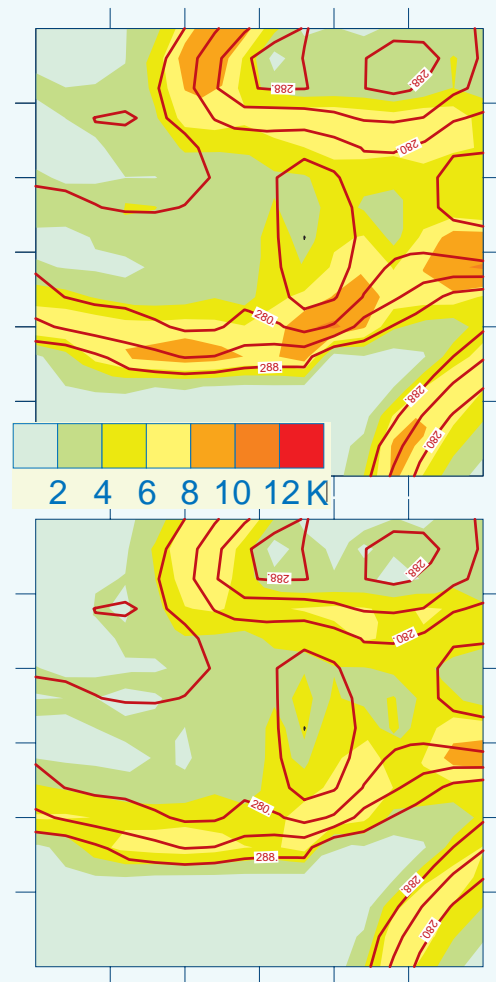
Figure SN1.8.2: *Assuming that the singular vector shown on Fig. SN1.8.1 has been properly sampled with good-quality, in-situ data, the study of Fischer et al. (1998) indicates that the actual impact of this data on the forecast uncertainty strongly depends on the assimilation technique employed once the data has been gathered. The top panel shows the impact of that data on the forecast error variance two days after the adaptive observation flight assuming a 3D-VAR-like system (isotropic covariance functions). It is the best use of an aircraft-like observing facility, but the impact is weaker than that of ships. The bottom panel shows the impact of the same data when flow dependent covariances are used, as cycling or long-period 4D-VAR system will have. In this case, even though no data is added after the "adaptive flight", the result is better than with ships constantly pouring information in. It appears possible that, providing the observation and assimilation problems are handled together, adaptive observation does have an impressive positive impact on ascertaining weather forecast.*

Operations in the Upstream Area were conducted with aircraft: a Learjet and, for some time, two C-130s, all three equipped for GPS dropsounding. The backbone facilities in the Midstream area were instrumented ships. Up to four ships with GPS radiosounding capabilities were available. Two of them also had a profiler radar and instruments developed for flux measurements. One also had a cloud radar. In the Multiscale Sampling Area, the platforms were a C-130, used primarily to drop sondes, and two other turboprop aircraft with airborne Doppler radars (see Section 1.7). The three aircraft were also able to perform *in situ* microphysical measurements and carried a number of remote-sensing instruments.

Finally, all three areas could be re-inforced with dropsoundings from a long-range, high-flying Gulfstream IV jet recently purchased by NOAA. In the course of the project, it was found that an efficient way of employing the Gulfstream was to send it from Shannon to St John's slightly in advance of a cyclone forming, by a relatively direct route and doing few measurements only. In a second flight from St John's, the Gulfstream added its capabilities to those of the Lear or C-130 in the Far Upstream zone. Then a day or so later, on the return flight to Shannon, it collected measurements in the midstream area or between the ships and the Multiscale Sampling Area.

Early in the planning of FASTEX, it was realised that the ships, in order to be useful all the time, would have to remain in the vicinity of the main baroclinic zone. The effectiveness of this approach was demonstrated in an idealized observing system simulation experiment (Fischer *et al.*, 1998, see Short Note 1.7). The idea of having ships moving with a weather feature in the middle of the ocean generated many comments from reviewers of the project. The idea, however, was simply to compensate for the relatively slow meridional motions resulting from the low frequency evolution of the flow, not to track the cyclone themselves. Indeed the longitude of the ships was chosen to help ensure that these motions were of reasonable amplitude. Practical experience during FASTEX revealed that the idea was quite feasible: the predictability on this scale was good enough and the resulting displacements manageable in spite of difficult seas.

1.7   Observations of mature cyclones

It is worth going into finner details in the plans for sampling the mature cloud systems. Three long-range turboprop aircraft were to operate in the Multiscale Sampling Area and collect the data needed in order to complete the dynamical objectives and to study the various aspects related to the cloud system. By decreasing order of range, these aircraft are the C-130 owned by the UK Meteorological Office (11 h endurance), one of the P3 operated by NOAA (9 h) and the Electra belonging to NCAR (7 h).

The C-130, as the two others, is very well equipped for all kinds of in-situ measurements, including microphysics and turbulence. However, it has been employed in FASTEX primarily to drop arrays of GPS sondes developed by VAISALA. The key instruments on the P3 are its lower-fuselage C-band radar, a scatterometer and several radiometers as well as a tail X-band Doppler radar, including a dual beam option. On the Electra, the main instrument is the ASTRAIA/ELDORA X-band dual beam Doppler radar. It has been developed jointly by NCAR/RSF and by the CNRS-CETP group in France.

The sonde deployment strategy for the C-130 is such as to obtain regularly spaced vertical profiles relative to the whole wave cyclone, from front to rear (with respect
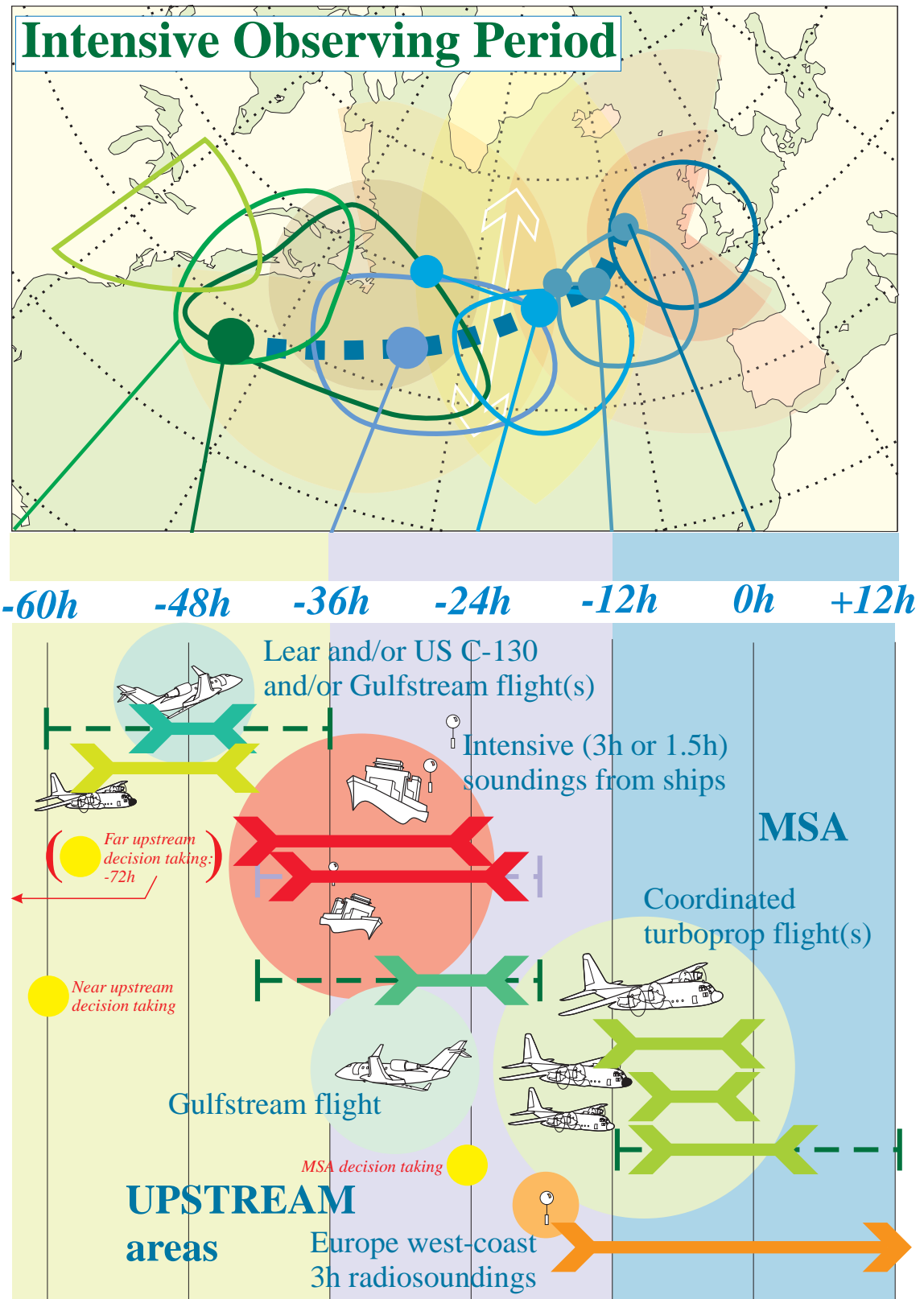
Figure 1.9: *Timelines and locations of the events composing a FASTEX IOP. The heavy arrows are proportional to the time of the flights (solid), the period of intensive soundings from ships (dash-dotted), the period of 3-hourly soundings from the UK, Ireland and France (dashed). Note the lapse of time taken into account between the cyclogenesis timeline and the Universal Time clock that determines some of the activities (the upstream flights, for example). The important decisions may have to be taken 12 h earlier than shown when they imply a shift from day to night actions.*

to cyclone motion). Sondes were to be dropped from heights varying from 6 to 8 km, depending on aircraft weight and air traffic constraints. In winter, this should just enable to catch the tropopause in the dry slot in the rear part. Because, by definition, the radar aircraft will not be able to collect significant data in this dynamically very interesting part of the cyclone, it will be important that the C-130 reaches this part relatively rapidly and samples it properly. For a large system, it may exceptionally share this task with the Gulfstream-IV. This strategy will be applied to all systems

Short Note 1.9:
Prototype IOP scenario

by A. Joly

The first characteristic of a FASTEX Intensive Observing Period is its duration. Facilities will be activated in turn during two to three days. Then, some warning lead time must be added to this. Given the very reason that led to set-up FASTEX (the uncertainties of west coast cyclone forecasting in the 36h–96h range), one can immediately see the importance of forecast experience, of the diversity of forecast products as well as the difficulty of the early decisions.

The second characteristic of FASTEX IOPs is that a new one is likely to begin while the previous one is fully buoying up. This is a direct consequence of the rapid chaining of events that is apparent in Fig. 1.4. This actually happened in several occasions during FASTEX: see the dates in Part 3.

The event that decides of the startup of an IOP is the extreme likeliness that a mature cyclone will go through the Multiscale Sampling Area 3 to 3.5 days after. We call the time when the cylones reaches the MSA $D0$. The extra 12 h are needed when there is a shift from flights to be conducted during the day to flights during the night. Note that the management of the ships (that are shared with other programmes) requires that their locations are changed depending on the 5-days evolution.

A summary of the sequence of events is then as follows (Fig. 1.9):

- $D - 3.5–D - 3$: Draft IOP schedule, tracking the various structures likely to be involved in the cyclogenesis. Start running the algorithms finding the locations for adaptive observations. A 24 h notice for a $D - 2$ upstream flight may be issued. Some of the ships location may be adjusted so that they can take part to the IOP.
- $D - 2.5–D - 2$: Updated IOP schedule. Notices to ship crews taking part to the IOP are issued, as well as to aircraft crews for a near upstream flight. Final targets for objective flights are determined enterely from a forecast (typically, a 60 h forecast of the mature cyclone, with the target location being itself a 24 h or 36 h forecast.)

Far upstream flights dealing with low level features could already happen at that stage.

- $D - 1.5–D - 1$: Upstream IOP. Intensive soundings from ships and upstream flights take place. The flights are monitored and may therefore be adjusted in real time (provided a satellite communication link is available). At the same time, the planning for the MSA IOP enters a critical stage: the air space booking NOTAM is issued, the crews are alerted. The ground radiosounding stations involved in the IOP in the UK, Ireland and France are alerted.

- $D - 0.5–D0$: Benefiting from the upstream measurements, the short-range forecast are used to prepare the final flight plans. The MSA flights begin. A number of ground radiosounding station launch sondes every 3 h.

- $D0–D+0.5$: MSA flights are executed and also monitored from the ground. The intensive radiosounding period continues. When the flights are completed, a first debriefing takes place.

There may be the possibility to extend an IOP with a further flight of the C-130 later on the same system.

A new weather system of interest may develop within 24 or 36 h of the previous one: this means that from $D - 2$ of the IOP described above onwards, the schedule of the new IOP overlaps the current ones and two series of tasks have to be conducted in parallel.
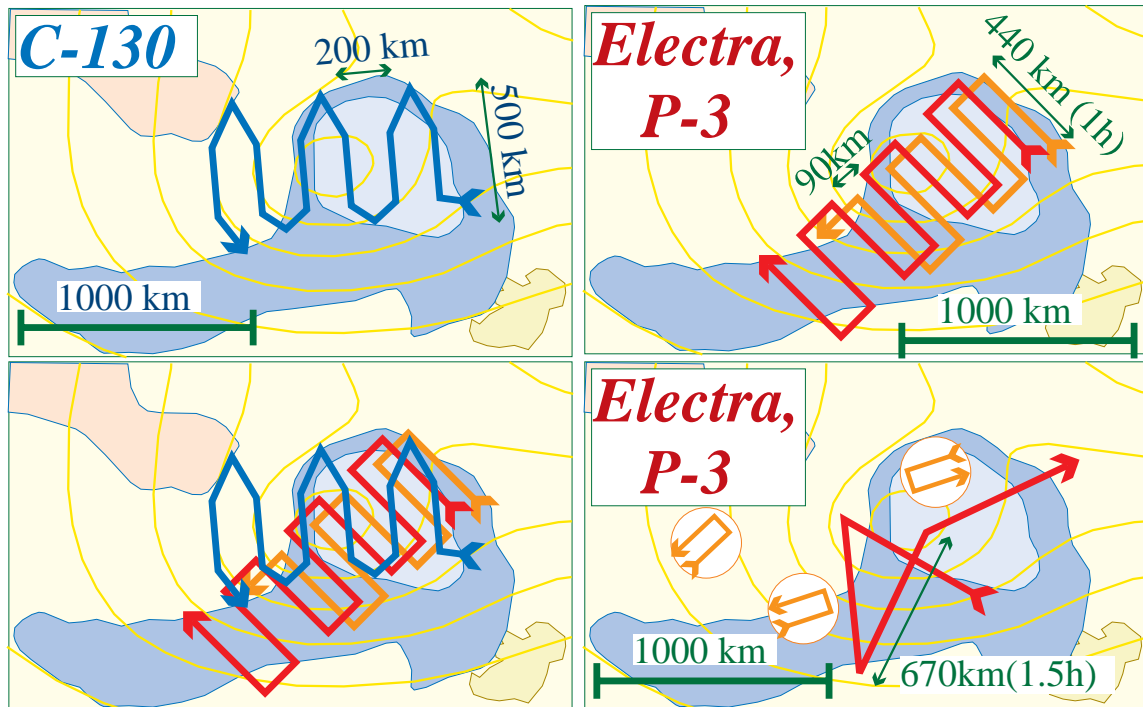
Figure 1.10: *Schematics of system-relative flight patterns to be employed by the turboprop aircraft in the MSA. The flight tracks are overlayed on the a composite structure for a second generation cyclone re-derived from automatic tracking and automatic classification of trajectories. The solid lines are surface pressure and the shaded areas are the vertical velocity at 700 mbar. The top-left panel shows the UKMO C-130 pattern going towards the clear air, low tropopause, components of the cyclone. This pattern is to be performed on all cases. Two other panels show the two main alternatives for the NCAR Electra (orange track) and NOAA P-3 (red track). The top right panel shows the so-called "lawnmower pattern" from which an overall observation of the ascent zone could be derived. The bottom right panel shows the overall exploration of the wave by the P-3 while circles mark possible areas where the Electra could performed a truly mesoscale sampling of rainbands and other structures (mesoscale investigation). The bottom left panel shows the full systematic survey pattern by overlaying the three aircraft tracks. These patterns are the result of the discussions within the MSA flight planning group. (Backround composite frontal wave: after F. Ayrault, Météo-France.)*

and will provide a cyclone-wide description of the thermal and wind fields as well as water vapour. This will be achieved by flying a series of 4 to 6 legs, about 500 km long, aiming at the dry slot following the cloud head. The sonde will be dropped about every 100 km. Relative to the system, legs should be spaced by about 100 or 200 km, depending on the scale of the cyclone.

Embedded within this systematic survey of the FASTEX cyclones that will provide a unique, multi-purpose documentation of their overall and internal structure, the Doppler aircraft were deployed according to two basic strategies. The first one reproduces, within the cloud system, the kind of systematic, regular survey proposed for the C-130. The P-3 and the Electra will fly parallel legs, so that the Doppler coverage of the two aircraft joins but does not overlap. The dual beam technique that permits recovery of the full wind vector from a single aircraft allows this new

Table 1.4: *Time table of the FASTEX project*

Dec 1991	"Proposition pour une expérience FRONTS 9x" document
Apr 1992	FRONTS 92 pilot experiment by the British JCMM
Jan 1993	The project begins at Météo-France, Research Dept
Sum 1993	The project becomes FRONTS 97, a joint CNRS and Météo-France programme
End 1993	British scientists from JCMM (Reading) join in the project and US scientists are also involved in early discussions
Feb 1994	FRONTS 97 becomes FASTEX, a new acronym for a higher level of international cooperation
Jui 1994	FASTEX Day in Bergen, presentations and discussions in order to enlarge the project group
Mar 1995	The main project groups begin their actions in Silver Spring, Maryland Emergence of the adaptative observation theme
Oct 1995	2nd plenary meetings near Oslo
Dec 1995	COAST Experiment: test of MSA-like flight plans in the Pacific Ocean
Jan 1996	Pre-FASTEX: real size simulation of the FASTEX operations centre in Toulouse and Bracknell
May 1996	3rd plenary meetings in Boulder, Colorado
Sum 1996	The Data Base development begins
Sep 1996	RMS and AMS Mesoscale Conference in Reading 4th plenary meetings
Dec 1996	Set-up and first test actions of the Operations Centre in Shannon
Jan 1997	The FASTEX field phase begins; unfavorable period
Feb 1997	Very favorable period; end of the FASTEX field phase
Mar 1997	The Data Base is opened to all scientists on the INTERNET
Nov 1997	First results submitted or published, e.g. in *Compte-Rendus de l'Académie des Sciences* (origin of Low 41, by Ph. Arbogast, see Short Note mininviop.)
Apr 1998	The first results are presented and discussed (EGS Annual Conference in Nice and FASTEX workshop in Toulouse)
Sum 1998	Most participating groups submit publications to the *Quarterly Journal* special issue.

approach. The aircraft are separated by about 100 km (the Doppler range being about 50 km on each side) and, as above, the leg length are about 500 km across the system, perpendicular to its motion. At regular interval along these legs (about every 120 km), complete 360°turns were executed, providing a kind a vertical conical scan similar to a ground-based VAD (results are shown in Part 5). This type of scanning allows for the unambiguous recovery of the terminal falling velocity of the reflecting droplets. This is an important microphysical information. It is also needed for inverting the vertical velocity of the air from the Doppler signals. This strategy is called the "lawnmower" pattern. This is a highly coordinated multi-aircraft plan. The Electra will fly at a height of 3 km, the P3 at 1.5 km.

This systematic survey allows a truly multiscale sampling of the structure of the cloud system. The end products depend on the way the signals are filtered and inverted. In the spirit of studying the overall wave dynamics, including cyclone-wide vertical motion, the overall distribution of microphysical fields, etc, a well suited technique is the MANDOP programme (Scialom and Lemaitre, 1990, Dou *et al.*, 1996). This algorithm is designed to recover the 3D wind field on a relatively large scale regular grid, as well as its main derivatives: see Part 6 for results in FASTEX. This wind field and the reflectivity can be used as input to other techniques that will provide thermodynamical and microphysical distributions. The same scans resampled in a different way can also provide information on the mesoscale substructures.

However, the mesoscale substructures and in particular, their own life cycles, could also be investigated mostly with the second flight strategy, called the "phenomena

investigation" pattern. The flights were coordinated in a different way. The P3 takes off about an hour earlier than the Electra and enters the system at the same time as the C-130 begins its survey. The P3, however, performs in the meantime an X-like pattern covering the cloud head and frontal systems within 3 to 4 hours (1 to 1.5 h per leg) and centered on the position of the minimum pressure. The idea is to derive a map of the precipitating structures present in the cyclone using the lower fuselage radar. Based on this information, the Electra is directed towards mesoscale substructures of interest. These can be cold frontal rainbands, cloud head or warm frontal rainbands or convective structures in the cold air. Rainbands can be studied in two possible ways. A front relative pattern gives an idea of along-front variability and enable to follow several rainbands, sampling them at two different times at least, as the same portion of front is covered from both sides in turn. A band-relative pattern enable the use of the highest rate sampling capabilities of ASTRAIA/ELDORA and give access to the internal structure of the band. The objectives here are to derive life-cycles of mesoscale features and frontal eveolution on the mesoscale. The retrieving techniques and the kind of results that can be obtained are shown by Wakimoto *et al.* (1992) in an explosive extreme cyclone. What is the activity on these scale in the generally much weaker FASTEX cyclones and their contribution to the overall budgets is one of the challenging questions of FASTEX.

Figure 1.10 provides an idea of these flight strategies shown on the objective composite of one type of frontal wave derived from Ayrault (1995). The P3 and the Electra will be based at Shannon (Ireland). The C-130 will be in Lyneham, in England, about 50 minutes flight away from Shannon. The entire low level airspace to be sampled by these flights will be blocked about 24 h in advance. Resources have been determined in order to allow the observation of 10 cases.

The detailed plans of operations, together with the various flight patterns to be considered for the different types of aircraft and missions, are described in the FASTEX Operations Plans (Jorgensen *et al.*, 1996). The schedule during which all these ideas were discussed and prepared is shown by Table 1.4.

1.8   References

Ayrault, F., 1995:
   Suivi automatique des tourbillons sur l'Atlantique Nord.
   D.E.A. (Masters Thesis) Université P. Sabatier, Toulouse.

Ayrault, F., 1998:
   Environnement, structure et évolution des dépres-

sions météorologiques: réalité climatologique et modèles types.
PhD thesis, Doctorat de Université P. Sabatier, Toulouse.
328pp.

Ayrault, F., F. Lalaurette, A. Joly, and C. Loo, 1995:
   North Atlantic Ultra-High Frequency variability:

an introductory survey.
Tellus, **47A**, 671–696.

Bergot, T., G. Hello, A. Joly, and S. Malardel, 1998:
Adaptive observations: a feasability study.
Mon. Wea. Rev., **127**, (5), 743–765.

Beugin, R. and M. Rochard, 1991:
L'hiver 1989–1990. Les tempêtes et quelques autres phénomènes.
Technical Report, Meteo-France, SCEM, Prévision générale et aéronautique.
184pp.

Bishop, C.H. and A.J. Thorpe, 1994a:
Frontal wave stability during moist deformation frontogenesis. part I. linear wave dynamics.
J. Atmos. Sci., **51**, (6), 852–873.

Bishop, C.H. and A.J. Thorpe, 1994b:
Frontal wave stability during moist deformation frontogenesis. part II. the suppression of non-linear wave development.
J. Atmos. Sci., **51**, (6), 874–888.

Bishop, C.H. and A.J. Thorpe, 1994c:
Potential vorticity and the electrostatics analogy : quasi-geostrophic theory.
Quart. J. Roy. Meteor. Soc., **120**, 713–731.

Bishop, C.H. and Z. Toth, 1998:
Ensemble transformation and adaptive observations.
J. Atmos. Sci., **55**, (-), *accepted*.

Bjerknes, J. and H. Solberg, 1922:
Life cycle of cyclones and the polar front theory of atmospheric circulation.
Geofys. Publikasjoner, **3**, 1.

Bjerknes, V., 1927:
Die atmospharischen storungsgleichungen.
Beitr. Phys. freien Atmos., **13**, (1), 1–14.

Blackmon, M.L., Y.H. Lee, and J.M. Wallace, 1984:
Horizontal structure of 500mbar height fluctuations with long, intermediate and short time scales.
J. Atmos. Sci., **41**, (6), 961–979.

Blackmon, M.L., J.M. Wallace, N.C. Lau, and S.L. Mullen, 1977:
An observational study of the northern hemisphere wintertime circulation.
J. Atmos. Sci., **34**, 1040–1053.

Browning, K.A., 1994:
GEWEX Cloud System Study (GCSS): science plan.
Volume 11, IGPO Publication Series.
62pp.

Browning, K.A., 1994b:
Survey of perceived priority issues in the parameterizations of cloud-related processes in gcms.
Quart. J. Roy. Meteor. Soc., **120**, 483–487.

Browning, K.A., S.A. Clough, C.S.A. Davitt, N.M. Roberts, T.D. Hewson, and P.G.W. Healey, 1995:
Observations of the mesoscale sub-structure in the cold air of a developing frontal cyclone.
Quart. J. Roy. Meteor. Soc., **121**, 1229–1254.

Browning, K.A. and N.M. Roberts, 1994:
Structure of a frontal cyclone.
Quart. J. Roy. Meteor. Soc., **120**, 1535–1557.

Buizza, R. and A. Montani, 1999:
Targeting observations using singular vectors.
Quart. J. Roy. Meteor. Soc., **125**, *submitted*.

Charney, J.G., 1947:
The dynamics of long waves in a baroclinic westerly current.
J. Meteor., **4**, 135–162.

Charney, J.G. and M.E. Stern, 1962:
On the stability of internal baroclinic jets in a rotating atmosphere.
J. Atmos. Sci., **19**, 159–162.

Clough, S.A. and J. Testud, 1988:
The FRONTS-87 Experiment and Mesoscale Frontal Dynamics Project.
WMO Bull., **37**, 276–281.

Davis, C.A. and K.E. Emanuel, 1988:
Observational evidence for the influence of surface heat fluxes on rapid marine cyclogenesis.
Mon. Wea. Rev., **116**, 2649–2659.

Dirks, R.A., J.P. Kuettner, and J.A. Moore, 1988:
Genesis of Atlantic Lows Experiment (GALE): an overview.
Bull. Amer. Meteor. Soc., **69**, 148–160.

Dou, X., G. Scialom, and Y. Lemaitre, 1996:
MANDOP analysis and airborne Doppler radar for mesoscale studies.
Quart. J. Roy. Meteor. Soc., **122**, 1231–1261.

Eady, E.T., 1949:
Long-waves and cyclone waves.
Tellus, **1**, (3), 33–52.

Ertel, H., 1942:
Ein Neuer hydrodynamischer Wirbelsatz.
Meteorologishe Zeitschrift, **59**, 271–281.

Farrell, B.F., 1984:
Modal and non-modal baroclinic waves.
J. Atmos. Sci., **41**, (4), 668–673.

Farrell, B.F., 1985:
Transient growth of damped baroclinic waves.
J. Atmos. Sci., **42**, (24), 2718–2727.

Farrell, B.F., 1988:
    Optimal excitation of neutral rossby waves.
    J. Atmos. Sci., **45**, (2), 163–172.

Farrell, B.F., 1989:
    Optimal excitation of baroclinic waves.
    J. Atmos. Sci., **46**, (9), 1193–1206.

Farrell, B.F., 1994:
    Evolution and revolution in cyclogenesis theory.
    Preprint Symposium on The Life Cycles of Extra-tropical Cyclones, , 101–110.
    Bergen, 27 June – 1 July 1994, vol.I.

Fischer, C., A. Joly, and F. Lalaurette, 1998:
    Error growth and kalman filtering within an ide-alized baroclinic flow.
    Tellus, **50A**, (5), 596–615.

Gelaro, R., R. Langland, and G.D. Rohaly, 1999:
    An assessment of the singular vector approach to targeted observing using the FASTEX data set.
    Quart. J. Roy. Meteor. Soc., **125**, *submitted*.

Gibson, J.K., P. Kallberg, S. Uppala, A. Hernandez, A. Nomura, and E. Serrano, 1997:
    ERA description.
    Technical Report, ECMWF Re-analysis report series.
    72pp.

Hadlock, R. and C.W. Kreitzberg, 1988:
    The Experiment on Rapidly Intensifying Cy-clones over the Atlantic (ERICA) field study: ob-jectives and plans.
    Bull. Amer. Meteor. Soc., **69**, (11), 1309–1320.

Hildebrand, P.H., W.C. Lee, C.A. Walther, C. Frush, M. Randall, E. Loew, R. Neitzel, R. Parsons, J. Testud, F. Baudin, and A. LeCornec, 1996:
    The ELDORA/ASTRAIA airborne Doppler weather radar: high-resolution observations from TOGA-COARE.
    Bull. Amer. Meteor. Soc., **77**, (2), 213–232.

Hoskins, B.J. and F.P. Bretherton, 1972:
    Atmospheric frontogenesis models : mathemati-cal formulation and solution.
    J. Atmos. Sci., **29**, 11–37.

Hoskins, B.J., M.E. Mc Intyre, and R.W. Robertson, 1985:
    On the use and significance of isentropic potential vorticity maps.
    Quart. J. Roy. Meteor. Soc., **111**, 877–946.

Hoskins, B.J., I.N. James, and G.H. White, 1983:
    The shape, propagation and mean-flow interac-tion of large-scale weather systems.
    J. Atmos. Sci., **40**, (7), 1595–1612.

Joly, A., 1995:
    The stability of steady fronts and the adjoint method : non-modal frontal waves.
    J. Atmos. Sci., **52**, (17), 3082–3108.

Joly, A. and A.J. Thorpe, 1990:
    Frontal instability generated by tropospheric po-tential vorticity anomalies.
    Quart. J. Roy. Meteor. Soc., **116**, 525–560.

Joly, A. and A.J. Thorpe, 1991:
    The stability of time-dependent flows: an appli-cation to fronts in developing baroclinic waves.
    J. Atmos. Sci., **48**, (1), 163–182.

Joly A. and F. Lalaurette, 1991:
    Une proposition pour une expérience FRONTS 9x.
    Internal report, Centre National de Recherches Météorologiques, Toulouse, 42pp.

Joly, A., A. Thorpe, Y. Lemaître, K. Browning, F. Lalaurette, 1994:
    FASTEX, Fronts and Atlantic Storm Tracks Ex-periment, scientific papers.
    Available from the FASTEX Project Office, febru-ary 1994, 60pp.

Jorgensen D. and A. Joly, 1995:
    FASTEX field programme, Operations overview.
    Available from the FASTEX Project Office, De-cember 1995, 55pp.

Jorgensen D., P. Bessemoulin, S. Clough and J.A. Moore, 1996:
    FASTEX Operations Plan.
    Available from the FASTEX Project Office, November 1996, 150pp.

Kleinschmidt, E., 1950:
    Über Aufbau und Enstehung von Zyklonen, I Teil.
    Met. Rundschau, **3**, 1–6.

Langland, R.H., R.L. Elsberry, and R.M. Errico, 1995:
    Evaluation of physical processes in an idealized extratropical cyclone using adjoint techniques.
    Quart. J. Roy. Meteor. Soc., **121**, 1349–1386.

Lemaître, Y. and G. Scialom, 1992:
    Three-dimensional mesoscale circulation within a convective post-frontal system. possible role of conditional symmetric instability for triggering convective motions.
    Quart. J. Roy. Meteor. Soc., **118**, 71–99.

Malardel, S., A. Joly, F. Courbet, and Ph. Courtier, 1993:
    Non-linear evolution of ordinary frontal waves in-duced by low-level potential vorticity anomalies.
    Quart. J. Roy. Meteor. Soc., **119**, 681–713.

Molteni, F., R. Buizza, T.N. Palmer, and T. Petroliagis, 1996:
The ECMWF Ensemble Prediction System: methodology and validation.
Quart. J. Roy. Meteor. Soc., **122**, 73–119.

Neiman, P.J., M.A. Shapiro, and L.S. Fedor, 1993:
The life cycle of an extratropical marine cyclone. part II: mesoscale structure and diagnostics.
Mon. Wea. Rev., **121**, 2177–2199.

Orlanski, I., 1968:
Instability of frontal waves.
J. Atmos. Sci., **25**, 178–200.

Rivals, H., J.P. Cammas, and I.A. Renfrew, 1998:
Secondary cyclogenesis: the initiation of a frontal wave observed over the eastern atlantic.
Quart. J. Roy. Meteor. Soc., **124**, 243–267.

Roebber, P.J., 1984:
Statistical analysis and updated climatology of explosive cyclones.
Mon. Wea. Rev., **112**, 1577–1589.

Rossby, C.G., 1940:
Planetary flow patterns in the atmosphere.
Quart. J. Roy. Meteor. Soc., **66**, Suppl., 68–87.

Ryan, B.F., 1996:
On the global variation of precipitating layer clouds.
Bull. Amer. Meteor. Soc., **77**, (1), 53–70.

Sanders, F. and J.R. Gyakum, 1980:
Synoptic-dynamic climatology of the "bomb".
Mon. Wea. Rev., **108**, 1589–1606.

Schär, C. and H.C. Davies, 1990:
An instability of mature cold front.
J. Atmos. Sci., **47**, (8), 929–950.

Scialom, G. and Y. Lemaître, 1990:
A new analysis for the retrieval of three-dimensional mesoscale wind fields from multiple Doppler radar.
J. Atmos. Oceanic Technol., **7**, 640–665.

Snyder, C., 1996:
Summary of an informal workshop on adaptive observations and FASTEX.
Bull. Amer. Meteor. Soc., **77**, (5), 953–961.

Stewart, R.E., 1991:
Canadian Atlantic Storms Program: progress and plans of the meteorological component.
Bull. Amer. Meteor. Soc., **72**, (3), 364–371.

Stewart, R.E., R.W. Shaw, and G.A. Isaac, 1987:
Canadian Atlantic Storms Program: the meteorological field project.
Bull. Amer. Meteor. Soc., **68**, 338–345.

Stewart, R.E., K.K. Szeto, R.R. Reinking, S.A. Clough, and S.P. Ballard, 1998:
Extra-tropical layer clouds: their nature and climatic importance.
Advances in Geophysics, **x**, (n), in press.

Sutcliffe, R.C., 1947:
A contribution to the problem of development.
Quart. J. Roy. Meteor. Soc., **73**, 370–383.

Thorncroft, C.D. and B.J. Hoskins, 1990:
Frontal cyclogenesis.
J. Atmos. Sci., **47**, (19), 2317–2336.

Thorpe, A.J. and C.H. Bishop, 1995:
Potential vorticity and the electrostatics analogy : Ertel-Rossby formulation.
Quart. J. Roy. Meteor. Soc., **121**, 1477–1495.

Thorpe A.J. and M.A. Shapiro, 1995:
FASTEX, Fronts and Atlantic Storm Tracks Experiment. The Science Plan.
Available from the FASTEX Project Office, July 1995, 25pp.

Vautard, R., 1990:
Multiple weather regimes over the north-atlantic : analysis of precursors and successors.
Mon. Wea. Rev., **118**, 2056–2081.

Vautard, R., B. Legras, and M. Déqué, 1988:
On the source of midlatitude low-frequency variability. part I: a statistical approach to persistence.
J. Atmos. Sci., **45**, (20), 2811–2843.

Vautard, R. and B. Legras, 1988:
On the source of midlatitude low-frequency variability. part II: nonlinear equilibration of weather regimes.
J. Atmos. Sci., **45**, (20), 2845–2867.

Wakimoto, R.M., W. Blier, and C. Liu, 1992:
The frontal structure of an explosive oceanic cyclone: airborne radar observations of ERICA IOP 4.
Mon. Wea. Rev., **120**, 1135–1155.

Part 2

The field experiment operations

by

Alain Joly[*], Keith A. Browning[**],
Pierre Bessemoulin[*], Jean-Pierre Cammas[•],
Yvon Lemaître[•], Dave Jorgensen[⋆],
Jean-Pierre Chalon[*], Tim Hewson[**],
Kieran Commins[♣], F.H. Sigurðsson[◇],
Zoltan Toth[⋆] and Trausti Jónsson[◇].

[*]*Météo-France, URA CNRS 1357, Groupe d'Etude de l'Atmosphère Météorologique, Toulouse, France,*
[**]*Joint Centre for Mesoscale Meteorology, University of Reading and Meteorological Office, Reading, United Kingdom,*
[•]*Centre National de la Recherche Scientifique, France,*
[⋆]*National Oceanic and Atmospheric Administration, Boulder and Washington, United States of America,*
[♣]*Met Éireann, Dublin, Ireland,*
[◇]*Veðurstofa Íslands, Reykjavik, Iceland.*

2.1 FASTEX Operations: from plans to reality

*T*his Part is meant to give a first idea of how well the goals laid out in Part 1 have been reached. This section summarizes how the plans for operations were implemented. Section 2.2 summarizes the large-scale weather characteristics during FASTEX. Then, two examples of FASTEX cases are presented so as to convey an impression of the type of systems of interest and of the type of operations. An overall summary of operations and a preliminary subjective characterization of all the cases is presented in section 2.5. A short section addresses the forecasts (section 2.6). This Part concludes with some highlights of the achievements of the operations.

2.1.1 Project schedule

FASTEX aims at constructing a dataset covering 10 complete cyclone cases and some extra cases in the upstream areas covered by the Gulfstream-IV. According to the climatology (summarized in section 1.3), a period of 2 months is necessary, on average, with best chances in January. Taking extra-meteorological reasons into account, the FASTEX field season was set on the two months period January and February 1997 (see Table 1.4 in Part 1 for an overview of the project schedule).

The extra radiosoundings all around the North-Atlantic basin have been performed during the whole two months. The FASTEX ships contributed to these soundings except when in port for two or three days at the end of January. The Victor Bugaev, Suroit and Ægir will be on station for roughly two periods of three weeks. The longest cruise is that of the Victor Bugaev coming from Odessa. The aircraft were to be ready to fly from their different bases from the 6th of January 1997 until the 28th of February.

2.1.2 Operations control

FASTEX observing platforms are distributed all over the Atlantic region and yet, they need to be activated in a highly coordinated fashion. In order to achieve this, a single centre had overall control of operations. The implementation heavily relied on satellite telecommunications (with ships and even with aircraft) and numerical data networks (see Short Note 2.1 for a summary on the telecom and computing aspect of FASTEX).

The Operations Centre was located at Shannon, on the West Coast of Ireland. It is a large international airport very suitably located for catching the wave cyclones of interest to FASTEX.

Because of the large scale of the systems of interest, also because of the emphasis put on cyclone life-cycles, the FASTEX operations are more than ever before a forecast and weather monitoring problem. A recent satellite or radar picture is not enough to decide on the strategy and draft a flight plan. The high degree of coordination between the facilities, the complexity of some flight strategies require relatively precise advance notices that will be based on forecast assessment and comparisons. The main part of the work related to planning and monitoring the activities was performed by a mixed group of forecasters and scientists from the operational and research branches of several national weather services: France, United Kingdom, Canada and Ireland.

It was an important secondary objective of FASTEX to allow for direct exchanges of views, techniques, products and methods between forecasters from different origins

Short Note 2.1:
Telecom and computing networks for FASTEX

by M. Chaigneau and P. Bessemoulin
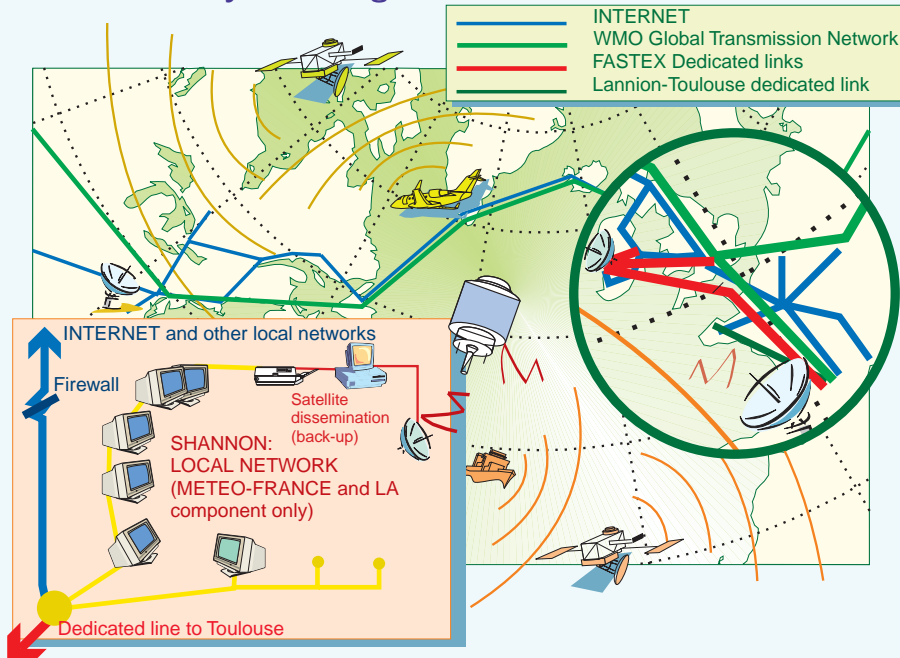
Figure SN2.1.1: *Summary of the main telecommunication links followed by the data with one example of local computing network set-up in Shannon to monitor the data and operations.*

Numerous data items, images, forecast products and so on were required in order for the FASTEX Operations Centre to operate properly. Most groups involved in running the Centre or working in it had to address a telecommunication problem between their base and Shannon, and, on the spot, had to set-up their equipment as part of a local network, all this without jeopardazing the security rules of their respective institutions.

The backbone of the weather data circulates around the globe on a dedicated network called the *Global Transmission System*, coordinated by WMO. GTS data arrived in Shannon from Dublin (via Met Éireann), Bracknell (via the UK Met Office) and Toulouse (via Météo-France), each with different products. Special dedicated data links made this possible:

- Met Éireann upgraded its dedicated link between Dublin and Shannon and extended it from the Shannon Forecast Centre to the FASTEX Operations Centre,

- the UK Met Office set-up a secured and sealed-off fast speed link between Bracknell and the FASTEX Operations Centre,

- Météo-France also set-up a fast speed link between Toulouse and Shannon,

- the other groups (from Canada and the USA mostly) deferred to the UCAR/JOSS unit to set-up an IN-TERNET connection between the University of Lim-erick and the FASTEX Operations Centre in order to tranfer information via INTERNET.

Fig. SN2.1.1 summarizes the various lines employed. It also shows an example of local computing network set-up in the FASTEX Operations Centre itself, the one from Météo-France. It included 4 workstations, one of them being provided by the Laboratoire d'Aérologie, 2 printers, 4 connections for portable PCs and one X-terminal and a few other things. This network was logically part of the Météo-France domain, but was open to the UCAR network and INTERNET via a local firewall. In the case of failure of the critical link to Toulouse, a backup with the satellite dissemination from Météo-France was also set-up (see the diagram). Met Éireann, UCAR/JOSS and the UKMO had similar looking implementations. Other impressive local computing networks were brought and installed for the maintenance and data processing of the aircraft based in Shannon. These were designed by NCAR and by NOAA/AOC respectively. They were connected via the INTERNET.

The main stream for satellite images was either via Bracknell to the specific terminal of UKMO, or via the Centre de Météorologie Spatiale of Lannion. This Centre receives data directly from both METEOSAT and the NOAA Polar Orbiting satellites. It transmits some products but it also produces new ones. All of them go on the dedicated line between Lannion and Toulouse and from there to Shannon.

A two-way fax-type link existed with each of the ships, based on satellite communications via INMARSAT mode C. Both information on operations from and to the ships and measurements from the ships went through this link. The observations were put on the GTS in Toulouse in real time.

A somewhat similar link was set-up by the NOAA groups and enabled real time exchanges between the FASTEX Operations Centre or the National Center for Environmental Prediction in Washington and the Gulfstream IV in flight. The Gulfstream IV dropsonde data, formatted in flight mostly through shear hard work by Diana Bartels, from NOAA/NSSL, was sent to Washington and immediately put on the GTS. Within minutes, it was available in Shannon and could be plotted in various ways and discussed on the phone with the flying aircraft, an extraordinary experience.

as well as discussions between forecasters and scientists. Past experience also strongly suggests that it is important that everybody have a direct access to all the available information: the alternative (to have sub-groups working in different places) strongly weakens the coordination.

The processing of the data was also to begin immediately after the completion of the missions as many investigators were at Shannon with groups of scientists and technicians from NCAR and NOAA.

These activities were managed by two bodies of senior scientists. The FASTEX Science Team was to take the major decisions (begin and end an IOP, select strategies, etc) and to oversee the planning. The Science Team, chaired by Prof. Keith Browning, is composed of representatives of the agencies funding major facilities. The other body, the FASTEX Operations Coordination Team, implemented these decisions and surveyed the status of the various components of the observing system. The Operations Coordination Team was lead by the Operations Directors, Drs James Moore and Richard Dirks from UCAR.

During an IOP, there were three types of activities going on at Shannon.

(i) During any flight, both its progress and the evolution of the weather will be monitored.

(ii) Twice a day, when new forecast products became available, the short-term planning (typically, the flight(s) of the next 24 to 36 h) were revised and the corresponding steps were taken (crew warning, Air Traffic Control warnings, small adjustments of ship positions).

(iii) Once a day, the longer-term planning was conducted, based on medium and short range forecast. It was accompanied by a detailed marine forecast for the ships covering the weather and sea state for next two days wherever they were. Outside an IOP, only the last type of activity was maintained.

The way by which the diversity of the interests and objectives of the various investigators were taken into account was simply through the usual process of proposal submission. Except that during FASTEX, proposals were examined on a daily or half-daily basis. The relevant committee was of course the Science Team.

2.1.3 The actual observing system

The previous Part of the report shows the planned observing system (Fig. 1.8). Moreover, all of its component had, in spite of numerous difficulties and uncertainties, been gathered in time. However, technical and logistical troubles always tend to make reality more unexpected and complicated than carefully devised plans imagine it to be.
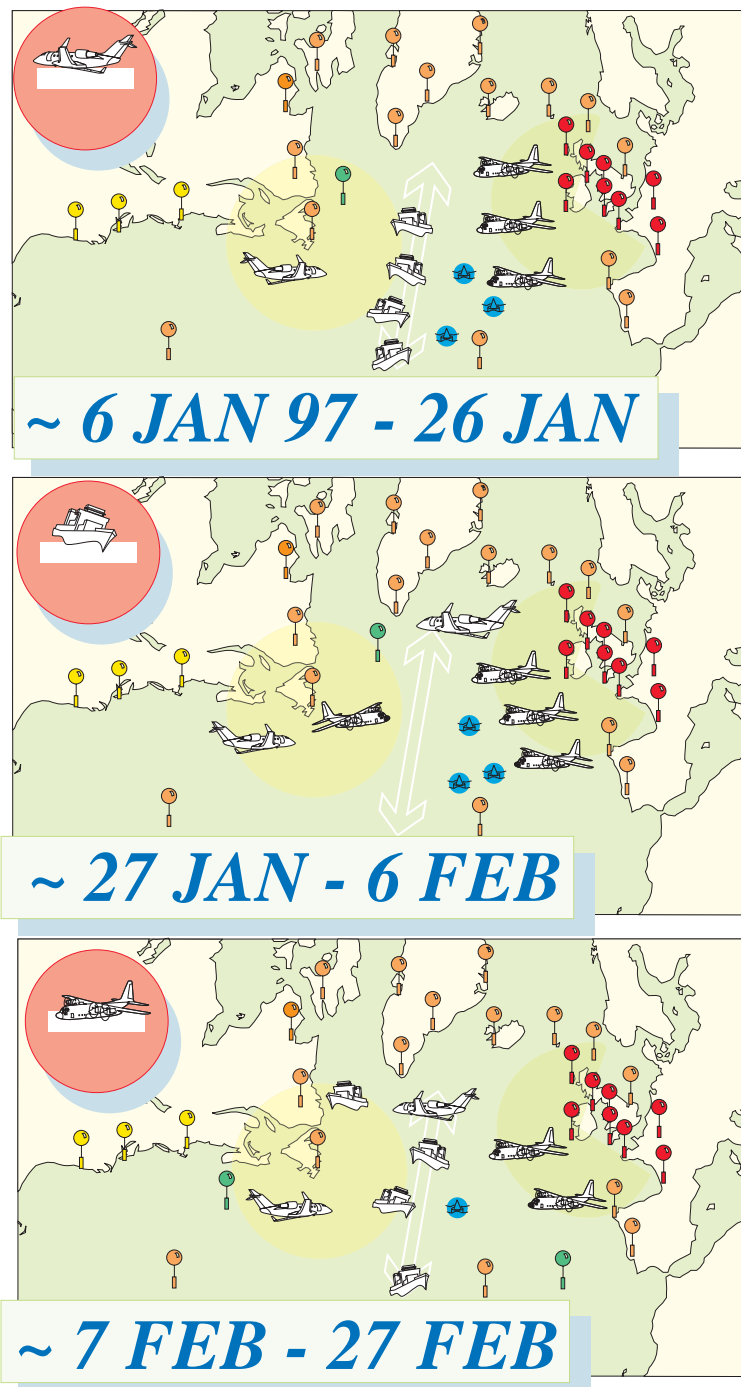
Figure 2.1: *A summary in 3 sketches of the actual observing platforms that were deployed during the field phase of FASTEX, also showing the location of the upper-air stations involved. The shaded zones refer to the areas of Fig. ??. The dates are somewhat approximate, since, for example, the ships were still operating en route when calling to ports in the middle period.*

The actual observing system available during the two months field season is shown in Fig. 2.1. Roughly speaking, the observing problems divided into three periods. During the first period the Gulfstream aircraft was largely unavailable. During the second period, the ships had to call into ports. During the last period the Electra aircraft had to be withdrawn for mechanical reasons just at the start of the MSA missions in IOP 12. One of the ships (the RV Knorr) was reassigned to another project, the Labrador Sea Experiment (however, the crew still maintained a link with FASTEX and actually took part in some IOPs). On the positive side, the first period was run with four ships as planned and an intercomparison of the flux measurements took place; all the other components performed quite well. In particular, the first complex coordinated flights in the Multiscale Sampling Area were a success. In the second period, the Gulfstream became fully available and two C-130 were provided by the US-Air Force: they took part mostly to the test of adaptive observations but, to some extent, they also replaced the ships (as in IOP 9, for example). Finally, during the last period, when some of the most interesting cyclones occurred, all the available components were employed at their full potential.

2.2   Meteorological conditions

In the course of the planning of FASTEX, it was found that the notion of weather regime, as defined by Vautard *et al.* (1988), is useful for highlighting conditions favourable to the type of event of interest to FASTEX (see Short Note 1.1).

Things did not turn out along the way determined by the preliminary climatological study, as far as regime frequency are concerned. It was, with hindsight, fortunate, as will be explained. Averaged meteorological conditions relevant to the FASTEX period are displayed in Fig. 2.2. Analysed fields have been projected on the weather regime fields to determine, daily, the closest one (see Santurette *et al.* (1999)). On this basis, it appears that there were three distinct periods. The year 1997 started with a fortnight of Greenland Anticylone regime, although in practice, it was more an Icelandic ridge than a true anticyclone. The actual mean flow for this period, although close to this reference climatological regime, also had some characteristics of the highly unfavourable Blocking Regime. It was characterized by a jet-stream confined near latitude 40°N and meridionally to the west of 40°W, and more intense than in the climatology. East of this area, there was a large variability (both in the wind and geopotential, not shown) which can be attributed to the lower frequency component of the flow and marks this tendency towards Blocking. Thus systems remained at relatively southern latitudes in general but were able, on occasion, to move north-eastwards and temporarily establish a baroclinic area extending from the end of the average wind maximum to iceland. It also means that the baroclinic driving of the weather systems near the European side was quite weak (on average) and their behaviour sometimes unusual.

The second half of January was dominated by Blocking. The jet-stream was weak compared with the other two periods, but close to its climatological value (about 40 ms^{-1}). These two periods were, from an operational point of view, useful for testing the procedures and gaining experience in readiness for the suitable weather that occurred in February.

The whole of February, finally, was characterized by the wanted Zonal regime. It was associated with rather low total variability, meaning that it was very stable. On average, the wind at 300 mbar was 10 ms^{-1} stronger than its climatological value
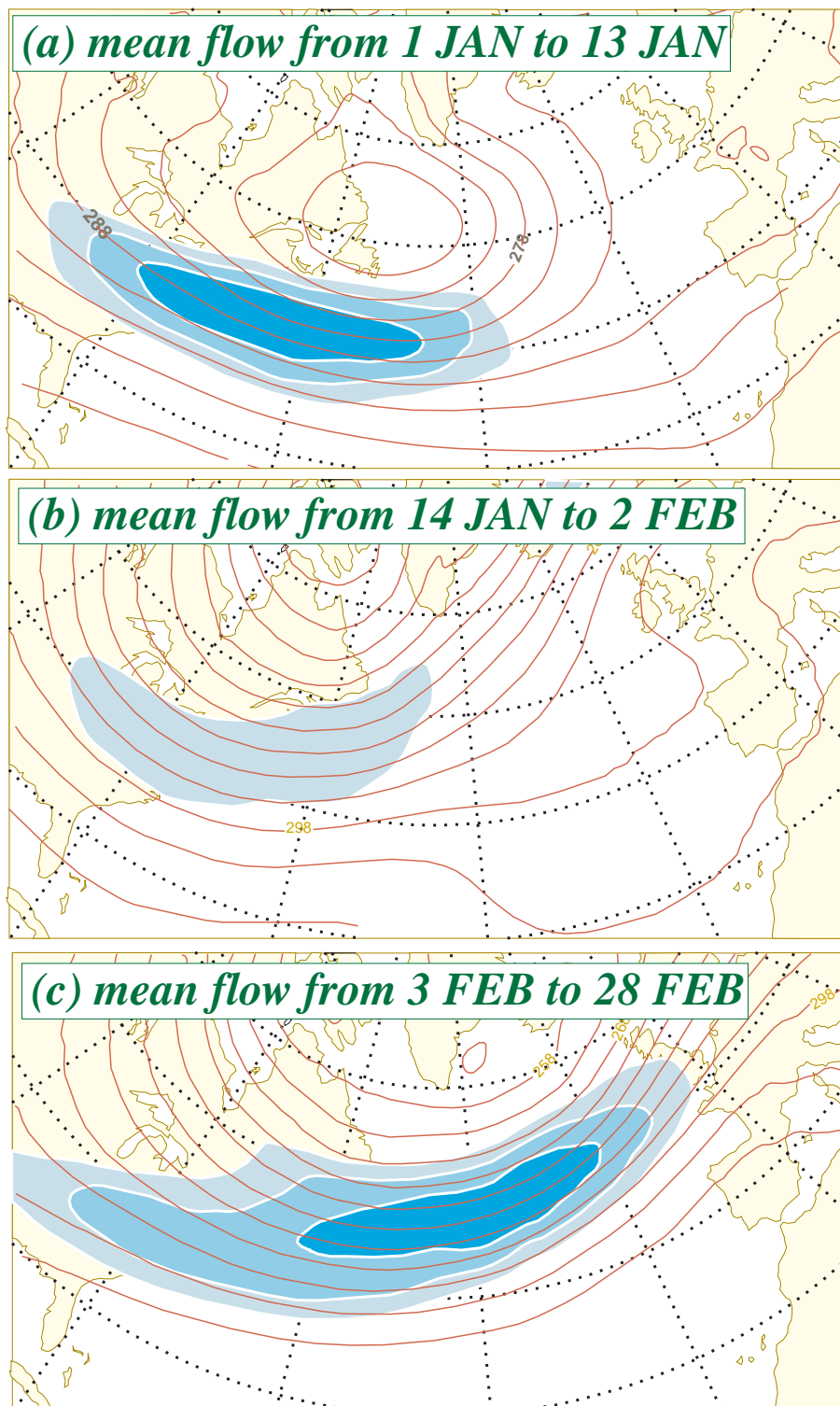
Figure 2.2: *A summary of the averaged meteorological conditions during FASTEX. Contours are 700 mbar geopotential (every 5 damgp) and the three intensities of shading indicate 300 mbar wind in excess of 40, 45 and 50 ms^{-1}. Figure prepared by B. Pouponneau, Météo-France, using the ARPEGE analyses included in the Data Base.*

(see Short Note SN1.1.1), although the overall shape of the jet-stream was close to the reference Zonal regime, with a baroclinic guide extending unbroken from Halifax to Kerry in Ireland. Around 17 February, the jet peaked at about 100 ms^{-1} for about two days. These conditions provided suitable cyclone events. People and machines were also well tuned by that time to the procedures of FASTEX.

During FASTEX, all the lows that moved over the North-Atlantic ocean were numbered sequentially. During the two months of the field experiment, about 50 lows have crossed this broad area. The density of tracks for January and February are shown in Short Note 1.2 and provide a necessary additional picture to the mean flow as shown in Fig. 2.2.

The FASTEX aircraft based in Shannon, Ireland.
Photo: N. Raynal, Météo-France.

The UKMO C-130 in action. Photo: UK Met Office.

Above: the NOAA P3 in operations during a previous experiment, TOGA-COARE. Photo: B. Smull, NOAA. Right: the NCAR Electra, also during TOGA-COARE. Photo: R. Bumpas, NCAR.
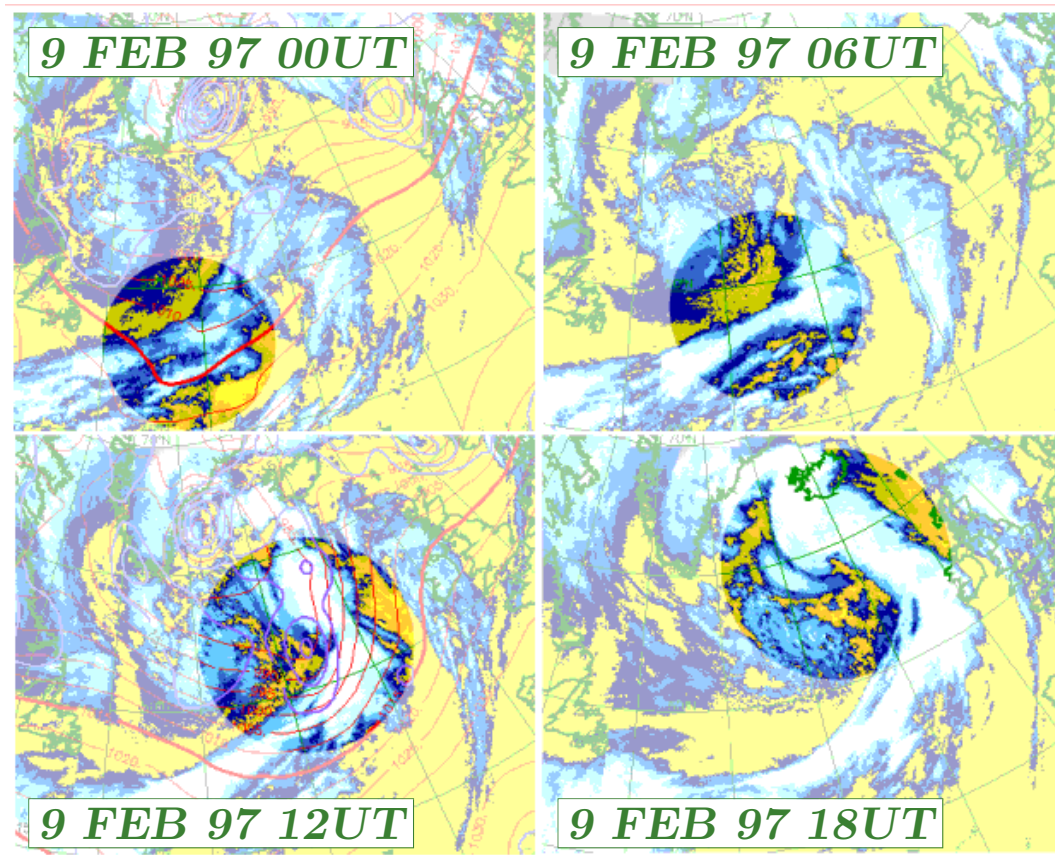
Figure 2.3: *Development of Low 34 on 9 February 1997, FASTEX IOP 12. Low 34 is encircled. Images are in the infra-red channel and are a composite of METEOSAT and GOES. On two images, two fields from the operational Météo-France analysis (that includes FASTEX data) are superimposed. The purple lines are absolute vorticity at 850 mbar from $1.5{\times}10^{-4}$ s^{-1} every $0.5{\times}10^{-4}$ s^{-1}. The red lines are mean-sea-level isobars, drawn every 5 mbar.*

2.3 Example of an Intensive Observations Period: IOP 12

The best way to convey a flavour of FASTEX operations is to summarize the story of one Intensive Observing Period. Because of its unique mixture of exciting meteorology and dramatic operational events, IOP number 12 is now presented.

The meteorology will be discussed first. IOP 12 was conducted on Low 34. This cyclone underwent, on 9 February 1997, the most explosive deepening of the period: roughly -54 mbar in 24h, with a phase of -23 mbar in 6h. This very rapid development goes along with a very short life-cycle. It is summarized by Fig. 2.3. The background shows infra-red images composited from both geostationary satellites GOES and METEOSAT. The figure also shows the mean-sea-level pressure and low-level vorticity analyzed by the Météo-France operational suite ARPEGE. An individual vorticity maximum can be tracked from 9 February 00UTC onwards, whereas closed

isobars can be seen only when the low is fully developed, after 18UTC. The analysed sea-level pressure falls from about 1015 mbar on 8 February 18UTC to 961 mbar on 9 February 18UTC. Between 6UTC and 18UTC 9 February, Low 34 moved about 1700 km at a phase speed of nearly 40 ms^{-1}. The life-history of this system began, however, on 8 February between 00 and 06UTC. This is somewhat to see with most usual fields, including the images. However, the use of time-filtering, for example, enables a separation between perturbations and background. Precursors can then be isolated.

Low 34 was preceded by a series of active systems. It marked the end of first most active portion of the zonal regime. After it, the activity in the eastern part of the Atlantic basin subsided somewhat before building up again about a week later. Panel (a) of Fig. 2.3 shows two of the preceding lows: Low 31, a quasi-steady system close to Greenland and Low 33 north of Ireland, a rapidly evolving "typical" cyclone that, for logistical reasons, could not be considered for an IOP. This category of case is discussed in the next section.

The dynamics of Low 34 will be briefly returned to in a paragraph or so. Its associated Cloud System is discussed in more details in Part 5 and Part 6 in this Report. See also, for example, Scialom *et al.* (1999) in this issue or Chaigne (1998) and compared to a Pacific case by Lemaître and Protat (1999). Consider now how the life-cycle of this cyclone has been followed.

The first tentative plan for a possible IOP 12 on a Low 34 was drafted on the basis of the forecasts starting on 5 February 00UTC and, for the ECMWF model, 4 February 12UTC. As the Low was expected to be in the western part of the MSA on 10 February 00UTC, it is important to note that these are 120h and 132h respectively. As summarized in section 2.6 below, decisions for FASTEX were prepared using an "ensemble" of many different numerical models. Needless to say that there was a wide discrepancy in the various forecasts, but at the same time, there was enough consistency to convince the team of forecasters that a new IOP might be declared. As soon as 5 February 12UTC, a westbound flight of the Gulfstream-IV jet aircraft was planned for 8 February, a return flight on 9 February and a coordinated MSA flight of turboprop aircraft on 10 February.

The reader has now to realize that these "long-term" decisions were taken in the midst of running IOP 11 on Low 30, a case that led to long, difficult discussions because of the possibility of a wave forming in its wake. And this IOP came immediately after a series of three in a row so that a number of logistical "clocks" were running out time: days without operations had to be set into the schedule for crews to rest and for some maintenance of the aircraft. For these reasons, a choice had to be made between Low 33 and Low 34 for an IOP: the latter, which turned out to be the more interesting one, was chosen. These decisions were confirmed on the following day, that is 2 days prior to the first airborne operation relating to IOP 12, and 3.5 days before the cyclone sped into the MSA: the schedule was defined more precisely (mid-times were assigned to a number of flights)with the coordinated flights in the MSA rightly moved closer to 00UTC 10 February. The ships were informed of the likely IOP scenario and that they would have to perform 3h radiosoundings for 24 hours as from 8 February 12UTC. These decisions were taken on the basis of 96h and 108h forecasts (which are, with hindsight, generally less good than the previous ones) and the decision not to fly the turboprops on Low 33 was maintained. In this series of forecasts and the following one, Low 34 deepened to only 980 mbar, with a dispersion of 8 mbar at most, making the decision far from clear cut. On 7 February,
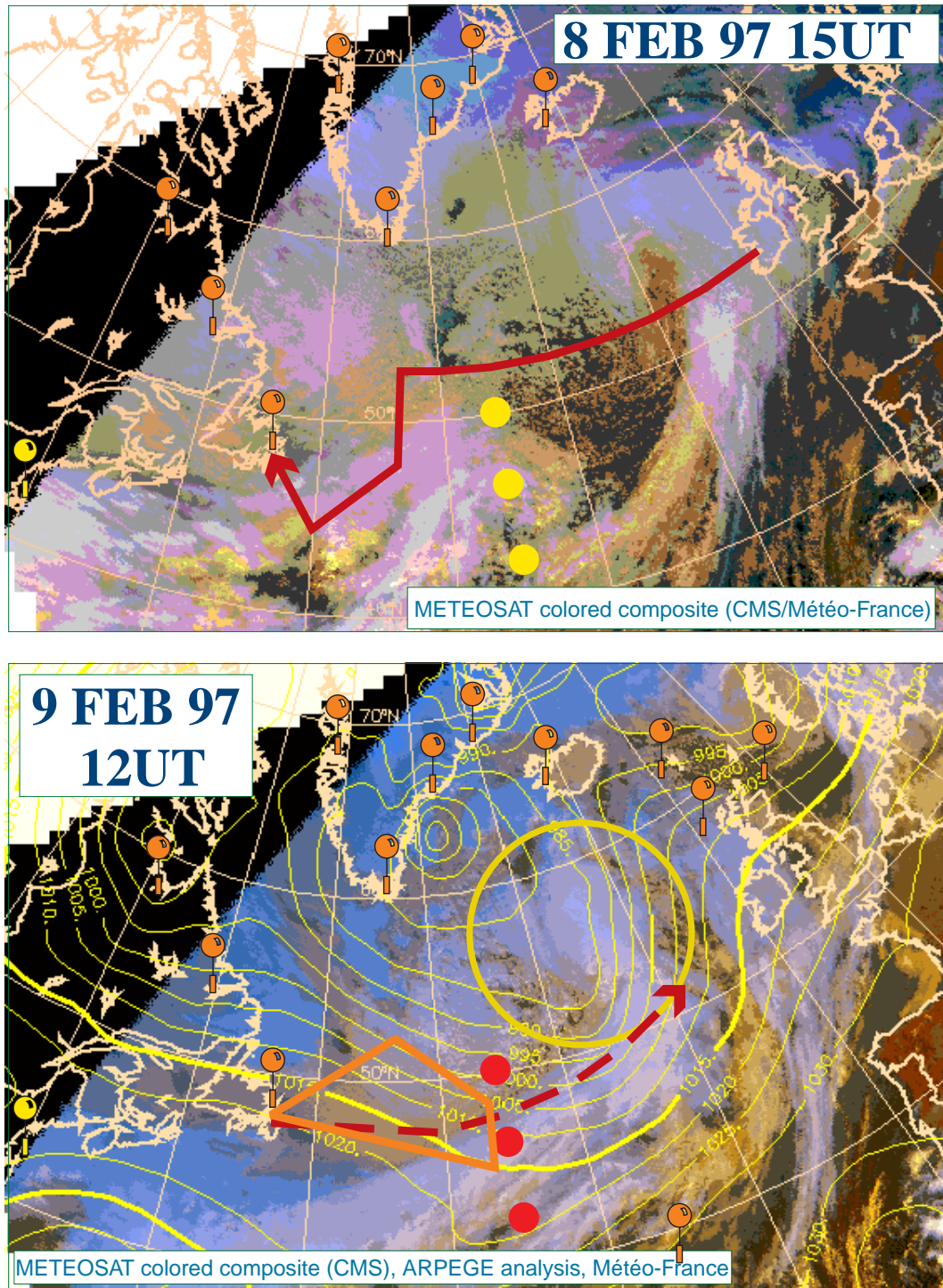
Figure *2.4*, beginning.
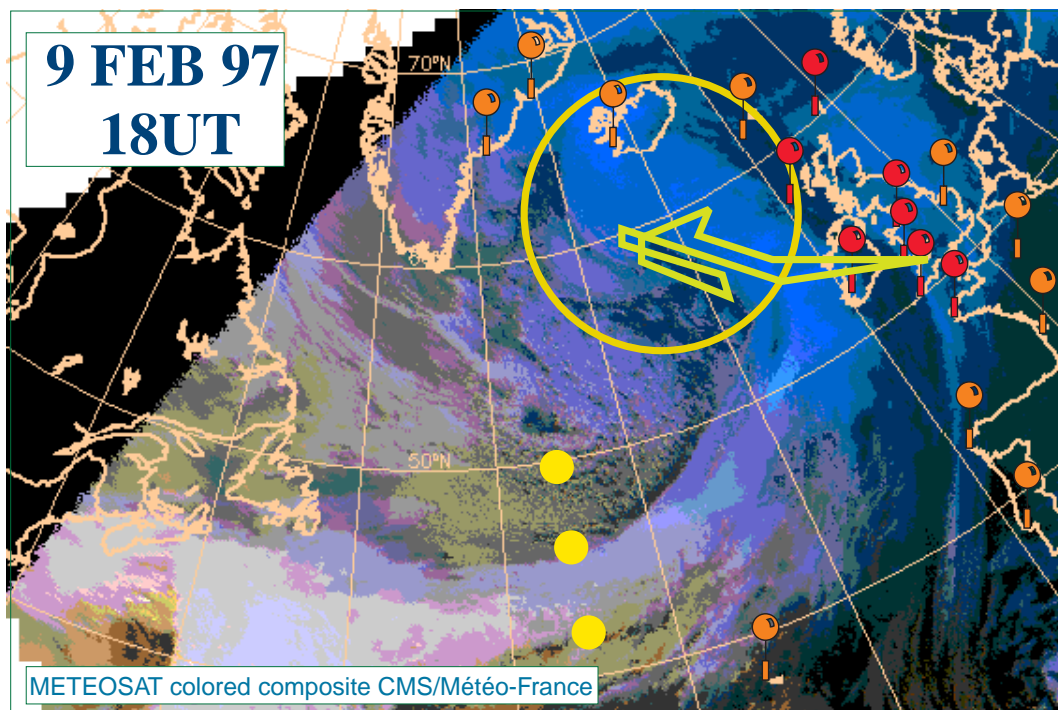
Figure 2.4: *A summary of operations during IOP 12. The lines show flight tracks (dark red: Gulfstream; orange: US C-130; green-yellow: UK C-130). The large dots show the ships location, performing intensive radiosoundings when red. All upper-air stations shown (balloon symbols) were operating every 6h except the red ones which were operating every 3h. The difficult and eventful St-John's–Shannon flight of the Gulfstream IV on 9 Feb is dashed; no data were taken. The backgound images are multichannel composite images from METEOSAT prepared by the Centre de Météorologie Spatiale, Météo-France. See also summary 3.15, page 112 in Part 3.*

the day prior to the beginning of IOP 12, the discrepancy between the various forecasts remained quite large and Low 34 still appeared to be unexceptional except in the 72h ARPEGE forecast. These are signs that the case could be a promising one for testing the adaptive observation strategy: specific targets for this system were determined by the various groups involved in this aspect of FASTEX: the NRL in Monterey, NCEP in Washington, ECMWF in Reading and Météo-France in Toulouse. Contacts were made between the project headquarters at Shannon and Washington to try to coordinate "targeting" flights between aircraft already based in St-John's and the Gulfstream-IV, set to join them on 8 February. The divergence amongst forecasts led two scenarios being considered: one close to the original plan, the other focused on a new system, called Low 34B, that was not present previously (and that did not turn up in the real world), but which required a delay of about 12h in a number of flights. A few more soundings were ordered from the ships.

The forecasts available in the early morning of 8 February showed a much better agreement between the various models and now predicted Low 34 with a minimum pressure between 953 mbar and 968 mbar, with little dispersion as to its location. On this basis, two flights dedicated to adaptive observations were prepared, one from the

Radiosounding launched from the
V. Bugaev in strong wind. Photo:
T. Douffet, Météo-France.
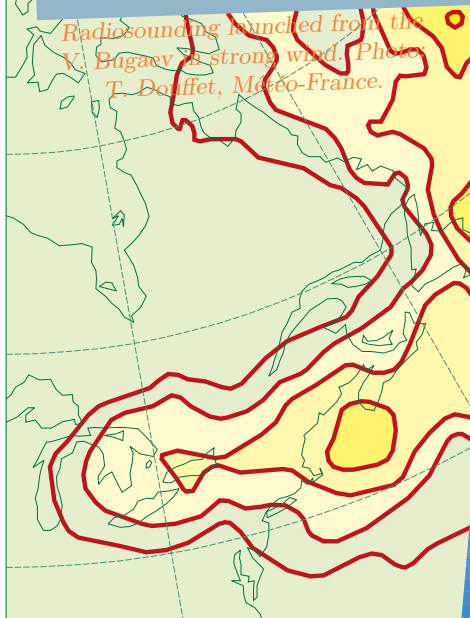
Thirty seconds on Le Suroit's quarterdeck
during FASTEX; It has been like this most
of the 6 weeks at sea. Stills from a video
film by G. Caniaux (at the camera) and
J. Salvano, Météo-France.
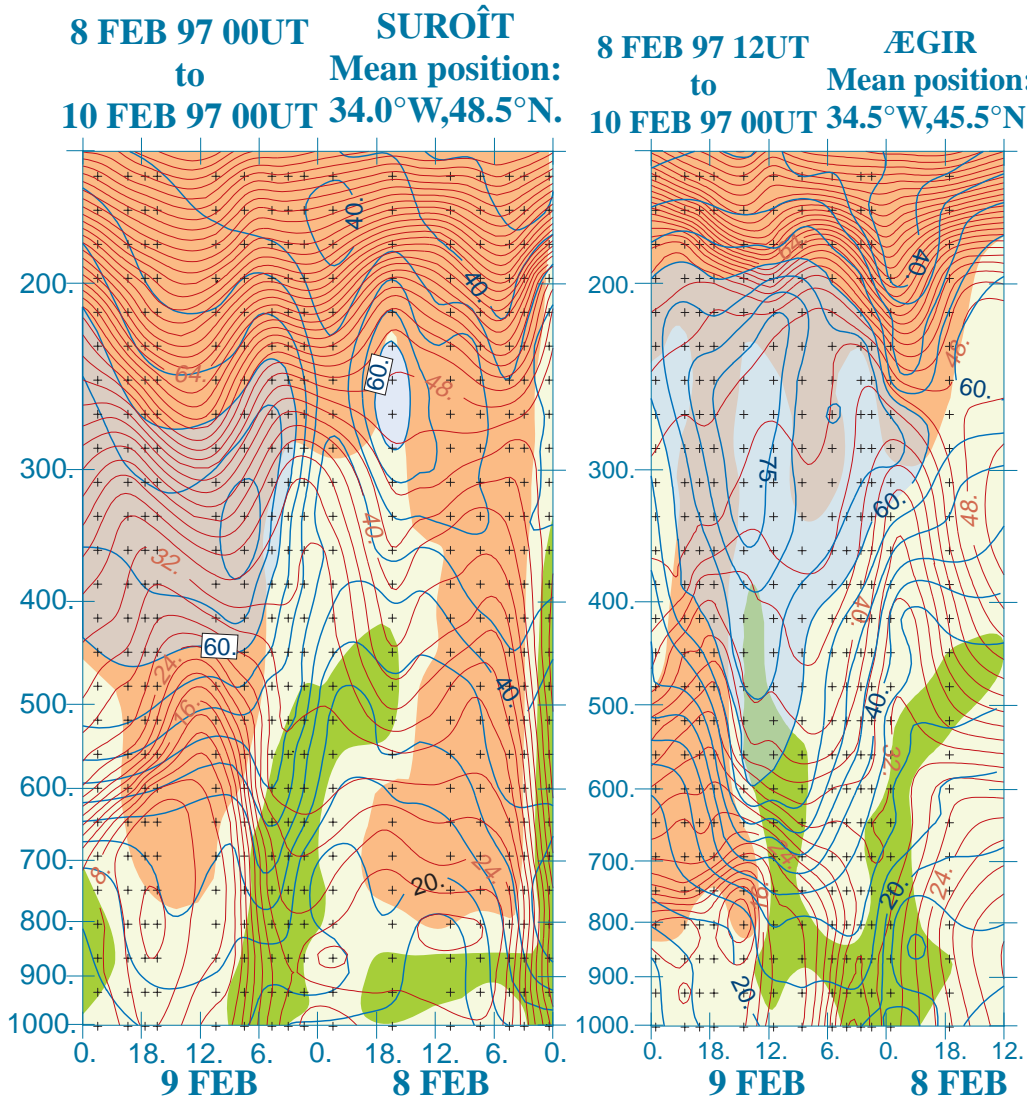
Figure 2.5: *Vertical-time cross-sections derived from the radiosoundings taken from RV Suroît (left) and CC Ægir (right) during IOP 12. The time scale has been reversed so that the figures are suggestive vertical cross-sections with West to the left and East to the right. The heavy blue lines show the wind speed every 5 ms^{-1}, shaded above 60 ms^{-1}. The light dark-red lines are θ_w every 2 K. Light orange shading marks the location of very dry air (less than 40 % relative humidity). Green shading indicates likely cloudy areas (more than 80 % relative humidity). The small crosses indicate the data points. The analysis has been performed with spline functions. Figure built from the soundings from the FASTEX Data Base by G. Desroziers, Météo-France.*

Gulfstream-IV (upon reaching the western Atlantic on that same day) and another by a USAF C-130 about 24h later, on 9 February. The Gulfstream data were also intended to study the early stages of the formation of Low 34. The next step in the plan was to collect data on the rapidly deepening phase using ship soundings and the return flight of the Gulfstream-IV back to Shannon on 9 February, at about 15UTC.

Finally, the three turboprops were to sample the mature system in the evening of 9 February while 8 upper-air stations along the west coast of Europe would be launching 3-hourly soundings.

The actual operations managed on this case are summarized by Fig. 2.4. Low 34 behaved more or less as anticipated from the 48h or so forecast runs. The Gulfstream-IV properly sampled the predictability "target". As was often the case, this target was located, at low levels, in the warm air to the south-east of the system of interest. The ships, although fully in the track of the cyclone and accompanying gale force winds, managed to perform the required soundings. The USAF C-130 flight on 9 February sampled the wake of Low 34 in case Low 34B showed up (the data may help explain why it did not). However, shortly after the Gulfstream-IV took off from St John's for what might have been an optimal flight sampling the structure of a deepening cyclone, one of its electric generators stopped functioning. The flight was completed safely, albeit with much anxiety and without a number of equipment and functions, but, of course, invaluable soundings were lost. However, there was still the possibility to study the detailed structure of the cloud system with dropsondes from the C-130 and both airborne Doppler radars. The UKMO C-130 and the P3 aircraft took off successfully but the mechanical problem of the Electra prevented it to join them. Radio communications with the other two turboprops allowed for in-flight adjustment of the plans to compensate for the absence of the Electra. Then, the C-130 met numerous difficulties with its first dropsondes. However, they were solved and a successful operation resulted. In spite of all these problems, valuable data were obtained at various stages of the evolution of Low 34 . Operations on this case had been planned over a period of 4 to 5 days and lasted two days only. In a number of other cases, the actual operations covered three days continuously and, in the case of the linked IOPs 9 and 10, four days consecutively, plus a several more days upfront for planning.

Fig. 2.5 illustrates features of interest during the development of Low 34, as seen from the ships. The Ægir Coast Guard vessel was directly in the path of the cyclone and its low-level thermal structure clearly shows up, between 0 and 6 on 9 February in the form of a narrow warm conveyor belt. Most interesting, however, is the tropopause anomaly that can be seen moving above the Ægir during the evening of 8 February. As shown in the figure, this anomaly is on the wrong side of the low for constructive baroclinic interaction. Analyses show that it took place earlier on 8 February, but the upper-level anomaly moved eastward at 43 ms^{-1}, while the surface precursor, a warm maximum in the soundings from the Ægir travelled at 19 ms^{-1}. The rapid development was due instead to the influence of a second upper-level anomaly, more intense, that can be seen in the soundings from the Suroît ship at 12UT on 9 February.

The importance of the two successive baroclinic interactions has been demonstrated by Chaigne (1998). He shows, using potential vorticity inversion, that if this second upper-level feature is removed, Low 34 does not develop. He also shows that if the surface precursor generated on 8 February is removed, Low 34 again does not develop. From the point of view of the dynamical objectives of FASTEX, this case shows the reality and importance of transient baroclinic interaction between two features as well as the fact that a strong cyclone does not emerge from continuous growth. Rather, it grows in steps and each can involve different features. This indicates that one needs to be very careful when defining a system of interest. This case illustrates one of the conclusions from the climatological work of Ayrault (1998): rapid deepening involves two *independent* precursors at least: one in the lower troposphere, the other at the tropopause.

22 FEB 97 00UT   **23 FEB 97 00UT**

23 FEB 97 12UT
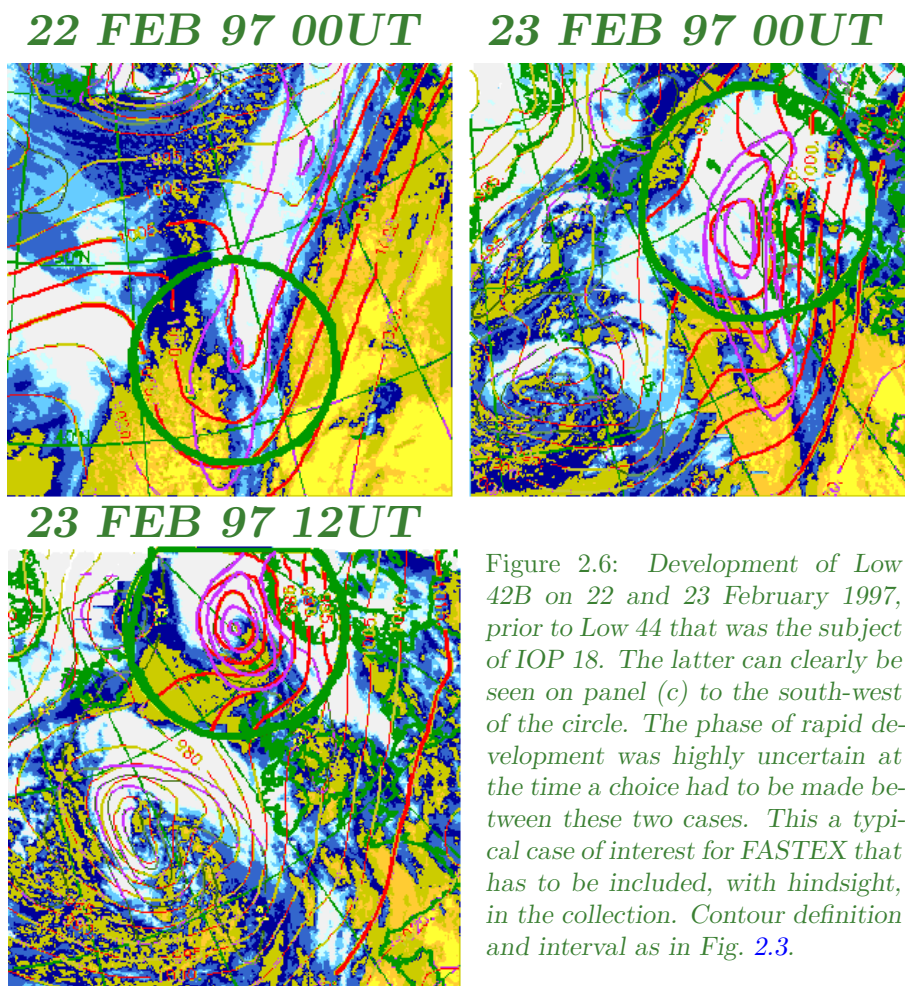
Figure 2.6: *Development of Low 42B on 22 and 23 February 1997, prior to Low 44 that was the subject of IOP 18. The latter can clearly be seen on panel (c) to the south-west of the circle. The phase of rapid development was highly uncertain at the time a choice had to be made between these two cases. This a typical case of interest for FASTEX that has to be included, with hindsight, in the collection. Contour definition and interval as in Fig. 2.3.*

2.4   The Lesser Observations Periods during FASTEX

According to the previous section critical decisions regarding IOP 12 were taken 3 days before the system even existed. Difficulties raised by the differences between forecasts have been alluded to, as well as those resulting from operational constraints. It was because of the operational constraints that Low 33, although the type of system of interest to FASTEX, was not the subject of intensive observations: the rapid succession of IOPs 9 to 11 imposed a break in the operations.

Yet Low 33 was by no means totally deprived of special observations. 54h prior to Low 33 entering the MSA, a long flight of an USAF C-130 from St-John's covered the broad area around 50°W and 45°N where the low started to form later. The ships were on the track of this low as well and performed 8 soundings per day on 7 and 8 February as Low 33 developed. And finally, as the Gulfstream flew towards St-John's on 8 February, it sampled the same low, still undergoing deepening, with a series of dropsoundings, providing a minimum set of data in the MSA. These are the components of a mildly successful IOP and so this case has been included in the FASTEX set. It was, indeed, labelled IOP 11A.

Low 33 is not an isolated case. After the field phase was completed, a second set of systems was added to the main FASTEX Intensive Observations Periods: the
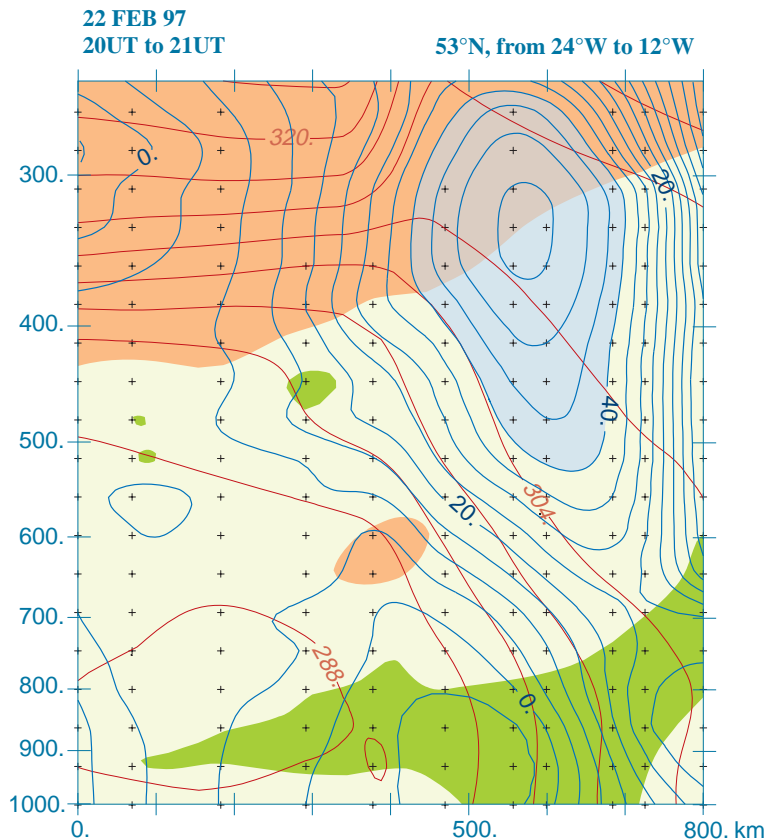
Figure 2.7: *Vertical cross-section derived from the dropsoundings taken from the Gulfstream-IV aircraft at the end of a flight part of IOP 18, but describing the cyclone 42B that was not selected for an IOP. Contours and shading are as in Fig. 2.5, except θ_w drawn every 4 K and the wind is shaded when larger than 40 m.s^{-1}. The analysis has been performed with spline functions by G. Desroziers (Météo-France) using the FASTEX Data Base.*

FASTEX Lesser Observations Periods (FLOP). They fall into two categories: the first is made up of the cases like Low 33 that were only partially covered for logistical reasons. The second category is, given the objectives of the project, quite an important one: it contains the cases only partially covered because they were wrongly anticipated from the forecasts. They epitomise the "FASTEX dilemma" mentioned in section 1.6 Since FASTEX is about understanding predictability, looking back on these cases can be helpful. Figure 2.7 illustrate a case falling in the second category, one model only having predicted its existence at the time a decision had to be made for an IOP 18. This figure also shows the capabilities of the Gulfstream-IV to map cyclone-scale features. These two cases are now included in this series of interesting cases as FLOP 2 and FLOP 5.

The story of IOP 12 is successful because the decisions taken early were confirmed and turned out to be the right ones. One cannot expect this to have been true all the time. Fig. 2.6 shows a cyclogenesis event belonging to this second category. At an early stage, an assumption has been made in order to choose between two cyclones (Low 42B shown on the figure and Low 44 that was the subject of IOP 18: it can be seen on panel (c) of Fig. 2.6) that turned out to be wrong. Low 42B is of a high priority for FASTEX because it is undoubtedly what a synoptician would call a frontal wave. Furthermore, the prediction of its evolution has been very difficult. Low 42B formed along the meridionally oriented cold front of Low 42 during the night between 21 and 22 February. However, most of 22 February, it moves northward along the front without really developing. It appears, on the satellite images, as a thicker

Short Note 2.2:
Surface fluxes in the North-Atlantic Current during FASTEX

by L. Eymard, G. Caniaux, H. Dupuis and L. Prieur

An oceanic component has been added to FASTEX: CATCH (*Couplage avec l'Atmosphère en Conditions Hivernales, Atmospheric Coupling in Winter Conditions*). It was performed from the research vessel Le Suroît, near 47°N and 40°W, an area characterized by the presence of the warm North-Atlantic Current (NAC) in a cold surrounding water.

CATCH aimed at studying the surface fluxes variability related to the passage of atmospheric fronts, of the role of strong sea surface temperature gradients associated with the North-Atlantic Current and of the parameterization of surface turbulent fluxes in strong and changing direction wind. The first results of the analysis of the ship data, relocated in the major mesoscale features, is presented in details in Eymard et al. (1999). They have been obtained by combining buoy measurements, satellite data and meteorological output together with the direct observations. The surface turbulent and radiative fluxes are derived from ship measurements and compared with model and satellite estimates.

The turbulent fluxes from the ship have been obtained using the inertial-dissipative method. A bulk algorithm has then been derived and the results of this parameterization are compared to other previously published ones. Fig. SN2.2.1 shows the results for the momentum fluxes. For this parameter, it appears that existing schemes systematically underestimate the stress.

The major novelty of this dataset is that it contains observations at large wind speeds (between 20 m/s and 30 m/s) under a variety of temperature and stability conditions. This area of the parameter domain has seldom been explored in the past. Results such as those shown in Fig. SN2.2.1 may have a dramatic impact in climate simulations, especially in coupled simulations.

About the authors:

L. Eymard and H. Dupuis are from the CNRS-CETP laboratory, L. Prieur is from the Laboratoire de Physique et Chimie et Marine and G. Caniaux from Météo-France.

Figure SN2.2.1: *Scatter plot of the momentum fluxes calculated from 6 bulk flux formulae according to the mean flux.*
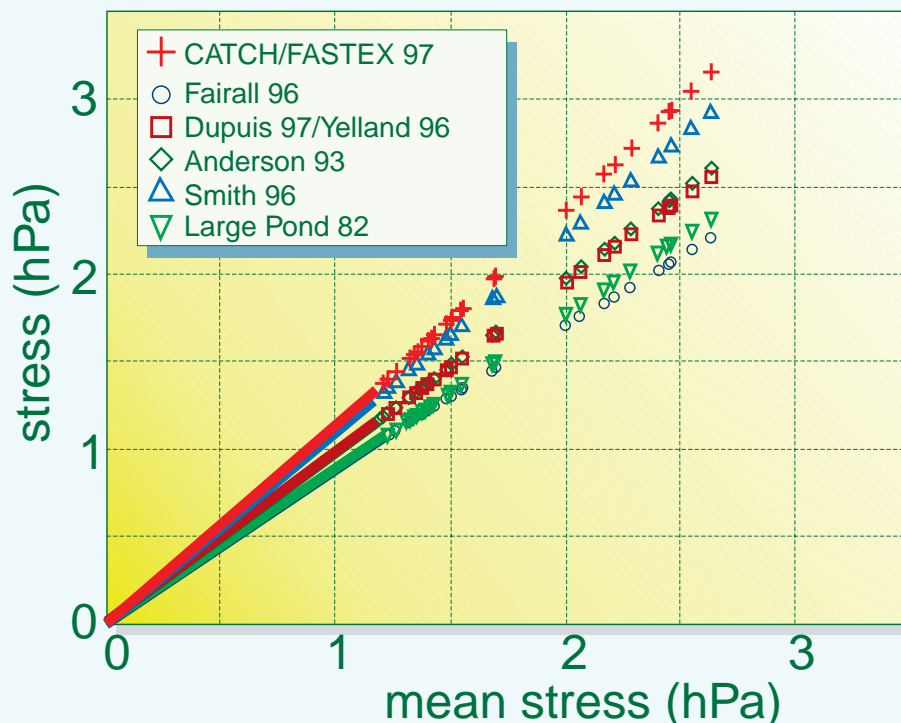
section of the frontal cloud band. And then, during the night between 22 and 23 February, it deepens rapidly and took, at the same time, a more usual shape.

The choice between Low 42B and Low 44 was made on 20 February on the basis of a series of 72h (84h for ECMWF) forecasts. One model, the UK Met Office global one this time, moderately developed Low 42B, the others not. Non developing cases were to be included in the FASTEX set, but they had already been met at that time. Although the transition from repressed development to explosive growth is of obvious interest as well, it was thought to be too uncertain. It is only on the 24h forecasts and less that things changed, but the operations on Low 44 were decided already. However, as was done on Low 33, Low 42B was sampled by a series of dropsondes from the Gulfstream-IV in the MSA on the evening of 22 February: the resulting section is shown as Fig. 2.7. This case therefore benefits from the improved background obsrvations as well as from special observations. It can be studied practically as any of the more standard IOP cases and is included in the FASTEX set as FLOP 5. It should also be noted that IOP 18 on Low 44 is important in the FASTEX sample, since it is a very well documented case of a life-cycle occurring on the northern side of the baroclinic zone. A transition from restrained growth to explosive deepening has been observed in IOP 19.

2.5   Summary of operations and overview of cases

The scene is now set for taking a broader perspective and presenting the complete set of FASTEX cases. There are 25 of them: 19 IOPs were declared and run as such, 6 LOPs were included at the end of the field phase, when the whole period was reassessed (FASTEX was initially planned to allow the study of 10 cases). Almost all cases concentrate on a particular type of cyclone or on a feature such as front that did not allow for a cyclone to form. All these cases are in line with the objectives of the project: the sole exception is IOP 8. IOP 8 took place, during the blocking period, when no cyclone could possibly reach the eastern Atlantic. In order to maintain a minimum of activity, a flight from the Gulfstream was set up and directed towards Greenland in order to document upper-level lee waves. However, apart from the fact that the flight intersected a coastal front, this IOP is difficult to include in the summary tables.

The achievements of the field phase of FASTEX are summarized in Table 2.1. Part 3 provides more detailed information on each FASTEX case (including IOP 8): key dates and locations, flights and other operations.

2.5.1   Potential for cloud-system and mesoscale studies

This category of objective has suffered from the premature withdrawal of the Electra. Nonetheless, good datasets were collected from the very start of the field phase as indicated in the last three columns of Table 2.1. This is due, to a large extent, to the high degree of cooperation achieved very early in the project by the scientists involved as well as to their ability to explain their operations to the aircraft crews. The success is also attributed to the development, by the JCMM and NSSL scientists of software to perform system-relative, multiple-aircraft flight planning. The complexity of coordination resulted from the need subsequently to analyse the structure of the core of the cyclones with quasi-regular flight pattern in system-relative space. In one configuration, the same sampling area was to be covered by both dropsondes and

Table 2.1: *Summary of operations on each FASTEX case*

	Soundings at 3 successive stages	Upstream data for targeting	Ship data for targeting	Upstream data for dynamics	Ship data for dynamics	MSA sampled with dropsondes	Airborne Doppler data in MSA	3hourly European west-coast soundings
IOP 1	–	–	–	–	end ampli	●	ss **	**
LOP 1	–	–	24h	–	beg ampli	–	–	**
IOP 2	●	36h	48h	–	–	●	mi ***	**
IOP 3	–	48h	24h	gen	ampli	–	–	**
IOP 4	–	–	48h	–	organ	–	–	**
IOP 5	●	48h	36h	–	organ	●	mi **	**
IOP 6	–	–	18h	–	beg sup	●	–	**
IOP 7	–	–	18h	–	front	● ●	ss ***	**
IOP 9	●	42h	(C130)	ampli	(circl)	●	mi **	***
IOP 10	●	18h	30h	gen	beg gen	●	ss ***	***
IOP 11	●	36h	18h	beg ampli	front	● ●	ss **	**
LOP 2	●	48h	18h	–	ampli	●	–	–
IOP 12	●	30h	12h	rear gen	beg ampli	●	ss **	***
IOP 13	–	48h	48h	circl	beg dec	–	–	–
LOP 3	–	48h	48h	–	beg gen	–	–	–
IOP 14	–	48h	24h	–	beg dec	–	–	–
IOP 15	●	24h	18h	rear	ampli	●	ss **	*
IOP 16	●	24h	12h	–	beg gen	●	ss ***	***
LOP 4	–	48h	24h	–	clust	–	–	***
IOP 17	●	42h	18h	ampli 1	wave	● ●	ss ***	***
LOP 5	–	–	36h	–	beg gen	●	–	–
IOP 18	●	36h	12h	gen	ampli	●	mi **	***
LOP 6	–	48h	36h	–	beg dec	–	–	***
IOP 19	●	30h	24h	wave	sup waves	●	–	**

Abbreviations for life-cycle stages:
beg: early step of stage
gen: genesis
rear: rear (western) component
circl: soundings all around system
clust: cloud cluster
ampli: amplification, deepening stage(s)
organ: organisation, "shaping"
sup: suppression (of waves)
dec: decay.

Symbol ● means "yes" or "present"
Symbol ● ● marks that 2 sets are available.

Targeting lead times: the figures are orders of magnitude based on the life-cycle of the systems. They are not the exact values employed by a particular targeting group.

Coverage in the MSA:
ss: systematic survey
mi: mesoscale investigation
**: 70–80% sucess rate of sampling
***: 100% success rate of sampling.
From IOP 12 onwards, the Electra is removed.

European west-coast radiosoundings:
* means that only the UK stations actually on the west coast were active.
** means that only the stations actually on the west coast were active.
*** means that all the participating stations were active.
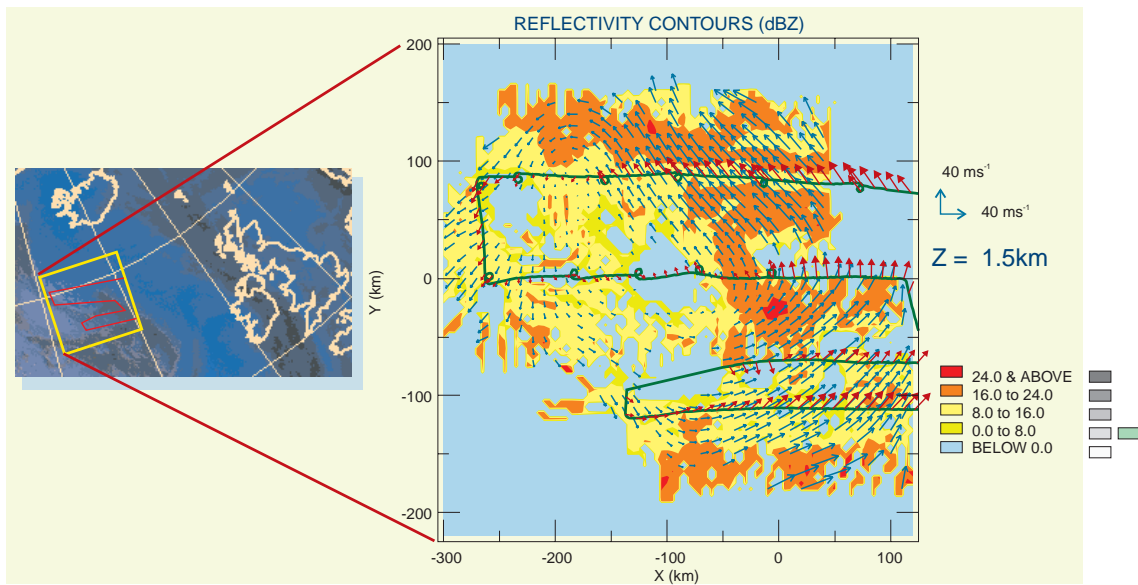
Figure 2.8: *METEOSAT multichannel composite image of Low 34, during IOP 12 (left), as in Fig. 2.4. Airborne Doppler analysis of winds at 1.5 km retrieved with the MANDOPA technique over the bow indicated on the satellite image. Shading on the radar image shows the reflectivity. Figure prepared by A. Protat, from CETP: see Part 6 for further details and results.*

adjoining airborne Doppler radar swaths. This mode of operation, called "systematic survey" was tested in the very first IOP. It turned out to be successful from this first attempt (see the work of Jorgensen *et al.* on this IOP). The flight planning problem is not simple and its proper handling by scientists and crews is one significant accomplishment of the project.

Systematic survey patterns have been achieved on 4 occasions with three aircraft and another 4 occasions with two aircraft. Bouniol *et al.* (1999) present results of such a flight made during IOP 16. In four other IOPs, detailed observations of of mesoscale features embedded within the cyclones were obtained by airborne Doppler radars in an environment sampled by dropsondes from the C-130. Some early results are presented in this Report (Part 5, 6 and 7). This is close to the target 10 cases. Fig. 2.8 illustrates the flow organisation within the cloud head of Low 44 (during IOP 18) derived from the P3 tail radar at NOAA/NSSL.

2.5.2   Potential for air-sea interaction studies

This component of FASTEX started as a kind of opportunistic adjunct to the project. Its contribution to studying the complex influence of surface fluxes on cyclogenesis addresses a not well resolved question. At the same time, its contribution to the problem of parameterizing properly these fluxes in the presence of high sea and under strong winds is more clear-cut: see Short Note 2.2 for a brief overview of the results in the domain of parametrization. In this area, a truly unique data set has been gathered by the Suroît and Knorr research vessels. The required conditions have been met (indeed, the ships were hit, on average, by a cyclone every other day) in a wide sample of vertical stability and temperature conditions. The reader is referred

to the overview of Eymard *et al.* (1999) to see that this topic should soon benefit from FASTEX data. These results have direct implication for climate simulations.

2.5.3   Potential for dynamical meteorology studies

The primary objective of the field operations was to collect special data, in the form of vertical profiles, at three or more stages of the evolution of a number of cyclones. The first column of Table 2.1 shows that this was achieved in 12 cases. The criteria for success are: special soundings have been taken successively in *(i)* the Far Upstream Area either at an early stage of the weather system of interest or in a likely sensitive area for predictability; *(ii)* the Midstream Area, mostly by the ships or by the Gulfstream or a C-130; and *(iii)* in the Multiscale Sampling Area, the last two being within or close to the weather system.

There is, of course, a hierarchy amongst the succesful cases, depending on the number of successful soundings, their location in space and time with respect to the system, the presence of upper-level data or the number of samples collected. The most comprehensively observed one is IOP 17. It took place from 17 to 20 February. The weather system, Low 41, formed off the East-Coast of America from multiple precursor features. It was tracked for 67h, over a distance of 5500 km. The ships were properly located, the Suroît having been moved in time to be on the track of this low. They managed, in spite of the wind and the sea, to perform soundings every 90 minutes as the low moved over them. Five successive flights were performed and another earlier flight, on the 16th, can perhaps also be included, from the predictability point of view. During three of these flights, dropsondes were launched from above the tropopause. About 400 soundings were taken in and around Low 41, 230 of which were made from the ships and the aircraft. Dynamically, this low illustrates many of the features or behaviour that led to FASTEX: non-spontaneous genesis in a complex environment, multiple phases of growth, temporary tendency to split into two lows with forecast development of these centres varying greatly between models and explosive deepening. Some of these features are discussed in the studies of Cammas *et al.* (1999), Mallet *et al.* (1999a, 1999b).

It can be said, therefore, that the key experimental objective of FASTEX has been reached. There are, furthermore, significant data for addressing more focused dynamical issues. There are a number of rapidly developing cyclones (see Table 2.2 for a summary) but, as a control for checking current ideas on the way development can be hindered under certain circumstances, there are a few non-developing systems as well (see the work of Chaboureau and Thorpe (1999) and Baehr *et al.* (1999). As will be discussed below, a large number of types of systems has been collected; several critical features or phases have been directly observed, such as the genesis of a wave (IOP 10), a number of cases of the amplification phase, jet inflows and outflows. The most characteristic ones are listed in columns 4 and 5 of Table 2.1.

2.5.4   Potential for adaptive observations studies

A large amount of data are available for impact studies on predictability. Column 2 of Table 2.1 lists the cases for which datasets have been obtained in the Far Upstream Area; the corresponding forecast range is also given. Note that in relative terms the quality of short-range forecasts for some FASTEX cyclones was below that of longer lead time forecasts. The data from the ships can be used in studies of

Short Note 2.3:
Precursor anomalies of cyclogenesis in action

by Ph. Arbogast

The model of cyclogenesis put forward by the Bergen School around 1920 (e.g. Bjerknes and Solberg, 1922) has been widely accepted and was the dominant one in the mid-thirties in operational forecasting. The search for a theoretical basis for this model also opened the way towards linear normal mode stability analyses.

By the end of the thirties, however, different views began to emerge. They are summarized by Sutcliffe (1947) and by Petterssen et al. (1955). The approach, called development, considers that cyclones result from the amplification, sometimes dramatic, of pre-existing and finite-amplitude features present in the atmosphere. The most well known synoptic model in this family is the one of surface cyclogenesis triggered by an upper-level anomaly in the form of a vorticity maximum. This proposal directly opposed the one expressed by, for example, Bjerknes and Holmboe (1944): for them, a cyclone actually starts as an unstable wave in the Polar Front close to low levels, propagates upward and generates the upper-level vorticity maxima. There is a continuing thread of studies that attempt to support the one or the other point of view. The discussion was, furthermore, soon muffled down by the success of the linear normal mode baroclinic instability model. An important landmark in this line is the paper by Petterssen and Smebye (1971) that presents cases representative of both points of view: quasi-linear, possibly surface triggered ones are called Type A and the ones triggered by an upper-level feature are called Type B. The latter are the most convincing ones and the conclusion states that, according to the author's (considerable) experience, they are the most frequent.

This paper clearly made the point that upper-level triggered cyclogenesis were most probably real. However, the direct proof that a given structure at a given time is the actual *cause* of a cyclogenesis event could not be obtained for lack of a proper theoretical tool.

This tool is provided by the emergence of *potential vorticity inversion and attribution*. It is summarized in Short Note 1.6. The building up of implementations of these ideas that can be employed to study actual cases is recent and accompanies the FASTEX programme. The first popular one is due to Davis and Emanuel (1991) and Davis (1992). It has been employed mostly in a diagnostic way. At a given time generally preceding a cyclogenesis event, a number of anomalies are isolated within the flow and their influence on the other parts of the flow at that time is diagnosed. Previous synoptic studies were not very different except that "influence" effects could be computed only globally and not definitely *attributed* to a particular anomaly.

FASTEX offered a good opportunity to make the next step towards the first direct proof that the presence of a given anomaly determines the development of a cyclone. This step consists of removing or adding anomalies in initial conditions and simulate the resulting time evolution with a realistic, finite-amplitude model of the atmosphere.

In this perspective, a new potential vorticity inversion code has been prepared at Météo-France. It is designed to interact directly with the operational ARPEGE primitive equation model. The inversion technique employed is also a new, variational one. The variational approach has been chosen initially because it can handle the presence of areas of negative potential vorticity (Arbogast and Joly, 1998). It can also easily be organized into a framework open to several formulations of the balance condition and the corresponding definition of potential vorticity.

Figure SN2.3.1: *Vertical cross-sections roughly meridional along 90°W, 16 February 1997. The fields are potential temperature θ (red contours, interval 10 K), potential vorticity (blue contours, interval 1 PVU) and vorticity (shading, outermost value 0.4×10^{-4} s^{-1}, interval 0.2×10^{-4} s^{-1}. Top panel: ARPEGE analysis. Middle panel: one upper-level structure has been removed using potential vorticity inversion. Bottom panel: the low level structure cut by the section has been removed in turn. At this time, Low 41 does not exist.*
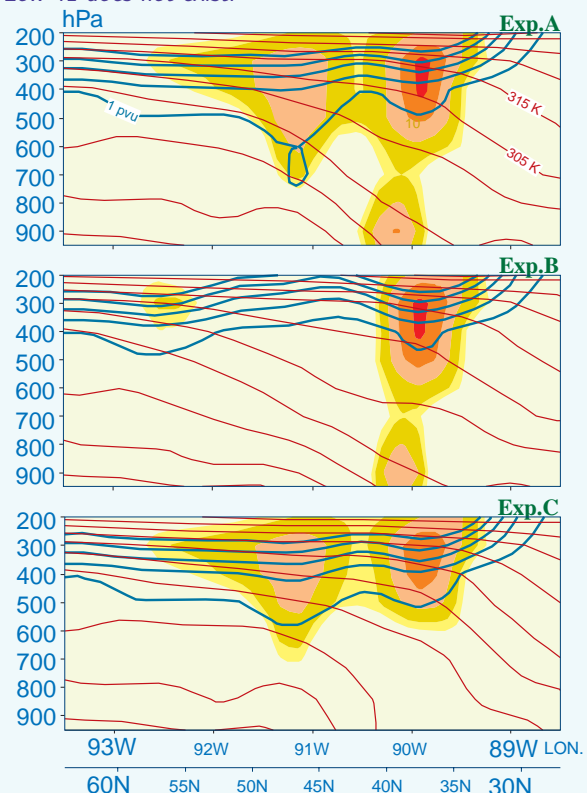
One of the best documented case in the FASTEX sample is Low 41 in IOP 17 (see section 3.21 in Part 3 , page 118 for a summary of this case). Low 41 is a definitely new system that appears on the warm side of a complex jet-inflow, developing surface front area between 6UT and 12UT, 17 February. Cammas et al. (1999) provide a detailed synoptic-dynamic study of the case. The search for precursors of Low 41 must be performed at an earlier time, for example, at 12UT, 16 February. Looking at maps, many features could be pointed out: this is one of the interesting aspects of this case. If the idea of development induced by a specific anomaly is to be proved, its influence must be shown and, simultaneously, the non-influence of neighbouring anomalies must also be shown. It is in the course of a systematic search that the mechanism of the genesis of Low 41 has been uncovered. The long-wanted result has been obtained, but it is accompanied by an unexpected surprise (Arbogast and Joly, 1998b).

Figure SN2.3.1 shows a small selection of possible precursors, seen in a vertical cross-section. At least three distinct features can be seen. The ability of potential vorticity inversion to manipulate the initial conditions in a consistent way is clearly shown on this figure, where two possible precursors are removed in turn. Others have been tested for influence, including large-scale ones: in all but two cases, no significant impact on the subsequent life-cycle has been shown.

The top panel of Fig. SN2.3.2 shows the reference evolution, 36 h after the analysis. Low 41 is then about 12 to 18 h old. Removing the upper-level anomaly as in the middle panel of Fig. SN2.3.1 leads to the complete removal of Low 41 (middle panel). Conversely, removing the other upper-level anomalies does not have this impact. This result is, therefore, the first direct proof of the correctness of the views of Sutcliffe, Petterssen and a few others.

But the actual mechanism is not exactly the one first put forward by Sutcliffe. Indeed, *leaving in* the only critical upper-level anomaly and removing the low-level one that is shown in the cross-section, it appears that the formation of Low 41 is just as severely hindered (bottom panel). The action of the upper-level precursor is not direct. Its direct effect is to enable the low-level system to survive through a weak baroclinic interaction. And it is the low level system, approaching the jet-front complex from the north-west that triggers Low 41. This part of the scenario has been studied in greater details by Mallet et al. (1999).

It remains that FASTEX has proved unambiguously that cyclogenesis results from the influence at a distance of pre-existing, finite amplitude structures interacting with other such structures, specifically here, the strong baroclinic zone in the western Atlantic. All the forms of finite amplitude interactions may, however, come into play and the Type B of Petterssen appears to be one specific kind among others.

The use of such ideas does not, however, solve the forecast problem. It geatly helps the interpretation of existing data and the rating of model runs. However, for the forecast to be correct, two conditions must be met simultaneously:

the distribution of possible precursor structures must be exact *and* the amplitude of the competing, rapidly growing structures supported by the large-scale flow component alone must be *strictly* exact, since otherwise the small errors here will amplify and introduce significant phase and amplitude errors in the interactions between the precursors.

Figure SN2.3.2: *ARPEGE has been integrated forward with the modified initial conditions shown in Fig. SN2.3.1 and others. The maps show the three corresponding 36 h forecasts. The fields are mean sea level pressure (red contours and shading, interval 5 mbar, thicker contour 1015 mbar) and potential vorticity at 300 mbar (blue contours, interval 1 PVU). Top panel: simulation started from the analysis, reasonably close to the analysis given the lower resolution employed. The plane of the cross-section of Fig. SN2.3.1 is also shown. Mid-panel: simulation without the critical upper-level precursor. Bottom panel: simulation without the low level precursor.*
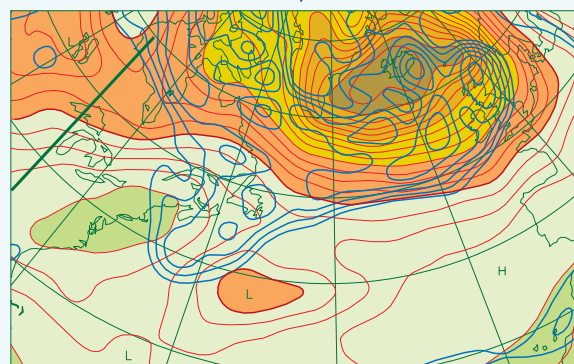
Initial time: 16 FEB 97 12UT - Forecast: 18 FEB 97 00UT (+36h)
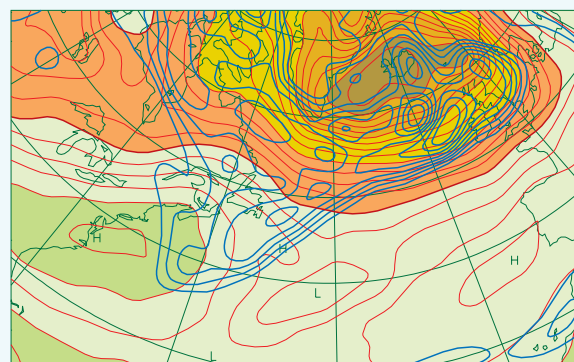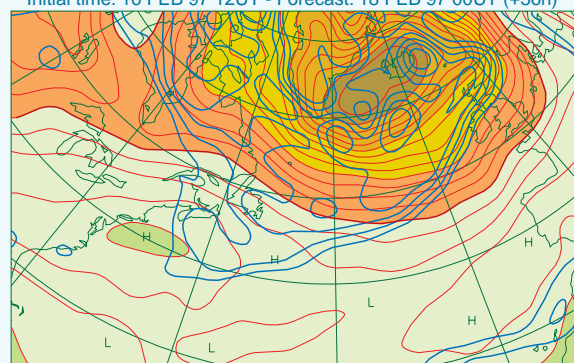
Short Note 2.4:
Implementation and evaluation of adaptive observation in FASTEX

by T. Bergot, G. Hello and S. Malardel
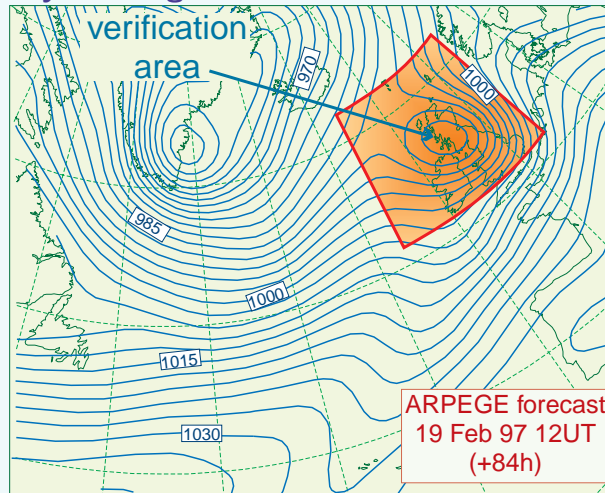
Figure SN2.4.1: *An early forecast for 19 Feb. 97 12UT, made from the analysis of 16 Feb. 00UT (the range is 84h) showing a possible Low 41. The low resolution system employed in real time is then asked "where should we observe on 17 Feb. 18UT in order to improve specifically the following (42h) forecast of Low 41 ?" in the verification area. The field shown is the pressure at the mean sea level, interval 3 mbar. The model employed is ARPEGE on a regular grid at resolution T63.*

Figure SN2.4.2: *The answer to the question asked with Fig. SN2.4.1 is shown here by considering the isolines: they represent the 700 mbar temperature perturbation of the most unstable singular vector that can develop between 17 Feb. 18UT and 19 Feb. 12UT (the amplitude is arbitrary; negative contours are dashed). A small error on the amplitude of this 3D perturbation will amplify as rapidly as this perturbation and is likely to wreck the forecast. A flight plan designed to collect extra data where this structure has a maximum amplitude at that time is superimposed, the dots showing where dropsondes were to be launched. This flight plan was proposed before the Gulfstream flew to StJohn's, but had to be confirmed several times afterwards, using more recent forecasts.*

Figure SN2.4.3: *The dropsonde data obtained during the 17 Feb. flight has been used operationnaly as well as after the field phase, in a better controlled environment. The figure shows the impact of this dropsonde data (shaded area, interval 2 mbar) on a high resolution forecast derived from a suite run without any of the special FASTEX data, except this particular flight. The impact in this case is to change the amplitude towards a better, less deep, value.*

An actual example of implementation of the idea of adaptive observation, as defined for example in Short Note 1.8 , is given by Figures SN2.4.1 (the forecast to make sure of and to improve), SN2.4.2 (the critical structure and area for this particular forecast and the resulting flight actually performed) and SN2.4.3 (the impact of the data collected during this flight). The US Naval Research Laboratory and ECMWF also performed rather close calculations. The NOAA National Center for Environmental Prediction proposed a different approach, based on score threat and the ensemble prediction (Bishop and Toth, 1998).

Given the many operational constraints (aircraft regulations, need to take observations close to 0, 6, 12 or 18UT, etc), many parameters of the target finding algorithm had to be changed, and the calculations often repeated. The Météo-France group has properly anticipated these practical problems. The NRL suite also had some flexibility, but its use was hindered by the time lag between Ireland and California.

All the groups involved in this first experiment with adaptive observation based on pre-defined algorithm undertook, after the field phase, to study the impact of the data. Using current assimilation techniques (essentially Optimal Interpolation and 3D-VAR, see Part 8 on Data Assimilation), this impact has been found to be, on average, positive but weak. However, adaptive observation has been proposed to improve the forecast on particular events, not on average. Figure SN2.4.4 shows one of the results of Bergot (1999) obtained in this perspective: assuming that the score of forecast derived from the raw guess field provides a measure of predictability, the figure shows that adaptive observation can significantly improve the situation when the predictability is low. When it is high, on the other hand, adaptive observation may be difficult to handle, as it can have a negative impact.

The next step is to combine adaptive observation with 4D-VAR. One reason is that, according to the feasability study of Bergot et al. (1999), many observations in the critical area are required to maximize the impact and current assimilation method force a severe selection when one does not wish to introduce phase errors: not all the data, by far, has been employed in these studies. The theoretical work of Fischer et al. (1998) also suggests that, with flow dependent covariances functions as in 4D-VAR, the impact can be extremely positive.

Figure SN2.4.4: *One important result from a systematic study of the impact of the adaptive observation flights on the subsequent forecast is shown on this figure. The improvement of the RMS score of surface pressure over Europe due to the adaptive observations (vertical axis, positive for actual improvement, negative for a negative impact on the forecast) is plotted as a function of an a posteriori measure of the quality of the guess field. It appears that adaptive observations can be very efficient when the quality of the guess is poor, but are neutral or even detrimental when the guess field is good.*
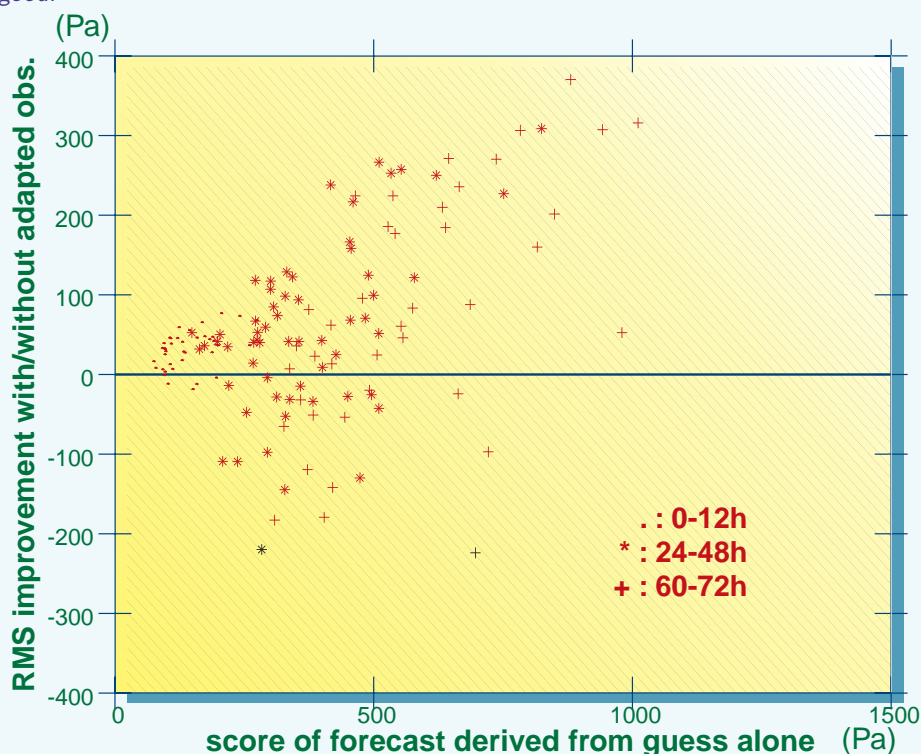
predictability at the shorter ranges. They are very often well located with respect to sensitive areas.

An important aspect not reflected in this table is the experience gained in the actual practice of "targeted observing". The feasibility of real-time adaptive observing has been demonstrated, but the degree of flexibility required is very significant.

An example of target determination, associated flight plan and impact of the data collected as a result is presented in Short Note 2.4, together with an example of overall assessment. See also Short Note 1.8 for the theoretical perspective opened by adaptive observation.

The effectiveness of this strategy is further discussed in the work of Szunyogh *et al.* (1999), Bergot (1999), Bishop and Toth (1998), Langland *et al.* (1999), Buizza and Montani (1999) and Pu and Kalnay (1999).

Table 2.2: *Subjective synoptic characterization of the FASTEX cases. The cases are summarized in Part 3 of the report. On the screen version, the page numbers are hypertext links.*

	Comma cloud-like feature	Second generation wave	Rapid development stage	Clear stage of baroclinic interaction	Suppressed waves (stable front)	See page
IOP 1	–	front	–	●	–	99
LOP 1	–	jet/front	–	–	–	100
IOP 2	●	front	–	–	slow gen	101
IOP 3	–	–	●	●	–	102
IOP 4	●	–	–	–	–	103
IOP 5	●	–	–	–	–	104
IOP 6	–	tempo	–	–	●	105
IOP 7	–	tempo	–	–	●	106
IOP 8	–	–	–	–	–	107
IOP 9	–	jet/front	–	●	–	108
IOP 10	–	front	–	–	–	109
IOP 11	–	–	●	●	–	110
LOP 2	–	front	–	●	–	111
IOP 12	–	jet/front	● ●	●	–	112
IOP 13	–	–	–	●	–	113
LOP 3	–	front	–	–	–	113
IOP 14	–	–	–	●	–	114
IOP 15	–	jet/front	●	●	–	115
IOP 16	–	jet/front	●	–	–	116
LOP 4	●	–	–	–	–	117
IOP 17	–	jet/front	●	●	–	118
LOP 5	–	front	●	–	–	119
IOP 18	●	–	●	●	–	120
LOP 6	–	fronts	–	–	–	121
IOP 19	–	front	●	●	tempo	122

Symbol ● means "yes" or "present"
An entry in column 2 means that the system started as a second generation wave. It gives an idea of its environment, "front" being obvious, "jet" meaning presence of a jet-streak or entrance, "tempo" meaning that waves existed temporarily or, in the case of IOP19, temporarily hindered.

2.5.5 The FASTEX cases

Another important aspect is the sample of cyclone types that was covered by these measurements. One of the ideas underlying FASTEX is that there is a large variety of cyclones (Ayrault, 1998) and no such thing as a single type (for example, a system growing on a front, always going through the same set stages and having the same structure, as imagined earlier in this century). There is no single "typical" FASTEX cyclone. It is important that the FASTEX sample reflects this diversity.

More or less in real time, B. Pouponneau, from Météo-France, prepared a basic atlas of maps based on the operational analyses made during FASTEX which included a significant amount of special FASTEX data. These maps were soon complemented by satellite images provided by the Data Base group (see Part 4). This enabled a subjective classification of the cases to be performed based on the morphology of the system and its environment (Table 2.2). It is meant to be used as a double-entry table: one can look for a short meteorological definition of a given IOP or LOP or alternatively, find in the table which IOP or LOP may provide data on a given type of weather system.

Figure 2.9: *Map showing the trajectories of the cyclones of interest to FASTEX, the location of maximum deepening and its amplitude in mbar/6h derived from the ARPEGE analyses. The trajectory lines and symbols marking the location of maximum deepening indicate the different types of cyclones resulting from the subjective classification of Table 2.2. Dark blue line and asterisk: IOP 12 (largest deepener); Blue lines and circled crosses: end-of-stormtrack cyclones in IOP, LOP are dash-dotted blue lines; purple lines and open triangles: comma-cloud like features, LOP are purple dash-dotted lines; Green lines and filled circles: baroclinic waves in zonal regime, LOP are dashed; Dark green lines and diamonds: baroclinic waves in southern zonal regime; light blue lines and empty sign: non developing waves. These trajectories have been constructed by gathering togather the individual trajectories that can be found in Part 3.*
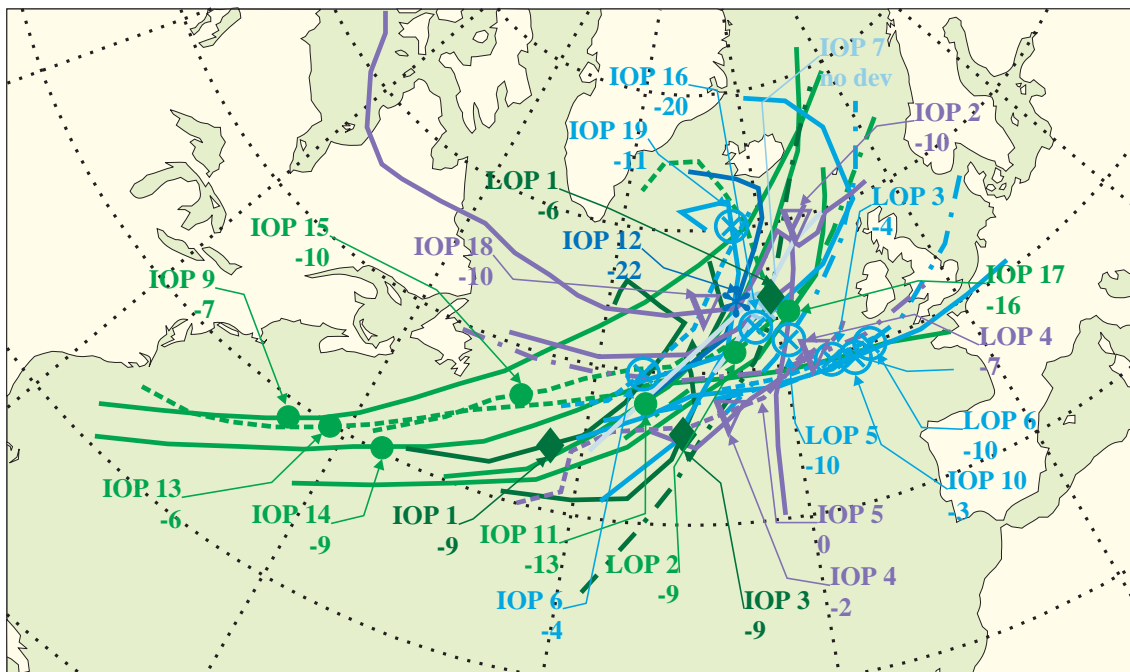
Short Note 2.5:
The forecast routine during FASTEX

by The forecast team from the Centre Météorologique Canadien, the Joint Centre for Mesoscale Meteorology, Met Éireann and Météo-France
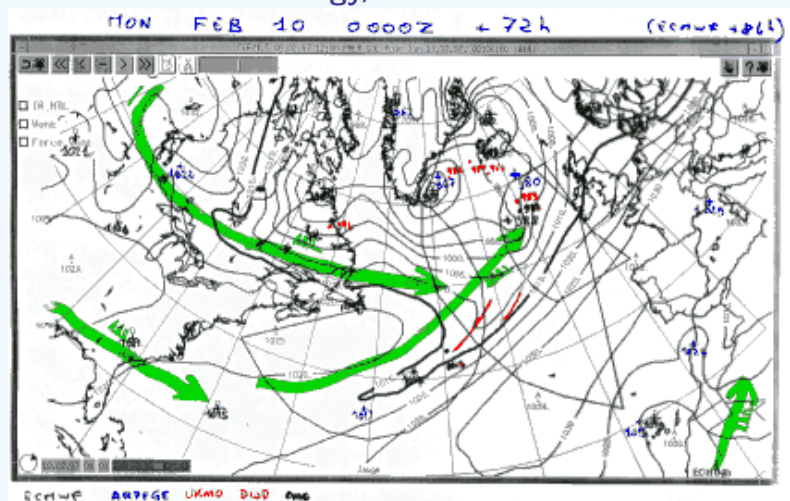
Figure SN2.5.1: *Example of one of the raw components entering the preparation of the consensus forecast: on a transparency based on the previous day's ECMWF forecast, the location and amplitude of the lows in the different models are plotted by the various groups. The example shown is one of the forecast preparing for IOP 12 (see Section 2.3).*

2.5.1 The main schedule and activities

The daily forecast routine set-up all along the field phase was resting on the following basic steps:

0600UT–0730UT Representatives from each group analyse their own numerical forecast products derived from the 00UT observation network. The Météo-France group, in particular, prepares the background transparencies for the summary of low location and amplitude.

From about 0700UT, some more specialized tasks also begin, such as the specific forecast for the ships in the Atlantic or the interpretation of the ensemble forecast from ECMWF (see Short Note 2.6 for one of the products).

0730UT–0800UT Each group completes the series of low location and amplitude summary (Fig. SN2.5.1). The resulting product is a daily series of 6 transparencies covering analysis (Fig. SN2.5.3) time up to 5 days ahead showing the potential cases of interest as well as the possible options and uncertainties.

0800–0830UT Discussion amongst forecasters. The aim is to turn the summary on low locations and amplitude as well as all the details collected within each group into a coherent presentation of the situation, summarized by the "consensus forecast" product (Fig. SN2.5.2). The discussion is led by the group's speaker at the briefing.

0830–0900UT The briefing is being prepared. The consensus forecast is drawn, the images and products

to be shown during the briefing are transferred to the appropriate machines.

0900UT–0940UT Daily weather briefing, described in more details below. The presentations were made by each group in turn, with changes every three days. The audience is the whole FASTEX group at Shannon: scientists, implementation group, the Science Committee, etc.

0940–1030UT The forecast work splits into several activities. Bulletins are written, for example for the ships. A specific 48 h forecast is prepared for each of the ships at sea, so this was generally a long task. Sometimes, operations were running in parallel: this also required specific short-range tasks, such as local evolution monitoring.

The main body of forecasters discusses in front of their respective screens fine points of the current or future weather events with the scientists who are preparing their proposals and come with questions.

1030–1100UT Forecasters attend the daily planning meeting, since they may have, sometimes, to clarify issues. The decisions taken at these meetings also strongly influence future work: aircraft operations typically require special attendance.

1100–1230UT The various bulletins are finalized and sent, a number of groups complete their pages for the World Wide Web, products are archived.

When an Intensive Observation Period was running (or when several of them were overlapping, as happened several times in February), additional monitoring tasks were ran, mostly regarding the aircraft flight: detailed weather forecast for the flight itself, with sometimes briefing of the crew, including the usual discussion of conditions at the main landing places and the alternates, and also a preparation of documents describing the conditions during the flight at a level of details specific of this kind of weather projects. This information was either printed and given to one or two crew members or gathered on a personal computer, such as for the flight planning programmes. Furthermore, during the preparatory stages of an IOP, an update briefing was prepared during the afternoon, starting at about 1530UT. The briefing was held at 1730UT or 1800UT and looked somewhat like a reduced version of the morning briefing, focusing only on solving the uncertainties that led to such or such option.

2.5.2   The Daily Weather Briefing

The briefing featured the following components:

- A GOES and METEOSAT composite image animation (in the "infra-red" or "water vapour" channels) of the previous 24 h is shown. The domain covers the East of North America, the North-Atlantic ocean and western Europe. This product was essentially prepared by the Centre de Météorologie Spatiale in Lannion (France).

- A quasi-hemispheric geopotential map or series of maps is presented in order to give an idea of the planetary scale circulation.

- The surface pressure and frontal analysis on the North-Atlantic is then shown as a transparency. This map usually came from the Central Forecast Office of Bracknell (UK).

- The consensus forecast is presented: the summary transparencies are followed by the expected trajectories of the various lows. As indicated above, the period covered extends from 0 to 5 days ahead.

- Some forecast products representative of the most likely scenario and the possible most likely alternate are then shown, generally in the form of animations on some kind of computer projected on the screen. The products shown vary greatly from day to day.

- The situation of the ships is then recalled and the weather outlook for them is given. The ships went through a storm every other day on average during the field phase.

- the medium-range outlook derived from ECMWF ensemble prediction closes the briefing.

Figure SN2.5.3: *The analysis corresponding to the forecast of Low 34A of IOP 12 (see Section 2.3 and 3.15) of Fig. SN2.5.1 and SN2.5.2. It is interesting to note that, even at this stage, there are some differences between the various numerical weather prediction systems.*

Figure SN2.5.2: *Example of the product called "consensus forecast" resulting from the collective model discussion: the most likely track of lows of interest to FASTEX is drawn, together with some indications on the uncertainties. This example is also one of the documents that were important to plan IOP 12, as in Fig. SN2.5.1 and Section 2.3.*
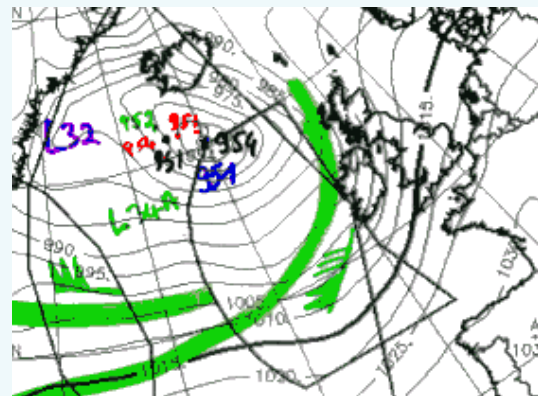
FASTEX is primarily oriented towards cyclones forming well within the oceanic storm-track, in contrast to East-Coast cyclogenesis as studied in programmes such as ERICA (Hadlock and Kreitzberg, 1988) or CASP (Stewart, 1991). The cyclones in FASTEX could be called, using traditional synoptic parlance, frontal waves. However, a more general description might be second generation cyclones, suggesting they form in the wake of another system (considered to be the parent, although this may not be always correct). This is the label retained in Table 2.2, and the parent structure is indicated for cyclones falling in this category of primary interest. An even better description would be end-of-stormtrack cyclones, which simply locates them geographically in a broad sense. Different views relating to the definition and description of these cyclones can be found e.g. in Kurz (1995) in relation to satellite imagery, Hewson (1997) for determining waves automatically or Ayrault *et al.* (1995) and Ayrault (1998) for composite structures extracted from long series of analyses. Figure 2.9 shows a summary of the tracks of all the major cyclones during FASTEX.

Table 2.2 shows that, apart from the non-developing and temporary small amplitude cyclones, there was a mixture of three types of systems forming well over the ocean in the FASTEX sample:

1. cold-air cyclones dominated by convective activity and characterized by their comma-shaped cloud system north of the main baroclinic area (or storm-track, roughly),

2. actual frontal cyclones and

3. cyclones forming within a complex environment combining a low-level front-like feature and an upper-level jet-streak or jet-entrance.

A case is entered in the first column when either a comma-cloud was involved in a life-cycle as precursor or the case itself was a comma cloud. The table also indicates the cases that developed explosively, using in a broad way the criterion of Sanders and Gyakum (1980): a phase of deepening equal to or larger than 24 mbar in 24h. The presence of such a phase is shown by a dot in the "Rapid development stage" column. This happened on 9 occasions.

Table 2.2 identifies those systems that had a clear-cut phase of baroclinic development during their life-cycle. It means that the development of the cyclone benefitted from baroclinic interaction with an upper-level structure, typically an upper-level cyclonic anomaly: such cases are labelled as having a "clear stage of baroclinic interaction". Cyclones having as their only feature this characteristic type of evolution (the simplest cyclones, in that sense) are not the most frequent ones: IOP 3, 11, 13, 14. Most cases add another degree of complexity to simple baroclinic interaction, either when they are generated or by undergoing several phases of growth (see Baehr *et al.* (1999) for a detailed documentation of this process). IOP 14 probably shows the simplest life-cycle, with a phase of growth in the western Atlantic followed by slow decay (however, this low is also the only one to have been clearly advected from the american continent to the ocean, so its past history may be more complex).

The last column of Table 2.2 lists the cases where structures such as fronts bacame wavy but the waves did not develop (dot), or developed very slowly (slow gen) or saw their development temporarily checked (tempo).

Table 2.2 illustrates two levels of diversity or complexity in the FASTEX sample: the existence of different types and the idea of complex life-cycles leading the same system to change type. Contrast IOP 10, that remains a frontal wave throught its marine life cycle with IOP 12, that starts in the same category and ends as a full-scale

Ukrainian participants to FASTEX talking in the radiosounding reception and monitoring room of the V. Bugaev. Photo: T. Douffet, Météo-France.

The Ægir calling to the Irish port of Cork for refuelling and crew relief at the end of January. Photo: P. Bessemoulin, Météo-France.

A rare opportunity: a radiosounding is launched in fair weather on the V. Bugaev. Photo: T. Douffet, Météo-France.
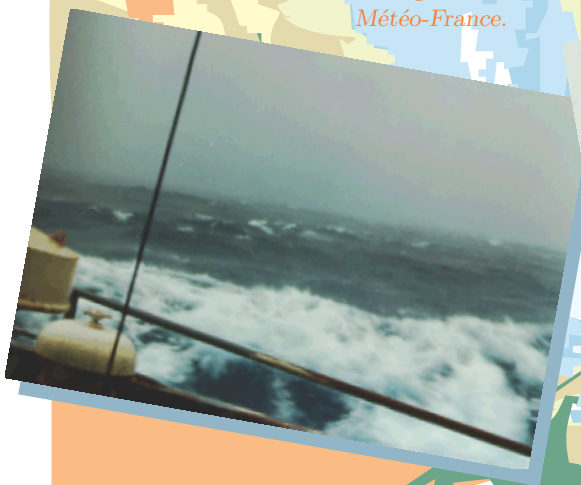
On board the V. Bugaev under the most frequent conditions: uniform grey sky, waves flattened by strong winds. Photos: E. Gizard, Météo-France.

storm. Another example is IOP 18, that turns into a major storm while beginning away from the main baroclinic area. Another subjective classification of the FASTEX cases is provided by Clough *et al.* (1998).

2.6   Forecasts during FASTEX

The forecast activity during the FASTEX field phase was, by design, an experiment within the experiment. The requirements were quite demanding: (1) produce once, and sometimes twice a day, medium-range forecasts of cyclone tracks, (2) refine forecast life-cycles enough to prepare flight plans, (3) monitor the evolution using fine-mesh models and satellite imagery in real time and over a long period.

The forecasts were prepared at Shannon operations centre by teams from four groups: the Canadian Meteorological Center, the Irish Meteorological Service, Météo--France and the UK Meteorological Office. An important aspect of this exercise was the cross-exchange of tools, concepts and approaches between members of these groups. All groups brought to Shannon their familiar working environments, namely their model output, display systems, etc. Most of the participants seemed pleased with this approach and learned a lot from each other.

The diversity of models extended beyond the ones provided by these participating groups: the ECMWF model was available from several sources (for example, the

Short Note 2.6:
The forecast of weather regimes

by G. Hello, F. Lalaurette, P. Santurette

The relevant weather pattern on the time scale of the week is, as explained in the Short Note 1.1, the weather regime. This as well as Short Note 1.2 and Fig. 1.4 in Part 1 reveal the strong connection between the occurrence of cyclones in the eastern Atlantic and the regime. It will not come as a surprise, as a result, that the advanced planning of FASTEX relied on a medium-range forecast of weather regime.

The basis for this forecast is the ECMWF Ensemble Prediction. During the field phase, it was made of 50 trajectories obtained with a T106L31 version of ECMWF IFS/ARPEGE model, plus the reference high resolution forecast (Molteni et al., 1996). The trajectories are initialized using singular vectors. ECMWF provided several products derived from the Ensemble Prediction for FASTEX (special classification, single maps, etc).

The Laboratoire de Prévision of the Operational Division of Météo-France has developed, from these products, a projection on the weather regime patterns shown in the Short Note 1.1. Each trajectory is projected, so that for each range, an empirical probability of occurrence of the four regimes is available. The forecasted weather regime is simply the most frequent one in the sample of 51. It is easy to add an information on uncertainty based on the size of the full distribution of frequencies (the larger is the majority of the forecasted regime, the most likely is the forecast).

The results are shown by Fig. SN2.6.1. It appears that the weather regimes are predicted very well up to day 7. This is a remarkable, practical result. It is a significant achievement of the ECMWF approach to medium-range forecast. It also embodies the current limit of predictability: while the forecast as implemented delivers a kind of deterministic information on the regime, the latter is only the large scale part of the flow: the characteristics of the finer scale features, including the cyclones, are known only statistically, either from the climatology associated to the regime or to the high-frequency information that can be extracted from the Ensemble Forecast.

Figure SN2.6.1: *Distribution of weather regimes forecasted during FASTEX using the ECMWF Ensemble Prediction, analyzed (bottom) and at 4, 7 and 10 days respectively.*
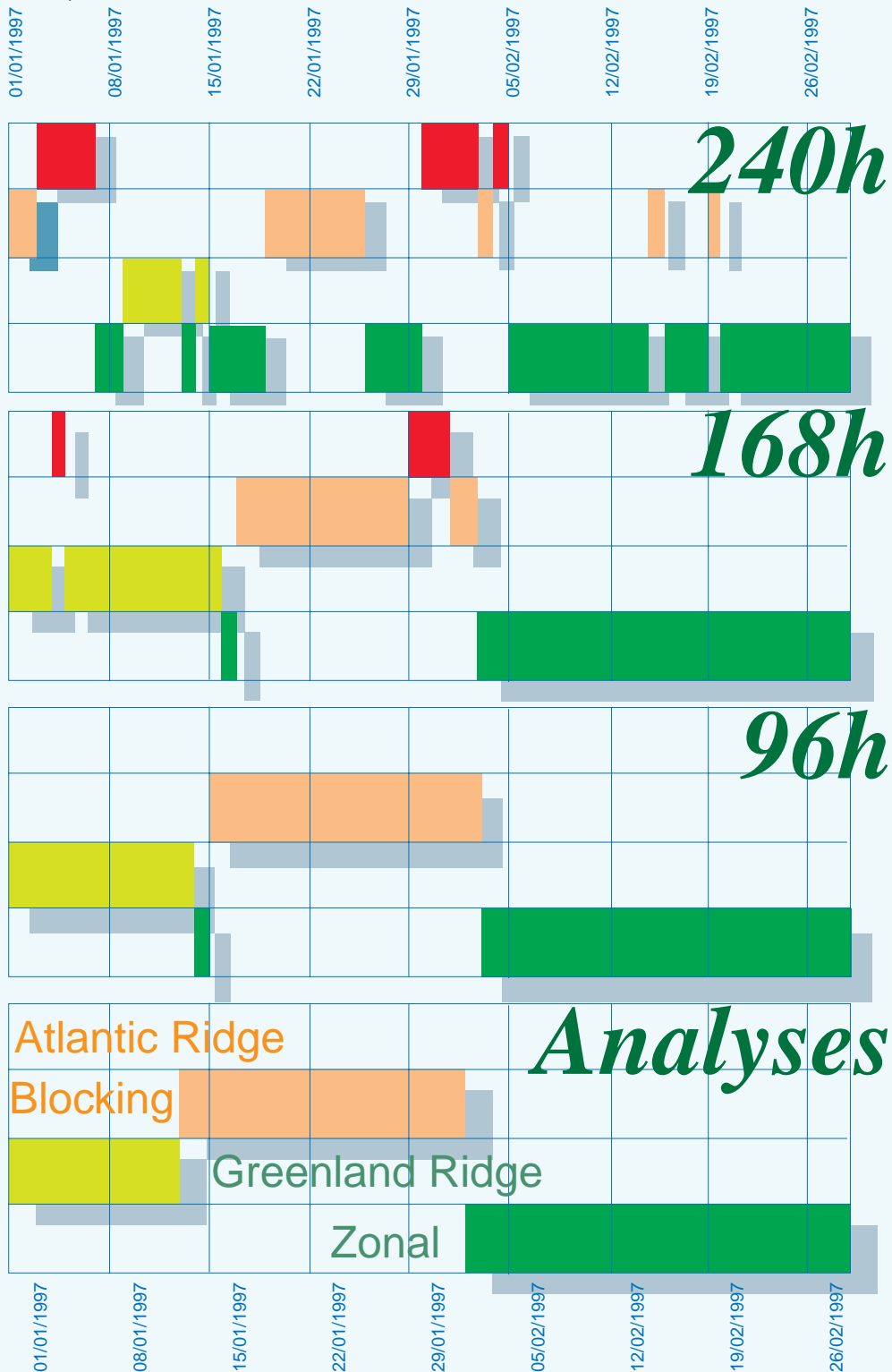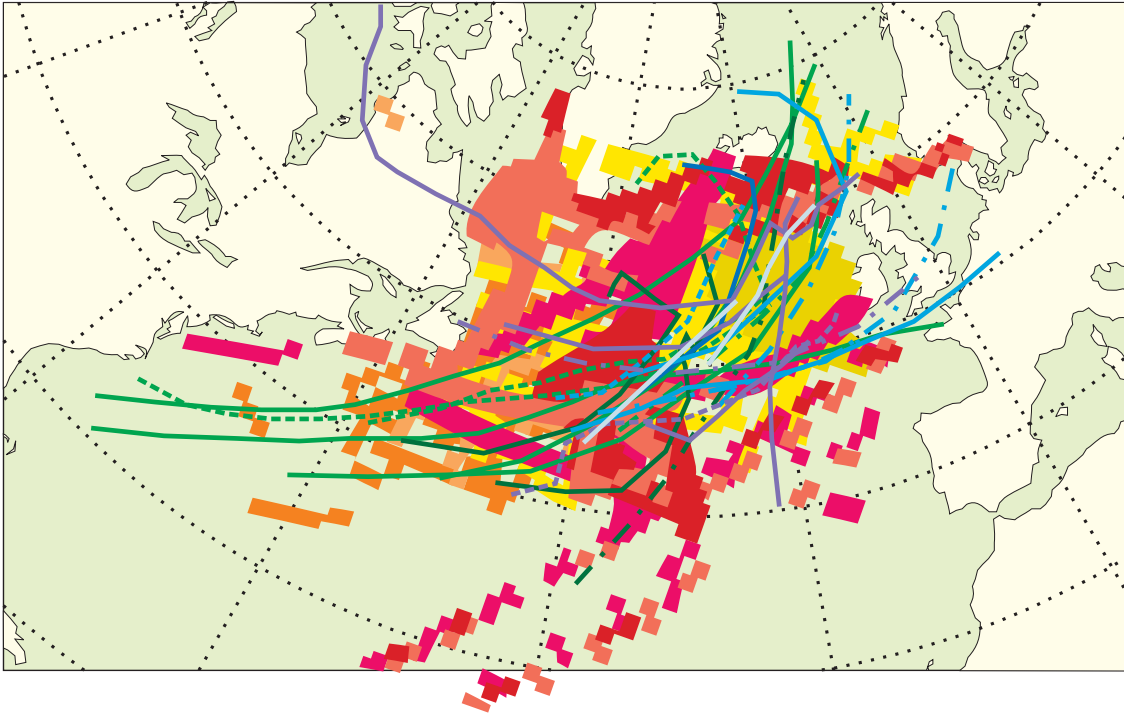
Figure 2.10: *A summary of FASTEX: the trajectories of the lows of interest to the project (as in Fig. 2.9) are superimposed on the distribution of the vertical soundings taken by the ships (reddish zones) and by the aircraft (other shaded areas). This is only a part of the FASTEX data, but the fitting indicates the life-cycle tracking has been quite effective. Distribution areas provided by G. Jaubert, (Météo-France) and shown in more details in Part 4.*

Irish Met Éireann provided the 00UTC ECMWF run) and the Deutscher Wetterdienst model was also employed on the longer ranges. On occasions, results from US models were also available.

The main outputs of the forecast teams were: (1) a medium-range forecast based on the ECMWF ensemble, expressed in terms of weather regimes (as defined in section 2.2), (2) maps of the dispersion of cyclone centers predicted by the different models, (3) a consensus 4-day forecast of cyclone tracks resulting from comparing and discussing all the available models explicitely identifying the uncertainties, for example by adding error-bars to the cyclone tracks, (4) a detailed 2-day forecast including winds and sea-state for each of the ships and (5) detailed weather information for each of the planned flights. An example of consensus forecast and the backbone schedule are presented in the Short Note 2.5.

2.7   Concluding remarks

The experimental objectives of FASTEX as a field project, as defined in section 1.5, have been fulfilled, this statement being justified by most of this Part. A number of cyclones have successfully been multiply sampled as they crossed the North-Atlantic. The cases sampled in this way and those observed in much more detail in the Multi-scale Sampling Area, do reflect some of the variability of recent mid-latitude cyclone

Briefing, or rather debriefing the MSA flights after IOP 5: P. Hildebrand from NCAR summarizes the events of the past day and the Shannon people listen. All briefings took place here. Photo: N. Raynal, Météo-France.
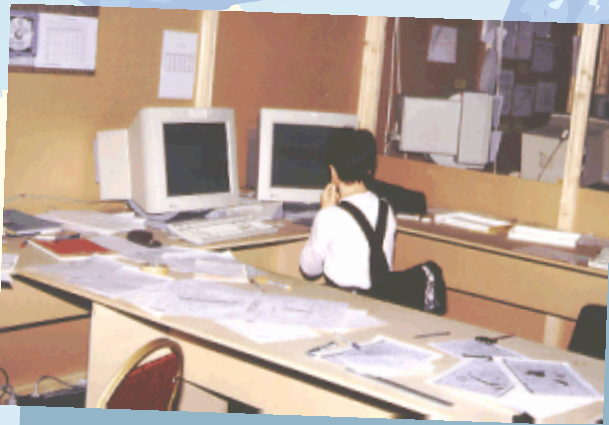
Head forecaster B. Benech in front of the twin-screen SYNERGIE workstation: a picture of the Shannon set-up prepared by Aer Rianta inside the air terminal. Photo: N. Raynal, Météo-France.
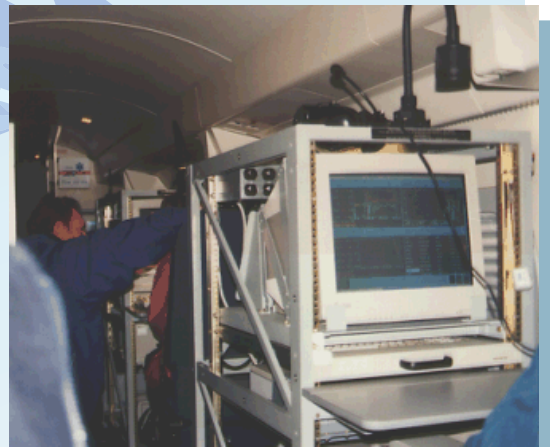
D. Jorgensen from NOAA inside the Gulfstream-IV in flight during IOP 6, trying to support D. Bartels, also from NOAA, preparing the TEMPDROP messages. Photo: F. Lalaurette, Météo-France.

Above: the Electra shortly after landing at Shannon. Leading the group: R. Wakimoto, from UCLA. Photo: N. Raynal, Météo-France. Left: the NOAA P3 ready to fly at night from Shannon. Photo: N. Raynal, Météo-France.

classifications typologies. Real time adaptation of the observations to areas critical to improving predictions for cyclones have actually been done for the first time. A unique turbulent fluxes dataset has been collected from the ships. The data have been made available to all within a short time scale.

There are other positive aspects of FASTEX. Between 1993 and 1996, as part of the preparations for the field season, focused scientific studies have been undertaken that proved to be useful to the project: the climatological study of Ayrault *et al.* (1995) determined the optimal period of year, locations and schedules, the idealized observing system experiments of Fischer *et al.* (1998) showed the necessity of the ships, Bishop and Toth (1998) provided some theoretical basis to adaptive observation, Bergot *et al.* (1999) directly addressed practical issues relating to its implementation. In fact, numerical tools and techniques are now reaching a stage where many aspects of costly projects like FASTEX can and should be simulated beforehand. As shown by the overall schedule (Table 1.4), too short a time has been allowed for these studies. New tools for retrieval of 3D-fields on the mesoscale have also been prepared at that time. They combine Doppler radar measurements and other sources such as dropsondes (Protat *et al.* 1997, Protat *et al.* 1998, Montmerle and Lemaître 1997) Training forecasters and flight track planning scientists for FASTEX was carried out in the UK and France during the winter preceding the experiment: this is done for other projects and remains a condition of success. But one can now go much further than this and test the impact different distributions of platforms or observational procedures and limit the consumption of expensive resources for trial or test runs.

The mode of operation of the forecasters was successful thoughout the project — actually, the forecasting routine was started early in December 1996, another condition of success. The consensus forecasts have proved to meet the needs of the project.

Another result is the demonstration of the feasibility of weather ships to be tied to the slowly migrating baroclinic area. Data systematically reaching upper-levels invaluable from a dynamical meteorology point of view have been obtained by the ships catching key components involved in the process of cyclogenesis. Current and future data impact studies add to the critical but successful character of this component of FASTEX (see e.g. Janisková *et al.* (1999) and Desroziers *et al.* (1999), a flavour of which is given in Part 8 of this Report).

The daily running of FASTEX has shown the usefulness, indeed the necessity, of computer aided flight planning. It was required for the MSA operations in order to meet the multiple constraints: the intrinsic complexity of the reference flight patterns, the actual weather and the logistical and air safety regulations. It was found compulsory for operating the Gulfstream because most objectives required its full range. (The computer programs for the MSA were developed by the NSSL and JCMM groups, the one for the Gulfstream by the Laboratoire d'Aérologie.)

Above all, the field phase of FASTEX as a whole has demonstrated the feasibility, despite the manifest difficulties, of a coordinated multi-base, multi-objectives observing system covering a whole ocean and closely associating scientists and meteorologists from many different countries. One way of summarizing the effectiveness of the tracking of the North-Atlantic cyclones is given by Fig. 2.10, where the overall distribution of the soundings taken from the FASTEX main platforms is superimposed on the system trajectories: apart from the earliest phases of some of the cyclones, tracks and data distribution remarkably overlap throughout the ocean: for two-monts, the Atlantic data gap has been filled.

Acknowledgment

2.8   References

Arbogast, Ph. and A. Joly, 1998:
Identification des précurseurs d'une cyclogenèse.
Compte-Rendus à l'Académie des Sciences, Sciences de la Terre et des planètes, **326**, 227–230.

Arbogast, P. and A. Joly, 1998b:
Potential vorticity inversion of a two-dimensional steady flow: application to symmetric instability.
Quart. J. Roy. Meteor. Soc., **124**, 317–339.

Ayrault, F., 1998:
Environnement, structure et évolution des dépressions météorologiques: réalité climatologique et modèles types.
PhD thesis, Doctorat de Université P. Sabatier, Toulouse.
328pp.

Ayrault, F., F. Lalaurette, A. Joly, and C. Loo, 1995:
North Atlantic Ultra-High Frequency variability: an introductory survey.
Tellus, **47A**, 671–696.

Bergot, T., 1999:
Adaptive observations during FASTEX: a systematic survey of the impact of upstream flights.
Quart. J. Roy. Meteor. Soc., **125**, *submitted.*

Bergot, T., G. Hello, A. Joly, and S. Malardel, 1998:
Adaptive observations: a feasability study.
Mon. Wea. Rev., **127**, (5), 743–765.

Bishop, C.H. and Z. Toth, 1998:
Ensemble transformation and adaptive observations.
J. Atmos. Sci., **55**, (-), *accepted.*

Bjerknes, J. and J. Holmboe, 1944:
On the theory of cyclones.
J. Meteorol., **1**, 1–22.

Bjerknes, J. and H. Solberg, 1922:
Life cycle of cyclones and the polar front theory of atmospheric circulation.
Geofys. Publikasjoner, **3**, 1.

Bouniol, D., A. Protat, and Y. Lemaître, 1999:
Mesoscale dynamics of a deepening secondary cyclone (FASTEX IOP 16): three-dimensional structure retrieved from dropsonde data.
Quart. J. Roy. Meteor. Soc., **125**, *submitted.*

Cammas, J.P., B. Pouponneau, G. Desroziers, P. Santurette, A. Joly, Ph. Arbogast, I. Mallet, G. Caniaux, P. Mascart, and M. Shapiro, 1999:
Initiation, triggering and development phases of the FASTEX cyclone (IOP 17): synoptic and dynamic overview.
Quart. J. Roy. Meteor. Soc., **125**, *submitted.*

Chaboureau, J.P. and A.J. Thorpe, 1999:
Frontogenesis and the development of secondary wave cyclones in FASTEX.
Quart. J. Roy. Meteor. Soc., **125**, *in press.*

Chaigne, E., 1998:
Application de l'inversion du tourbillon potentiel.
Master's thesis, Ecole Nationale de la Météorologie, Note de Travail n 618, Toulouse, 86pp.

Clough, S.A., H.W. Lean, N.M. Roberts, H. Birkett, J.P. Chaboureau, R. Dixon, M. Griffiths, T.D. Hewson, and A. Montani, 1998:
A JCMM overview of FASTEX IOPS.
Technical Report 81, Joint Centre for Mesoscale Meteorology, Reading, UK.

Davis, C.A., 1992:
Piecewise potential vorticity inversion.
J. Atmos. Sci., **49**, (16), 1397–1411.

Davis, C.A. and K.E. Emanuel, 1991:
Potential vorticity diagnostics of cyclogenesis.
J. Atmos. Sci., **119**, 1929–1953.

Desroziers, G., B. Pouponneau, J.N. Thépaut, M. Janisková, and F. Veersé, 1999:
Four dimensional variational analyses of FASTEX situations. part II: use of additional observations.
Quart. J. Roy. Meteor. Soc., **125**, *submitted.*

Eymard, L., G. Caniaux, H. Dupuis, L. Prieur, H. Giordani, R. Troadec, and D. Bourras, 1999:
Surface fluxes in the North-Atlantic Current during the CATCH/FASTEX experiment.
Quart. J. Roy. Meteor. Soc., **125**, *submitted*.

Fischer, C., A. Joly, and F. Lalaurette, 1998:
Error growth and kalman filtering within an idealized baroclinic flow.
Tellus, **50A**, (5), 596–615.

Hadlock, R. and C.W. Kreitzberg, 1988:
The Experiment on Rapidly Intensifying Cyclones over the Atlantic (ERICA) field study: objectives and plans.
Bull. Amer. Meteor. Soc., **69**, (11), 1309–1320.

Hewson, T.D., 1997:
Objective identification of frontal wave cyclones.
Meteorol. Appl., **4**, 311–315.

Janisková, M., F. Veersé, J.N. Thépaut, G. Desroziers, and B. Pouponneau, 1999:
Four dimensional variational analyses of FASTEX situations. part I: impact of a simplified physical package in the assimilating model.
Quart. J. Roy. Meteor. Soc., **125**, *submitted*.

Kurz, M.
synoptic-scale waves., chapter .
Volume Images in weather forecasting, M.J. Bader, G.S. Forbes, J.R. Grant, R.B.E. Lilley, A.J. Waters eds, Cambridge University Press, 1995.
187–200.

Langland, R.H., R. Gelaro, G.D. Rohaly, and M.A. Shapiro, 1999:
Targeted observations in FASTEX: adjoint-based targeting procedures and data impact experiments in IOPs-17 and 18.
Quart. J. Roy. Meteor. Soc., **125**, *submitted*.

Lemaître, Y. and A. Protat, 1999:
Pacific and Atlantic bomb-like deepenings in mature phase: a comparative study.
Quart. J. Roy. Meteor. Soc., **125**, *in preparation*.

Mallet, I., Ph. Arbogast, Ch. Baehr, J.P. Cammas, and P. Mascart, 1999:
Effects of a low level precursor and frontal stability on cyclogenesis during FASTEX IOP17.
Quart. J. Roy. Meteor. Soc., **125**, *submitted*.

Mallet, I., J.P. Cammas, P. Mascart, and P. Bechtold, 1999b:
Effects of cloud diabatic heating on the FASTEX cyclone (IOP 17) early development.
Quart. J. Roy. Meteor. Soc., **125**, *submitted*.

Molteni, F., R. Buizza, T.N. Palmer, and T. Petroliagis, 1996:
The ECMWF Ensemble Prediction System: methodology and validation.
Quart. J. Roy. Meteor. Soc., **122**, 73–119.

Montmerle, T. and Y. Lemaître, 1997:
Three-dimensional variational data analysis to retrieve thermodynamical and dynamical fields from various nested measurements.
J. Atmos. Oceanic Technol., **15**, 360–379.

Petterssen, S., G.L. Dunn, and L.L. Means, 1955:
Report on an experiment in forecasting of cyclone development.
J. Meteor., **12**, 58–67.

Petterssen, S. and S.J. Smebye, 1971:
On the development of extratropical cyclones.
Quart. J. Roy. Meteor. Soc., **97**, 457–482.

Protat, A., Y. Lemaître, and G. Scialom, 1997:
Retrieval of kinematic fields using a single beam airborne doppler radar performing circular trajectories.
J. Atmos. Oceanic. Technol., **14**, 769–791.

Protat, A., Y. Lemaître, and G. Scialom, 1998:
Thermodynamic analytical fields from Doppler radar data by means of the MANDOP analysis.
Quart. J. Roy. Meteor. Soc., **124**, 1633–1669.

Pu, Z.X. and E. Kalnay, 1999:
Targeting experiments with the quasi-inverse linear and adjoint NCEP global model: the performance and evaluation during FASTEX.
Quart. J. Roy. Meteor. Soc., **125**, *in preparation*.

Sanders, F. and J.R. Gyakum, 1980:
Synoptic-dynamic climatology of the "bomb".
Mon. Wea. Rev., **108**, 1589–1606.

Santurette, P., F. Lalaurette, Y. Bachimont, and G. Hello, 1999:
A review of forecast during fastex: an overview and some météo-france highlight.
Quart. J. Roy. Meteor. Soc., **125**, *submitted*.

Scialom, G., A. Protat, and Y. Lemaître, 1999:
Vertical structure of a FASTEX secondary cyclone derived from dual-beam airborne radar data.
Quart. J. Roy. Meteor. Soc., **125**, *submitted*.

Stewart, R.E., 1991:
Canadian Atlantic Storms Program: progress and plans of the meteorological component.
Bull. Amer. Meteor. Soc., **72**, (3), 364–371.

Sutcliffe, R.C., 1947:
A contribution to the problem of development.
Quart. J. Roy. Meteor. Soc., **73**, 370–383.

Szunyogh, I., Z. Toth, K.A. Emanuel, C.H. Bishop, C. Snyder, R. Morss, J. Woolen, and T. Marchok, 1999:
Ensemble-based targeting experiments during fastex: the impact of dropsonde data from the Learjet.
Quart. J. Roy. Meteor. Soc., **125**, *submitted.*

Vautard, R., B. Legras, and M. Déqué, 1988:
On the source of midlatitude low-frequency variability. part I: a statistical approach to persistence.
J. Atmos. Sci., **45**, (20), 2811–2843.

Part 3

Summary of the 25 FASTEX cases

by
Alain Joly,
Béatrice Pouponneau,
Geneviève Jaubert,
Catherine Piriou.

Météo-France, URA CNRS 1357, Groupe d'Etude de l'Atmosphère Météorologique, Toulouse, France.

3.1 Reading the graphical case summary

Table 3.1: *The subjective synoptic characterization of the FASTEX cases is repeated at the beginning of this part to be used as a case selection table. On the screen version, the page numbers are hypertext links.*

	Comma cloud-like feature	Second generation wave	Rapid development stage	Clear stage of baroclinic interaction	Suppressed waves (stable front)	See page
IOP 1	–	front	–	●	–	99
LOP 1	–	jet/front	–	–	–	100
IOP 2	●	front	–	–	slow gen	101
IOP 3	–	–	●	●	–	102
IOP 4	●	–	–	–	–	103
IOP 5	●	–	–	–	–	104
IOP 6	–	tempo	–	–	●	105
IOP 7	–	tempo	–	–	●	106
IOP 8	–	–	–	–	–	107
IOP 9	–	jet/front	–	●	–	108
IOP 10	–	front	–	–	–	109
IOP 11	–	–	●	●	–	110
LOP 2	–	front	–	●	–	111
IOP 12	–	jet/front	● ●	●	–	112
IOP 13	–	–	–	●	–	113
LOP 3	–	front	–	–	–	113
IOP 14	–	–	–	●	–	114
IOP 15	–	jet/front	●	●	–	115
IOP 16	–	jet/front	●	–	–	116
LOP 4	●	–	–	–	–	117
IOP 17	–	jet/front	●	●	–	118
LOP 5	–	front	●	–	–	119
IOP 18	●	–	●	●	–	120
LOP 6	–	fronts	–	–	–	121
IOP 19	–	front	●	●	tempo	122

Symbol ● means "yes" or "present"
An entry in column 2 means that the system started as a second generation wave. It gives an idea of its environment, "front" being obvious, "jet" meaning presence of a jet-streak or entrance, "tempo" meaning that waves existed temporarily or, in the case of IOP19, temporarily hindered.

1
6 pictures run-down: satellite images and ARPEGE analyses

Operational ARPEGE analyses, extracted from the online Atlas, on the same area as the images. Continuous lines: mean sea level pressure, interval 5 mbar. Shading and dashed lines: 2m air temperature, interval 2°C.

2.nn   IOP nn, jj–jk JaFeuary

IOP nn		
low n°		30
formation time	4/2 06	(60W, 37N)
max deepening rate (mbar/6h)	5/2 06	(39W, 44N) -13
max amplitude (mbar)	7/2 00	(5W, 68N) 950
end of tracking time	7/2 00	(5W, 68N)
US RS	→	4/2 00
LearJet	4/2 1415	0330 15
C130 USAF	4/2 1615	0945 13
Gulfstream (1)		
KNORR	6/2 0000	48 15 (51W, 51N)
ÆGIR	6/2 0300	24 9 (24W, 47N)
SUROÎT	6/2 0000	48 12 (31W,44N)
V. BUGAEV	5/2 0000	48 8 (35W,41N)
Other ships		
Gulfstream (2)		
C130	5/2 2300	1000 38
P3 NOAA	6/2 0145	1000
Electra	5/2 2200	0700 ss
Gulfstream (3)	6/2 0530	22

jj mm hhUT

Date and time.

2
Weather system and operations overview table

GOES and METEOSAT infra-red images, centered on the system of interest, extracted from the on-line Atlas.

On occasions, this 850 mbar map is shown. Light blue lines are geopotential. Red lines show absolute vorticity maxima, dark blue lines vorticity minima.

IOP nn

3
Schematic summary showing tracks

Two-part table:
- top: some key properties of the weather system,
- bottom: operations summary, by zone and by facility.

US RS: 4 East-Coast radiosounding stations move to launch every 6h. Indicated:
- date/time of beginning (left) or end (right)of increased frequency.
- $\longrightarrow$ symbol meaning continuation.

Upstream flights by LearJet, USAF C-130 or Gulfstream. Indicated for all flights:

Midflight date - time	Flight duration	Number of dropsoundings in Data Base

Ship operations, with indications on the period of intensive soundings (either 3h or 1.5h):

Mid-period date - time	Period duration	Number of soundings in Data Base (ship location)

US RS	$\longrightarrow$	4/2 00
LearJet	4/2 0330	15
	1415	

SUROÎT	6/2 48	12
	0000	(31W,44N)

Multiscale Sampling Area flights. Indications as for other flights with "ss" for Systematic Survey flight pattern and "mi" for Mesoscale Investigation by the Doppler radar carriers.

Increased frequency of european West-Coast soundings. Indicated (left to right): date-time of *beginning* of intensive period; duration; number of *stations* involved.

Electra	5/2 0700	ss
	2200	

European RS	6/2 06 18	4

Relevant weather system trajectories, 6 hourly marks:
- filled circle: depression
- empty circle: trough
- white wedge: open wave
- filled wedge: wave depression
- thin lines: link simultaneous marks

Radiosounding land stations launch frequency:
- 2 soundings/day
- 4 soundings/day on alert
- 4 soundings/day permanent
- 8 soundings/day on alert

Other symbols for weather systems:
- comma cloud
- weak vorticity maximum
- significant fronts
- weak convective cloud cluster
- upper-level anomaly of P and its trajectory

Sketch of relevant flight tracks:
Orange: LearJet, US-C130
Dark red: Gulfstream IV
Blue: one of the MSA tracks chosen from generally combined flights

FASTEX dedicated research ships, at their intensive sounding position (dot).
From left to right: Ægir; Suroît; Knorr; Victor Bugaev.
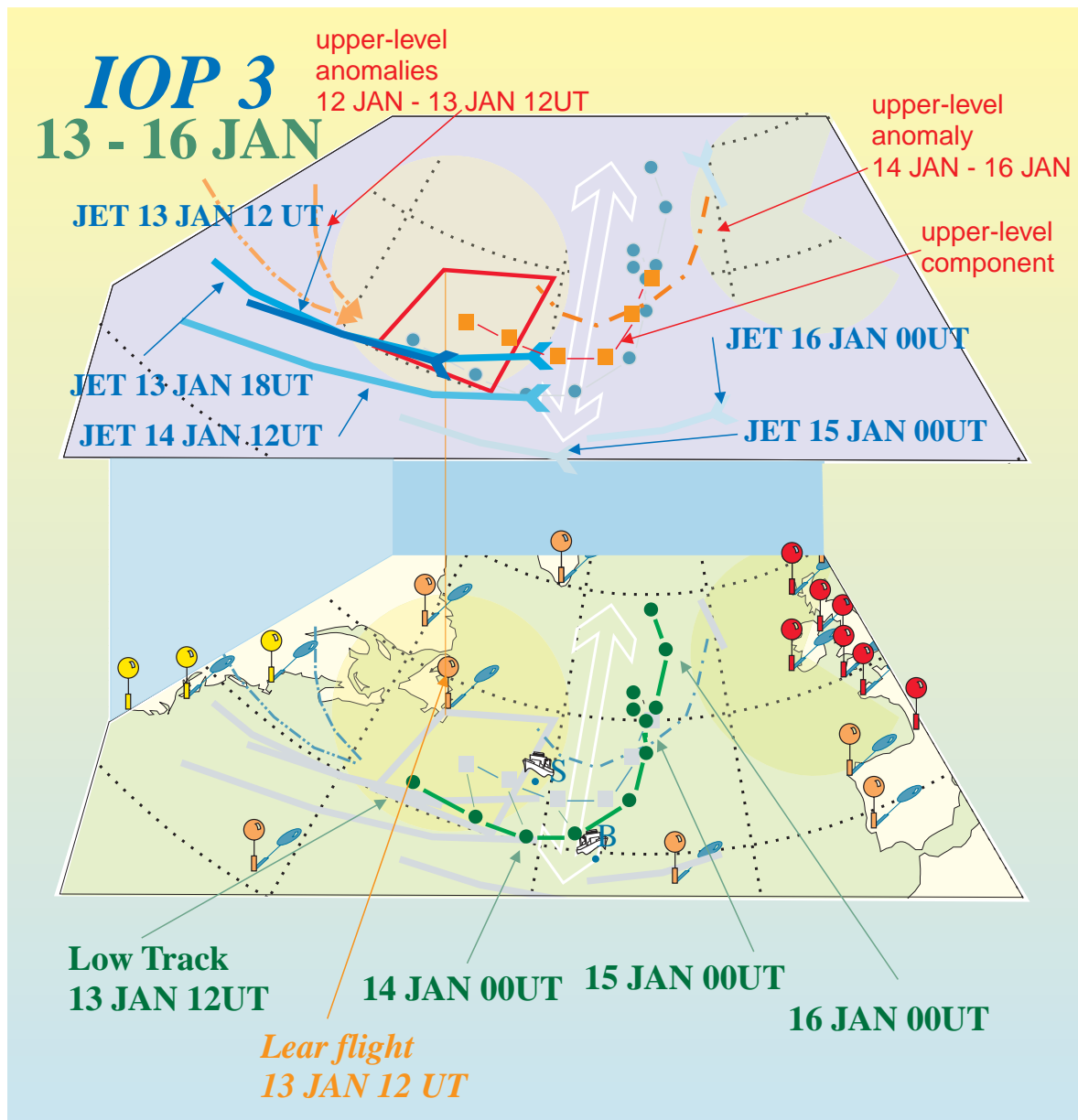Arrow indicates ship displacement when this happened.

Figure 3.1: *One early example of schematic summary for an IOP. This type of diagram attempts to provide a dynamical interpretation of the case together with where and when the observing facilities were employed.*

3.2   IOP 1, 8–11 January

8 JAN 06UT
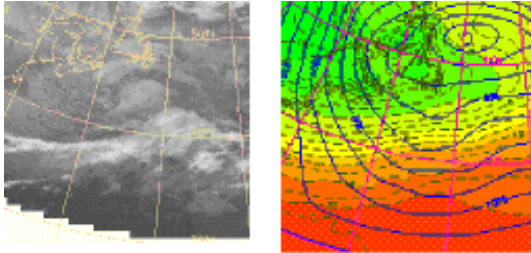
9 JAN 06UT
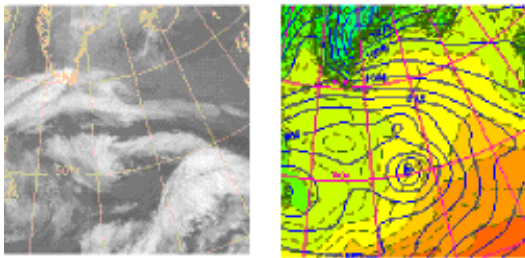
10 JAN 06UT
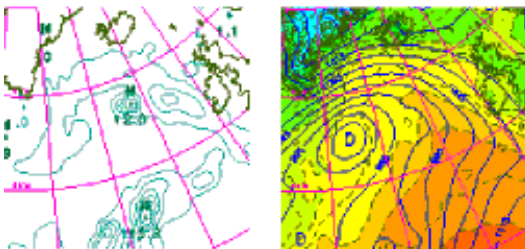
IOP 1

	8A		low n°
8/1 06	(54W, 41N)		formation time
8/1 12	(47W, 42N) -9		max deepening rate (mbar/6h)
10/1 00	(33W, 54N) 968		max amplitude (mbar)
11/1 00	(40W, 55N)		end of tracking time
8/1 18	→		US RS
			LearJet
			C130 USAF
			Gulfstream (1)
9/1 1200	24 (35W, 42N)	4	KNORR
9/1 0900	18 (35W, 46N)	6	ÆGIR
9/1 1200	24 (31W, 39N)	2	SUROÎT
			V. BUGAEV
			Other ships
			Gulfstream (2)
10/1 0745	0730	21	C130
10/1 0630	0840		P3 NOAA
10/1 0600	0500	ss	Electra
			Gulfstream (3)
10/1 12	24	5	European RS
			Other facilities

3-hourly soundings from ships; 9 JAN 12UT

P3, Electra, C130 10 JAN 06UT

Low 8A trajectory; begins 8 JAN 12UT

IOP 1
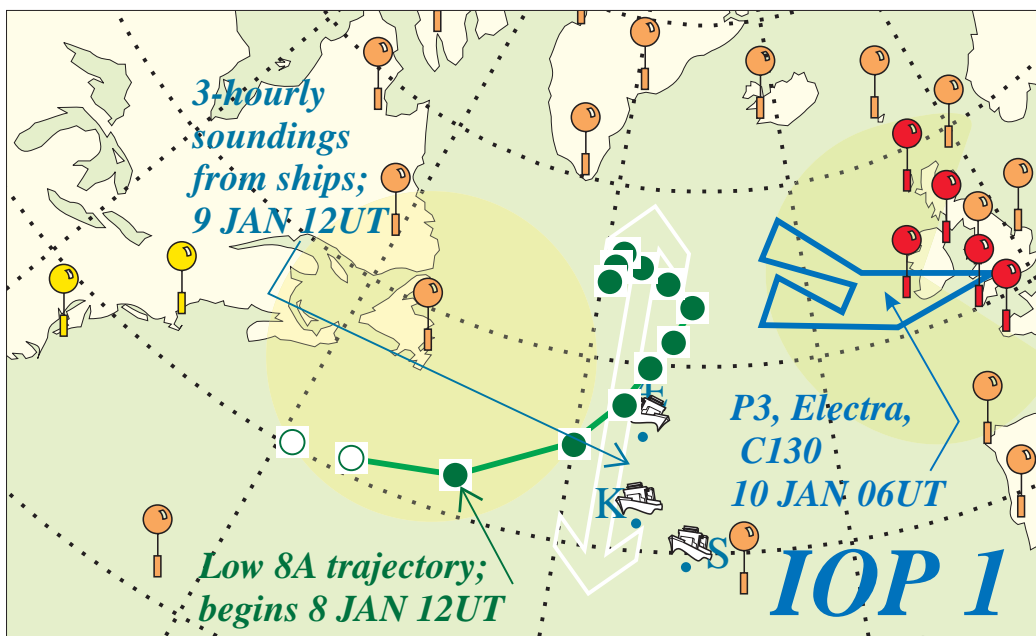
3.3 LOP 1, 10–12 January

LOP 1		
low n°	10	
formation time	10/1 00	(37W, 40N)
max deepening rate (mbar/6h)	11/1 00	(22W, 53N) -6
max amplitude (mbar)	11/1 12	(29W, 59N) 973
present in MSA end of tracking time	11/1 06 12/1 12	(20W, 56N) (1W, 68N)
Upstream data	US RS	
Ships	3 ships 9/1 10/1 Bugaev 10/1	4 s/d K, Æ, S 8 s/d (35W, 38N)
Downstream data	Eur RS	→11/1 12

10 JAN 12UT

11 JAN 06UT

11 JAN 12UT

Bugaev: 8 s/d; 10 JAN

Low 10 trajectory; 9 JAN 18UT

FLOP 1

3.4 IOP 2, 11–13 January

12 JAN 00UT

12 JAN 12UT

13 JAN 00UT
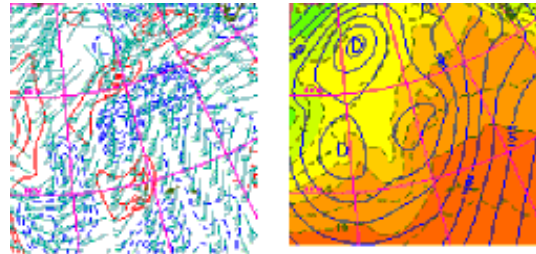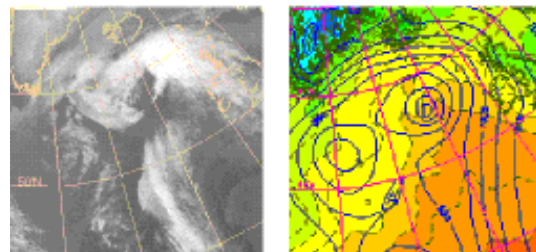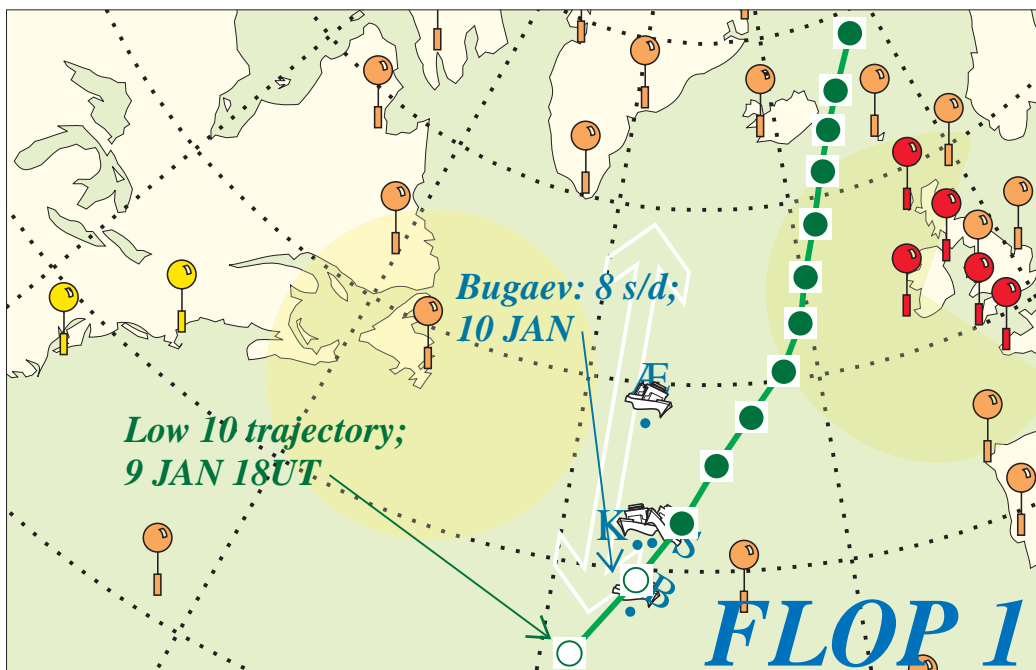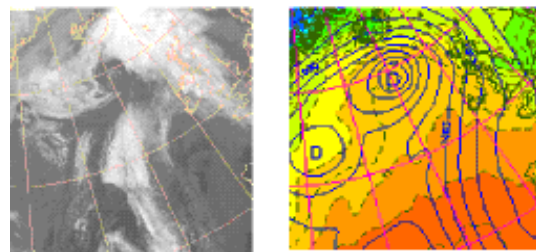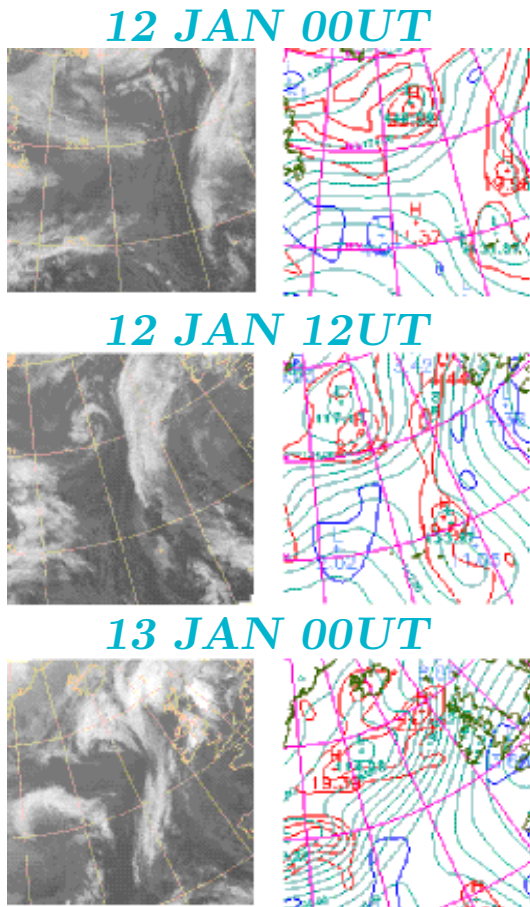
IOP 2		
	11	low n°
11/1 18	(23W, 40N)	formation time
13/1 00	(18W, 53N) -10	max deepening rate (mbar/6h)
13/1 00	(15W, 59N) tlw 978	max amplitude (mbar)
13/1 00	(15W, 59N)	end of tracking time
⟶	12/1 18	**US RS**
11/1 1500	0345 11	**LearJet**
		C130 USAF
		Gulfstream (1)
10/1 2230	15 4 (35W, 42N)	**KNORR**
		ÆGIR
10/1 2230	15 4 (34W,41N)	**SUROÎT**
10/1 1800	36 10 (35W,38N)	**V. BUGAEV**
11/1 06-18	2 ASAP	**Other ships**
		Gulfstream (2)
12/1 1500	0945 42	**C130**
12/1 1615	0900	**P3 NOAA**
12/1 1615	0700	**Electra**
		Gulfstream (3)
12/1 12	24 5	**European RS**
		Other facilities
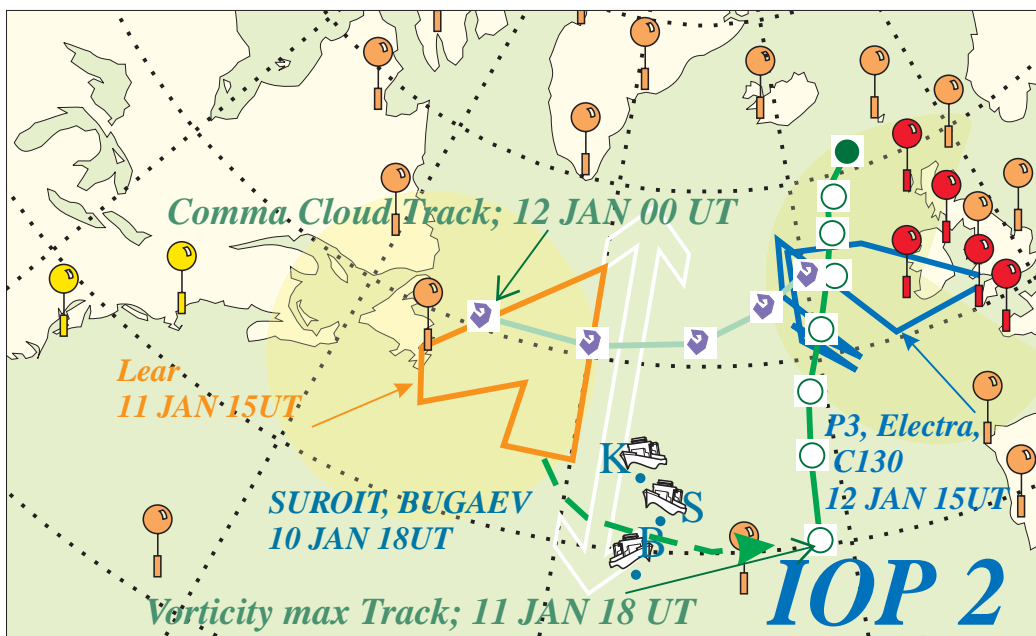
3.5   IOP 3, 13–16 January

IOP 3		
low n°		14
formation time	13/1 12	(53W, 41N)
max deepening rate (mbar/6h)	14/1 12	(32W, 43N) -9
max amplitude (mbar)	15/1 18	(29W, 51N) 973
end of tracking time	16/1 06	(28W, 58N)
US RS	13/1 06	14/1 06
LearJet	13/1 1215	0430 14
C130 USAF		
Gulfstream (1)		
KNORR	14/1 2100	18 4 (35W, 45N)
ÆGIR	15/1 0300	18 6 (35W, 49N)
SUROÎT	14/1 0900	18 11 (41W, 46N)
V. BUGAEV	14/1 0900	18 13 (35W, 42N)
Other ships		
Gulfstream (2)		
C130		
P3 NOAA		
Electra		
Gulfstream (3)		
European RS	16/1 06	24 5
Other facilities		

13 JAN 12UT

14 JAN 12UT

15 JAN 12UT

Lear 13 JAN 12UT

Genesis area; 13 JAN

Æ

SK

B

Numerous soundings from ships 14-15 JAN

Low 14 trajectory; 13 JAN 18UT

IOP 3
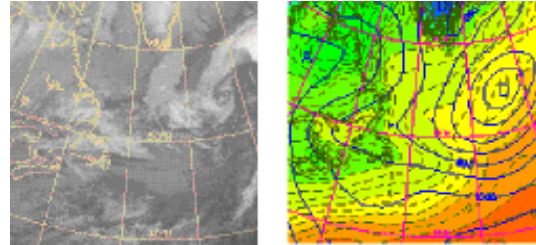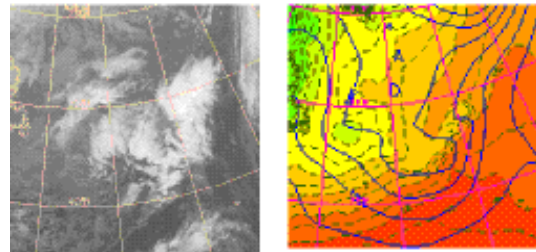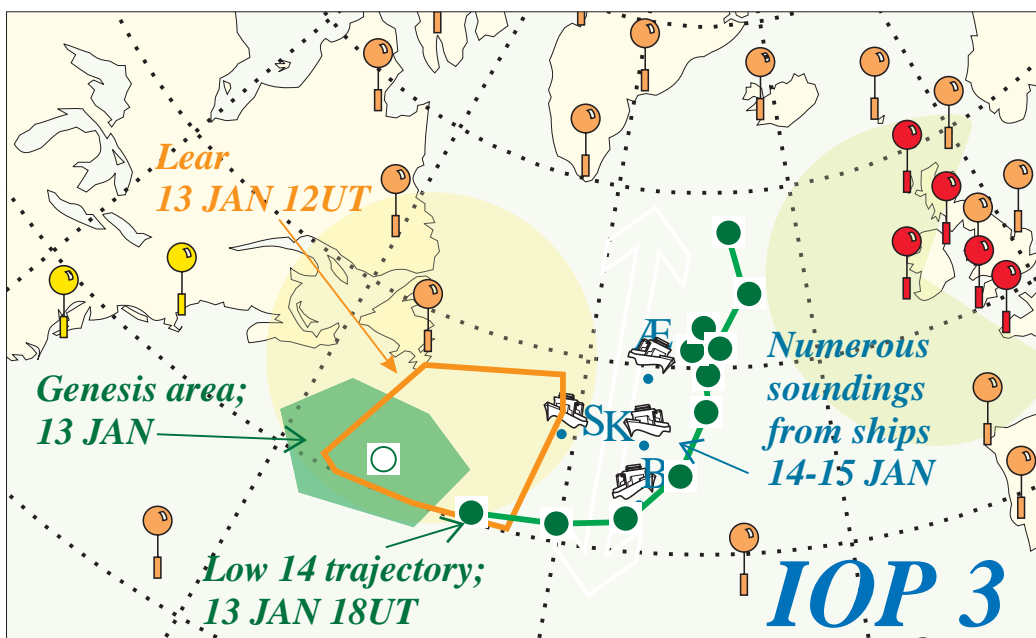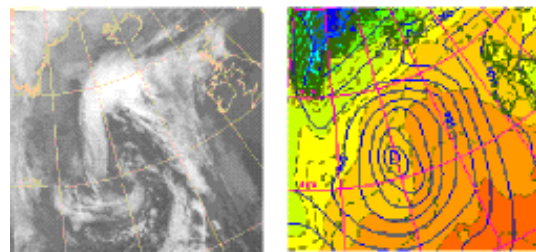
3.6   IOP 4, 16–18 January

16 JAN 12UT
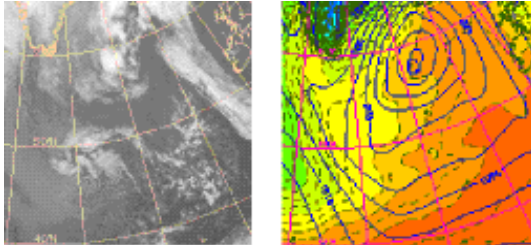
17 JAN 00UT
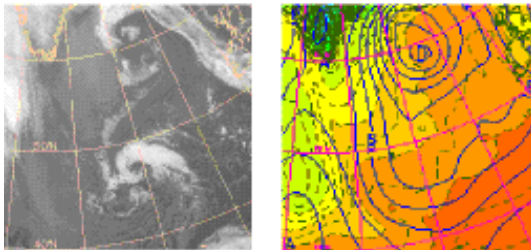
17 JAN 06UT
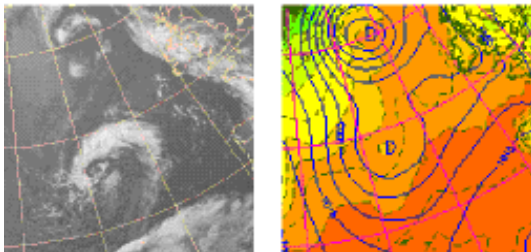
IOP 4		
	18	low n°
16/1 18	(33W, 47N)	formation time
17/1 06	(27W, 47N) -2	max deepening rate (mbar/6h)
17/1 12	(25W, 48N) 995	max amplitude (mbar)
18/1 06	(15W, 52N)	end of tracking time
		US RS
		LearJet
		C130 USAF
		Gulfstream (1)
16/1 1500	18 (35W, 46N)	2	**KNORR**
16/1 1500	18 (35W, 50N)	11	**ÆGIR**
16/1 1500	18 (43W, 47N)	11	**SUROÎT**
16/1 1500	18 (35W, 42N)	7	**V. BUGAEV**
		Other ships
		Gulfstream (2)
		C130
		P3 NOAA
		Electra
17/1 1215	0645	22	**Gulfstream (3)**
18/1 18	24	5	**European RS**
19/1 00	24	7	
		Other facilities

Gulfstream
17 JAN 12UT

Æ

S

Low18 trajectory;
16 JAN 12UT

B

IOP 4
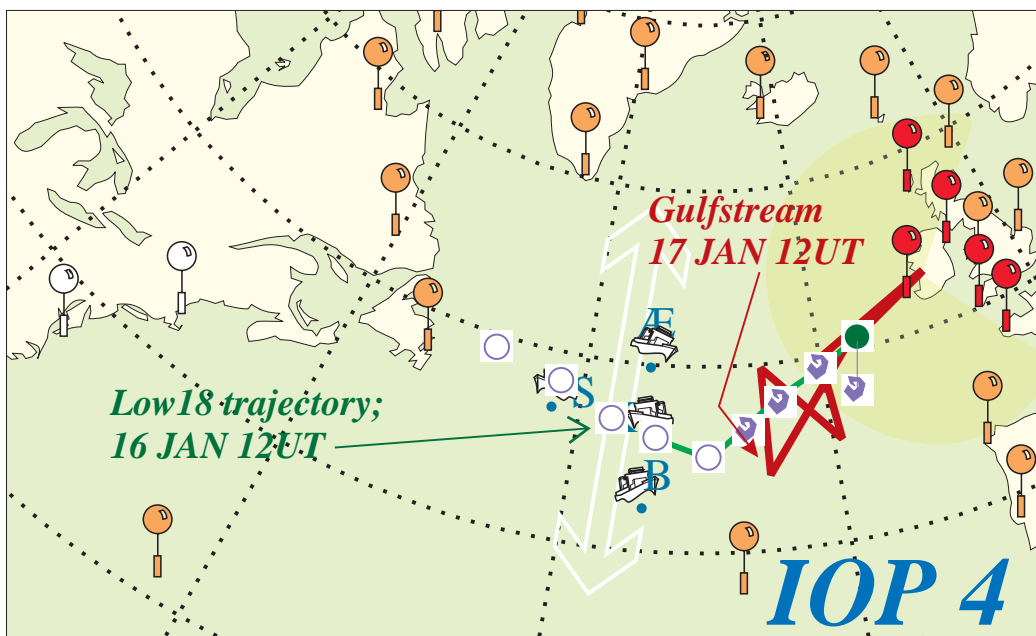
3.7   IOP 5, 22–23 February

IOP 5			
low n°	19 A/B		
formation time	22/1 00	(25W, 47N)	
max deepening rate (mbar/6h)	no significant pressure fall		
max amplitude (mbar)	22/1 18	(17W, 44N) 1008	
end of tracking time	23/1 06	scission	
US RS	19/1 18	20/1 18	
LearJet	20/1 1130	0445	14
C130 USAF			
Gulfstream (1)			
KNORR	20/1 2100	18 (48W, 45N)	0
ÆGIR	22/1 0000	48 (35W, 52N)	10
SUROÎT	20/1 2100	18 (35W,47N)	11
V. BUGAEV	21/1 0600	24 (35W,45N)	7
Other ships			
Gulfstream (2)			
C130	22/1 0915	0430	∼0
P3 NOAA	22/1 1345	0930	
Electra	22/1 1200	0600	ss
Gulfstream (3)	22/1 1215	0315	0
European RS	22/1 15	24	7
Other facilities			

22 JAN 00UT

22 JAN 12UT

23 JAN 00UT

310K P anomaly trajectory; 20 JAN 00UT

(Gulfstream 22 JAN 12UT)

P3, Electra, (C130) 22 JAN 14UT

Lear 20 JAN 12UT

System 19A trajectory; 21 JAN 12UT

IOP 5
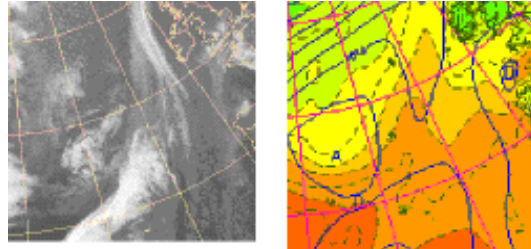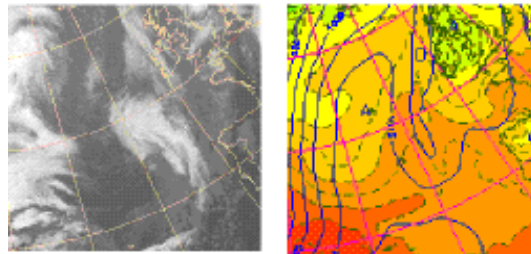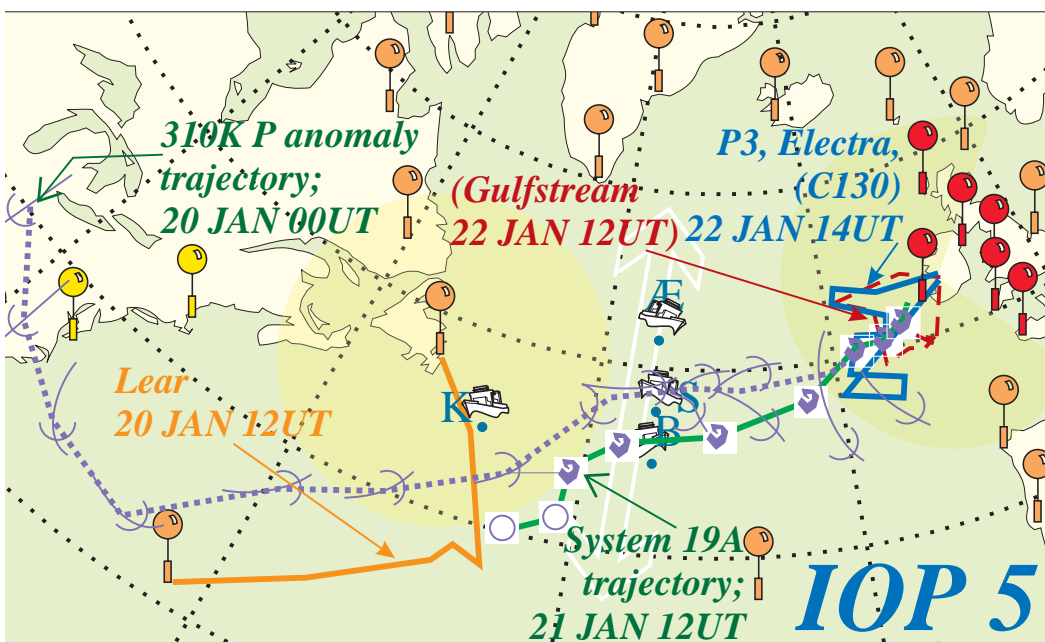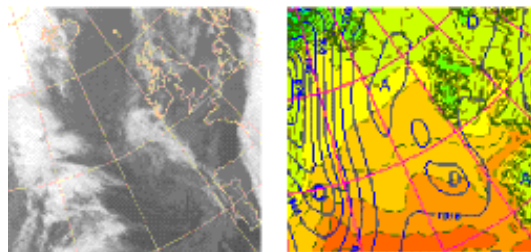
3.8   IOP 6, 22–23 January

22 JAN 18UT
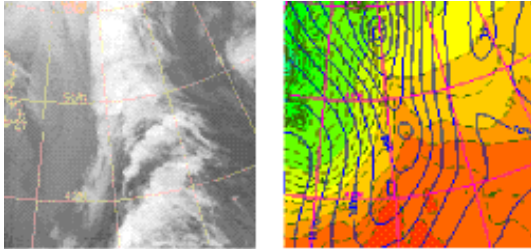
23 JAN 06UT
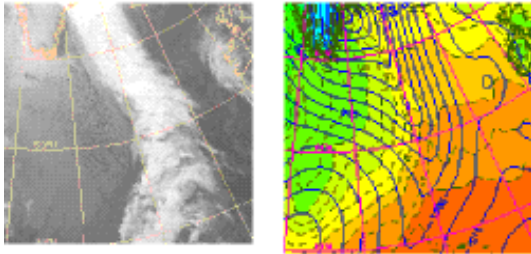
23 JAN 18UT
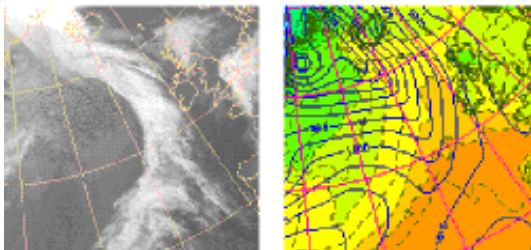
IOP 6		
	20	low n°
22/1 12	(43W, 46N)	formation time
23/1 00	(35W, 50N) −4	max deepening rate (mbar/6h)
23/1 00	(35W, 50N) 984	max amplitude (mbar)
23/1 12	(25W, 57N)	end of tracking time
	22/1 18	US RS
		LearJet
		C130 USAF
		Gulfstream (1)
22/1 1200	24 (49W, 45N) 4	KNORR
23/1 0300	24 (35W, 51N) 6	ÆGIR
23/1 0300	24 (35W, 49N) 7	SUROÎT
23/1 0300	24 (35W, 45N) 10	V. BUGAEV
23/1	1 ASAP	Other ships
		Gulfstream (2)
		C130
		P3 NOAA
		Electra
23/1 1945	0745 16	Gulfstream (3)
24/1 03	24 6	European RS
		Other facilities

Low 20 trajectory; 21 JAN 06UT

Wave 20A trajectory; 22 JAN 18UT

Gulfstream 23 JAN 20UT

Fronts and pseudo-fronts, 23 JAN 18UT

IOP 6
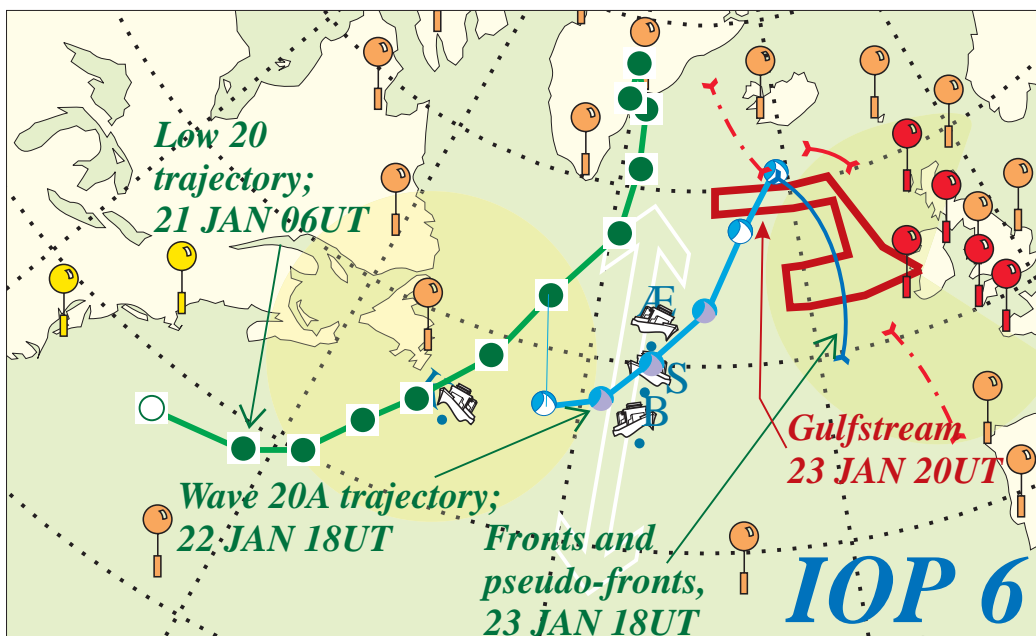
3.9   IOP 7, 25–26 January

IOP 7

low n°	22 A/B		
formation time	25/1 12	(27W, 50N)	
max deepening rate (mbar/6h)	25/1 06	(32W, 47N) < 1	
max amplitude (mbar)	26/1 00	(18W, 55N) tlw 1012	
end of tracking time	26/1 12	(15W, 55N)	
US RS			
LearJet			
C130 USAF			
Gulfstream (1)			
KNORR			
ÆGIR	25/1 0600	24 (35W, 49N)	9
SUROÎT	25/1 0600	24 (35W, 52N)	8
V. BUGAEV	25/1 0600	24 (35W, 45N)	8
Other ships			
Gulfstream (2)	25/1 2015	0630	21
C130	26/1 0030	0700	32
P3 NOAA	26/1 0100	0800	
Electra	26/1 0245	0600	ip
Gulfstream (3)			
European RS	26/1 00	12	4
Other facilities			

25 JAN 00UT

25 JAN 12UT

26 JAN 00UT

Low 22 trajectory; 24 JAN 00UT

Fronts; 26 JAN 00UT

Gulfstream 25 JAN 20UT

Wave 22B trajectory; 25 JAN 12UT

P3, Electra, C130 26 JAN 00UT

Block southern component low, 24-26 JAN

IOP 7
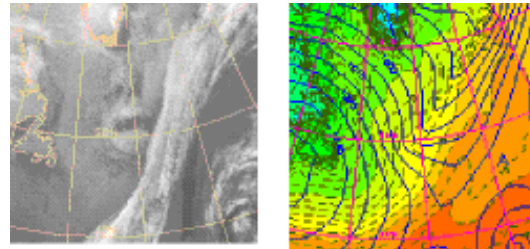
3.10 IOP 8, 27–29 January

27 JAN 00UT

28 JAN 12UT

29 JAN 12UT
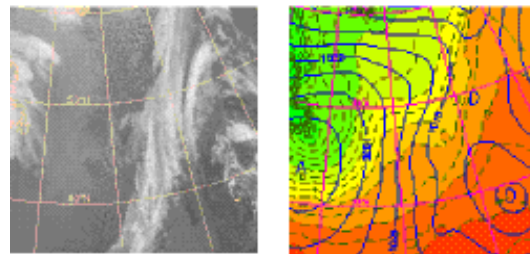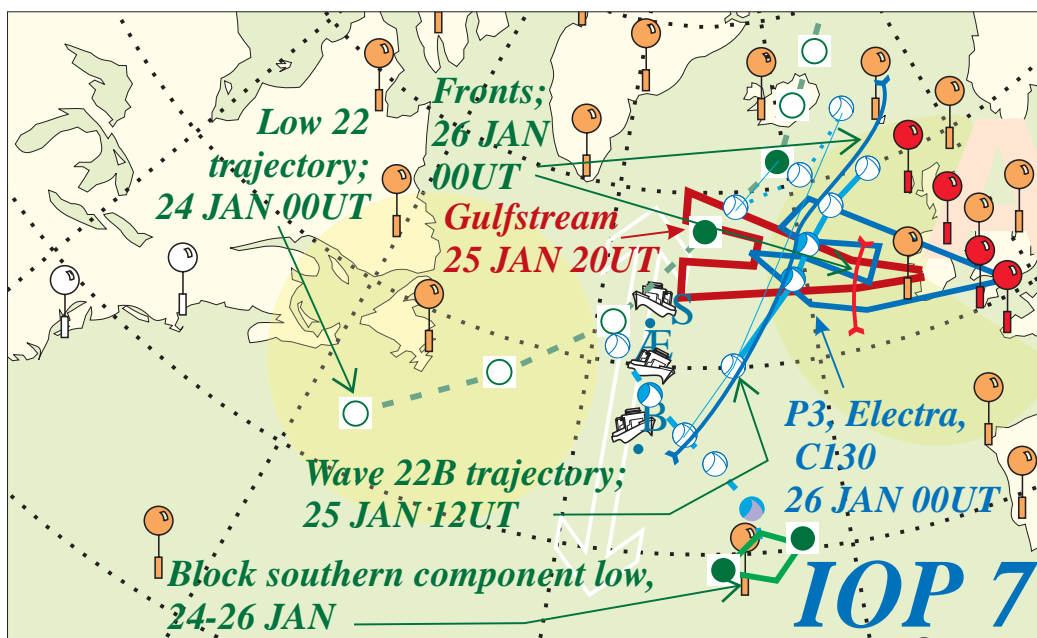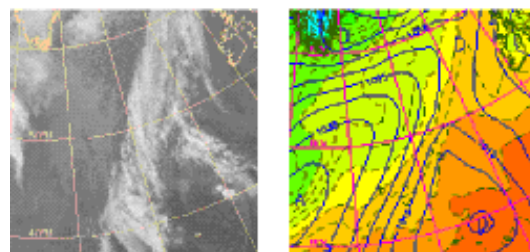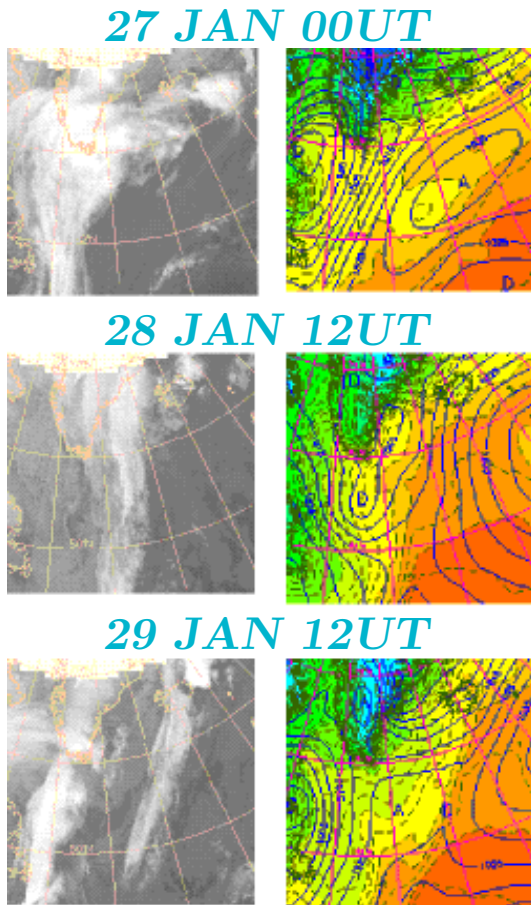
IOP 8	
Greeland Waves	low n°
	formation time
Complex interaction low(s)/orography	max deepening rate (mbar/6h)
	max amplitude (mbar)
	end of tracking time
	US RS
	LearJet
27/1 0600 14 0100	C130 USAF
	Gulfstream (1)
	KNORR
	ÆGIR
29/1 5 (39W,45N)	SUROÎT
	V. BUGAEV
	Other ships
29/1 0715 13 1230	Gulfstream (2)
	C130
	P3 NOAA
	Electra
	Gulfstream (3)
	European RS
	Other facilities

Orography-low-front interaction, 29 JAN

Gulfstream 29 JAN 13UT

Low 24 trajectory; 26 JAN 12UT

US-C130 27 JAN 01UT

Weak waves; 28 JAN 00UT

IOP 8

3.11   IOP 9, 30 January–3 February

IOP 9		
low n°		27
formation time	30/1 12	(78W, 31N)
max deepening rate (mbar/6h)	31/1 12	(66W, 37N) -7
max amplitude (mbar)	3/2 06	(18W, 63N) 975
end of tracking time	3/2 18	(2W, 68N)
US RS	31/1 06	⟶
LearJet	1/2 0000	0330 10
C130 USAF		
Gulfstream (1)	1/2 1145	0530 26 Sh →StJ
KNORR		
ÆGIR		
SUROÎT		
V. BUGAEV	2/2	24 3 (56W, 44N)
Other ships		
Gulfstream (2)		
C130		
P3 NOAA	2/2 2000	0900 7 ss
Electra	2/2 2300	0700 ip
Gulfstream (3)		
European RS	3/2 03	18 5
Other facilities	Norssarsuaq 1/2 18 8	

1 FEB 00UT

2 FEB 00UT

3 FEB 00UT

Gulfstream 1 FEB 12UT

US C130 2 FEB 17UT

P3, Electra 2 FEB 20UT

Lear 1 FEB 00UT

Parent Cyclone Track; 1 FEB 00 UT

Frontal wave Track; 3 FEB 18 UT

Gulfstream 3 FEB 18UT

P3, Electra, C130 4 FEB 10UT

IOP 9 - IOP 10
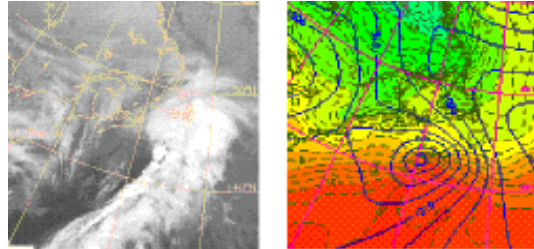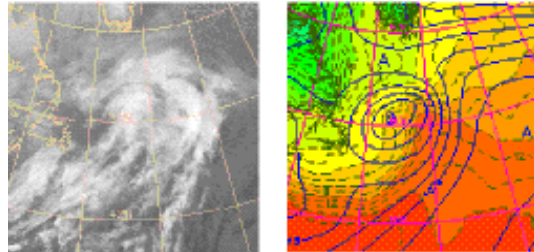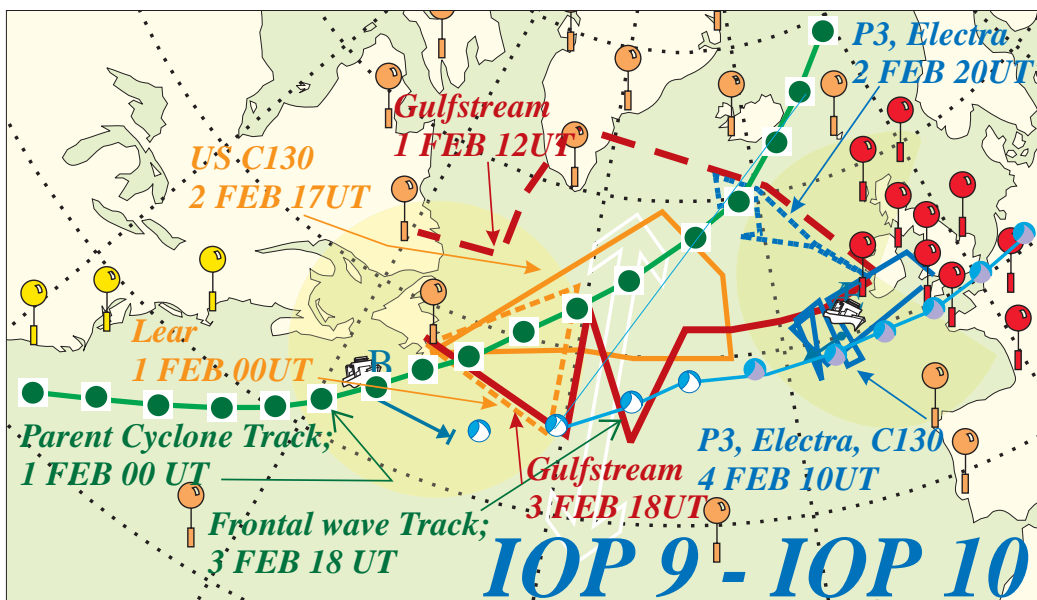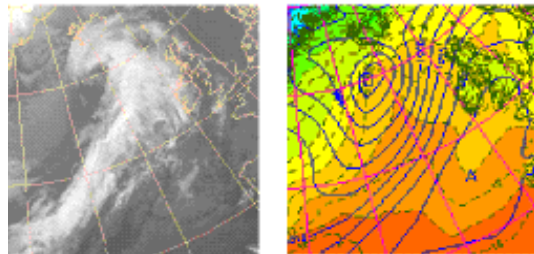
3.12 IOP 10, 3–5 February

4 FEB 00UT
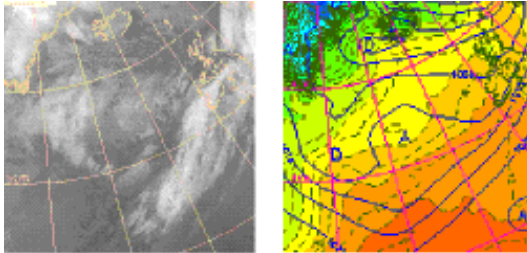
4 FEB 12UT
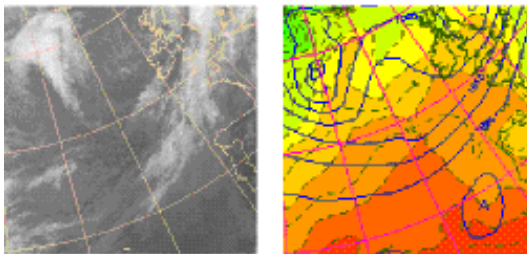
5 FEB 00UT
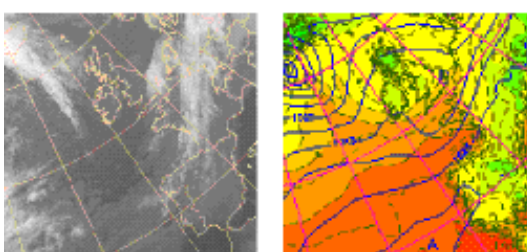
IOP 10		
	28	low n°
3/2 12	(40W, 45N)	formation time
4/2 12	(17W, 48N) -3	max deepening rate (mbar/6h)
4/2 18	(10W, 50N) 1010	max amplitude (mbar)
5/2 12	(5E, 50N)	end of tracking time
⟶	⟶	**US RS**
		LearJet
2/2 1700	1045 19	**C130 USAF**
		Gulfstream (1)
		KNORR
4/2 1200	24 10 (12W, 50N)	**ÆGIR**
		SUROÎT
3/2 0600	24 7 (50W, 43N)	**V. BUGAEV**
		Other ships
3/2 1815	0545 32 StJ →Sh	**Gulfstream (2)**
4/2 0930	0900 16	**C130**
4/2 1030	0915 1	**P3 NOAA**
4/2 0915	0730 ss	**Electra**
		Gulfstream (3)
4/2 03	24 12	**European RS**
2 ARAT flights 4/2		Other facilities
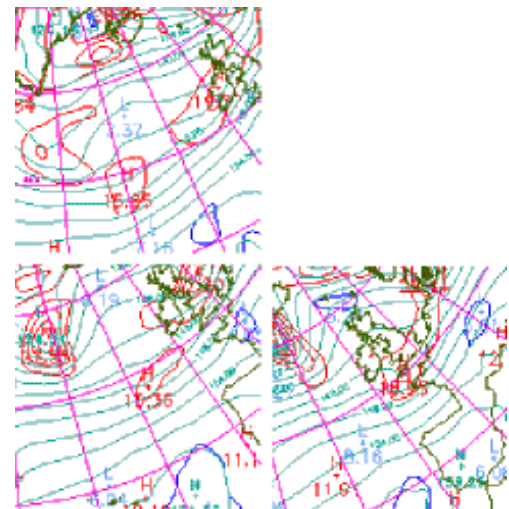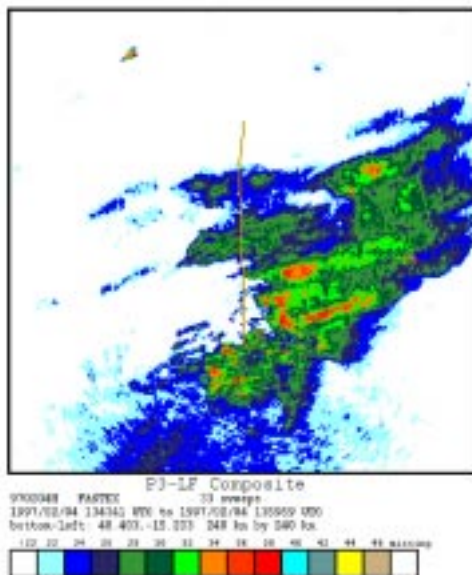
3.13   IOP 11, 4–7 February

IOP 11			
low n°		30	
formation time	4/2 06	(60W, 37N)	
max deepening rate (mbar/6h)	5/2 06	(39W, 44N) −13	
max amplitude (mbar)	7/2 00	(5W, 68N) 950	
end of tracking time	7/2 00	(5W, 68N)	
US RS	⟶	4/2 00	
LearJet	4/2 1415	0330	15
C130 USAF	4/2 1615	0945	13
Gulfstream (1)			
KNORR	6/2 0000	48 (51W, 51N)	15
ÆGIR	6/2 0300	24 (24W, 47N)	9
SUROÎT	6/2 0000	48 (31W,44N)	12
V. BUGAEV	5/2 0000	48 (35W,41N)	8
Other ships			
Gulfstream (2)			
C130	5/2 2300	1000	38
P3 NOAA	6/2 0145	1000	
Electra	5/2 2200	0700	ss
Gulfstream (3)	6/2 0115	0530	22
European RS	6/2 06	18	4
Other facilities			

4 FEB 00UT
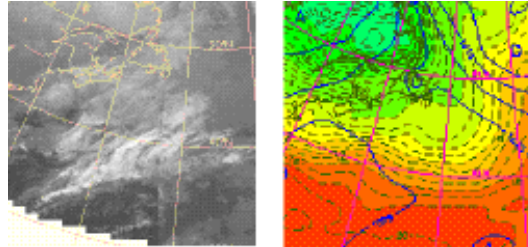
5 FEB 00UT
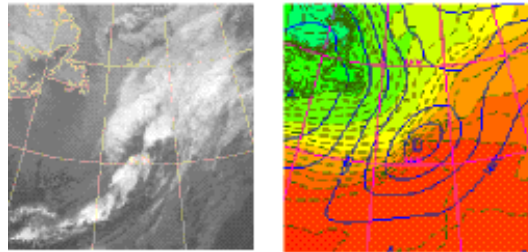
6 FEB 00UT

3.14   LOP 2, 7–9 February

8 FEB 00UT

8 FEB 12UT

9 FEB 00UT
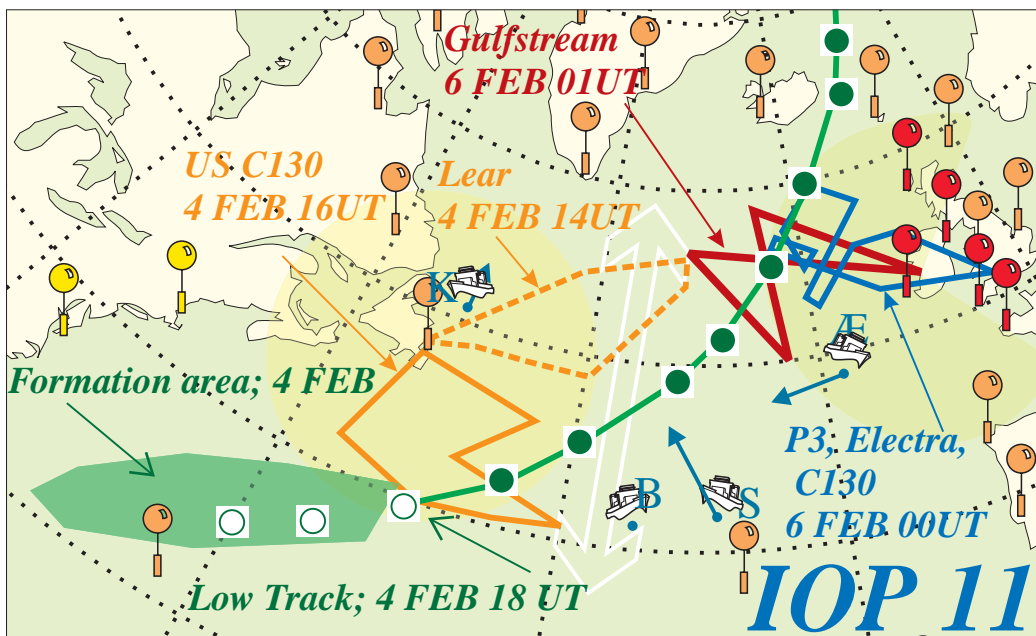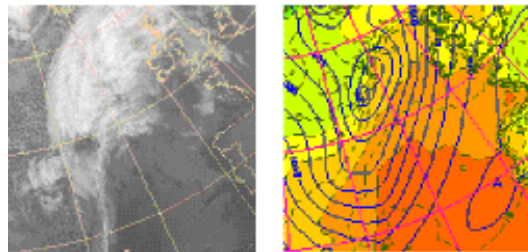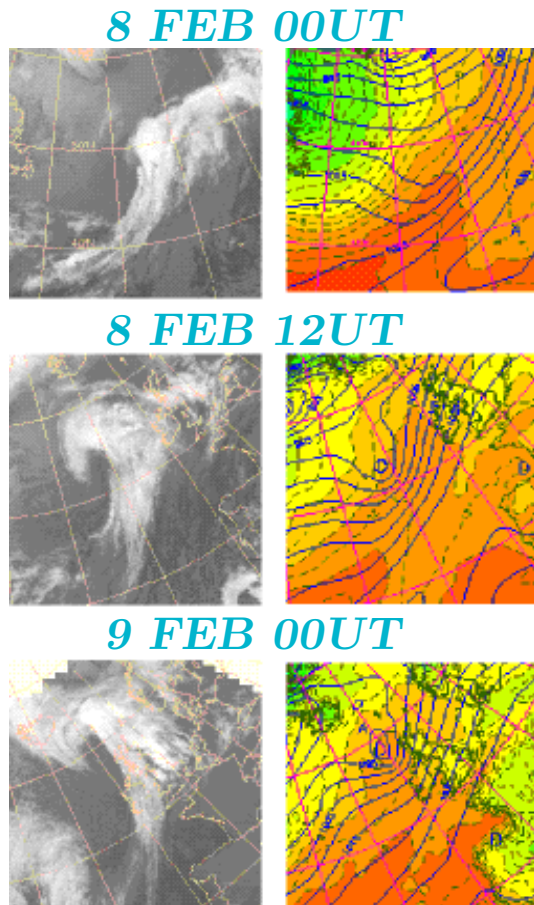
LOP 2		
	33	low n°
7/2 00	(52W, 40N)	formation time
8/2 06	(29W, 50N) -9	max deepening rate (mbar/6h)
9/2 06	(5W, 64N) 985	max amplitude (mbar)
8/2 18	(15W, 55N)	present in MSA
9/2 12	(2E, 64N)	end of tracking time
C130 US 5/2 1300	1030 18	Upstream data
C130 US 6/2 0730	1000 15	
Knorr 7/2	8 s/d (49W, 51N)	Ships
Ægir 7/2	8 s/d (30W, 47N)	
Suroît 8/2	7 s/d (33W, 47N)	
Bugaev	8 s/d (35W, 41N)	
Gulfstream 8/2 0530 1215 en route		Downstream data

C130 US
6 FEB 07UT

Gulfstream
8 FEB 12UT

K

Genesis area, 7 FEB

Low 33 trajectory;
8 FEB 00UT

B

S

FLOP 2
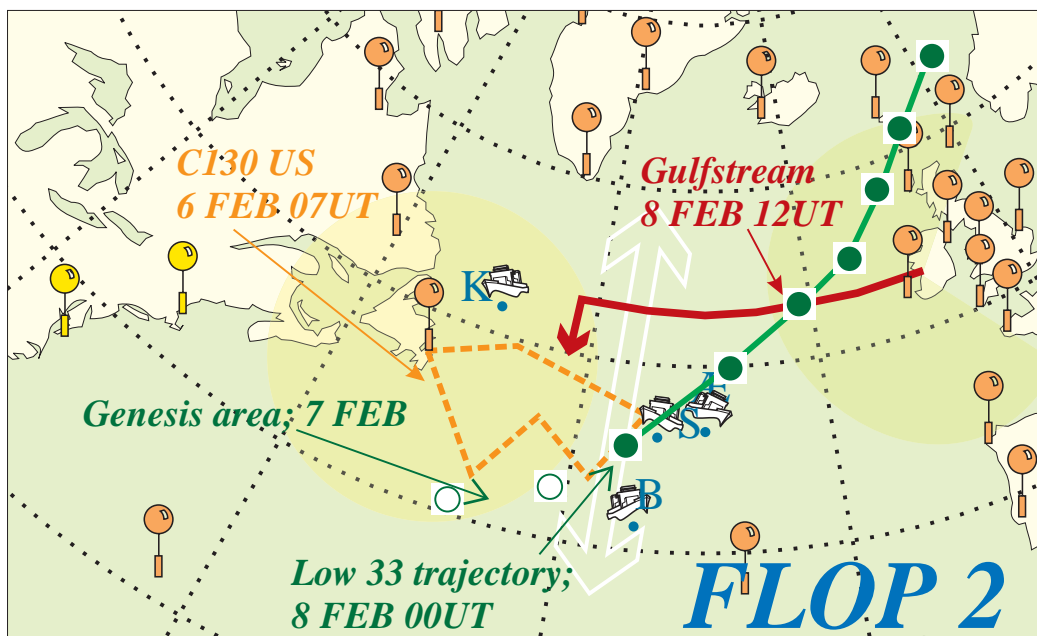
3.15   IOP 12, 9–11 February

IOP 12		
low n°		34
formation time	9/2 06	(35W, 48N)
max deepening rate (mbar/6h)	9/2 12	(27W, 52N) -22
max amplitude (mbar)	10/2 06	(20W, 62N) 947
end of tracking time	11/2 00	(30W, 65N)
US RS	8/2 06	⟶
LearJet	8/2 0545	1100 8 (NB:C130)
C130 USAF	9/2 1315	0730 7
Gulfstream (1)	8/2 1215	0530 26 Sh →StJ
KNORR	9/2 1200	24 7 (51W, 56N)
ÆGIR	9/2 1500	24 11 (35W, 46N)
SUROÎT	9/2 1500	24 9 (35W, 50N)
V. BUGAEV	9/2 1500	24 14 (35W, 41N)
Other ships	9/2	1 ASAP
Gulfstream (2)		retour StJ →Sh
C130	9/2 1745	1130 21
P3 NOAA	9/2 1800	1000 ss
Electra		
Gulfstream (3)		
European RS	10/2 09	24 8
Other facilities		

8 FEB 18UT

9 FEB 12UT

9 FEB 18UT

US C130 8 FEB 06UT

US C130 9 FEB 13UT

Gulfstream 8 FEB 14UT

P3, C130 9 FEB 18UT

Low level precursor 8 FEB

Low Track; 9 FEB 06 UT

IOP 12
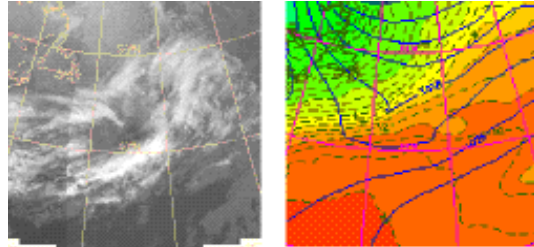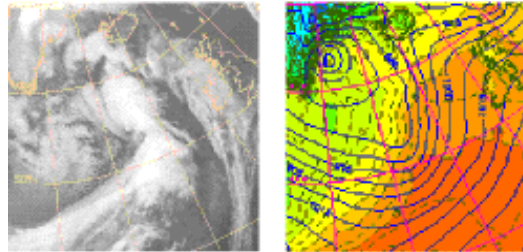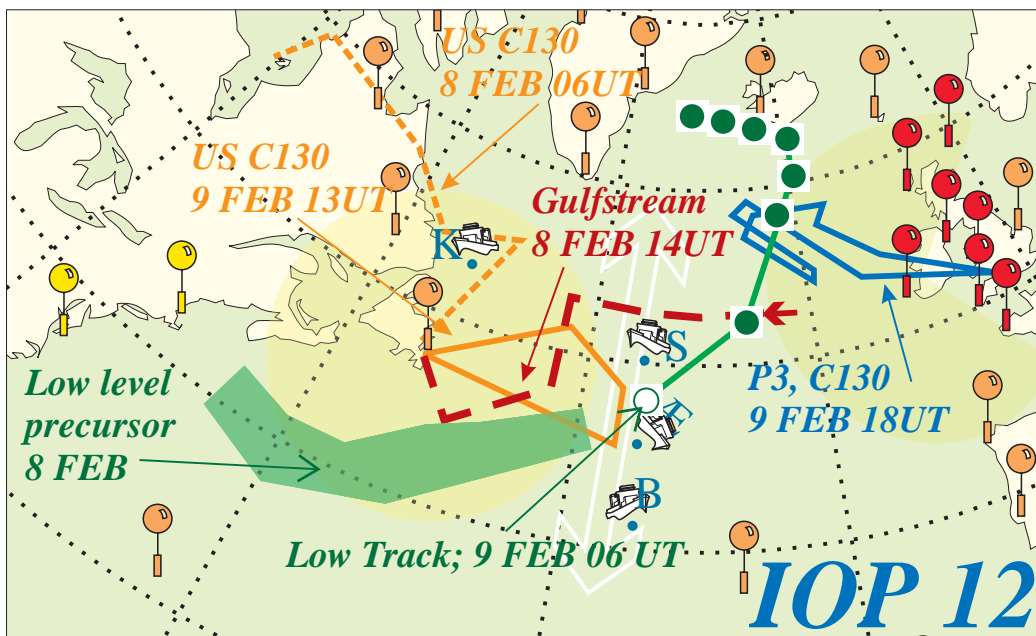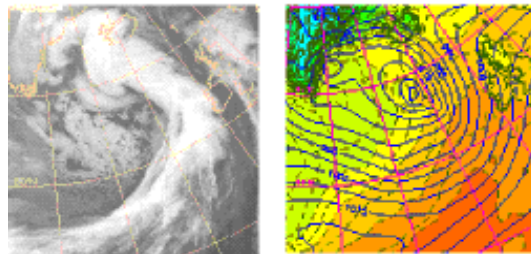
3.16 IOP 13/LOP 3, 8–13 February

10 FEB 06UT
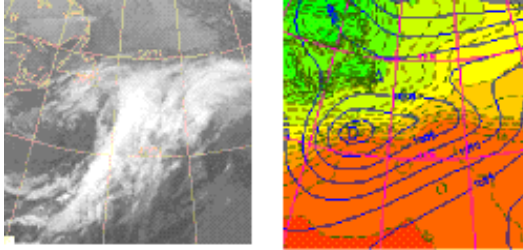
11 FEB 12UT
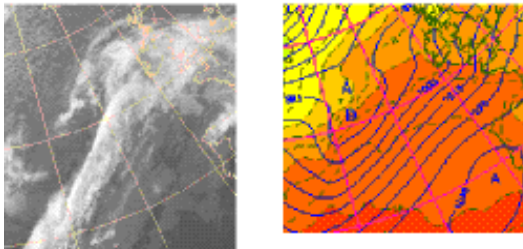
12 FEB 12UT
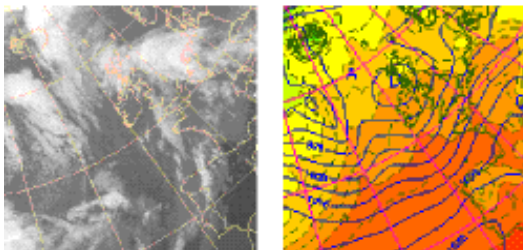
IOP 13/LOP 3		
	35/35A	low n°
8/2 06	(85W, 32N)	formation time
9/2 18	(62W, 39N) -6	max deepening rate (mbar/6h)
10/2 18	(43W, 46N) 989	max amplitude (mbar)
13/2 00	(2W, 59N)	end of tracking time
→	9/2 18	US RS
10/2 1100	0500 18	LearJet
		C130 USAF
		Gulfstream (1)
10/2 1200	24 6 (54W, 57N)	KNORR
10/2 2100	18 12 (35W, 46N)	ÆGIR
10/2 2100	24 18 (35W, 52N)	SUROÎT
10/2 2100	18 15 (35W, 41N)	V. BUGAEV
		Other ships
		Gulfstream (2)
		C130
		P3 NOAA
		Electra
		Gulfstream (3)
		European RS
		Other facilities

Lear 10 FEB 11UT

Low disruption, waves formation; 12 FEB

Low Track; 9 FEB 18 UT

Wave Track; 11 FEB 18 UT

Many soundings by ships; late 10 FEB

IOP 13-FLOP 3
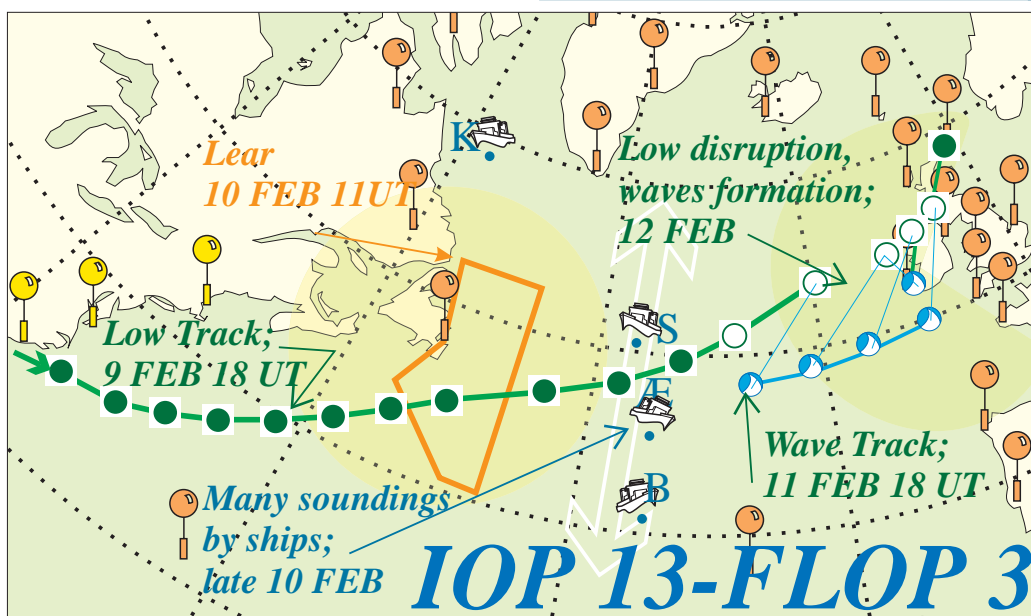
3.17   IOP 14, 10–15 February

IOP 14

low n°		37
formation time	10/2 18	(77W, 28N)
max deepening rate (mbar/6h)	11/2 18	(65W, 37N) -9
max amplitude (mbar)	12/2 18	(45W, 43N) 986
end of tracking time	15/2 00	(3W, 48N)
US RS	11/2 06	12/2 06
LearJet	12/2 1030	0415 20
C130 USAF		
Gulfstream (1)		
KNORR		
ÆGIR	13/2 0000	18 6 (35W, 46N)
SUROÎT	13/2 0000	18 7 (38W,50N)
V. BUGAEV	13/2 0000	18 9 (35W,41N)
Other ships	13/2 06	1 ASAP
Gulfstream (2)		
C130		
P3 NOAA		
Electra		
Gulfstream (3)		
European RS		
Other facilities		

12 FEB 00UT

13 FEB 00UT

14 FEB 00UT

Lear 12 FEB 11UT

Low begins to fill; 13 FEB 00TU

Low 37 trajectory; 11 FEB 18UT

IOP 14
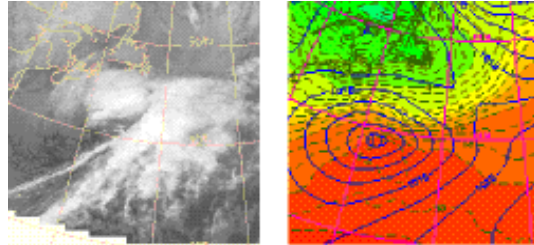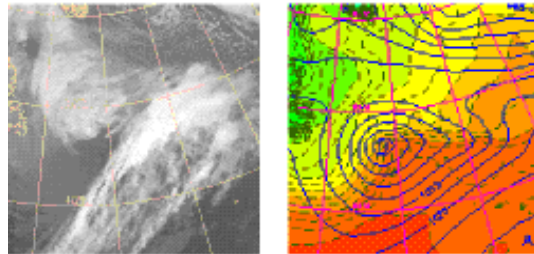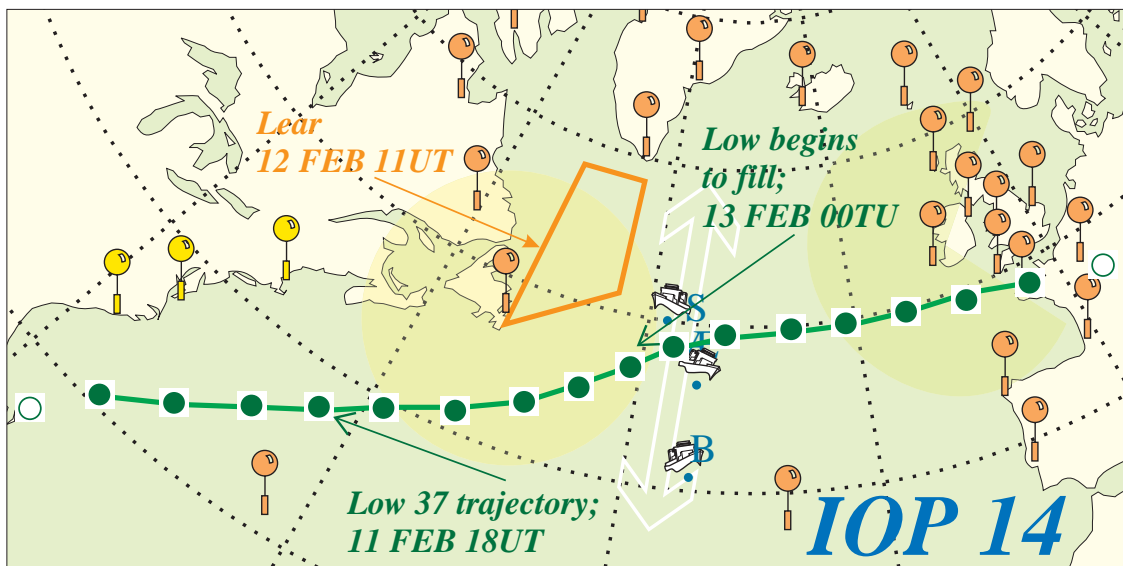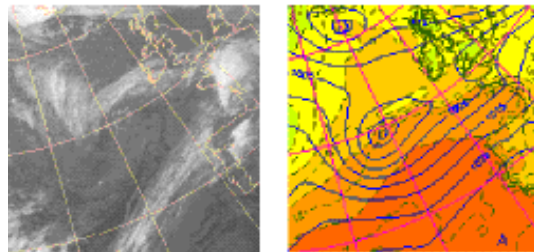
3.18 IOP 15, 13–17 February

13 FEB 12UT
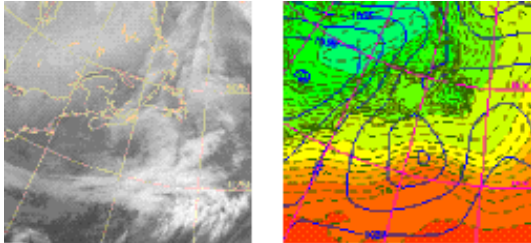
14 FEB 12UT
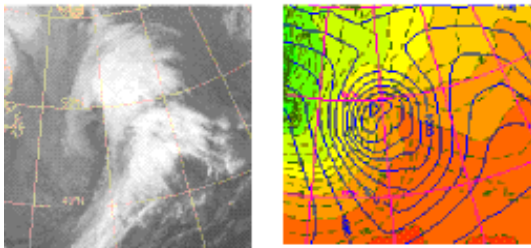
15 FEB 12UT
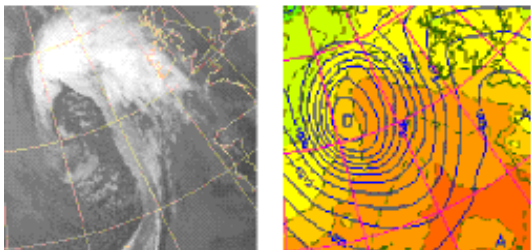
IOP 15		
	38	low n°
13/2 12	(58W, 42N)	formation time
14/2 00	(50W, 46N) -10	max deepening rate (mbar/6h)
15/2 18	(24W, 53N) 973	max amplitude (mbar)
17/2 18	(38W, 63N)	end of tracking time
13/2 06	14/2 00	US RS
14/2 1330	0400 16	LearJet
		C130 USAF
13/2 1430	0500 0 Sh →StJ	Gulfstream (1)
13/2 1500	24 8 (55W, 59N)	KNORR
14/2 1800	24 7 (35W, 46N)	ÆGIR
14/2 1800	24 6 (39W, 50N)	SUROÎT
14/2 1800	24 7 (35W, 41N)	V. BUGAEV
15/2 06	1 ASAP	Other ships
15/2 0615	0630 28 StJ →Sh	Gulfstream (2)
15/2 1130	1100 19	C130
15/2 1145	0830	P3 NOAA
		Electra
		Gulfstream (3)
16/2 15	9 2	European RS
		Other facilities

Lear, 14 FEB 14UT

Gulfstream 15 FEB 06UT

P3, C130 15 FEB 12UT

Precursor trough; 13 FEB

Low 38 Track; 13 FEB 12 UT

IOP 15
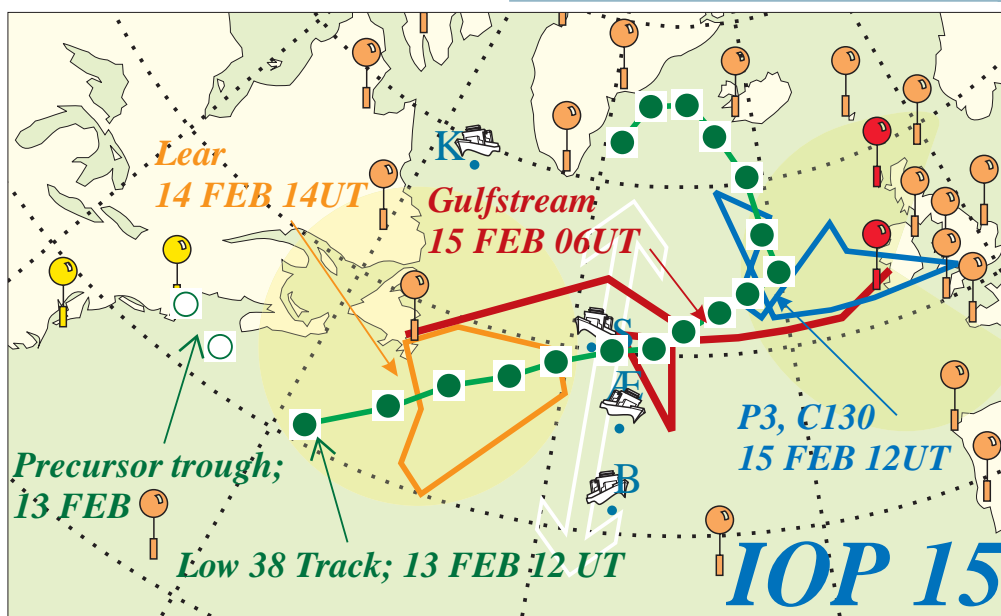
3.19   IOP 16, 17–18 February

IOP 16		
low n°		39A
formation time	17/2 00	(37W, 49N)
max deepening rate (mbar/6h)	17/2 06	(25W, 52N) -20
max amplitude (mbar)	18/2 06	(12W, 68N) 943
end of tracking time	18/2 06	(12W, 68N)
US RS	15/2 12	⟶
LearJet	16/2 1345	0830 21
C130 USAF		
Gulfstream (1)	(17/2)	(06) Sh →StJ
KNORR	16/2 1200	24 8 (53W, 61N)
ÆGIR	16/2 2230	15 6 (35W, 52N)
SUROÎT	16/2 2230	15 5 (38W, 48N)
V. BUGAEV	16/2 2230	15 6 (35W, 41N)
Other ships		
Gulfstream (2)		
C130	17/2 0730	1100 26
P3 NOAA	17/2 0700	0645
Electra		
Gulfstream (3)		
European RS	17/2 18	24 10
Other facilities		

16 FEB 18UT

17 FEB 12UT

17 FEB 18UT

Parent low 39 trajectory; 15 FEB 12UT

Lear 16 FEB 14UT

Wave 39A trajectory; 17 FEB 00UT

P3, C130 17 FEB 07UT

IOP 16
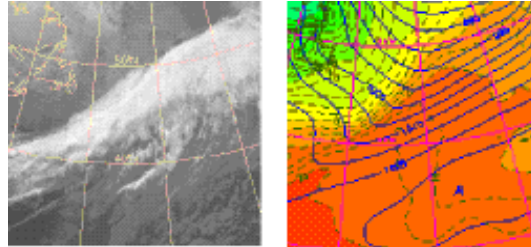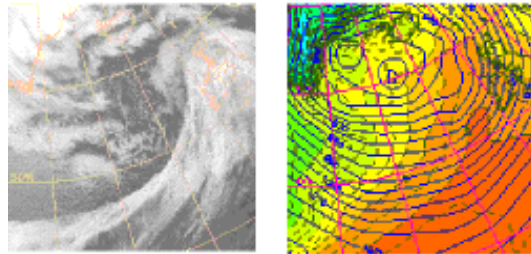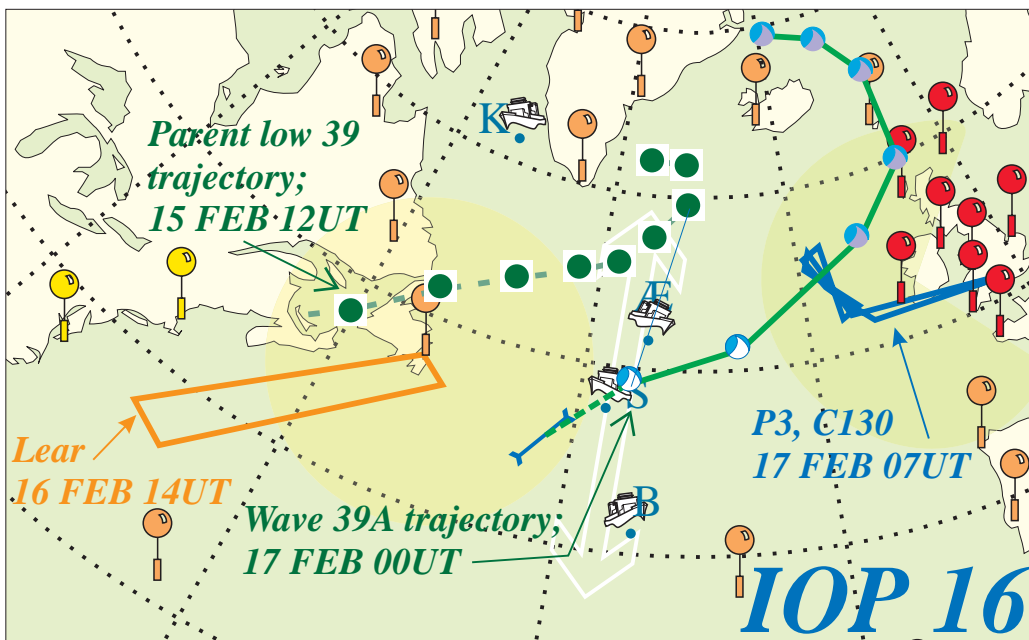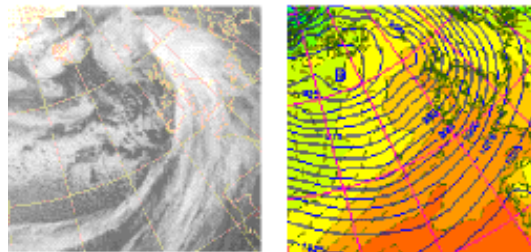
3.20   LOP 4, 17–19 February

17 FEB 00UT
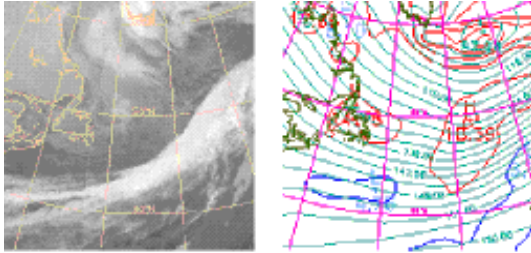
17 FEB 12UT
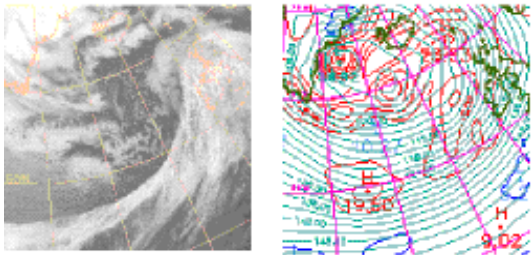
18 FEB 00UT
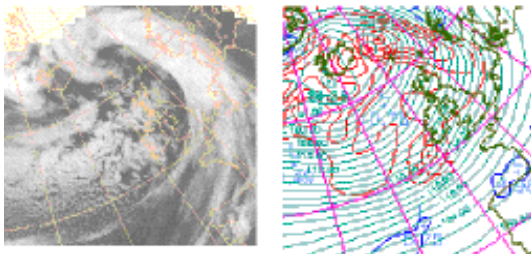
LOP 4		
	39B	low n°
17/2 06	(45W, 48N)	formation time
17/2 18	(20W, 50N) -7	max deepening rate (mbar/6h)
17/2 18	(9E, 57N) 990	max amplitude (mbar)
17/2 18	(20W, 50N)	present in MSA
19/2 00	(10E, 58N)	end of tracking time
US RS		**Upstream data**
LearJet 16/2 1345	0830 21	
3 ships 17/2	5 s/d K, Æ, B	**Ships**
Eur RS	→18/2 18	**Downstream data**

Lear, 16 FEB 14UT

Development into a low; 18 FEB 18UT

Æ

S

B

System 39B trajectory; 16 FEB 18UT

FLOP 4
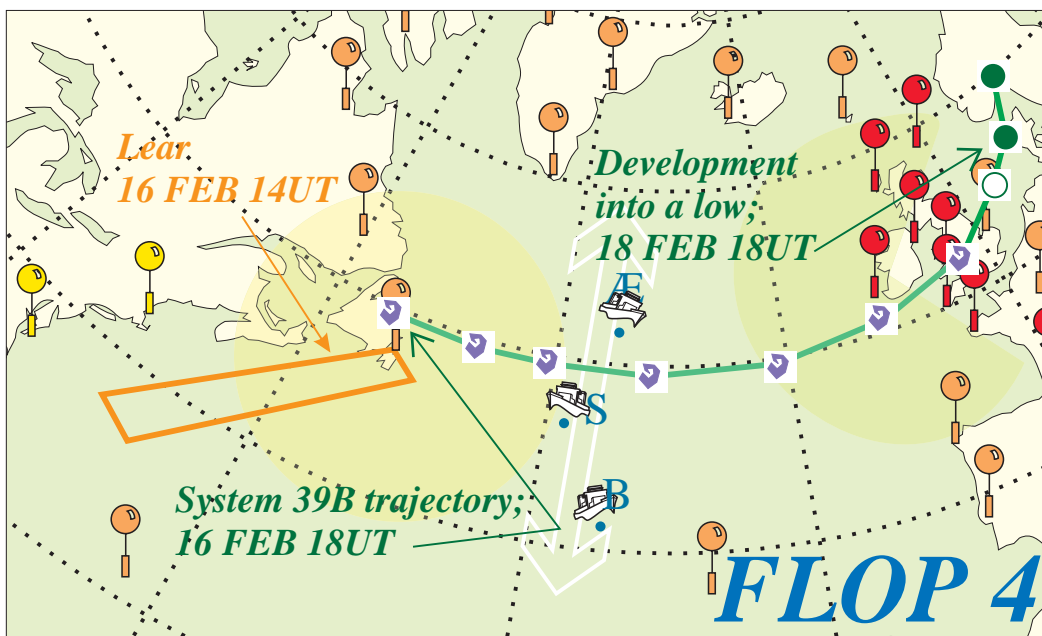
3.21   IOP 17, 17–20 February

IOP 17			
low n°		41	
formation time	17/2 12	(61W,35N)	
max deepening rate (mbar/6h)	19/2 00	(22W, 51N) -16	
max amplitude (mbar)	20/2 00	(7W, 62N) 943	
end of tracking time	20/2 00	(7W, 62N)	
US RS	⟶	18/2 00	
LearJet	18/2 0015	0245	13
C130 USAF			
Gulfstream (1)	17/2 1730	0500	20
KNORR	18/2 1200	24 (51W,62N)	5
ÆGIR	19/2 0000	18 (35W, 52N)	9
SUROÎT	18/2 1800	18 (36W,46N)	12
V. BUGAEV	18/2 1800	18 (35W,41N)	15
Other ships			
Gulfstream (2)	18/2 1830	0700	52
C130	19/2 0645	1030	35
P3 NOAA	19/2 0730	0900	
Electra			
Gulfstream (3)	19/2 2030	0700	27
European RS	19/2 15	24	10
Other facilities	Nors'aq 18/2 12 24 8		

17 FEB 12UT

18 FEB 12UT

19 FEB 12UT

Gulfstream
20 FEB 21UT

Lear
16 FEB 12UT
18 FEB 00UT

Gulfstream
17 FEB 18UT
18 FEB 18UT

Æ

S

B

P3, C130
19 FEB 06UT

Low 41 trajectory; 17 FEB 12 UT

IOP 17
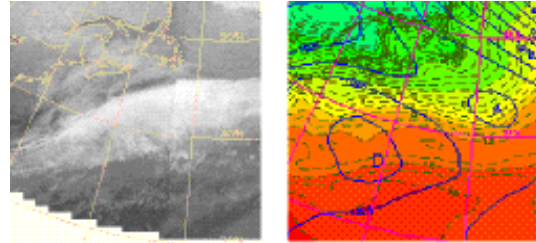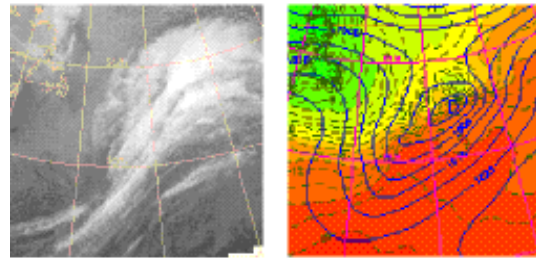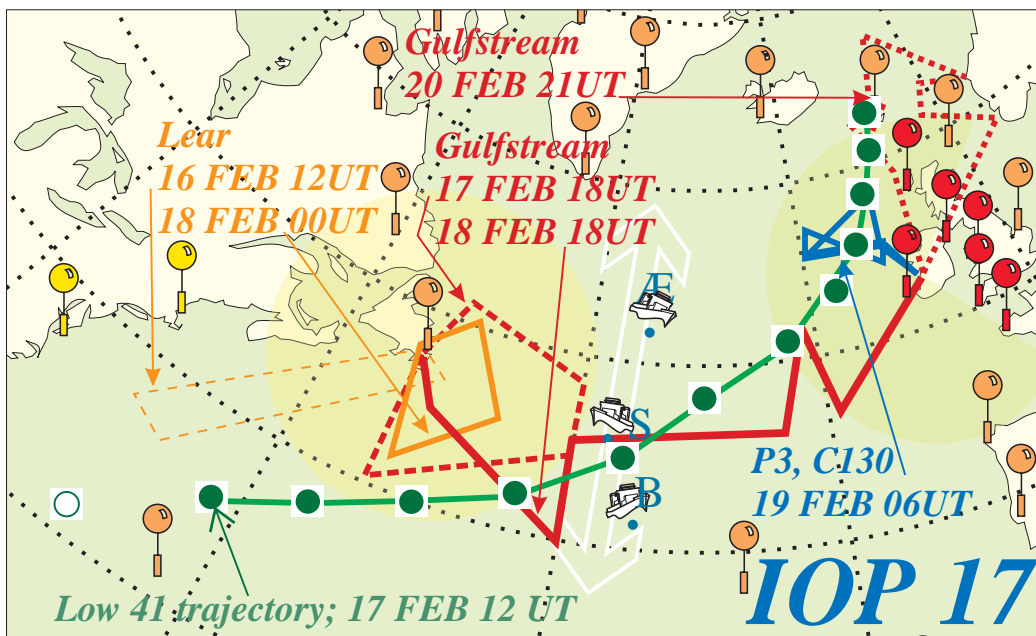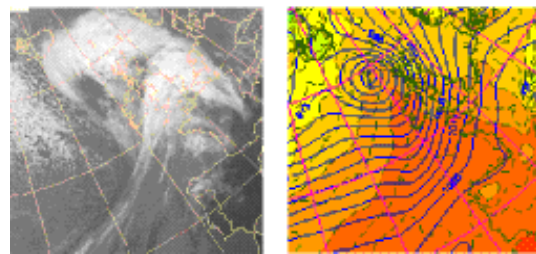
3.22 LOP 5, 22–23 February

22 FEB 00UT
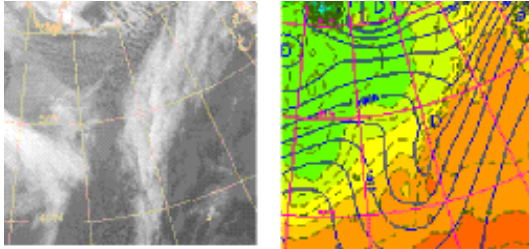
22 FEB 12UT
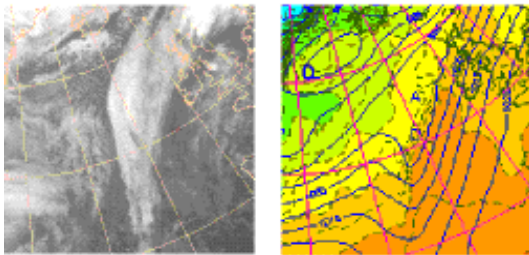
23 FEB 00UT
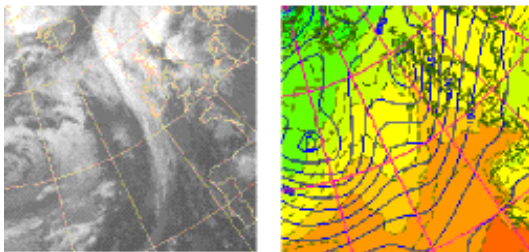
LOP 5		
	42B	low n°
22/2 06	(27W, 47N)	formation time
22/2 12	(21W, 51N) -10	max deepening rate (mbar/6h)
23/2 12	(1E, 63N) 967	max amplitude (mbar)
22/2 18 23/2 12	(15W, 54N) (1E, 63N)	present in MSA end of tracking time
US RS		**Upstream data**
3 ships 21/2	4 s/d Æ, S, B	**Ships**
Gulfstream 22/2 1845	0445 en route	**Downstream data**

Parent wave 42 trajectory; 20 FEB 18UT

Genesis area; 21-22 FEB

Wave 42B trajectory; 22 FEB 06UT

Gulfstream 22 FEB 19UT

FLOP 5
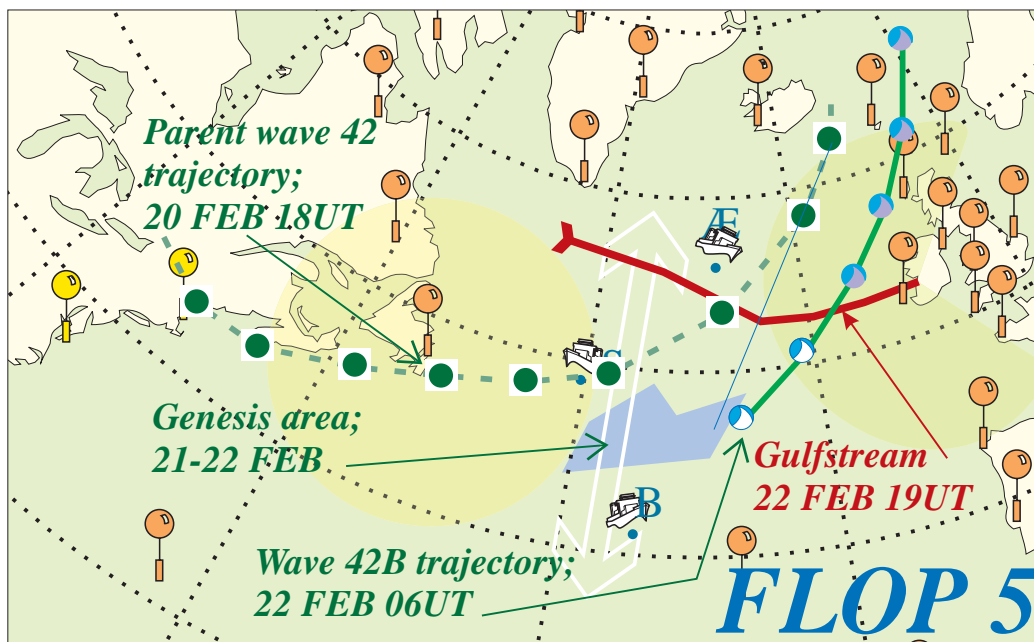
3.23   IOP 18, 22–25 February

IOP 18		
low n°		44
formation time	22/2 12	(44W,54N)
max deepening rate (mbar/6h)	23/2 00	(32W, 53N) -10
max amplitude (mbar)	24/2 18	(4W, 60N) 950
end of tracking time	25/2 00	(4W, 60N)
US RS	19/2 18	22/2 18
LearJet	22/2 0000	0400 18
C130 USAF		
Gulfstream (1)	22/2 1115	0630 25 Sh →Gob
KNORR	22/2 0600	24 8 (57W, 57N)
ÆGIR	23/2 0000	24 12 (28W, 60N)
SUROÎT	23/2 0000	24 9 (42W, 48N)
V. BUGAEV	23/2 0000	24 7 (35W, 41N)
Other ships	23/2 06	1 ASAP
Gulfstream (2)	22/2 1845	0445 33 Gob →Sh
C130		
P3 NOAA	23/2 1515	0915 22
Electra		
Gulfstream (3)		
European RS	24/2 09	30 12
Other facilities	Nors'aq 22/2 00 24 8	

22 FEB 12UT

23 FEB 12UT

24 FEB 12UT

surface projection of upper-level precursor; 20 FEB 12UT

Gulfstream 22 FEB 11UT

Lear 22 FEB 23UT

Lear 22 FEB 00UT

Low 44 trajectory; 22 FEB 12UT

P3 23 FEB 15UT

IOP 18

K   Æ   S   B

3.24   LOP 6, 24–25 February

24 FEB 00UT

24 FEB 12UT

25 FEB 00UT
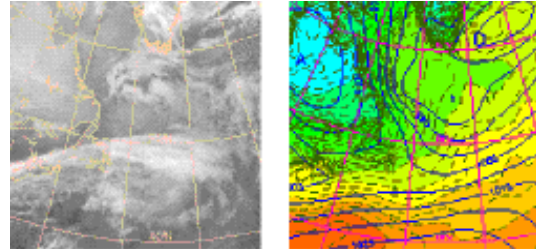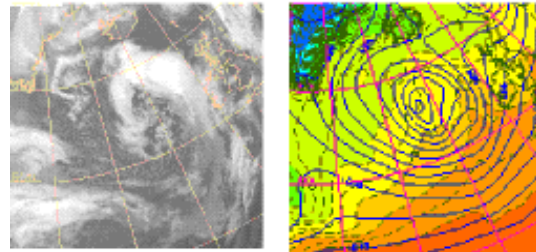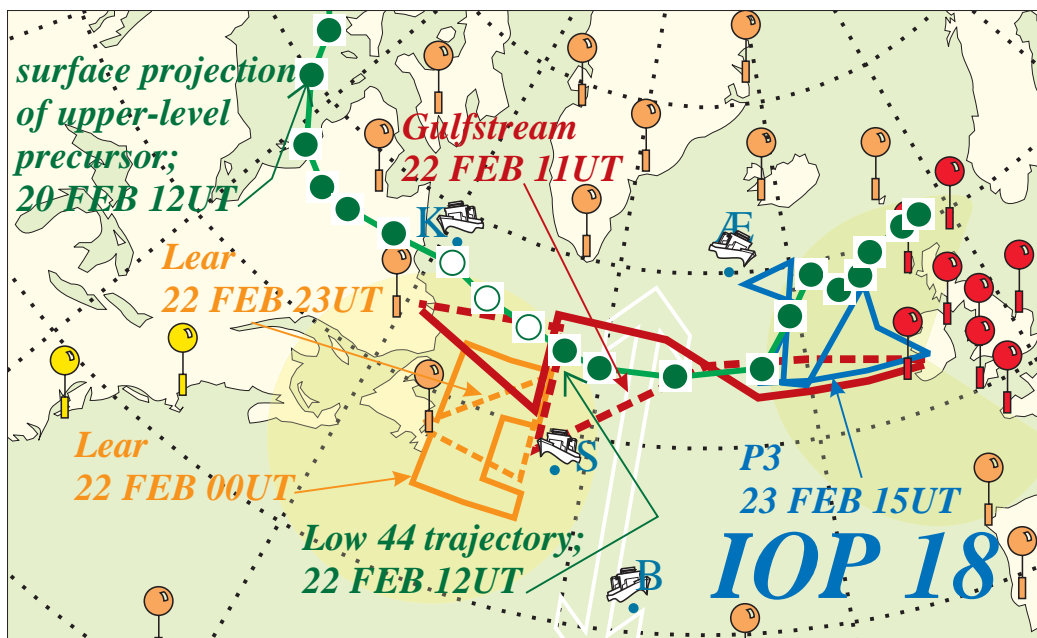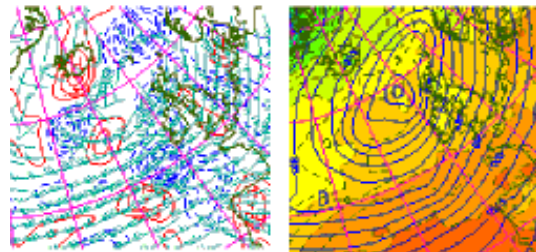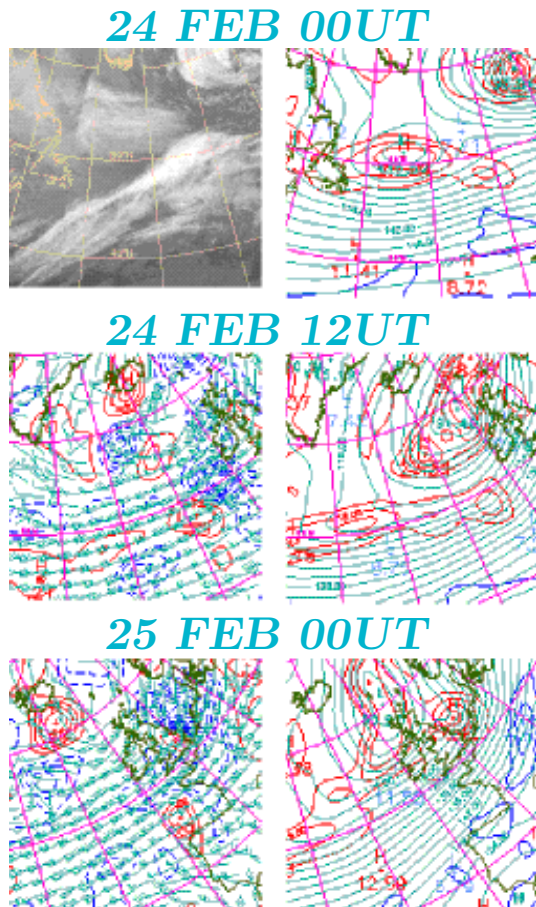
LOP 6		
	43A	low n°
24/2 00	(33W, 47N)	formation time
24/2 12	(16W, 49N) -10	max deepening rate (mbar/6h)
25/2 06	(10E, 57N) 965	max amplitude (mbar)
24/2 12	(16W, 49N)	present in MSA
25/2 06	(10E, 57N)	end of tracking time
US RS		Upstream data
LearJet 22/2 0200 10 2300		
Suroît 23/2 8 s/d 24/2 (43W, 47N) Bugaev 4 s/d 24/2 (35W, 41N)		Ships
Eur RS →25/2 18		Downstream data

Parent low 43 trajectory; 22 FEB 12UT

Recalling low 44 location; 24 FEB 12UT

Fronts: 24 FEB 12UT 25 FEB 00UT

Lear 22 FEB 23UT

Wave 43A trajectory; fronts, 24 FEB 00UT

FLOP 6
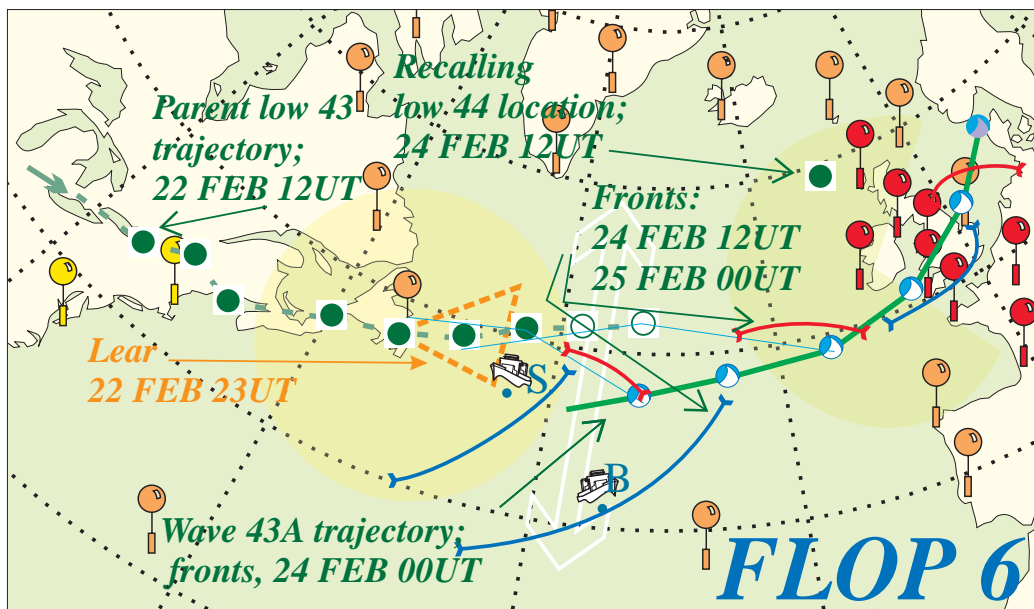
3.25 IOP 19, 26–28 February

IOP 19			
low n°	46B		
formation time	26/2 12	(38W, 41N)	
max deepening rate (mbar/6h)	27/2 06	(23W, 60N) -11	
max amplitude (mbar)	27/2 12	(25W, 62N) 957	
end of tracking time	28/2 06	(28W, 58N)	
US RS	23/2 18	27/2 00	
LearJet	26/2 0000	0345	16
C130 USAF			
Gulfstream (1)			
KNORR	27/2 1200	24 (49W, 60N)	7
ÆGIR			
SUROÎT	26/2 1500	18 (40W, 45N)	13
V. BUGAEV	27/2 0000	18 (28W, 40N)	10
Other ships			
Gulfstream (2)			
C130	27/2 0730	1100	21
P3 NOAA			
Electra			
Gulfstream (3)	27/2 1345	0730	48
European RS	27/2 18	24	5
Other facilities			

25 FEB 12UT

26 FEB 12UT

27 FEB 12UT

Low 46 trajectory; 25 FEB 06UT

Lear 26 FEB 00UT

C130 27 FEB 07UT

Gulfstream 27 FEB 14UT

Wave 46A trajectory; 25 FEB 18UT

Wave 46B trajectory; 26 FEB 12UT

IOP 19
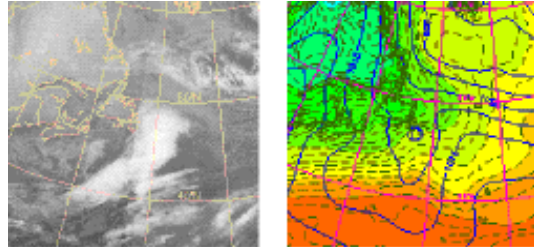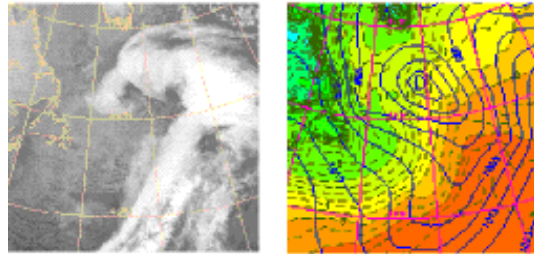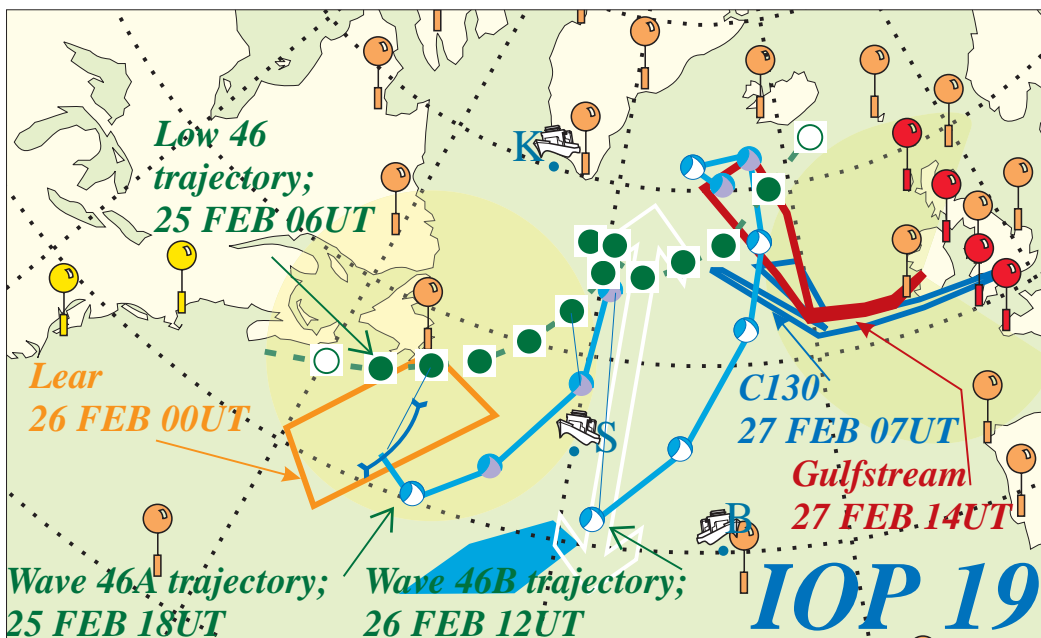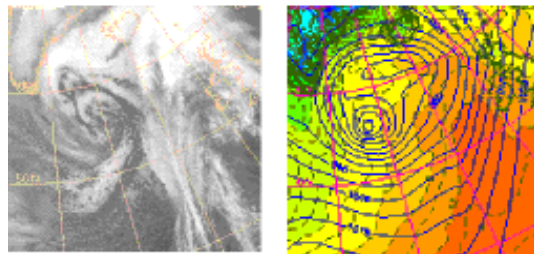
Part 4

The Archive and Data Base

by
Geneviève Jaubert[*],
Catherine Piriou[*],
Scot M. Loehrer[**],
Alain Petitpa[*]
and James A. Moore[**].

[*]*Météo-France, URA CNRS 1357, Groupe d'Etude de l'Atmosphère Météorologique, Toulouse, France,*
[**]*University Corporation for Atmospheric Research, JOSS, Boulder, Colorado, USA.*

4.1   Introduction

*T*he requirement to collect, check and make readily available to the scientific community the data measured during the Fronts and Atlantic Storm-Track Experiment is important to achieving the scientific objectives.

The FASTEX Core Steering Group (CSG) gave the Météo-France/Centre National de Recherches Météorologiques (CNRM) the responsibility for the design of the FASTEX Data Archive in October 1995. CNRM, in consultation with the FASTEX scientific community, recorded the Specialised Data Archives who take responsibility in the dissemination of the raw data and developed a Central Archive (FCA) to provide the community with a large part of the quality controlled measurements that are easily accessible, via the Internet, to all interested investigators.

This part of the report shows the original elements of this archive, which made possible the availability of some data sets in March 97, two weeks after the end of the field phase, and describes the different services and data sets available from the FASTEX Data Archive. Section 4.2 explains the FASTEX Data Archive design, with the locations of the Specialised Data Archives. Documentation and graphics available on-line on the FCA are described in section 4.3. The FCA building processes are described in section 4.4, and its technical design in section 4.5. Information on data set availability is given in section 4.6 and FCA checking procedures in section 4.7. A summary of the radiosonde quality control conducted by the University Corporation for Atmospheric Research/Joint Office for Science Support (UCAR/JOSS) is included in section 8.

4.2   FASTEX Data Archive overview

FASTEX leadership made a strong commitment to provide timely and efficient access to all special data sets collected during the field phase of the program. The primary point of contact and repository of archived data is the FASTEX Central Data Archive (FCA). Other organisations and agencies, however, also maintain subsets of FASTEX data. Collectively all of these data centres are referred to as the FASTEX Data Archive (FDA). The FCA Internet address is (see Fig. 4.1):

<p align="center">http://www.cnrm.meteo.fr/fastex/</p>

and its Email address is:

<p align="center">fastex-dba@cnrm.meteo.fr.</p>

The FCA contents include technical documentation about the measurements made during FASTEX, the on-line field catalog built during the field season and the locations of the specialised data bases. Many graphics are available, such as maps from the Météo-France operational forecast model, and images and products from satellites. On-line data access is provided through a client/server configuration based on a World Wide Web (WWW) Interface.

The main function of the FCA is to provide processed data, in geophysical units. The main part of the data sets processed from the raw data archived in the specialised data bases are available in the FCA. Some processed data sets are only available in the FCA. When it is possible, the measurements from several instruments are provided in the same format. Some raw data sets are also retained on the FCA for long-term archival.

Figure 4.1: *The FASTEX Home Page on the INTERNET and its address.*

The main function of the specialised data bases is to provide the scientific community with raw data from the research instruments involved in FASTEX. Some qualified data sets processed from the archived raw data, and provided in the specialised data bases own format, could be available from the specialised data bases.

The list of the specialised data bases is in section 4.2.3.

4.2.1 Data Policy for the FASTEX Experiment

Data Access

Access to the FASTEX Data Archive is consistent with World Meteorological Organisation (WMO) Resolution 40. Accordingly, use of the FASTEX Data Archive is unrestricted for scientists who utilise the data for research and educational purposes. The use or redistribution of data for commercial purposes may engender certain restrictions that vary depending on the source and type of data under the guidelines of WMO Resolution 40.

The FASTEX Data Archive sites provide a "best" effort in data validation. However, data sets are provided "as is" without warranty of any kind.

Data Attribution

In all cases, proper acknowledgements should be given in publications that utilise FASTEX data to specific scientists and institutions that made the collection of data possible.

Where appropriate, all authors considering publication of FASTEX related research results should offer co-authorship to investigators that had a primary role in the collection of data utilised in the study.

4.2.2   Requirements for the FASTEX Central Archive

Requirements for the FCA call for:

- •Facilitated access to selected data of interest to the international FASTEX scientific community. All FASTEX data are not available on the FCA, but a large subset of the data collected during the field phase are on the FCA.

- •The long-term archival of the original FASTEX data.

- •A catalog of available data, in the general FASTEX Data Archive.

Archive data validation

The FCA takes no responsibility in the FASTEX data validation. This is the data provider's responsibility. The data providers are the best persons to provide scientists with well validated data sets. However, the FCA takes a global view from all the data collected. It is also the first contact between FASTEX data users and data providers. The FCA can perform a global check when a scientist informs it of a possible problem. The FCA can also compare different data sets. The technical design of the FCA (section 4.5) make this checking easier.

For each problem appearing, the FCA informs the data provider. The data provider sends a new data set, well validated, to the FCA, or, for easy corrections, accepts that the FCA modifies the data set. The new data set replaces the older, and is quickly available for all the FCA users. The FCA always gives users access to the most recent versions of validated data sets.

4.2.3   The specialised data bases

The specialised data bases take responsibility in the raw data distribution for the instruments involved in FASTEX. They are specialised in the data processing and can also distribute validated data sets. Some specialised data bases maintain WWW sites. Here is the list of the specialised data bases:

- •NCAR/RAF (P.O. Box 3000, Boulder, Colorado 80307-3000, USA) for all NCAR aircraft data (Electra and Lear 36)

- •NOAA/NSSL (3450 Mitchell Lane, Boulder, Colorado 80301-2260, USA) for all NOAA aircraft data (Gulfstream IV and WP-3D). The on-line documentation site: http://mrd3.mmm.ucar.edu/FASTEX/FASTEX.html provides informations about the coordinated operations in the Mesoscale Sample Area with the turboprop aircraft (NCAR Electra, NOAA WP-3D, UK-C130).

- •DERA/Meteorological Research Flight (Farnborough, Hants GU14 6TD, UK) for the UKMO aircraft data (UK-C130).

- •University of Reading/JCMM (Whiteknights Road, PO Box 240, Reading RG6 6FN, UK) for the UKMO aircraft dropsondes. The on-line documentation site: http://www.met.rdg.ac.uk/FASTEX/ offers an overview of the Intensive Observational Period during FASTEX.

- •INSU/CETP (10-12 avenue de l'Europe, 78140 Vélizy, France) for the airborne radar data (NOAA WP-3D and NCAR Electra)

- •UCAR/JOSS (P.O. Box 3000, Boulder, Colorado 80307, USA) for the high resolution soundings. The sounding data set and the FASTEX on-line field catalogue are available at the following address: http://www.joss.ucar.edu/fastex/

Figure 4.2: *Total Ozone content from NOAA-12/TOVS for 16 February, 1997*
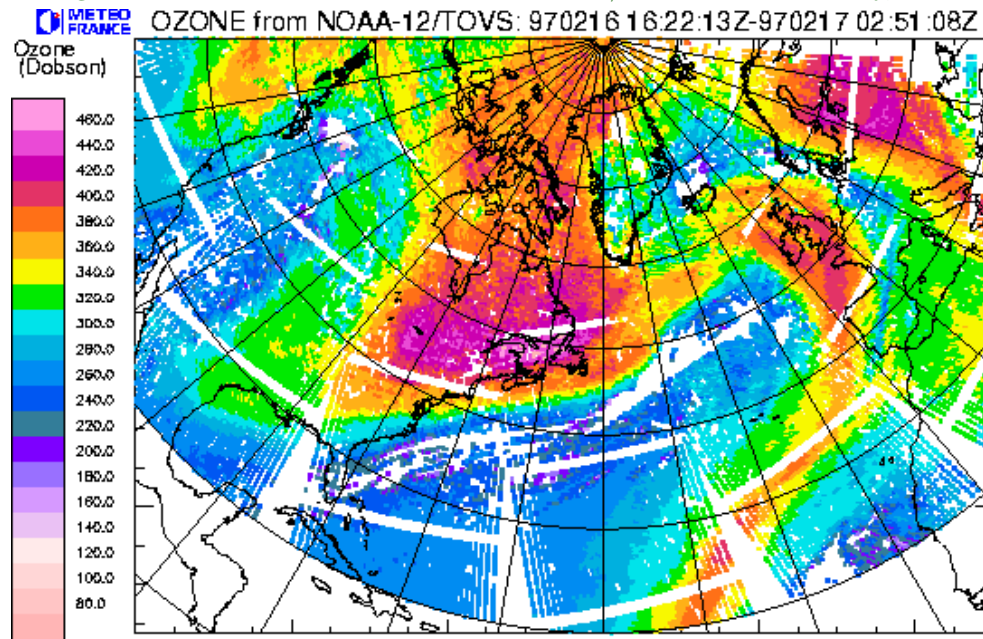
- Météo-France/CMS (B.P.147, 22302 Lannion Cedex, France) for NOAA 12 & 14 HRPT, Meteosat and GOES-EAST Imagery.

- The Hurricane Center for the US Air Force aircraft data (USAF C130). Data and operation reports are available on the WWW site: http://www.hurricanehunters.com .

4.3 FASTEX Central Archive overview

In the FASTEX Central Archive, documentation and/or data can often be reached in two ways: by instrument, or by data set. Instrument refers to all data collected by the same aircraft, ship or site. Data set refers to the same kind of measurements. Some instruments made the same kind of measurements. For example, six aircraft involved in FASTEX dropped sondes. All the ships, as well as radiosounding ground stations, launched soundings. When several instruments provided the same type of measurements, all the data are available in the same format and form a data set.

4.3.1 The technical documentation

A description of the instruments involved in FASTEX, including for each instrument a summary of the instrumentation, the period of measurements, and measurements reports, is available on the WWW site. The data provider is also noted, and when it is possible, WWW sites with technical documentation are linked. This documentation provides an overview of the measurements made during FASTEX by a particular instrument, aircraft or ship. A list of the data sets including measurements of this particular instrument is provided.

The documentation of the data sets available or planned to reside at the FCA, with a list of the different instruments which provided these measurements, provide information about data format, checks and control procedures applied.

A detailed description of the data available, listed as data sets as well as instruments, is updated when new data are available, or when some data are corrected. Information about the data number and position, and the state of qualification of the data are available. All past data updates are mentioned.

Some technical documents, such as the "FASTEX Operations Plan" (D. Jorgensen *et al.* 1996), are available in postscript format.

4.3.2   The FASTEX On-Line "Real-Time" Field Data Catalog

The Daily Operations Summaries, the forecasts, scientist logs and summaries, were included daily during the FASTEX field phase in an on-line catalog provided by the FASTEX Operations Coordination Team at Shannon (Ireland). This catalog also included special imagery or graphics such as the GOES-EAST/Meteosat Infrared imagery mosaic, 6 hourly winds deduced from GOES-EAST by the University of Wisconsin (Velden *et al* 1997), forecast maps from the Ireland Model HIRLAM, the daily consensus forecast, and the sea state forecast for the FASTEX ships. Built and updated daily by UCAR/JOSS during the field phase, this catalog is available both on the UCAR/JOSS WWW site and on the FCA site.

4.3.3   The graphical documentation

The graphical documentation collected during the field phase in the "Real-Time" Field Data Catalog was updated in delayed time on the FCA site. New satellite products and many charts from the ARPEGE Model were included. A new interface, with animation capability, was developed.

Satellite Imagery and products

The 6 hourly mosaic imagery from the infrared channel of the GOES-EAST and METEOSAT geostationary satellites are available for each day of the FASTEX field phase. The domain is the North Atlantic ocean. The main part of these images were provided in real-time to the field Catalog by Météo-France. The remaining part was processed in delayed time, from the data files available in the FCA.

The SSMI Imagery provided by NOAA/NESDIS in support of the FASTEX Experiment, and available in real time on its site, was archived at the FCA and is now available on the FCA site. This imagery included, on the North Atlantic domain and each 2 hours, the most recent data from the SSMI Imagers aboard the three DMSP polar satellites. Available products are rain rate, rain, water vapour and wind speed (Hollinger *et al* 1987).

The Total Ozone content data was processed by Météo-France/CNRM from the raw data files of the NOAA 12 & 14 TOVS sounders (Lefèvre *et al* 1991). Data files, as well as maps, are available in the FCA. Two different maps sets are available: the first set shows all the measurement from a satellite during 12 hours (Fig. **??**), the second shows the measurements for each satellite pass.

The satellites ephemerides were provided during the field phase by the CNES (France) and the Air Force Institute of Technology (USA). The ground trace was cal-

culated for the NOAA 12 & 14, ERS-2, DMSP 10,11 & 13 and TOPEX/POSEIDON satellites. Daily graphics are available for each satellite (Fig. 4.3).

Figure 4.3: *ERS-2 Ground trace for 16 February, 1997*

The Maps from the analysis of the ARPEGE Meteorological Model

Special outputs of the analysis of the Météo-France ARPEGE Meteorological Model were processed during the FASTEX Experiment. The following 6 hourly fields are available on the North Atlantic domain: mean sea level pressure, temperature and wind at the surface and at the 500 hPa level, geopotential height at the 500 and 300 hPa levels, and vertical motion at the 500 hPa level. (Fig. 4.4)

4.3.4   The data distribution

The data may be ordered on-line, through a WWW client/server configuration. The files requested are extracted from the FCA and put on an FTP server in near real-time. This provides the FASTEX scientists access to the up-to-date version of the data. CD-ROMs will be edited when the Archive content includes mainly validated data sets.

Through the data selection interface, both the instrument type or/and the specific data sets can be selected. The time and position windows can be specified. The FCA site returns information about the number and the location of the data selected. The choices can then be modified interactively. At the first request of data, the new user must subscribe to the FCA, and to state his agreement with the FASTEX data policy.

The data requests are automatically processed within 30 minutes after the end of the data selection process. Fields are extracted from the FCA Database Management System or copied from the FCA storage disks, and sent with a documentation to the FTP server. An email is sent to the FASTEX user with information about the location of the files extracted.

Figure 4.4: *The WWW page for ARPEGE map access*

The main part of the data are sent in ASCII format, which is easily readable for the major part of the users. Some data sets, such as the model fields or the satellite imagery, are stored in WMO GRIB format. Some very specialised data sets, such as the Electra in-situ measurements or some satellites products, are sent in its original form, along with a method to read them.

The documentation sent with the data includes information about the data origin, the data processing and eventually the corrections made, rights to be applied for these data and format description.

4.4 History

To design the FASTEX archive, lessons of the past were provided by the data management of previous experiments, and particularly the Tropical Ocean Global Atmosphere Coupled Ocean Atmosphere Response Experiment (TOGA-COARE, Webster and Lukas 1992) and the PYRenean EXperiment (PYREX, Bougeault *et al* 1990). These experiments are not comparable in term of size of the data archive, or by the number of laboratories and countries involved in. The design of the TOGA-COARE and PYREX archives are different. However, a significant effort in data management, validation and delivery was done for these two archives. We retain from the TOGA-COARE data management the use of specialized centers for data validation,

Table 4.1: *Steps of the FASTEX Central Archive Construction*

	FASTEX Archive building
Summer 95	Project defined
Fall 95	Project accepted by the FASTEX Scientific Steering Group
Spring 96	Agreement for the satellite products delivery
	The satellite Imagery to be processed at Météo-France/CMS is defined
	Contacts with the scientific teams who provide data
	Definition of the FASTEX data bases requirements
Summer 96	FCA Computer and Software Installation
	FCA WWW site is opened
	FASTEX Data Policy is written
Fall 96	Contacts with the meteorological services which provide the high resolution sounding data sets
	Software Interface between the Météo-France operational archive and the FCA for GTS data sets is written
	Software Interface between the FCA Users and the FCA is written
	FASTEX Experiment Field Phase
January - February 97	Operational data received through the GTS are included in the FCA
	High resolution sounding data are sent by the meteorological services to the FCA
	Beginning of the inclusion, and the checking, of the high resolution sounding data in the FCA
	Satellite Ephemerides are archived
	SSMI images from NOAA/NESDIS are archived
	Data availability on FCA
March 97	The FCA is opened, some data sets received from the GTS are available to the FASTEX community, consistent with the WMO Resolution 40
Spring 97	High resolution soundings from the ground sites participating in FASTEX
	Operational Surface measurements and high resolution soundings from the 4 FASTEX ships
	High resolution soundings from the ASAP ships participating in FASTEX
	Low resolution dropsonde data set from FASTEX aircraft
Summer 97	Full satellite Imagery
	ARPEGE analysis fields
	High resolution soundings from the R/V Knorr during LabSea Experiment
Fall 97	1s in-situ measurements from US Research aircraft (Electra, WP-3D, Gulfstream IV)
	Reflectivity Composite images from aircraft Radar (WP-3D)
	First data set of the high resolution US dropsonde
	High resolution UK-C130 dropsonde data set during some IOPs
Winter 97	Full High resolution sounding data set, including UCAR/JOSS QC flags
	EGOS buoy data set validated by Météo-France/CMM
	R/V Knorr 15 min and 1 hour surface measurements validated data set
	R/V Le Suroît 1 min surface measurements validated data set
	Total Ozone Content from NOAA/TOVS
	TOPEX/POSEIDON Wind/Wave product
	Surface measurements from some World Weather Watch principal ground stations
Spring 98	Full High resolution UK-C130 dropsonde data set
	Real Time profilers data set from the R/V Knorr and the R/V Le Suroît
	Corrected High resolution US dropsonde data set
Summer 98	ERS-2 Wind product
	Profilers data set from the European network

specialized data bases for raw data distribution, on-line access and a primary point of contact. From the PYREX experiment, a central point for processed data archive and delivery, the necessity of a dialog between the archive manager and the data providers, and between archive users and archive manager to point out and correct erroneous data, the delivery of up-to-date data sets.

In another connection, a major problem appears after the field phase of meteorological experiments: scientists wish to work quickly with the data collected, but the data providers need time to validate the data sets. Data exchange between scientists during the field phase, or just after, force the scientists to work with real time data sets. Fairly often, validated data sets, when they are available, are not in the same format. These practices bring difficulties in the use of validated data sets.

Following these observations, the FCA was planned to provide timely and efficient access to special data sets collected during the field phase of the FASTEX experiment. The FCA was planned a long time before the field phase. The Internet facilities were largely used, before the field phase for the preparation of the archive, and during and after the field phase for sending the data to the archive, and to provide efficient access to the data. Table 4.1 presents a summary of the steps of the FASTEX Central Archive construction.

The FASTEX Archive was designed eighteen months before the field phase. The plan was presented and accepted during the first FASTEX Scientific Steering Group meeting in October 1995.

During the year 1996, the agencies which provide data were contacted in order to establish collaboration. In particular, satellite agencies and data providers for satellite products were contacted, as were meteorological agencies which provided the high resolution soundings from ground stations and Atmospheric Sounding Automated Program (ASAP) ships. In the Météo-France service, several teams were contacted and proposed their collaboration for data retrieved through the Meteorological Global Telecommunications System (GTS), imagery computing and buoy supervising. The Central Archive hardware and software technical environments were installed. The WWW site, with data sets and instruments documentation, was opened in summer 96. The software for data archival was written. Figure 4.6 presents a schematic of the important components of the FCA architecture.

During the field phase, many data were processed and archived:

- The Météo-France/Centre de Météorologie Spatiale (Lannion, France) processed the imagery received in real-time from METEOSAT and GOES-EAST. The remaining part of the METEOSAT imagery, sent by EUMETSAT to the CMS, was also processed. The HRPT from NOAA 12 & 14 for the CMS coverage zone was received and processed.

- Data from the World Weather Watch and some FASTEX data, received through the GTS at Météo-France, were decoded and archived in the FCA. This includes a fair amount of the dropsondes.

- Some high-resolution soundings from ground stations were verified by the Meteorological services and sent to the FCA.

The FCA data archives were open 2 weeks after the end of the field phase. Many data sets received from the GTS have been available since this date for the FASTEX community:

- sounding data from TEMP and TEMPSHIP messages

- real-time buoy data from BUOY messages

- surface data from commercial ships and some data from the FASTEX ships (SHIP messages)

- Commercial aircraft data (AIREP, ACARS and AMDAR messages)

The complete satellite imagery , many fields from the ARPEGE model analysis, and low resolution data from the FASTEX dropsondes were available 4 months after the field phase.

Some FASTEX measurements were quickly validated by the data providers. The high resolution sounding data from FASTEX ships, ASAP ships and ground stations were available between 2 and 6 months after the field phase. The in-situ measurements from NOAA and NCAR aircraft (WP-3D, Gulfstream IV and Electra) were available 6 months after the field phase.

The complete high resolution sounding data set, verified both by FCA and UCAR/-JOSS has been available since the winter 97-98 with the UCAR/JOSS quality control flags.

During the year 1998, many data sets were included in the archive, or replaced by validated data.

The FASTEX Archive will be in its final form during the year 1999.

4.5 FASTEX Central Archive Technical Constitution

4.5.1 A data base built around a Database Management System

The FASTEX Central Archive was designed with these main ideas:

- exactness for the data management

- easiness for the data checking

- facility for data sets cross validations

- uniqueness for the accessible archive

- easiness to insert new data sets

- interactive access to all the available data sets

- quickly sending the available data sets, without human interaction

All data bases have to establish a catalog of the data archived; usually, this catalog is maintained by a Database Management System (DMS). This is also the case for the FASTEX Central Archive. The FCA DMS catalog is interfaced with the WWW server, and produces for each request exact and up-to-date information of the available data.

The FCA has to meet several conditions. The FCA has to send data, coming from several instruments but belonging to the same data set, in the same format. These data sets have to be verified, and sometimes replaced by a qualified data set. Any user could have access at any time to the best available data sets. The format must not change, as the data set is replaced. To satisfy all these requirements, the Database Management System does not only manage the data catalog, but also manages a large part of the data sets. Every parameter of a measurement is stored in its physical unit. So, to compare and compute the same parameter coming from different instruments or data sets is easily done. For example, the temperature measurements aboard the R/V Le Suroît during one day in IOP5, coming from the automatic station, the

Figure 4.5: *An example of the comparison of measurements coming from different data sets and instruments. The temperature measurements are from the R/V Le Suroît: 1-minute data, from research instrumentation (continuous line), operational surface measurements provided by the Météo-France automatic station Batos (rhombs) and the routine messages sent by the crew (squares), potentiel temperature at the surface pressure calculated with the first sonde measurement (10 s after launch) and the sounding ground pressure (triangle).*
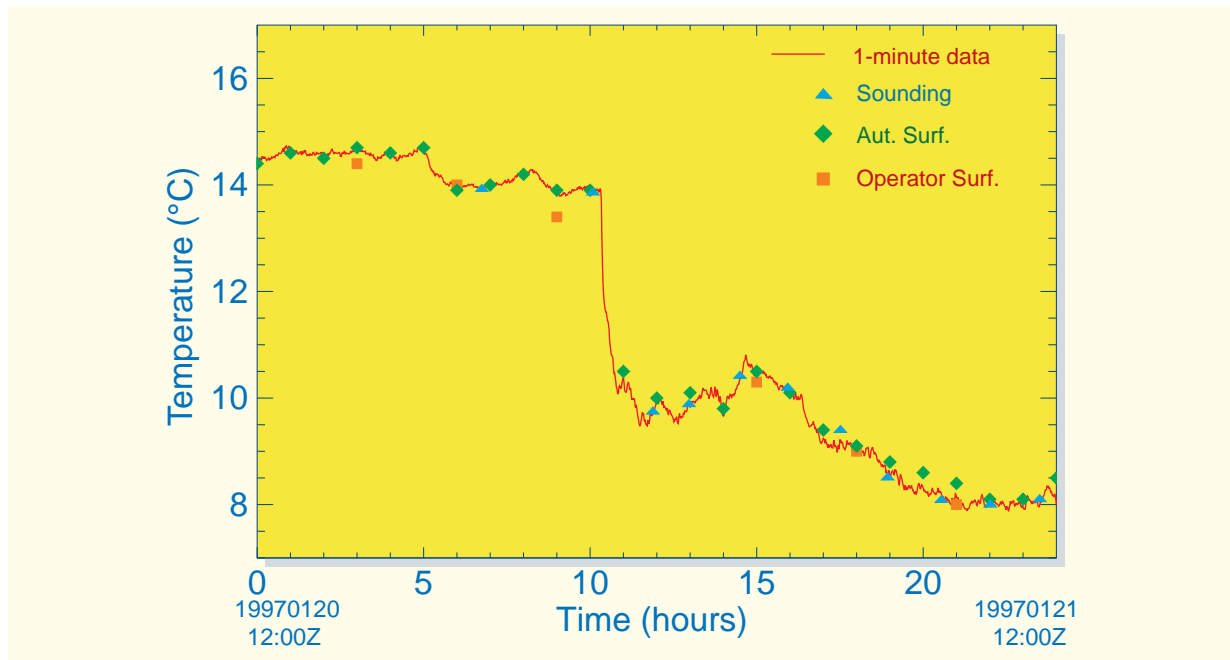
operator measurements, and the soundings at low levels are compared to the 1-minute surface data on figure 4.5.

Each data set is introduced in one or several DMS tables. As an example, the ship surface measurements data set, archived from the SHIP messages, is inserted in a table named 'SHIPS'. The 'SHIPS' table is composed of as many columns as informations informed in a SHIP message. The informations from each message are inserted in a row of the 'SHIPS' table. The pressure measurement, in hPa, is inserted in the 'Pressure' column, the temperature one, in degrees C, is inserted in the 'Temperature' column, etc...

The DMS functionalities are used to verify, when it is possible, the uniqueness of each measurement and to apply the gross-limit checks. A measurement inserted in the DMS must satisfy all the specifications. As an example, each measurement in the 'SHIPS' table has a site identifier, a date and time, and a location in latitude and longitude. These specifications are unique, and the date and location are bounded. All the measures are bounded numbers, or are coded as a chain of characters as defined in the WMO codes. If one of the specification rules is not satisfied, the measurement is rejected. Human intervention is necessary, to verify the measurement, correct it (or the software) if it is possible, or reject definitively the information. Many anomalies were detected in this manner, in the data sets sent to the FCA.

When a new measurement is inserted, each measure can be selected independently. The statistics tools and group selection possibilities of the DMS are used for validation. The quality control procedures applied to each data set are described in section 4.7.
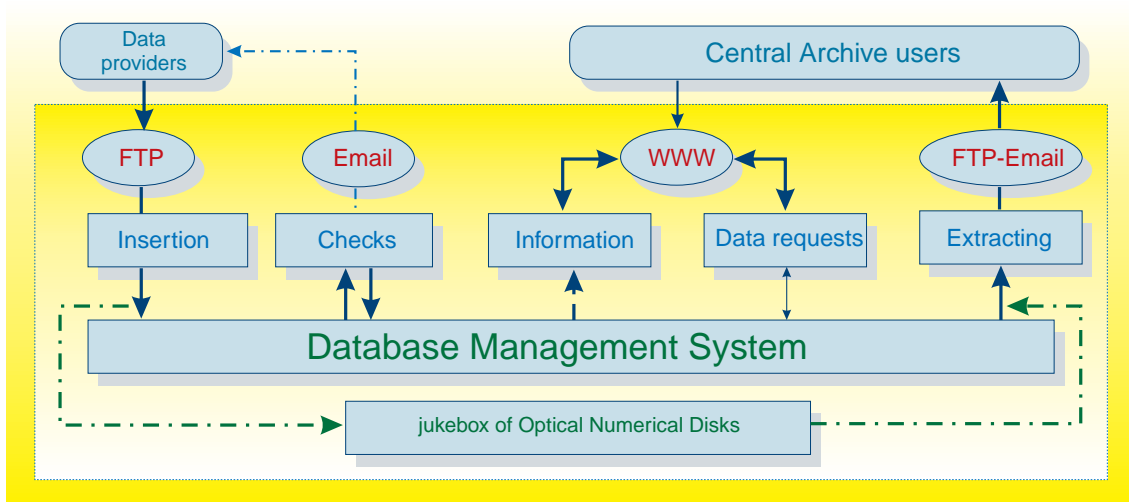
Figure 4.6: *FASTEX Central Archive Structure*

The DMS functionalities are also used for data updates. Uniqueness and gross-limit checks are automatically applied for each update. The DMS functionalities for updating independently each row/column are very useful to minimise the human errors. For example, these functionalities are used to modify the quality flags without data modification. A timestamp is updated for each line when a column is updated. This information is useful to verify if a new data set, well validated, includes all the data previously inserted in the DMS. The timestamp is sent with the data for each request, so, any user is informed of the date of the last update.

As soon as a measurement is inserted (or updated) in the DMS, it is available for all the FCA users.

The data requests are defined through a WWW form. The WWW server sends the request to the DMS. The DMS responses allow the user to adjust, interactively, the request to the data actually available. When the request is definitely written, it is archived in the DMS. Some minutes after, typically 30 minutes, an automatic process asks the DMS, the data requested are extracted from the DMS, and the files are written. The files are put on an FTP server and an email is sent to the user.

Data extracted from the DMS are written in ASCII files, each measure in physical units. The data extracting from the DMS is done for each request. The typing format was defined when the data set table(s) is(are) defined, and stored in the DMS. This allows any user to have access to the up-to-date data sets at any time, and every time in the same format.

4.5.2   The data sets structure

Measurements stored in the FCA are classified according to the measurement method and/or the processing method. The method used to build the PYREX data base (Bougeault *et al* 1993) was extended to all the FASTEX data sets. For example, the surface measurements received from the ground stations (SYNOP messages) are not included in the same data set as the surface measurements received from the ships (SHIP messages). Parameters are not exactly the same, and the site location is fixed in the SYNOP messages, not in the SHIP messages. The sounding

measurements are included in two different data sets, according to the data processing. The high-resolution data, sent by the FASTEX participants, are included in the 'high-resolution sounding data set'. The soundings processed as per WMO conventions, in standard and significant levels, are included in the 'low-resolution sounding data set'. This data set includes soundings received from the GTS (TEMP messages) and soundings provided by the FASTEX participants. A type identifier is attributed to each class measurement.

The archive structure is not the same for all the measurements:

- •For measurements in a single point, data set identifier, site identifier, and date assume the uniqueness of the measurement. The data set is stored in one table of the DMS.

- •For profile measurements, to add a level identifier is necessary to assume the uniqueness of the measurement. This level identifier depends on the data set: it is time for high resolution soundings data, pressure for low resolution soundings data, and altitude for profilers data. Two tables are necessary to store the data set: one table includes profile informations, like site identifier, date, and comments, another table include the measurements, a row for each level. The two tables are linked by a foreign key.

- •For the two-dimensional fields, and special data, the FCA distribute these data, with no validation. Files provided to the FCA are stored in a juke box of Optical Numerical Disks. The DMS includes only the file catalog, not the measurements.

Three DMS tables are used to summarise the information:

- •The description of each data set, including name, identifier, tables used for the catalog or data storage, are stored in a table

- •The description of each site measurement, including name, site identifier, position (for fixed site), data set type and data provider information are stored in a table.

- •A table summarises the relation between instruments and data sets.

4.6 Data available in the FASTEX Central Archive

4.6.1 The FASTEX instruments measurements

The research aircraft

Seven aircraft participated in FASTEX. The Lear 36 and two US Air Force C130 were based at St John's (Newfoundland,Canada) to document the "Far Upstream Area". The NOAA Gulfstream IV, based at Shannon (Ireland), documented, depending on the Intensive Observational Period (IOP), one of the three FASTEX sampling areas: the "Far Upstream Area" near St John's, the "Near Upstream Area" centered about 35°W longitude, or the "Multiscale Sampling Area" near Shannon. The two turboprop aircraft with Doppler radar, the NOAA WP-3D and the NCAR Electra, based at Shannon, and the UKMO C130 turboprop,based at Lyneham (UK), operated coordinated flights in the "Multiscale Sampling Area". See Joly *et al.* (1997) for the description of the observing strategy and Joly *et al.* (1999) for a summary of operations and cases.

The raw aircraft measurements are available in the specialised data bases. The 2s and low-resolution dropsonde data sets are available in the FCA, as well as the 1s

Table 4.2: *Summary of the FASTEX aircraft measurements available in the FCA*

	LEAR jet	USAF C130	NOAA Gulfstream IV	UK-C130	NOAA WP-3D	NCAR Electra
Number of flights	13	9	16	11	12	7
Number of available dropsonde measurements	220	108	498	439	31	
Number of hours of in-situ meteorological measurements		78h	60h	101h[+]	138h	57h
Composited images from aircraft radar					All flights	
Dynamical fields from Doppler radars					+	+

[+]: planned

Figure 4.7: *Dropsondes location resulting from all the flights performed during the fiel phase*
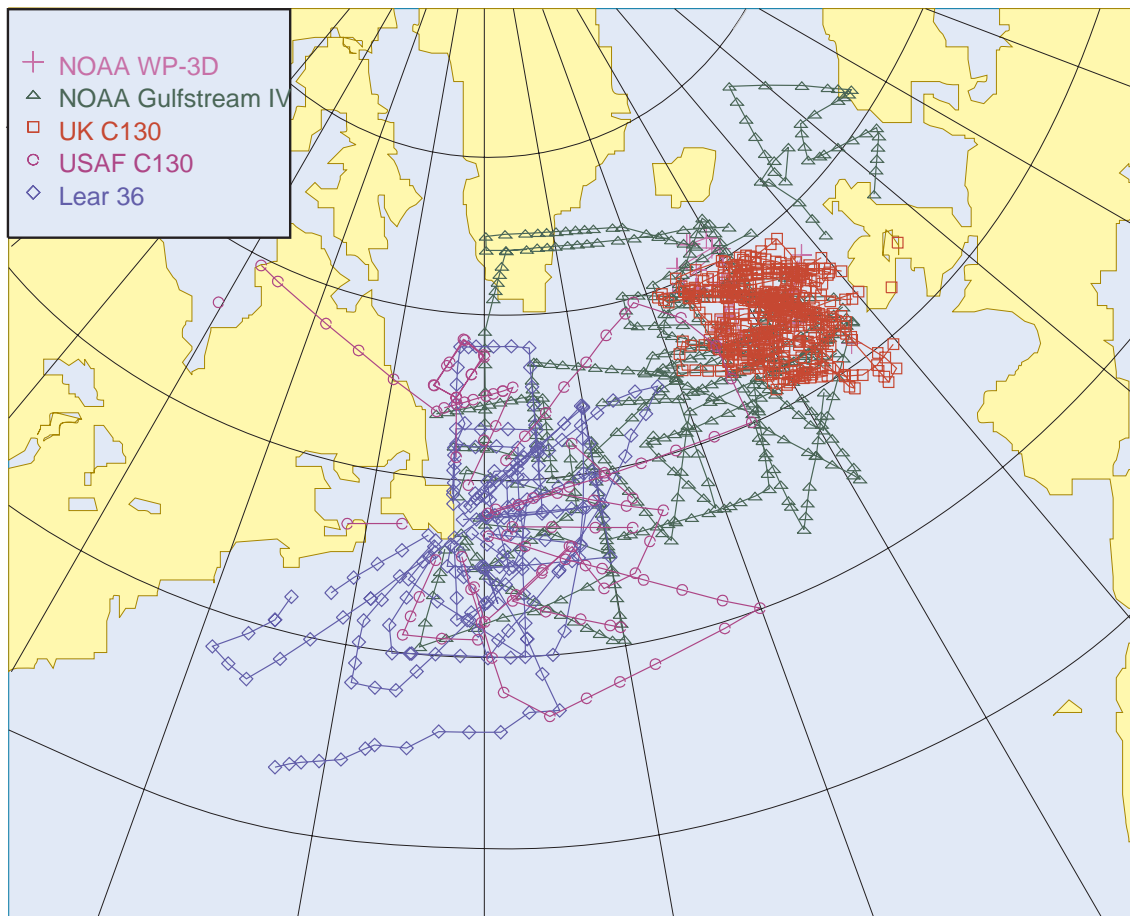
meteorological measurements of the Gulfstream, the WP-3D and the Electra. The composite images of reflectivity from the WP-3D radar are also available. Selected 3-D analysed wind and reflectivity fields and PERL profiles computed from the airborne Doppler radars will be available when provided by PIs, following formal publication of results. Measurements available or planned for each aircraft are indicated on Table 4.2. The dropsonde locations are on Fig. 4.7.

Table 4.3: *FASTEX ship measurements*

| | FASTEX ships | | | | ASAP ships | | |
| | R/V | R/V | Victor | | 4 | 2 | 1 |
	KNORR	Le SUROÎT	BUGAEV	ÆGIR	French	Danish	Swedish Icelandic
Days with measurements	52	53	50	44	109	75	26
Number of soundings	282	271	283	264	208	219	81
Operational Surface measurement frequency	6h	1h	1h	3h/1h	6h	3h	3h
Research Surf. and Oceano. measurements	15min avg /33 days	1min avg /52 days					
Flux measurements	+	+					
Profilers	25 days	50 days					

[+]: planned

The FASTEX and ASAP ships participating in FASTEX

The FASTEX ships are two research vessels, the R/V Knorr from NOAA and the R/V Le Suroît from IFREMER (France), a Ukrainian Meteorological Vessel, the Victor Bugaëv, and an Icelandic Coast Guard ship, the Ægir. The four FASTEX ships were approximately aligned on 40W longitude between 40N and 55N latitude. All routinely performed operational surface measurements and 6 hourly soundings. During IOPs, they performed more frequent soundings, up to every 90 minutes for 18 hour periods.

An air-sea interaction program was conducted by the two research vessels, the R/V Knorr and the R/V Le Suroît, using a 915 MHz Wind Profiler and in-situ atmospheric and oceanic instruments. Measurements made by the R/V Le Suroît are documented in L.Eymard *et al.* (1999). The R/V Knorr participated in FASTEX, in the middle of the North Atlantic Ocean, during January 97. During February 97, she participated in the LabSea Experiment, in the Labrador Sea. The LabSea PIs have provided the high resolution data from the soundings performed by the R/V Knorr to the FCA.

Seven commercial ships equipped with radiosounding equipment (ASAP), performed routine 12 hour soundings and participated in FASTEX by taking soundings each 6 hours during IOPs. The four French ASAP ships cross the Atlantic between Le Havre (France) and the French West Indies. The two Danish ASAP ships operate between the Denmark and Godthaab, on the Greenland West Coast. The Swedish - Icelandic ASAP ship crosses the North Atlantic between Reykavik (Iceland) and Norfolk (Virginia, USA). The Icelandic, Danish and French meteorological services sent, in delayed time to the FCA, the high-resolution data from the soundings performed by the ASAP ships.

Table 4.3 summarises the ship measurements and Fig. 4.8 provides the location of soundings performed by each of these ships.

Figure 4.8: *Locations of the high resolution soundings released from FASTEX and ASAP ships and ground sites participating in FASTEX*
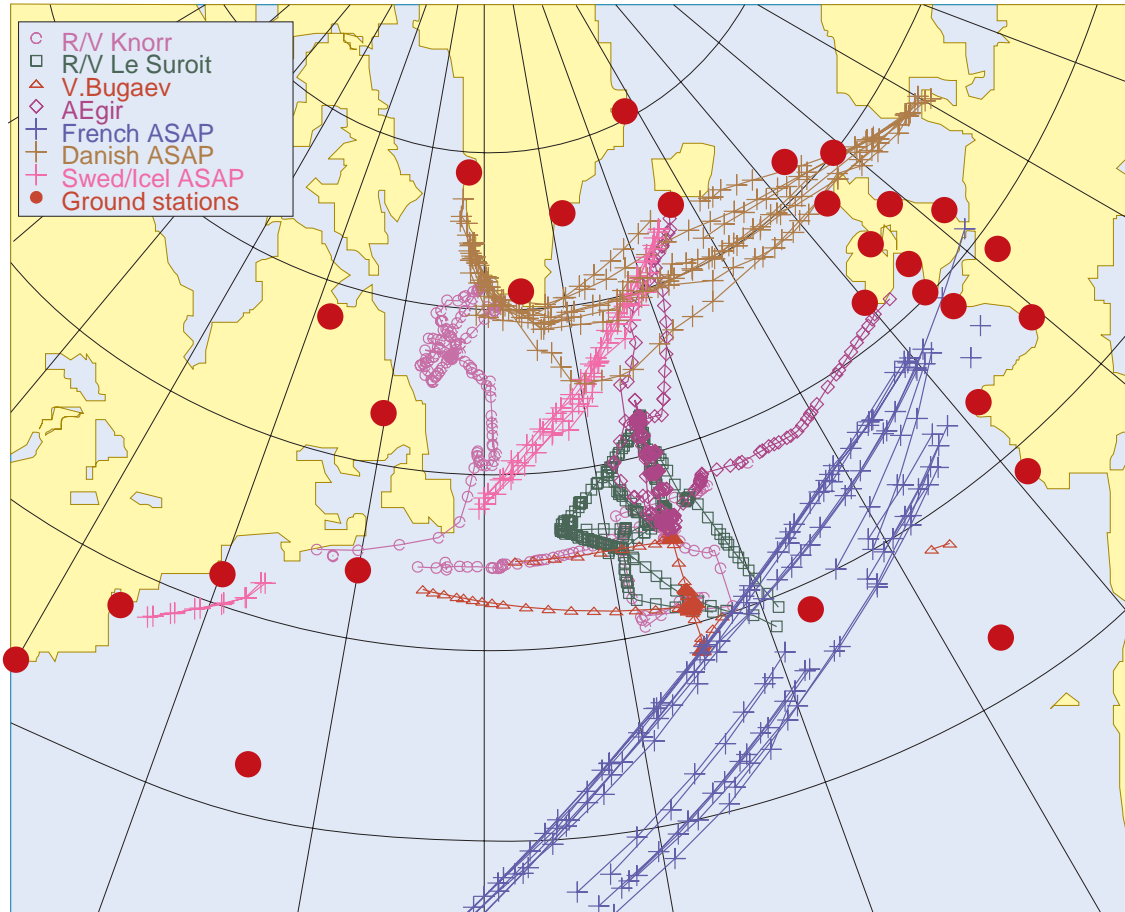
The radiosounding ground stations participating in FASTEX

Twenty nine ground sites performed more frequent soundings during FASTEX. The meteorological services have sent the high resolution data set, validated, to the FASTEX Archive. Table 4.4 summarises the location, frequency and measurement method at each site. The location of these sites are in Fig.4.8.

The buoy network

The European Group of Oceanic Stations (EGOS) maintains an operational network of buoys in the North Atlantic. The coverage of this network was maximised during the two months of the experiment. Additional buoys were deployed by the FASTEX ships: the R/V Knorr deployed six EGOS buoys, the R/V le Suroît eight, and the Ægir four NOAA/EGOS buoys.

All the measurements from the EGOS buoys with pressure measurements, when they were located in the North Atlantic, were validated by Météo-France / Centre de Météorologie marine (CMM) at Brest (France). The CMM processed the raw data files, from the Argos archive, of 53 buoys. The measurement location is interpolated

Table 4.4: *Radiosounding ground stations participating in FASTEX*

Site	WMO code	Lat	Long	Alt (m)	System	Sounding Frequency	Vertical resolution	Number
Greenland	Staff: DMI							
Egedesminde	04220	68.70N	52.87W	40	RS80-N/Omega	4/day	10 s	234
Narssarssuaq	04270	61.18N	45.44W	4	RS80-N/Omega	4/day	10 s	248
Scoresbysund	04339	70.50N	22.00W	68	RS80-N/Omega	4/day	10 s	229
Angmagssalik	04360	65.62N	37.65W	51	RS80-N/Omega	4/day	5/10 s	215
Denmark	Staff: DMI							
Thorshavn	06011	62.02N	06.77W	55	RS80-N/Omega	4/day	10 s	238
France	Staff: Météo-France							
Brest	07110	48.45N	04.42W	98	RS80-L/LoranC	4/day IOP: 8/day	10 s	289
Trappes	07145	48.77N	02.02E	168	RS80-L/LoranC	4/day IOP: 8/day	10 s	219
Bordeaux	07510	44.82N	00.68W	48	RS80-L/LoranC	4/day IOP: 8/day	10 s	242
Iceland	Staff: IcMS							
Keflavic	04018	63.97N	22.60W	38	RS80-N/Omega	4/day	5/10 s	230
Ireland	Staff: IrMS							
Valentia	03953	51.93N	10.25W	14	RS80-N/Omega	4/day IOP: 8/day	2 s	313
Portugal	Staff: INMG							
Lajes	08508	38.73N	27.07W	112	RS80-N/Omega	4/day (Jan:2/day)	variable	173
Lisboa Gago	08579	38.77N	09.13W	104	RS80-N/Omega	2/day	2 s	
Funchal	08522	32.63N	16.90W	56	RS80-N/Omega	4/day	2 s	233
Spain	Staff: INM							
La Coruna	08001	43.37N	08.42W	67	RS80-N/Omega	4/day	10/30 s	206
United King.	Staff: UKMO							
Lerwick	03005	60.13N	01.18W	84	RS80-L/LoranC or VIZ/LoranC	4/day IOP: 8/day	2 s or VIZ wind 20 s	285
Stornoway	03026	58.22N	06.32W	13	RS80-L/LoranC	4/day IOP: 8/day	2 s	302
Boulmer	03240	55.41N	01.6W	23	RS80-L/LoranC	4/day IOP: 8/day	2 s	266
Hemsby	03496	52.68N	01.68W	14	RS80-L/LoranC	4/day IOP: 8/day	2 s	268
Aberporth	03502	52.13N	04.57W	121	RS80-L/LoranC	4/day IOP: 8/day	2 s	277
Camborne	03808	50.22N	05.32W	88	RS80-L/LoranC	4/day IOP: 8/day	2 s	312
Hillsborough	03920	54.48N	06.10W	38	RS80-L/LoranC	4/day IOP: 8/day	2 s	304
Canada	Staff: AES							
Sable Island	71600	43.93N	60.02W	4	RS80-L/LoranC	4/day	10 s	240
St Johns	71801	47.62N	52.73W	140	VIZ/LoranC	4/day	variable wind 1 mn	206
Goose Bay	71816	53.32N	60.36W	38	RS80-L/LoranC	4/day	5 s	212
Kuujjaq	71906	58.10N	68.42W	60	RS-80/Omega or RS-80/CommVLF	4/day	10 s	215
USA	Staff: NOAA							
Charleston	72208	32.9N	80.03W	15	VIZ/Radiotheodolite	2/day IOP: 4/day	6 s	146
Wallops Isl.	72402	37.93N	75.48W	12	VIZ/Radiotheodolite	2/day IOP: 4/day	1.2 s wind 1 mn	170
Chatam	74494	41.67N	69.97W	14	VIZ/Radiotheodolite	2/day IOP: 4/day	6 s	169
Bermuda	Staff: USNavy							
Kindley	78016	32.36N	64.68W	6	RS80-N/Omega	4/day	10 s	236

when the meteorological measurements and Argos locations have different times. If necessary, recalibration based on the buoys monitoring statistics is applied to the meteorological measurements.

Measurements from nine NOAA buoys, retrieved from the GTS, were validated by CMM. CMM also validated the data from five UKMO moored buoys, from the raw Argos files.

The location and the meteorological measurements were drawn and visual checks were performed for each of these 67 buoys. The location of buoys with pressure measurements is shown in Fig. 4.9.

Figure 4.9: *Location of buoys with pressure measurements. large dots: UKMO moored buoys validated by CMM*

European COST-76 Wind Profiler Network

Eleven wind profilers in Europe performed hourly profiles during FASTEX. Some of these are operational profilers, the others are research ones. Table 4.5 summarises their characteristics. Measurements from the three French profilers are described in W. Klaus (1998). The data from all the profilers are available in the FCA.

4.6.2   Measurements from the World Weather Watch and commercial aircraft

A large subset of the measurements done during the FASTEX field phase (January and February 1997) and received from the GTS is available in the FCA. Data archived are included in a large domain centered on the North Atlantic: 20N-90N,140W-40E. Messages were decoded and geophysical measurements and significant WMO codes

Table 4.5: *European Wind Profilers*

Site	WMO Code	Lat	Lon	Alt (m)	Frequency (MHz)	Staff	Type
Aberystwyth (UK)	03501	52.42N	4.00W	50	46.5	UKMO	operational
Camborne (UK)	03807	50.13N	5.10W	88	40.3	UKMO	research
Brest (France)	07113	48.45N	4.42W	15	1238.0	Ets.Degreane	research
Lannemezan (France)	07114	43.08N	0.21E	597	45.0	CNRS/LA	research
La Ferté Vidame (France)	07112	48.61N	0.87E	244	52.0	Météo-France	operational
Toulouse (France)	07115	43.56N	1.36E	158	45.0	Météo-France	research
Hamburg (Germany)	10999	54.00N	9.50E	20	1240.0	Met.Obs.	research
Lindenberg (Germany)	10394	52.21N	14.13E	101	482.0	Met.Obs.	research
Lindenberg (Germany)	10394	52.21N	14.13E	101	1290.0	Met.Obs.	research
Cabauw (Netherlands)	06348	51.95N	4.88E	0	1290	KNMI	research
Payerne (Switzerland)	06610	46.82N	6.95E	491	1290.0	Swiss.Met.I.	research
Bilbao (Spain)	08025	43.37N	3.03W	60	1290.0	Univ.of Bilbao	research

are available in ASCII files. This allows easy access on these measurements to the whole scientific community. Data sets available include commercial aircraft data sets, from AMDAR, AIREP and ACARS messages, surface measurements from ground principal stations (SYNOP messages) and ships (SHIP messages), soundings from TEMP and TEMPSHIP messages, sea measurements from ships (BATHY messages) and buoy measurements (BUOY messages).

All the data sets are provided with quality control flags. These flags were calculated by the operational service of Météo-France, according to the WMO recommendations, when the data were received. If a validated data set replaces the GTS data set, or if manual checking is done by the FCA, the quality control flags values are updated.

Surface measurements from ships have a great interest for FASTEX analysis. This data set was validated by the FCA. Control procedures are described in section 4.74.7.2. The geographic coverage of this data set is shown in Fig. 4.10.

4.6.3   Satellite Imagery and products

Satellite Imagery

Météo-France/CMS provided the imagery from the geostationary satellites METEOSAT and GOES-EAST, and the polar orbiting satellites NOAA 12 & 14, for all the channels of the imagers. Special computations were made from FCA requests. The data from the four satellites are in the same geographical projection. The domain is shown in Fig. 4.11. The image resolution choosen for the satellite imagery is higher or close to the imager resolution at 45 degrees latitude, and allows for the easy use of several channels of the same satellite, and for the use of imagery from several satellites (see Table 4.6).

Thirty minute data from the 5 channels of the GOES-EAST Imager were received in real time at CMS. Thirty minute data from the 3 channels of the METEOSAT imager were partly received in real-time at CMS, and partly in delayed time, sent by the EUMETSAT Archive Service. The EUMETSAT Archive Service provided full resolution visible data and some Infrared and Water Vapor slots which were not disseminated in real time in full domain. The HRPT NOAA 12 & 14 data were received in real time at CMS (Eastern domain) and at the Canadian Atmospheric Environment Service (AES) in Halifax (Western domain). The CMS computed all

Figure 4.10: *Location of the operational surface measurements from commercial and FASTEX ships during FASTEX*
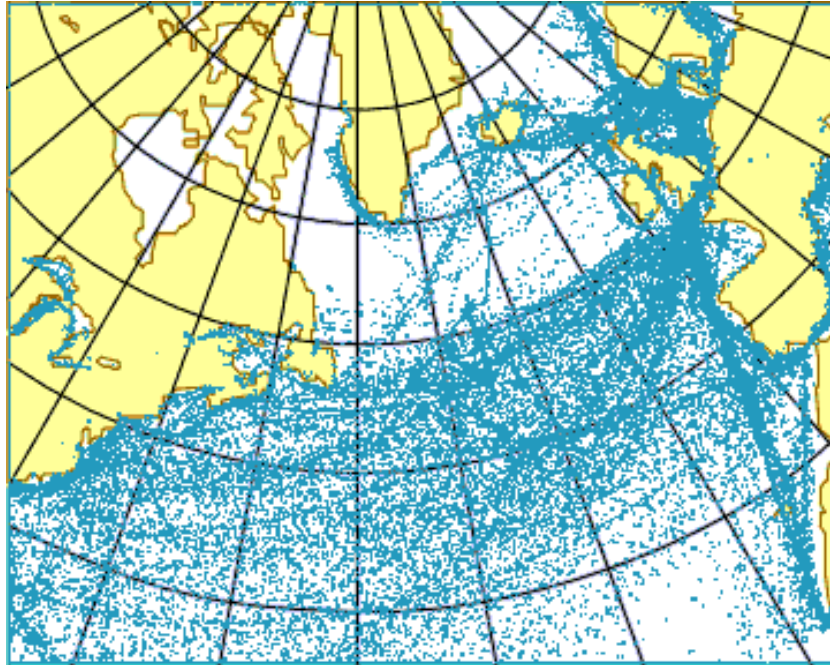
Table 4.6: *Satellite imagery specifications*

Satellite	Channels	Size (km)		Resolution		Size(pixels)	
		X(km)	Y(km)	x(km)	y(km)	columns	rows
GOES-EAST	1,2,4,5	7875	6750	7.5	7.5	1050	900
GOES-EAST	3	7875	6750	15.0	15.0	525	450
METEOSAT	VIS	6000	6750	5.0	5.0	1200	1350
METEOSAT	IR, WV	6000	6750	7.5	7.5	800	900
NOAA	all	5000	6000	2.0	2.0	2500	3000

the imagery received at Halifax and Lannion for the 5 channels. There is one data file per orbit scan and channel.

The satellite products

The NOAA/TOVS Total Ozone Content was prepared by Fernand Karcher (Météo--France) from the NOAA/TOVS raw data (level-1b files) produced by the NOAA/-NESDIS for the 2 satellites (Lefèvre *et al.* 1991). This product is provided at the spatial resolution of the sounder, that is 17x17km at nadir and 59x30 km at the end of the scan. The geographical domain is the FASTEX domain (20N-90N,140W-40E).

The significant wave height and the average surface wind speed, both at a resolution of 5x5km, are computed from the TOPEX-POSEIDON Altimeter data. The TOPEX-POSEIDON WIND/WAVE product was prepared by the CLS/AVISO Operations Center, Ramonville St-Agne (FRANCE). The product is provided along the altimeter trace, when it is in the FASTEX domain.

Figure 4.11: *Geographical coverage of the satellite imagery*

GOES-EAST
NOAA geostationary satellite
located at 75W 0N
half-hourly imagery from the 5 channels
resolution:
7.5km at 45N for channels 1,2,4,5
15km at 45N for channel 3

METEOSAT
EUMETSAT geostationary satellite
located at 0W 0N
half-hourly imagery from the 3 channels
resolution:
5km at 45N for VIS
7.5km at 45N for IR and WV

NOAA-12 and NOAA-14
NOAA polar orbiting satellite
orbit by orbit imagery from the AVHRR
5 channels scanning radiometer
resolution: 2km at 45N

The following other products are also available:

• the GOES cloud drift winds product prepared by Chris Velden from the raw data of the NASA geostationary satellite GOES-East (Velden et al., 1997),

• the 30 km resolution SATEM prepared by CMS from the HRPT NOAA data received at CMS and AES (Lavanant et al., 1997),

• the 25 km resolution speed and direction of the surface wind from the ERS-2 scatterometer data prepared by CERSAT.

4.6.4   The ARPEGE model analysis fields

Analyses are performed with the operational data assimilation and forecasting model ARPEGE/IFS at Météo-France. Since 1987, Météo-France and the European Center for Medium Range Weather Forecasts (ECMWF) have developed a new forecast system called ARPEGE/IFS (Courtier *et al.*, 1991). At the time of the experiment, the ARPEGE/IFS model was running with a semi- Lagrangian semi-explicit scheme. The resolution was T149, 27 levels with stretching 3.5. Time step: about 600s. The average resolution over the Atlantic is (roughly) equivalent to T300, T400 and more over western Europe (the pole is over France). The six hourly ARPEGE analyses are the outcome of the data assimilation suite run by Météo-France in Toulouse during the field phase. This data set was obtained from the operational analyses and covers entirely the two months of the FASTEX experiment. They incorporate the extra-FASTEX data that have been transmitted in real time to Toulouse. The analysis scheme was an optimal interpolation followed by digital filter initialization. The idea is to provide a self-contained data set enabling:

- •the study of the model simulation, global or in limited area, and

- •the computation of diagnostics from the analyses with good precision on spatial derivatives.

This data set is available for the period from 1 January 1997 0Z to 28 February 1997 18Z, with a frequency of 6 hours. The data set is projected on a global grid, latitude × longitude, with a resolution of 1.5 degrees. Vertically, the atmosphere is described through 24 pressure levels. Parameters available are geopotential height, the zonal and meridional wind components plus the zonal and vertical derivatives, the horizontal wind divergence and the vertical component of vorticity, the temperature and its 3 derivatives, and the specific humidity and its 3 derivatives. Six surface fields are also available: pressure, orography used for vertical interpolation, surface temperature including analysed Sea Surface Temperature, soil temperature and water content. The format used is WMO GRIB. The ECMWF software to read GRIB files can be provided by the FCA on special request.

4.7   Quality Control Procedures applied by the FCA

The measurements from the research instruments were processed by scientists or organisations participating in FASTEX. Checks applied by the FCA included:

- •all the files are read,

- •the uniqueness of each measurement is checked,

- •average, minimal and maximal values for each parameter are computed,

- •some samples are drafted to verify spatial and time consistency.

The data provider was informed if a problem appeared, and correction, or new release, or comment for documentation, was provided.

The data sets retrieved from the GTS are provided with Quality Control (QC) flags on the observation, and on some measurements like position, pressure, temperature, humidity and wind. These QC flags were calculated when the BUFR messages were decoded. The tests have been settled from controls made at the ECMWF, which have in general been extracted from the WMO guide on data processing (WMO 1982) . For each type of message, there are 3 different steps of control:

1. Unconditional checks when parameters can take only some defined values.

2. Gross limit checks for air, dew point and sea temperatures, pressure and its tendency, wind speed, geopotential height , etc...

3. Internal consistency checks between some parameters of an observation, like wind speed and direction, pressure and its tendency, and vertical wind shear for soundings.

The quality controls are presented in a Météo-France/SCEM note (1996). An english version is available on the FCA WWW site.

Some real-time data sets, retrieved from the GTS, were replaced by validated data sets. This was the case for EGOS buoys, UKMO moored buoys, and surface measurements from ships. When a data set is replaced, QC values are updated.

The surface measurements from the commercial ships data set contains precious informations on the meteorological environment of the FASTEX measurements. The FCA has done a best effort for quality control of this data set, which was not operationaly controlled by an international committee, as the buoys were.

Careful attention was given to verifying the location of the FASTEX and ASAP ships. A reference position data set was provided by the FASTEX ship data providers. The FCA used it to update the measurement locations in all the data sets, including the low resolution sounding one. The ASAP ship location from the surface measurement data set and the low and high resolution sounding data sets were compared. The ASAP ship velocity deduced from the ASAP ship positions, was calculated. Suspect positions were manually verified and corrected.

The FCA had in its charge to collect and to transpose in the same format the high resolution sounding data sets from the 29 ground stations, the 7 ASAP and the 4 FASTEX ships. The dropsonde from the 6 FASTEX aircraft were put in the same format as the radiosoundings. UCAR/JOSS was responsible for the Quality Control of the entire dropsounding and radiosounding data set. The methods used at UCAR/JOSS and at the FCA to verify the data set were slightly different. The method used at the FCA is explained below, the method used at UCAR/JOSS to attribute the QC flags is described in section 4.8. Table 4.7 summarises the QC procedures applied to the data sets available in the FCA.

4.7.1   FCA verifications on the sounding data set

Each data set was verified by the data provider before it was sent to the FCA. At Toulouse, each sounding was plotted and visually verified. The data insertion in the Data Management System allowed the assumption of the uniqueness of each measure identified by the sounding site, the launch date and time, and the time passed from the launch time. Errors dues to transmission, writing or reading the data, were detected first during the data insertion, and after when the minimum and maximum values for each sounding and each parameter were computed. For each problem, a dialog between the data provider and the FCA allowed its correction. Sometimes a new data set was provided, sometimes the data set was corrected at the FCA. The European meteorological services provided the FCA with the soundings launched in Europe and aboard the ASAP ships. UCAR/JOSS provided the FCA with the soundings launched in Canada and USA.

All soundings provided, except those from Lajes (Azores), are archived operationally by the Meteorological Services. The measurements were included without change in the FASTEX Archive. The Lajes data set was hand entered at the site by

the Portuguese Weather Service (INMG). Due to the lower resolution of these data in the upper levels, the FCA included data from the TEMP (GTS) messages within the high resolution data set.

When all the soundings from a site were included in the DMS, the complete data set was sent to UCAR/JOSS. UCAR/JOSS applied its Quality Controls Procedures (see Section 4.8) on each sounding and initialized the QC flags for each measurement line. The data set was sent back to the FCA, where the available data set was updated. The soundings data set is available in the same version and in the same format (JOSS quality control format) both in the FCA and in the UCAR/JOSS database.

The very good collaboration of the meteorological services has to be noted. They sent the data very quickly - many of them sent the data during the field phase - and answered additional questions with efficiency and efficacy.

The sounding data set from the FASTEX ships was also provided very quickly after the experiment, by Météo-France/GMEI (R/V Le Suroît, V.Bugaëv and Ægir) and NOAA/ETL and US-Navy/NPS (R/V Knorr).

8391 soundings compose this data set, 6785 soundings were launched by the ground stations, 406 soundings were launched by the ASAP ships, and 1100 by the FASTEX ships. The full high resolution sounding data set, validated and controlled, has been available since winter 97-98.

The same controls were applied to the dropsonde data set. The UK-C130 dropsonde measurements were processed and validated by the JCMM/University of Reading (UK), and quality controlled by UCAR/JOSS. The dropsondes launched by the US Air Force C130 were processed by the US Air Force, and validated and controlled by UCAR/JOSS. UCAR/JOSS processed and controlled the measurements from the NCAR GPS dropsondes (Lear jet, Gulfstream IV and WP-3D). See section 4.8 for a complete discussion of UCAR/JOSS sounding processing.

4.7.2   SHIP Message Quality Control

The automatic QC procedures, proposed by WMO and applied by Météo-France, allow the elimination of the major part of the wrong or doubtful measurements, before the data assimilation in an operational forecast system. For meteorological experiments analyses, and especially for case studies, a measurement could be very important in the interpretation. The validation of the surface measurements from the commercial ship data set is not internationaly organized, as the buoy data set validation is. So, the validation was done by the FCA. The procedures applied to the surface measurements done by the commercial ships during FASTEX allowed the cleaning of this data set, and sometimes the correction of the data.

The measurement, coding and transmission of the surface data aboard ships are often made in hard conditions, sometimes by people with little experience. Errors in this data set are due to different possibilities and can add up. The measurement errors are difficult to correct, whereas coding errors can be sometimes corrected. Some transmission problems can induce difficulties or errors in the automatic decoding of the message, sometimes to a duplication of messages, complete or not.

Checks are done on:

●the doubtful ship WMO codes,

●the location and the trajectory of each ship,

●the pressure and pressure tendency measurements,

●the temperature measurements.

Table 4.7: *Quality Control procedures applied to the data sets available in the FCA*

Dataset	Provenance	Checking
Commercial Aircraft Data	GTS (AIREP, AMDAR, ACARS messages)	WMO checks
Bathythermal Data	GTS (BATHY messages)	WMO checks
Buoy Data	EGOS Buoys: Météo-France/CMM from Argos raw files	CMM
	9 USA/GDC SVP drifters in the North Atlantic: GTS (BUOY messages)	CMM
	Other Buoys: GTS (BUOY messages)	WMO checks
Sea Temperature and Salinity from BUOY	3 EGOS Buoys: Météo-France/CMM from Argos raw files	CMM
	Other Buoys: GTS (BUOY messages)	WMO checks
SYNOPs Surface in-situ Data	GTS (SYNOP messages)	WMO checks
SHIPS Surface in-situ Data	R/V Le Suroît, V.Bugaëv, Ægir: GTS + ship archive	CNRM/GMEI
	Other ships: GTS (SHIP messages)	WMO checks + FCA checks
Average meteorological and Oceanic data from Research Vessels	R/V Le Suroît: Météo-France/CNRM/GMEI processing	CNRM/GMEI
	R/V Knorr: NOAA/ETL processing	NOAA/ETL
High resolution radiosonde Data	Data providers	data provider + FCA + UCAR/JOSS
Low resolution radiosonde Data	R/V Le Suroît, V.Bugaëv, Ægir: GTS + ship archive	WMO checks
	Other sites: GTS (TEMP, TEMPSHIP messages)	WMO checks
High resolution dropsounding Data	Lear36, NOAA Gulfstream IV, NOAA WP-3D: UCAR/JOSS processing	UCAR/JOSS
	USAF C130: USAF processing	UCAR/JOSS
	UKMO C130: JCMM processing	JCMM + UCAR/JOSS
Low resolution dropsounding Data	GTS + aircraft archive	WMO checks
Profiler on the FASTEX ships	ship measurements	real-time data set
Aircraft in-situ Meteorological Data	NOAA Gulfstream IV, NOAA WP-3D: NOAA/NSSL processing	NOAA/NSSL
	NCAR Electra: NCAR/RAF processing	NCAR/RAF
	USAF C130 : USAF processing	USAF
Composited images from Aircraft radar	NOAA WP-3D: NOAA/NSSL processing	NOAA/NSSL
Satellite Imagery	GOES-EAST, METEOSAT, NOAA-12, NOAA-14: Météo-France/CMS processing	CMS
Others Satellite products	Data provider processing	
Model analyzed fields	Météo-France ARPEGE Model	

A total of 164,000 GTS messages were received, validated and archived by FCA from ships other than the four FASTEX ships. The FASTEX ship measurements were validated by the data providers.

The unusual or doubtful ship WMO codes

The ship WMO codes usually use 4 to 8 letters. A long code could be erroneous. Also, a transmission problem could transform a WMO code into an unusual one. The WMO code attributed to a ship which broadcasted less than 5 messages during the 2 months of the experiment may be doubtful. Some messages come with the date or the name 'SHIP' instead of the WMO code. Some codes are not referenced in the WMO list of ships. All of these messages were considered to have doubtful codes. For each doubtful code, the message was compared to the other messages received in a spatio-temporal window of $\pm$ 12 hours and $\pm$ 3 degrees in latitude and longitude. The message was also compared to the messages sent by ships with closely related WMO codes. 820 messages were suppressed due to duplicated transmissions. 451 messages, with doubtful codes, were attributed without any uncertainty to another WMO code ship. The unknown codes of 2137 messages were replaced by the code 'SHIP'. 954 messages, from 306 unusual codes, could not be reattributed; the original code was maintained. 1.8 % of the received messages have a doubtful or unknown code.

Checks on ship location and trajectory

The successive locations of each ship were used to calculate its average speed. If this average speed and the ship course speed difference is greater than 12 km/h, the location is doubtful. When the ship course speed is not included in the message, an average speed greater than 50 km/h is doubtful. The ship locations were also compared to the locations calculated with the ship course heading and speed. When the distance between these two locations is greater than a limit value, the ship locations, heading and speed are checked. This limit value depends on the ship speed, the time between two successive observations and the heading steadiness, and also includes the lack of precision due to the WMO coding itself. Each doubtful location was edited. Typical code errors (latitude and longitude inversion, transposed figures in latitude or longitude value, erroneous coding of negative longitude) were corrected if possible. When this kind of error could not be corrected the quality code flag was set to doubtful or bad.

One of the automatic QC procedures applied at Météo-France is to compare the ship location with a land/sea mask. The land/sea mask, from the US-Navy, had a resolution of 10 minutes. If the four grid points surrounding the position of the ship are all land points, then the ship is considered to be over land. This procedure is effectual on the high sea or on the continents, but not for ships located on estuaries or on narrow rivers. A more accurate land/sea mask was used, calculated from the USGS Microwave databank II coastlines, lakes and islands at 0.1 degrees resolution, which is the precision of the ships location. The location of the ships considered to be over land by the automatic QC procedure were checked with this new land/sea mask. If 4 or more of the 8 points surrounding the position of the ship are water points, then the ship is considered to be over water. This procedure is more accurate than the automatic one, but again eliminates ships on some narrow rivers. The locations of these ships were checked with a geographical atlas. Some coding errors

were corrected. There remain 681 measurements with a doubtful or bad location, that is 0.4% of the available measurements.

Pressure and pressure tendency measurements

Some of the usual errors done in coding pressures higher than 1000 hPa (in hPa instead of in decimal hPa, allowing pressure values greater than 1060 hPa) were checked (1065 hPa instead of 1006.5 hPa). The doubtful pressure values were compared to the neighbouring pressure measurements when they exist, or to the sea level pressure field from the ARPEGE analysis.

The temporal evolution of the pressure was compared to limit values depending of the time between the two measurements. Limit values used were: 6 hPa per 1 h, 13 hPa per 3 h, 20 hPa per 12h, 30 hPa per 12h and 40 hPa per 24 h. When the pressure tendency was present, the temporal evolution of the pressure was compared to the pressure tendency. When the difference was greater than $3hPa$ per 6 hours, the pressure was visually checked. Measurements where corrected when an obvious coding error appeared. In other cases, the QC pressure flag was set to doubtful or bad.

2 % of the pressure measurements were flagged as doubtful or erroneous.

Temperature measurements

The temporal evolution of the temperature was calculated. When it was greater than a limit value depending of the time between the two measurements, the data were edited. Measurements were corrected when an obvious coding error appeared. In other cases, the QC temperature flag was set to doubtful or bad. Limit values used were: 6 degrees for 1h, 8 degrees for 3 h, 12 degrees for 12h, 15 degrees for 12h and 18 degrees for 24 h.

2 % of the temperature measurements were flagged as doubtful or erroneous.

4.8 Quality Control of High Resolution Sounding Data by UCAR/JOSS

UCAR/JOSS was given responsibility for the quality control (QC) of the FASTEX high resolution sounding data from the aircraft dropsondes (see Table 4.2), ships (see Table 4.3) and ground stations (see Table 4.4). The sounding QC procedures for FASTEX were based on those used by JOSS for the Tropical Ocean Global Atmosphere Coupled Ocean-Atmosphere Response Experiment (TOGA COARE; Loehrer *et al.* 1996). There were four processing steps used to QC the over 9000 soundings from FASTEX. The first process was the conversion of all data to a single, easily used format. The second process was the application of a series of automated internal consistency checks. The third process was a visual examination of every sounding. Finally, a special examination was conducted on the data from the aircraft dropsondes. This took the form of intercomparisons between the various aircraft dropsondes as well as between the dropsondes and the upsondes released from the FASTEX ships.

4.8.1 Format conversions

Each data provider had its own format(s) for its sounding data. In order to make the data easily useable by the scientific community UCAR/JOSS and Météo-France converted all soundings to a single ASCII format that both agencies agreed upon, the UCAR/JOSS quality control format (QCF). For a complete description of this format and an example please see Loehrer *et al.* (1996) . JOSS QCF has 15 data fields for measured and derived parameters and six additional fields for QC flags (see Loehrer *et al.* 1996 for the JOSS QCF flagging conventions). For the purpose of conducting a consistent QC methodology for the entire FASTEX data set, JOSS ignored any flags provided by the provider agencies.

The format conversion process also included the calculation of some derived parameters not initially available in the raw data. These were most often simple calculations (i.e. dew point, wind components, ascent rate of the radiosonde, and latitude/longitude position of the radiosonde). However, in the case of US National Weather Service (NWS) radiosondes, both wind speed and direction were calculated from the azimuth and elevation angles and the altitudes provided in the data set. This is a complex process due to the presence of oscillations within the measured angle data which can lead to oscillations in the winds. For complete information on the evolution of the UCAR/JOSS processing of high resolution winds in the US NWS radiosonde data see Williams *et al.* (1993) and Williams *et al.* (1998) .

The very high resolution dropsonde data from the Lear 36, Gulfstream IV, and NOAA WP-3D were reprocessed by UCAR/JOSS during this format conversion process. These data arrived to JOSS as 0.5 s vertical resolution data files with the data beginning prior to release of the dropsonde from the aircraft. Two modifications to the raw data set were made. First, JOSS determined the actual release point and started the data files about 20 s after that time, in order to allow for the acclimation of the dropsonde instrument package to the environment outside the aircraft. Second, JOSS developed 2 s vertical resolution data files from the 0.5 s data. This was done due to the presence of significant amounts of "bad" data within the 0.5 s data files. JOSS conducted a loosened version of its automated quality control processes on the 0.5 s data files to determine "bad" data points. These "bad" data points were then removed from the recalculation of the 2 s data files.

4.8.2 Automated internal consistency checks

UCAR/JOSS has for several years used an evolving set of automated internal consistency checks on high resolution sounding data from a variety of field programs (Loehrer *et al.* 1998) . These checks provide a quick and consistent test on every data point, thereby alerting users to potential problem areas within soundings. This process also helps to ensure that all format conversions were properly completed. All checks are applied from the surface up through the profile.

There are four types of automated checks used by UCAR/JOSS. They are:

1. inclusion of only numerical values

2. values within QCF format limits

3. values within reasonable climatology limits (see Table 4.8)

4. vertical consistency within a sounding/dropsonde (see Table 4.9)

The first two groups of checks typically do not result in flags being applied in the final version of the data but are used to verify the format conversion process. The third group of checks ensure that the values are within reason for the North Atlantic region climatology during winter and use a set of gross limits (Table 4.8). The flags are automatically applied within the data file to the affected data point. No flags are changed to the "good" value during this procedure. The checks for dropsondes varied slightly from those applied to the upsondes, the maximum allowable descent rate was 30 m s^{-1} due to the quicker rate of dropsonde descent versus radiosonde ascent. These gross limit checks (except the dew point $\leq$ -99.9°C check) affected a very small segment of the data with only 0.44% of data points flagged by these checks. Most of those flags were applied via the ascent rate checks. About 1% of all data points were flagged using the dew point $\leq$ -99.9°C check.

Table 4.8: *Gross limit checks applied to the FASTEX high resolution sounding data set.*

Parameter	Gross Limit Check	Parameter(s) Flagged	Flag Applied
Pressure	< 0 hPa or > 1050 hPa	p	B
Altitude	< 0 m or > 40000m	p, T, RH	Q
Temperature	< −80°C or > 30°C	T	Q
Dew Point	< −99.9°C or > 25°C	RH	Q
	> Temperature	T, RH	Q
Relative Humidity	< 0% or > 100%	RH	B
Wind Speed	< 0ms^{-1} or > 100 ms^{-1}	u, v	Q
	> 150 ms^{-1}	u, v	B
u Wind Component	< −100ms^{-1} or > 100 ms^{-1}	u	Q
	< −150ms^{-1} or > 150 ms^{-1}	u	B
v Wind Component	< −100ms^{-1} or > 100 ms^{-1}	v	Q
	< −150ms^{-1} or > 150 ms^{-1}	v	B
Wind Direction	< 0°or > 360°	u, v	B
Ascent Rate	< −10 ms^{-1} or > 10 ms^{-1}	p, T, RH	Q

p = pressure, T = temperature, RH = relative humidity.
u = zonal wind component, v = meridional wind component.
B = bad, and Q = questionable.

The final group of automated checks examined for vertical consistency within each sounding (Table 4.9). These were the most stringent checks applied during the processing. Again, these checks were applied beginning at the surface and were applied to neighboring data points except in a few cases where (for the purposes of QC only) some averaging of the data was employed. Again, the dropsonde checks varied slightly from those used for upsondes. In this case, the pressure (altitude) was checked to ensure it increased (decreased) with time. Over the entire FASTEX data set 1.33% of data points were flagged by these checks. Most of the flags were due to large inversions (some of which were deemed valid during the visual quality control procedure), large changes in ascent rates, and superadiabatic layers.

In summary, out of the about 9.5 million data points contained within the FASTEX high resolution data set there were about 265 000 reported "errors" (or about 2.8%). However, different checks can often find different errors affecting the same data points so the actual percentage of flagged data points is somewhat less. In comparison with other field programs, the FASTEX data set has a smaller proportion of flagged data points. This is mostly due to less frequent occurrence of superadiabatic layers than in the tropics, as would be expected in mid-latitude winter.

Table 4.9: *Vertical consistency checks applied to the FASTEX high resolution sounding data set.*

Parameter	Vertical Consistency Check	Parameter(s) Flagged	Flag Applied
Time	decreasing/equal	None	None
Altitude	decreasing/equal	p, T, RH	Q
Pressure	increasing/equal	p, T, RH	Q
	$> 1\text{hPas}^{-1}$ or < -1 hPas^{-1}	p, T, RH	Q
	$> 2\text{hPas}^{-1}$ or < -2 hPas^{-1}	p, T, RH	B
Temperature	$< -15°\text{Ckm}^{-1}$	p, T, RH	Q
	$< -30°\text{Ckm}^{-1}$	p, T, RH	B
from surface to 850 hPa:	$> 25°\text{Ckm}^{-1}$	p, T, RH	Q
	$> 40°\text{Ckm}^{-1}$	p, T, RH	B
for 275 hPa $< p <$ 800 hPa	$> 5°\text{Ckm}^{-1}$	p, T, RH	Q
	$> 30°\text{Ckm}^{-1}$	p, T, RH	B
Ascent Rate	change of $> (<) (-)3$ ms^{-1}	p	Q
	change of $> (<) (-)5$ ms^{-1}	p	B

p = pressure, T = temperature, RH = relative humidity.
u = zonal wind component, v = meridional wind component.
B = bad, and Q = questionable.

4.8.3　Visual examination

The next process in the UCAR/JOSS QC for FASTEX was the visual examination of each sounding. This process permitted a closer examination of the humidity and wind data. This QC step was identical to that undertaken by JOSS for TOGA COARE and the full details on this process can be found in Loehrer *et al.* (1996) . JOSS has developed an interactive skew *T*-log *p* diagram plotting routine which allows the scientist to automatically change the quality control flags within the sounding data file based on their knowledge of sounding structure. The severity of the flags can be increased or decreased by the scientist, so if the automated procedure flags a feature that upon visual examination appears to be an accurate representation of the atmospheric conditions, that flag can be decreased in severity from what the automated procedure provided. In the case of FASTEX, many large inversions that were flagged by the automated procedure were determined to be realistic features during the visual examination.

One problem that was found during this visual examination process during FAS-TEX was the existence of some significant "mismatches" between the independent surface humidity measurements and the initial radiosonde humidity measurements. This was especially true on some of the ships. A particularly severe example of this can be seen in Figure 4.12. Here, in the case of the ASAP ship *Irena Arctica*, the first several data points from the radiosonde show much drier conditions than the independently measured surface humidity. The radiosonde values then appear to recover to values that appear to be more representative. This problem has been noted to a significant degree in association with the soundings from TOGA COARE (Cole 1993 and Loehrer *et al.* 1996) as well as from other programs (Loehrer *et al.* 1998) . There have been many suggested causes for these problems, but in this case the problem appears to lie in not allowing the radiosonde to properly acclimate itself to the environment prior to its release. For most of the FASTEX sites, this problem occurred rarely, with $\leq 1\%$ of soundings affected. However, the ASAP ships *Nuca Arctica* ($\sim 20\%$) and *Godafoss* ($\sim 10\%$) had significant numbers of soundings

affected. Also, *Godafoss* had another $\sim 10\%$ of soundings where the independently measured surface humidity value was significantly drier ($\geq 5°$C dew point difference) than the radiosonde values.

Figure 4.12: *An example of a mismatch problem between the surface and initial radiosonde data. The sounding is from the ASAP ship Irena Arctica at 1200 UTC on 16 January, 1997. Note the reduced pressure scale.*
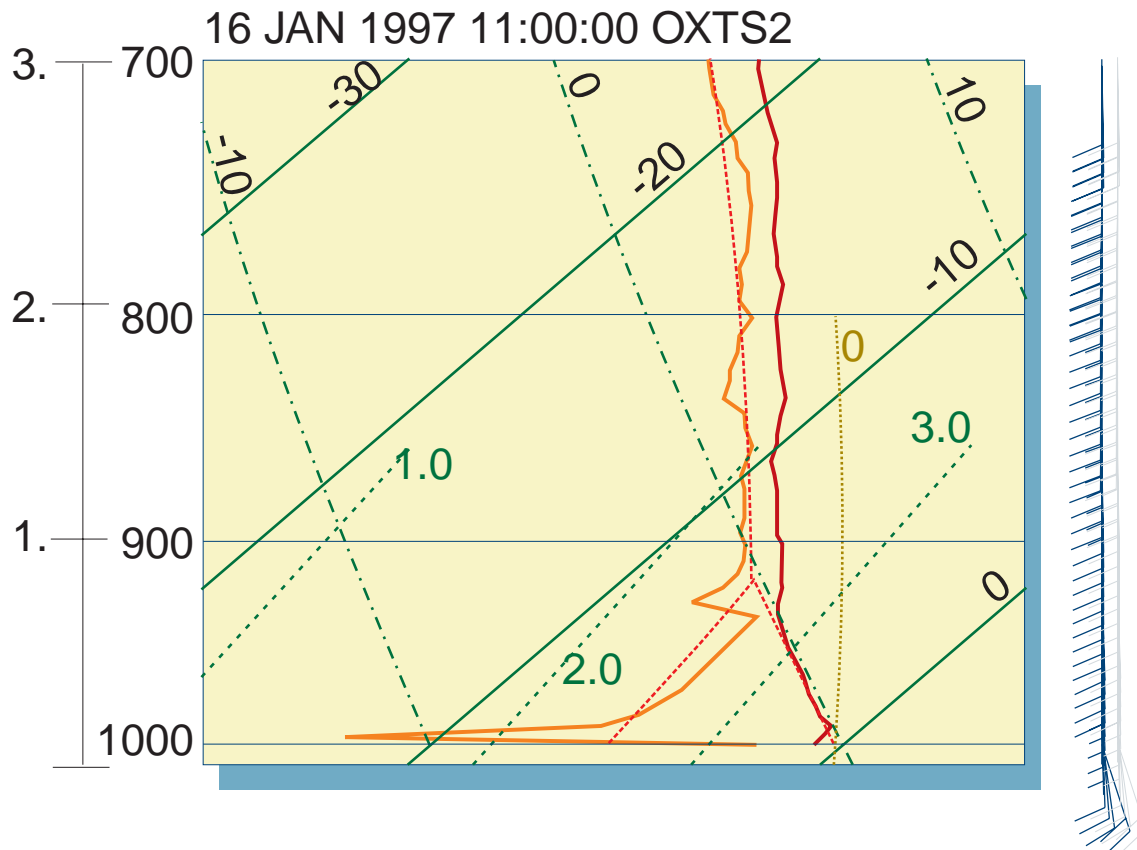
Another problem that needs to be noted occurs in US NWS soundings from Chatham, MA, USA and Charleston, SC, USA. As was mentioned previously, the calculation of the winds at these sites was complicated by the presence of oscillations in the measured angle data. As described in Williams *et al.* (1998) , JOSS applies a scheme that includes outlier removal, smoothing, as well as the application of a notch filter. JOSS focuses the notch filter to the periods most often seen in the oscillations (90 to 190 s). This is done to allow the removal of the effect of the majority of the oscillations, but still keep the mesoscale wind features in the wind profile. However, the tight focus of the notch filter allows some oscillations to remain within the wind data. The problem is particularly still present in conditions that lead to elevation angles $\leq 15^o$ (i.e. strong winds). This was the case in $\sim 6\%$ of soundings from Charleston, SC and $\sim 5\%$ of soundings from Chatham, MA.

In summary, the visual examination in FASTEX often led to a decrease ($\sim 0.5\%$) in the number of temperature and pressures flagged as "questionable" or "bad" due to occasional over flagging by the automated QC in the case of large inversions. These parameters have little additional flagging done in visual examination due to

the overall good performance of the automated QC, which identifies most problems involving these parameters adequately.

In the case of the winds, at most sites the additional flags applied during this process were quite small $\leq 1\%$. However, some sites (i.e. US NWS, French operational, and dropsondes) had from 3-5% of all winds flagged during visual examination.

The relative humidity from the surface to about 350 hPa again had few additional flags applied during this process ($\leq 1\%$). From 350 hPa to 50 hPa (the highest point checked in the visual examination) the amounts of humidity data points flagged could be very high ($\geq 10\%$). The humidities flagged were typically in regions of the sounding that were very cold ($\leq -40^oC$) and dry ($\leq 15\%$) where humidity measurements become difficult and filled with problems. Often the humidity sensor becomes frozen and on a skew T-log p diagram the dew point curve mirrors the temperature curve. Also, at sites which report the relative humidities only to the nearest whole percent, at low humidities the dew point values change large amounts with small changes in relative humidity, which leads to an erratic appearance.

4.8.4 Dropsonde intercomparisons

One of the important and unique aspects of the FASTEX data collection strategy was the use of dropsondes released from aircraft to specifically target and/or document cyclones or areas of potential development. These data are critical to achieving a primary objective of FASTEX concerning forecast improvement. As the initial processing and quality control of nearly 1300 dropsonde launches from the research aircraft platforms progressed, some problems arose that required special attention. Specifically, inconsistencies were found in the measurement of humidity made by several groups using different types of dropsonde expendables. At the time of publication some of these issues are still being examined. However, the authors felt it important that the community be aware of these problems and take them into consideration when dropsonde data are used in analyses.

The known problems with the dropsonde data sets include:

- Incorrect temperature was used to correct humidity. This problem was discovered during processing and has been corrected.

- Contamination of the capacitive sensor's dielectric material by outgassing products from the radiosonde's case and some of the bonding agents. This typically leads to a "dry bias" in the humidity measurement. A resolution to this problem is still being considered.

- Wetting of the humidity sensor during descent causing saturation during most of the profile. This problem remains under investigation.

- Possible effects of heating the humidity sensor on the latest model of expendable package used. This potential problem remains under investigation.

We have identified corrections, if any, that have been made to the data sets that are available from the FCA and JOSS. The first problem concerns the initial calculation of relative humidity (RH) and its adjustment for changing environmental conditions as required by the manufacturer. The Vaisala humicap humidity sensor has a temperature coefficient that is applied in the calibration equation to correct the humidity measurement. It was determined by the data provider that the internal radiosonde package temperature was used to adjust the humidity rather than the ambient outside temperature. This problem existed for the Gulfstream IV, Lear 36 and WP-3D data sets. It has now been corrected.

The next problem concerns contamination of the humidity sensor by outgassing from the resin impregnated radiosonde case and from some of the sealant and bonding products used in the manufacture of the expendable package. A portion of this problem was discovered during FASTEX (i.e. resin impregnated case material) so some of the dropsondes used by the Gulfstream IV and Lear 36 were modified to eliminate that portion of the problem. However, other outgassing problems were discovered after FASTEX and those problems will affect the FASTEX dropsonde data and remain unresolved. An error correction curve has been established but it can only be applied on a sensor by sensor basis. In addition, the amount of time the sensor is stored, and therefore exposed to the outgassing products has an impact on the magnitude of the measurement error. It is clear that the measurement error introduces a dry bias to the humidity observation. Any sort of "correction" process will be both tedious and risky especially if there is no corroborating in-situ humidity measurement. The possibility of making a correction for the dry bias is still being considered but can only be done on soundings exhibiting a known reference condition (e.g. saturation in cloud) (Cole, personal communication).

As JOSS continued its processing and quality control of the sounding data set, it was deemed useful to do some simple comparisons between dropsondes and upsondes, sensor types, and temperature and humidity regimes. Tables 4.10 and 4.11 provide a general summary of these intercomparisons. Table 4.10 provides the percent occurrence (regardless of temperature) of binned RH values in the lower levels (surface to 700 hPa) of the dropsonde data from the Gulfstream IV, Lear 36 and UK C-130 and the upsondes from the *Ægir*. The *Ægir* is taken to be representative of all four of the FASTEX ships (see Table 4.3) as they all had similar sounding statistics and instrumentation. The *Ægir* used a Vaisala RS80-18 Global Positioning System (GPS) radiosonde, the Lear 36 and Gulfstream IV used a Vaisala RD93 GPS dropsonde which uses Vaisala's most recently developed module which has dual humidity sensors that can be heated, and the UK C-130 used a Vaisala RD82 GPS dropsonde. The Aegir and the UK C-130 use the same single humidity sensor which does not have any heating capability. There are two extremes obvious from Table 4.10. The dropsondes from the UK C-130 had $\sim 64\%$ of all data points at these levels with RHs $\geq 90\%$, while the Gulfstream IV and especially the Lear36 had significantly lower occurrences of $\sim 25\%$ and $\sim 10\%$ respectively. The FASTEX ships fell between the extremes at $\sim 30\%$. The humidity sensor used by the UK C-130 was not heated, and there is some evidence here that once the dropsonde was deployed from the aircraft and the humidity sensor reached saturation, there was a tendency for it to remain saturated for the remainder of the flight (e.g. sensor got wet). This problem is currently being investigated by JCMM. Investigators should consider this fact and contact JCMM when using these data in their analysis efforts. Also in Table 4.10, the occurrence of very low RH values at these sites was quite varied. In this case, however, the Lear 36 is quite different from all of the others, including the Gulfstream IV. The Lear 36 had $\sim 16.4\%$ of all data points with RHs $< 20\%$ while the Gulfstream IV and Ægir were ~ 5-6% and the UK C-130 only 1.8%.

Table 4.11 provides the percent occurrence of radiosonde reported saturated conditions for temperatures $\leq 0^oC$ and $> 0^oC$ for the same sites as in Table 4.10. The differences here are dramatic. The same general pattern appears here as in Table 4.10, i.e. a very moist UK C-130 data set, much drier Lear 36 and Gulfstream IV data sets and the *Ægir* data set between the extremes. Note, however, that there is a difference in the occurrence of reported saturated conditions in different temperature

Table 4.10: *Percent occurrence (regardless of temperature) of binned relative humidity values for data points from the surface to 700 hPa for the Gulfstream IV, Lear 36 and UK C-130 dropsondes and the FASTEX ship Ægir upsondes.*

RH %	Gulfstream IV %	Lear 36 %	UK C-130 %	Ægir %
$\geq$ 100	3.5	2.9	33.6	12.5
90–99	20.7	8.0	30.4	19.9
80–89	26.9	22.7	13.3	18.1
70–79	18.0	18.1	7.7	15.2
60–69	10.0	12.6	4.5	11.1
50–59	5.8	8.8	3.4	7.8
40–49	3.3	4.2	2.3	3.7
30–39	2.8	2.6	1.7	3.0
20–29	3.0	3.6	1.5	3.2
10–19	2.9	6.9	1.1	3.2
0–9	3.2	9.5	0.7	2.3

Table 4.11: *Percent occurrence of reported saturated conditions for data points with temperatures $\leq$ 0°C and > 0°C (regardless of pressure) for the Gulfstream IV, Lear 36 and UK C-130 dropsondes and the FASTEX ship Ægir upsondes. Relative humidity (RH) is related to liquid water*

Site	$\leq$ 0°C, $RH = 100\%$	> 0°C, $RH = 100\%$
Ægir	9.4	17.5
UK-C130	20.4	51.1
Lear 36	1.3	10.3
Gulfstream IV	1.6	8.5

regimes depending on the radiosonde type. The two sites that used an unheated humidity sensor (the UK C-130 and *Ægir*) had about a factor of two higher reported saturated conditions in the warmer temperatures versus the colder temperatures. However, the two sites that used a heated humidity sensor (Lear 36 and Gulfstream IV) reported saturated conditions a factor of five and eight (respectively) higher in the warmer temperatures versus the colder temperatures. Thus while the sites using the heated sensors reported fewer saturated conditions in general (i.e. regardless of temperature) than those sites using the unheated sensors, the effect becomes even more pronounced when temperatures are below 0C. It has already been noted above that there is a known dry bias based on the contamination of the sensor by outgassing by-products from sealant materials. In addition, there may be some effect by the cyclic heating of the humidity sensor during descent. This analysis of the heated sensor has not occurred as of this publication.

4.9   The FASTEX Data Base: Conclusion

The data collected during FASTEX are archived in the FASTEX Data Archive. The raw data are available from specialised data bases. The main part of processed data from FASTEX measurements, in geophysical units, are available from the FASTEX Central Archive at Météo-France. Its Internet address is:

http://www.cnrm.meteo.fr/fastex/.

Operational meteorological measurements in the FASTEX area, as well as the satellite imagery and some satellite products, and fields from the meteorological model ARPEGE analysis are also available in the FCA. The data sets diffused are the up-to-date qualified ones. The high resolution soundings data set, which is one of the most important FASTEX data set, was quality controlled by UCAR/JOSS. The FASTEX Central Archive is open to the whole scientific community, for research and educational purposes. It is planned to diffuse a large part of the FASTEX data sets on CD-ROMs when the major part of the data is in their final form.

The planning for a data management strategy to support the FASTEX project began two years before the field experiment. There is a very important lesson that projects must consider as they prepare for the field. As the scientific objectives and measurement strategies are being developed and finalized so should the policies, procedures and tools needed to handle the data sets be considered and implemented. Meteo France provided the central nucleus of manpower and resources to develop the FCA, reach agreement with national and international data centers for vital project related data sets, and help participants to organize and submit data for archival. This has permitted a rich and varied data set to be readily accessible at the FCA via the WWW.

4.10   Acknowledgments

4.11   References

Bougeault P., B. Benech, P. Bessemoulin, B. Carissimo, A. Jansa Clar, J. Pelon, M. Petitdidier, and E. Richard, 1990.
Momentum budget over the pyrénées: The PYREX experiment.
Bull. Amer. Meteor. Soc., **71**, 806–818.

Bougeault P., R. Benoit, and G. Jaubert, 1993.
The PYREX data base.
Technical Report 9, Note Météo-France/CNRM/GMME.
Available from CNRM, 42, avenue Gustave Coriolis, 31057 Toulouse cedex, France.

Cole H., 1993.
The TOGA COARE ISS radiosonde temperature and humidity sensor errors.
Technical report, Surface and SOunding Systems Facility Rep., National Center for Atmospheric Research.
26 pp. [Available from Surface and Sounding Systems Facility, National Center for Atmospheric Research, P. O. Box 3000, Boulder, CO 80307-3000.].

Courtier Ph., C.Freydier, J-F.Geleyn, F.Rabier, and M.Rochas, 1991.

The arpege project at meteo-france.
ECMWF seminar proceedings.
September 1991 Reading(UK).

Eymard L., G. Caniaux, H. Dupuis, L. Prieur, H. Giordani, R. Troadec, and D. Bourras, 1999.
Surface fluxes in the north atlantic current during the CATCH/FASTEX experiment.
Quart. J. Roy. Meteor. Soc., **125**, *submitted.*

Hollinger J., R. Lo, G. Poe, R. Savage, and J. Peirce, 1987.
Special sensor microwave/imager user's guide.
Technical report, NOAA/NESDIS.

Joly, A., D.Jorgensen, M.A.Shapiro, A.Thorpe, P.Bessemoulin, K.A.Browning, J.P.Cammas, J.P.Chalon, S.A.Clough, K.A.Emanuel, L.Eymard, R.Gall, P.H.Hildebrand, R.H.Langland, Y.Lemaitre, P.Lynch, J.A.Moore, P.O.G.Persson, C.Snyder, R.M.Wakimoto, 1997:
The Fronts and Atlantic Storm-Track Experiment (FASTEX): Scientific Objectives and Experimental Design.
Bull. Amer. Meteor. Soc., **78**, (9), 1917–1940.

Joly, A., K.A. Browning, P. Bessemoulin, J.P. Cammas, G. Caniaux, J.P. Chalon, S.A. Clough, R. Dirks, K.A. Emanuel, L. Eymard, R. Gall, T.D. Hewson, P.H. Hildebrand, D. Jorgensen, F. Lalaurette, R.H. Langland, Y. Lemaitre, P. Mascart, J.A. Moore, P.O.G. Persson, F. Roux, M.A. Shapiro, C. Snyder, Z. Toth, and R.M. Wakimoto, 1999:
Overview of the field phase of the Fronts and Atlantic Storm-Track Experiment (FASTEX) project.
Quart. J. Roy. Meteor. Soc., **125**, *submitted.*

Jorgensen D.P., P. Bessemoulin, S. Clough, and J.A. Moore.
Fastex operations plan, 1996.
Technical Report 5, FASTEX Project Office, Centre National de Recherches Météorologiques, 164pp.

Klaus W. and I. Seloyan, 1998.
Campagne CWINDE 97: Validation des profileurs de vents de La Ferté-Vidame, Toulouse et Lanemezan.
Technical Report 18, Note Météo-France/CNRM/GMEI.
Available from CNRM, 42, avenue Gustave Coriolis, 31057 Toulouse cedex, France.

Lavanant L., P. Brunel, G. Rochard, T. Labrot and D. Pochic, 1997.
Current status of the ICI retrieval scheme.
Preprints, 9th International TOVS Study Conference.

Lefevre F., D. Cariolle, S. Muller, and F. Karcher, 1991.
Total ozone from TOVS/HIRS2 infra-red radiances during the formation of the 1987 ozone hole.
Journal of Geophysical Research, **96**, 12893–12911.

Loehrer S. M., T. A. Edmands, and J. A. Moore, 1996.
TOGA COARE upper-air sounding data archive: Development and quality control procedures.
Bull. Amer. Meteor. Soc., **77**, (11), 2651–2671.

Loehrer S. M., S. F. Williams, and J. A. Moore, 1998.
Results from UCAR/JOSS quality control of atmospheric soundings from field projects.
Preprints, 10th Symp. on Meteorological Observations and Instrumentation, Phoenix, AZ, Amer. Meteor. Soc., 1–6.

SCEM/TTI/DEV, 1996.
DIAPASON preprocessing.
Technical report, Note Météo-France/SCEM.
Available from SCEM, 42, avenue Gustave Coriolis, 31057 Toulouse cedex, France.

Velden C. S., C. M. Hayden, S. J. Nieman, W. P. Menzel, S. Wanzong, and J. S. Goerss, 1997.
Upper-tropospheric winds derived from geostationary satellite water vapor observations.
Bull. Amer. Meteor. Soc., **78**, (2), 173–195, 1997.

Webster P. J. and R. Lukas, 1992.
TOGA COARE: The coupled ocean- atmosphere response experiment.
Bull. Amer. Meteor. Soc., **73**, 1377–1416.

Williams S. F., C. G. Wade, and C. Morel, 1993.
A comparison of high resolution radiosonde winds: 6-second microart winds versus 10-second class loran winds.
Preprints, Eighth Symp. on Meteorological Observations and Instrumentation, pages Anaheim, CA, Amer. Meteor. Soc., 60–65.

Williams S. F., S. M. Loehrer, and D. R. Gallant, 1998.
Computation of high-resolution national weather service rawinsonde winds.
Preprints, 10th Symp. on Meteorological Observations and Instrumentation, Phoenix, AZ, Amer. Meteor. Soc., 387–391.

World Meteorological Organization, 1982.
Guide on the global data processing system.
Technical Report 305, WMO.
Available from Secretariat of the World Meteorological Organization, Geneva, Switzerland.

Wind derivatives and terminal fall velocities retrieval from "purls" flight patterns in IOP 12

by
Georges Scialom,
Alain Protat,
and Yvon Lemaître

Centre d'étude des Environnements Terrestre et Planétaires, CNRS, Vélizy, France.

5.1 On the interest of Dual-Beam Airborne Velocity Azimuth Display

ince the beginning of modern meteorology, and especially of radar meteorology, the description of the dynamical structure and organization of precipitating systems is a problem of crucial interest for many scientists. This interest has been progressively evolving from the large scale and convective scale motions toward the mesoscale motions on the one hand, and to the scale interactions on the second hand. The evolution toward the mesoscale studies is due to the possible importance of the mechanisms acting at this scale in the origin and the organisation of precipitation. As for cyclogenesis itself, two points of views have been put forward in recent years in order to account for the mesoscale organization of precipitations. One calls to an instability mechanism, slantwise moist convection driven by Conditional Symmetric Instability (Bennetts and Hoskins, 1979; Emanuel 1983; Bennetts and Sharp, 1982; Lemaître and Testud, 1988; Lemaître and Scialom, 1991). The other relies on the existence of an "external" forcing, indeed the frontogenetic forcing itself (Fischer and Lalaurette, 1995), that controls, via diabatic effects, the fine structure of ascent zones, and in particular the formation of weakly stable, strongly sheared areas. The mesoscale is also important because it interacts strongly with the larger scale by energy transfer and with the convective scale by humidity transfer. Another example of the importance of the mesoscale and of the scale interaction is the role shown to be played by the stratiform parts of the precipitating systems, e.g. the squall lines, in the maintenance of the system during several hours, and its propagation as long as it encounters environmental conditions of instability.

The feedback between current theory, experiment, and modelization, along with the crucial role of the mesoscale phenomena has impulsed a considerable development of the radar systems which are facilities particularly suited to this scale. While about twenty years ago, some field experiments (e.g. the GATE experiment, Houze and Betts, 1981) implied no Doppler radar, nowadays the major experiments, either devoted to tropical or to midlatitude meteorology, cannot be conceived and designed without these facilities.

An illustration of this feedback is the huge effort made for more than thirty years in the field of radar meteorology, particularly on devices (Doppler radars), and on analyses allowing the retrieval of the wind field. Concerning the devices, the most original part of the effort was devoted to developing airborne Doppler radars, while the activity on ground-based radars mainly consisted in setting up radar networks, like the NEXRAD network presently deployed over the USA (Alberty et al, 1991). Indeed, for more than ten years, airborne Doppler radars have proved to be an essential step in the evolution of radar meteorology, because of their ability to follow precipitating systems where they are, especially over oceans (Jorgensen et al, 1983; Hildebrand and Mueller, 1985). The first airborne Doppler radars possessed a single antenna scanning planes perpendicular to the aircraft track, offering a single view of the precipitating system. A second view is needed, in order to obtain (by using the mass conservation, or continuity equation) the three-dimensional wind field. Thus, if the aircraft performs successive perpendicular tracks around the precipitating area, the two angles of view allow to obtain the 3D wind field assuming stationarity of the observed system for the considered analyzed data set. Thus in this case, only large scale structure can be described adequately since smaller scale structures are not resolved.

When smaller scale motions are aimed at, two simultaneous scannings are required. This is why the FAST scanning was proposed by Frush et al (1986), and why dual-beam antennas were developed, scanning respectively cones with axis along the aircraft track and having an angle fore and aft with respect to the perpendicular to the track. This was the second step in the improvement of the airborne Doppler radar. The French-US ELDORA-ASTRAIA (Electra Doppler RAdar-Analyse Stéréoscopique par Radar à Impulsion Aéroporté) facility was the first radar of this type. While the ELDORA-ASTRAIA project was going on, the P3-43 radar of the NOAA was equipped with a French dual-beam antenna similar to that of ELDORA-ASTRAIA (Hildebrand and Moore, 1990). Several experiments were conducted which involved one or both of these radars. The CaPE experiment was the first in which the dual-beam antenna, newly installed on the P3-43 radar was operated within squall lines over Florida during summer 1991.
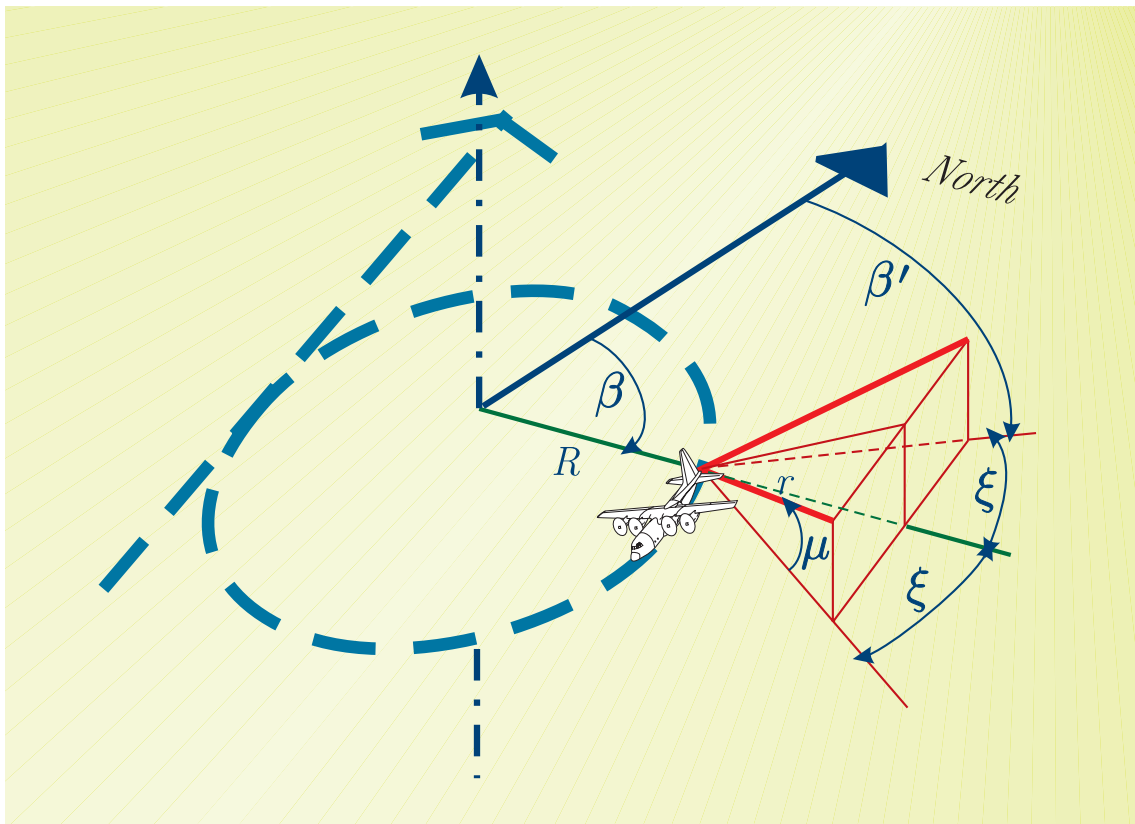
Figure 5.1: *Schematic view of the relevant elevation angles of the dual beam Doppler radar and as well as the azimuth angles.*

From then on, this radar is regularly used to scan tropical cyclones in the Caribbean area. Along with ELDORA-ASTRAIA, both radars were used during the TOGA--COARE experiment (1992-1993). While a lot of analyses are available for the wind field retrieval from ground-based radar data, the various case studies accumulated during the pioneer airborne radar experiments had evidenced the lack of analyses devoted to the wind field retrieval.

Thus, new wind analyses at several scales were developed and tested on the data sets extracted from these experiments. In particular, the cartesian method (Chong

and Campos, 1996), the COPLANE method (Chong and Testud, 1996), and the MANDOP method (Dou et al, 1996), currently used for ground-based radars, were adapted to airborne Doppler radar data. As for the classical (ground-based) VAD analysis which relies upon conical scannings, it can be adapted to airborne radars performing "purls", i.e. circles, in order to provide the mesoscale environmental wind field. When the radar is single-beam, the principle of the adaptation is straightforward but many specific problems must be resolved, as pointed out by Protat et al (1997) who implemented it under the name of SAVAD analysis, and applied it to the data of TOGA-COARE. If the airborne Doppler radar is dual-beam, we show in the following that it is possible to retrieve from the data gathered during the purls the linear approximation of the 3D wind field and the associated physical parameters of crucial importance, such as the vertical vorticity. This approach is called the DAVAD (Dual-beam Airborne Velocity Azimuth Display) analysis.

Developing such new analyses devoted to the retrieval of the wind field at the mesoscale was of crucial importance in view of the international field experiment FASTEX (Fronts and Atlantic Storm Tracks Experiment) which was held on january-february 1997. This experiment was aimed at studying the frontal waves and the cyclogenesis in the Atlantic Ocean. For this objective, frontal systems had to be scrutinized at several scales using in particular the above-noticed two aircraft with their dual-beam antennas. Performing purls all along the experiment allows obtaining the mesoscale wind field and fields of related parameters (vertical vorticity, divergence, deformation, terminal fall velocity of the hydrometeors), in the environment in a very regular way. This strategy of inserting purls along straight line tracks was systematically followed during FASTEX. Moreover, parallel to the development of new instrumentation, considerable efforts have been made on modelling. The design of FASTEX has taken into account the recent merging of both approaches, experimental and by modelling.

In this context, it was decided to include in the Data Base (described in Part 4 of this report) the vertical profiles of the wind and related parameters previously mentioned obtained throughout each sampled system in view of the validation and initialization of models by meteorological fields of experimental origin. Providing the database with the abovementioned parameters will allow to initiate this process.

A very brief and rough summary of the principle of the DAVAD analysis used in the present part of the Report is given. The potential of the approach is then shown, in sections 5.3 to 5.5, through its application to IOP (Intensive Observation Period) 12. This is the same case study as the one of Part 6, where the fields are reconstructed from the radar signal over a large area: this gives access to the 3-D structures present in the cloud system. A quick-look summary of the case is available in section 3.15 of Part 3, page 112 of this Report.

5.2   Outline of the DAVAD retrieval method

The original VAD analysis has been introduced by Browning and Wexler (1968). It relies on the conical scans that can be obtained from a single ground based Doppler radar. Scialom and Testud (1986) have extended this technique to two ground-based Doppler radars, leading to the more accurate Dual VAD.

The nearest equivalent for an airborne Doppler radar results from the aircraft performing a 360°turn around a fixed point, a pattern called "purl". The fixed point in question plays the role of the radar location in the classical problem.

The major difference results from the fact that the antenna(s) are not scanning in the direction of a radius taken from the center of the circle flown by the aircraft (denoted O), unlike a ground base radar. Airborne antennas are (or is, for single beam antennas) looking at an angle from the radius, denoted ξ (Fig. 5.1). It is nevertheless possible to circumvent this difficulty for both single beam antennas (Protat et al., 1997) and dual beam ones (see the submitted version of the present work, Scialom et al., 1999).

The goal is to obtain, at O, vertical profiles of the wind components ($u(z)$, $v(z)$, $w(z)$) together with the terminal fall velocity $V_f(z)$ of the cloud droplets and the first derivatives of the horizontal wind field about point O which combine into the vorticity $\zeta(z)$, the components of the deformation tensor $D_{eT}(z)$ and $Des(z)$ and the divergence $D(z)$. The terminal fall velocity V_f is an important information on the kind of cloud particle and it is also an important component of the observed signal: it is both useful and necessary to retrieve it in order to access the vertical velocity of the air w and, actually, even the horizontal components of the motion.

The input are measurements of the radial velocities V_r (radial with respect to where the antenna are pointing to, *not* with respect to O) for various elevation angles (with respect to the aircraft flight level) μ and at various distances r from the aircraft. Two sets are available in the case of a dual beam antenna. Measurements are available on each of the circles described by each sampling gate in which signal is received back. There is, however, a significant amount of noise in these raw observations and the whole problem is to limit oneself to that part of the scales that can be retrieved with some certainty. The noise is eliminated by creating redundancy in the available data and adjust to them the largest of the scale theoretically available.

At a given level z and a given radius $R + r$ from O, the observed wind V_r is a function of the azimuth β: this function is expanded into a Fourier series limited to order 2 in β:

$$V_r = V_0 + V_{c1} \cos\beta + V_{s1} \sin\beta + V_{c2} \cos 2\beta + V_{s2} \sin 2\beta. \qquad (5.1)$$

The raw measurements of V_r are turned into a number of values for the five coefficients V_0, V_{c1}, V_{s1}, V_{c2}, V_{s2}, obtained from a discrete set of radiuses and levels.

Another expansion of V_r can be written, first in terms of the wind conditions at the observed point:

$$V_r = -(u \sin\beta \cos\mu + v \cos\beta \cos\mu) + W(\beta)\sin\mu, \qquad (5.2)$$

where u and v are the usual horizontal wind components and $W(\beta)$ is the observed vertical component of the motion: the latter is dominated by V_f but also contains the vertical wind component w, generally very small, especially in stratiform clouds.

Finally, the horizontal wind itself is expanded to first order (linearly) with respect to its value at the center of the circle, so that equation 5.2 can be turned into an expansion of V_r as a function of β, but with coefficient explicitly given in terms of the various angles (μ, ξ) and distances (R, r) and the unknowns V_f, ζ, D_{eT}, D_{eS} and D, which, for a given level z are assumed to be constant. The detailed expression are beyond the scope of this short summary: see Scialom *et al.*, 1999. Identifying terms from Equation 5.1 and those from the first order development of 5.2 in terms of the wind derivatives yields the equations to be inverted.

To give an example, the first coefficient reads:

$$V_0 = V_f \sin\mu - 0.5 D \cos\mu (r\cos\mu + R\cos\xi) - 0.5R \zeta \sin\xi \cos\mu.$$

Ground base radars are such that $\xi = 0$, so that the first coefficient V_0 in this case is essentially related to the vertical motion (V_f and D, which, because of continuity, relates directly to w). For an airborne radar, this component now mixes up with vorticity ζ.

As the problem is still, by construction, strongly overdetermined, it is solved by a variational technique that makes the most of the measurements made available by the radar specifications. Provided the radar delivers enough data, the variational technique can take care of the new terms. Again, see Scialom *et al.*, 1999 for details.

5.3   Sampling strategy in IOP 12

The present section is devoted to an application of the DAVAD analysis to real data collected during FASTEX. This case study concerns Low 34 observed during FASTEX IOP 12. This low has been documented by Lemaître et al (1999).
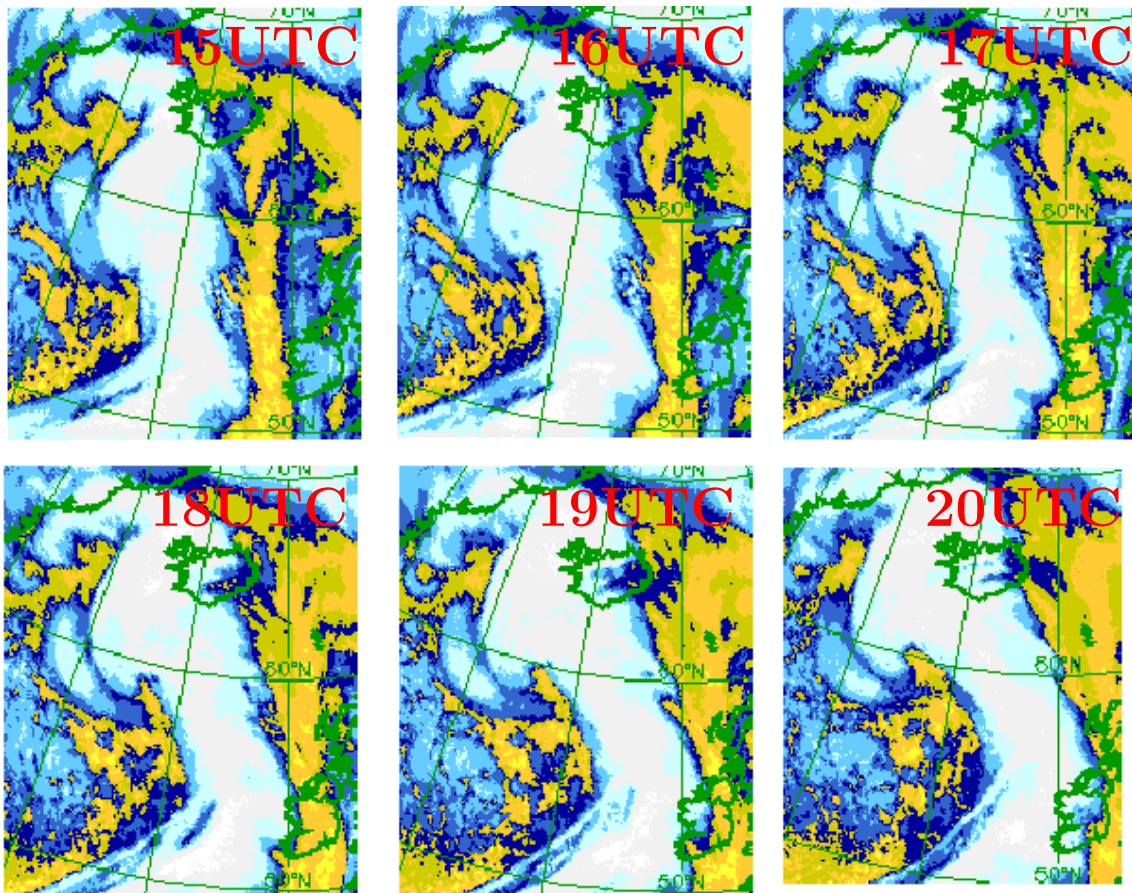

Figure 5.2: *METEOSAT Infra-Red images showing the motion and shape evolution of Low 34 during IOP 12 in the end of its phase of rapid development. Images courtesy of EUMETSAT and the Centre de Météorologie Spatiale of Météo-France.*

The main experimental facilities for that part of the study were the British C130 able to launch dropsondes, the French-US ELDORA-ASTRAIA radar, and the P3-42

NOAA aircraft Doppler radar both equipped with the dual-beam French antenna. The two airborne Doppler radars performed various types of trajectories among which lawnmower-type tracks regularly interrupted by purls (FASTEX Operations Plan, Jorgensen et al, 1996). The lawnmowers allow multiscale description of the lows using the MANDOP analysis (Scialom and Lemaître, 1990, Dou et al, 1996), while purls give mesoscale profiles of the wind and its first derivatives, as shown previously.

The case study which the DAVAD analysis is applied on is the most explosive deepening, roughly -54 mbar in 24 h (Joly et al, 1999) observed during FASTEX (9 february 1997). The METEOSAT satellite IR picture exhibits the evolution of the synoptic situation between 1500 UTC and 2000 UTC, with a drammatic (explosive) formation of Low 34a (as shown by the progressive growth of a cloud head and a dry slot feature that moves northeastward at 40 ms^{-1}, deepens and then tracks toward Iceland (Fig. 5.2). This low was sampled on the northwestern corner of the MSA. The reader is referred to Fig. 6.1 in Part 6, showing the IR picture at 1700 UTC with superimposed the aircraft trajectory in the frame of reference linked to the sampled system. It can be seen that the secondary low has been crossed over and sampled by the aircraft (in the present case, only the P3-42 aircraft was available, the Electra aircraft which bears the ELDORA-ASTRAIA radar being down). This figure illustrates the chosen sampling strategy, "lawnmower" type, which was intended to sample the precipitating systems at several scales and was intensively used during the FASTEX campaign.

The box in Fig. 6.1 delimits the $430{\times}430$ km^2 area in which the mesoscale scale retrieval of the dynamics presented in Lemaître et al (1999) was performed using the MANDOP analysis.

Fig. 5.3 exhibits the horizontal cross-section of the 3-D reflectivity field deduced from the P3 tail -radar mesurements, with the aircraft track put in the frame of reference relative to the whole precipitation area. This figure displays the main purls flown by the aircraft along the track between 1500 and 1800 UTC which will be referred to in the rest of this Part.

Lemaître et al (1999), by locating precisely the area covered by the radar within the satellite picture, identified three flows around the secondary low as it can be seen on their cross-section at 0.5 km showing the radar reflectivity and the retrieved wind fields (Fig. 6.4 and 6.5 in Part 6): the Cold Conveyor Belt (CCB) in the northern part of the figure (north of the convective band, with air at intermediate temperature); just south of this flow, the Warm Conveyor Belt (WCB) which wraps around the secondary cyclone. The convective area around the cyclone is the eastern part of the cloud head. The flow in the northwest part is possibly of polar origin, and the one in the southwest part is associated with the dry intrusion. The purls were mostly performed in this radar area as it appears on Fig. 5.3. The wind pattern displayed Fig. 6.5(a) suggests that vorticity on the mesoscale, is cyclonic at flight altitude in the secondary low area. We now summarize the main results from the DAVAD analysis.

5.4 Terminal fall velocity distributions

The vertical profiles of the terminal fall velocity V_f in stratiform or moderately convective areas are generally characterized by values about 5–12 ms^{-1} in the rain, below the 0°C isotherm, and 0–2 ms^{-1}, in the snow, above. In the present case, the processing of purls within stratiform precipitation is given by sample profiles in Fig. 5.4. It shows similar values within error bars. Profiles at 1625, 1634, 1659
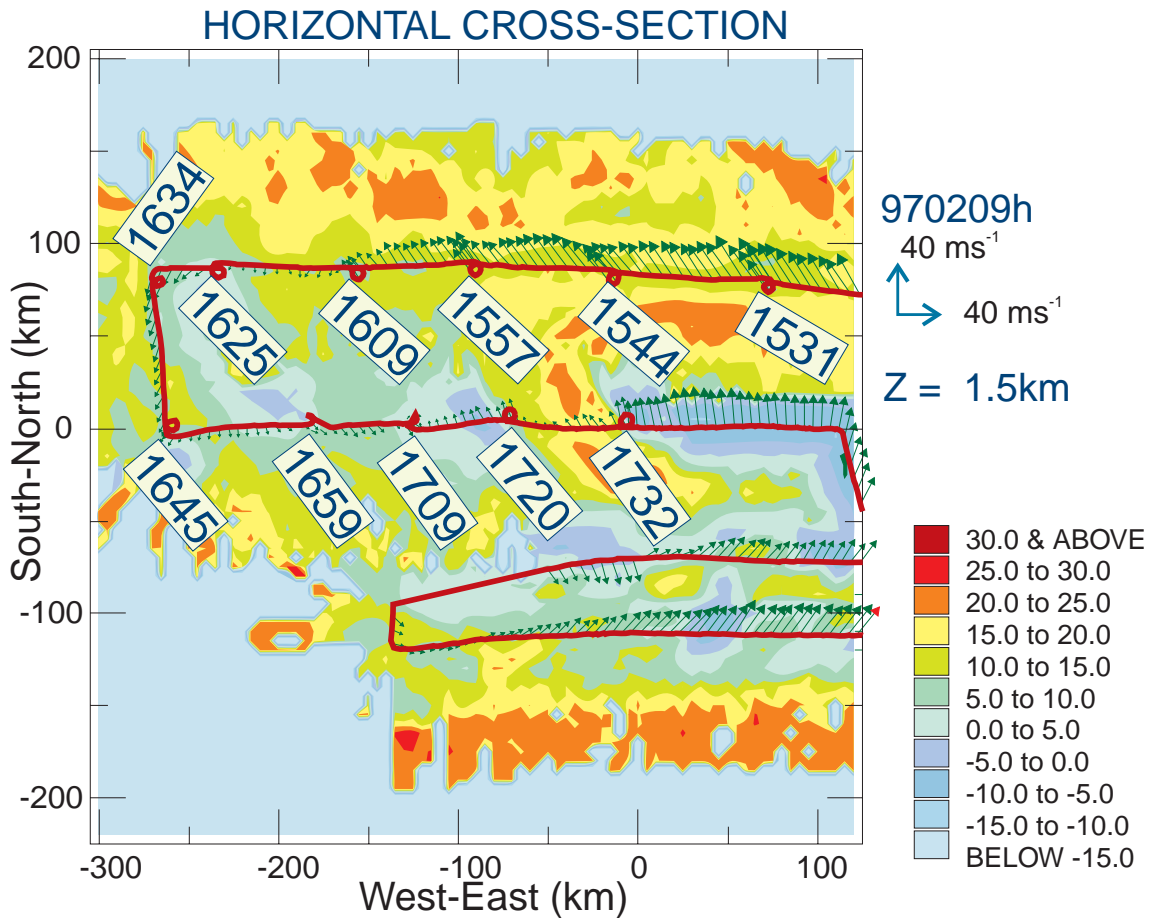
Figure 5.3: *Horizontal cross-section of the 3-D radar reflectivity field deduced from the tail-radar measurements at the flight altitude (1.5 km). The flight track is shown together with the purls labelled by the time at which they have been performed.*

and 1732UTC (not shown), do not exhibit such vertical patterns, which is consistent with the fact these profiles are mainly in nonprecipitating areas (see Fig.5). At last, profiles at 1709 and 1720UTC (also not shown) are intermediate and are obtained in mixed areas.

Fig. 5.5 shows two profiles of reflectivity Z and terminal fall velocity V_f taken in the two main regions of the cyclone, i.e. the CCB area (with overlapping WCB) for the 1531 UTC profile, and the colder northeasterly flow for the 1609 UTC profile; see also Fig. 5.3 for the location of the purls).

The dropsoundings performed by the UK C130 aircraft close to the purls processed to get these profiles show a layer (0°,-10°C layer) located between 1 and 2.5 km altitude, and 0.5 and 2 km for the 1531 and 1609 purls, respectively. This indicates that terminal fall velocity corresponds to ice particles above, and to water below.

We observe that globally, at 1531, the terminal fall velocity is sligly weaker than at 1609. This suggests that precipitating particles are bigger in the CCB area than in the northeasterly flow area. This is consistent with the localization of these purls rather in the high cloud and strong precipitation, for the first one, lower cloud and
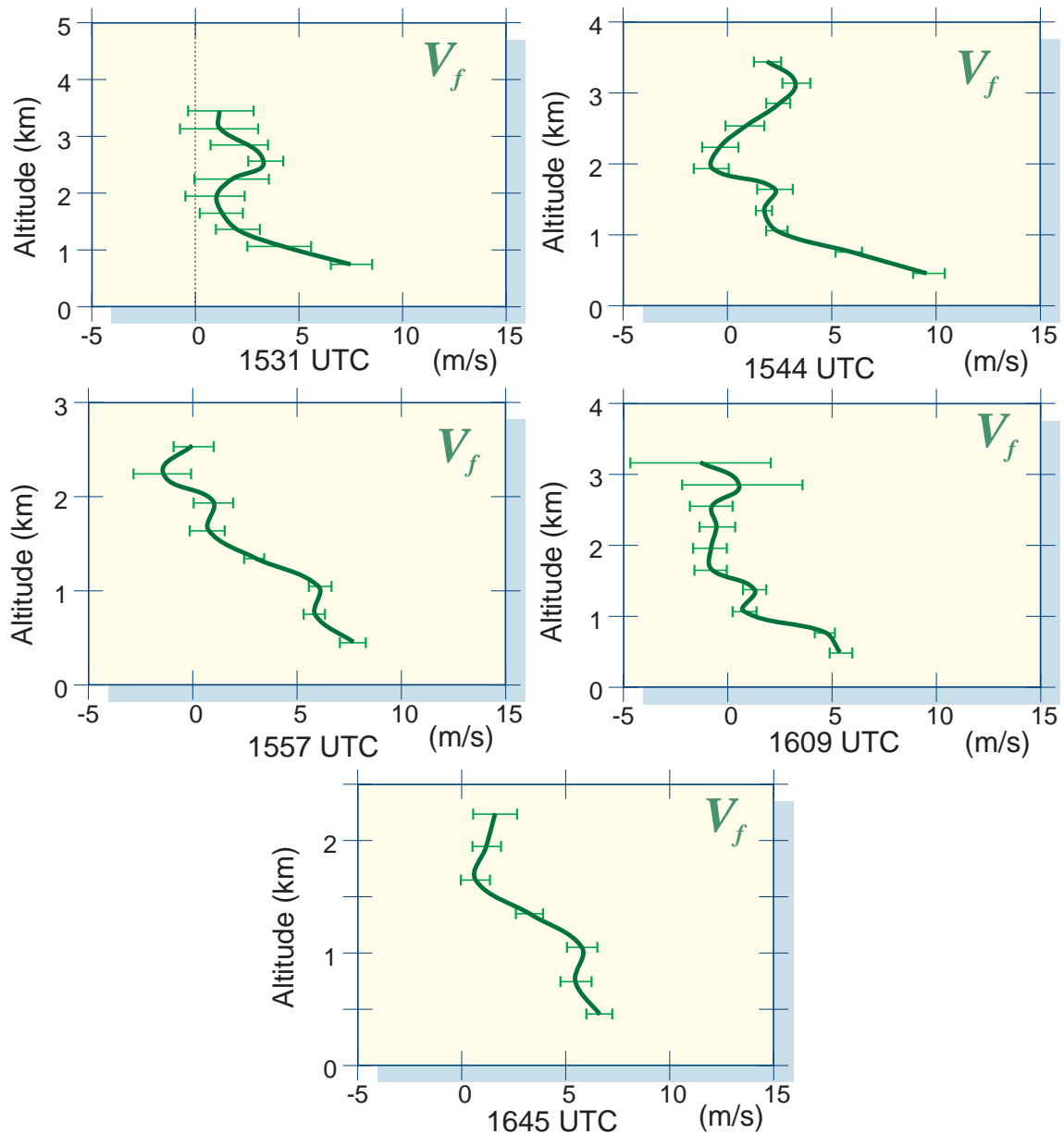
Figure 5.4: *Profiles of the terminal fall velocity V_f obtained for various purls that can be located on Fig. 5.3.*

lighter precipitation for the second. The fall velocity profile exhibits an increase of the fall speed from 0.5 ms^{-1} at 3.5 km to 2.5 ms^{-1} at 2.5 km, which implies that the ice particles tend to become heavier and probably denser. The transition area (0°, -10°C) at 1531 is characterized by a relative decrease in reflectivity and fall velocity, suggesting an evaporation process in that region. Note that the secondary maximum of reflectivity (bright band detected on the radar signal on stratiform precipitation) at 1531 corresponding to the melting layer is located at altitude 750 m. This maxi-

Figure 5.5: *Profiles of the terminal fall velocity V_f together with the corresponding reflectivity Z at two times.*

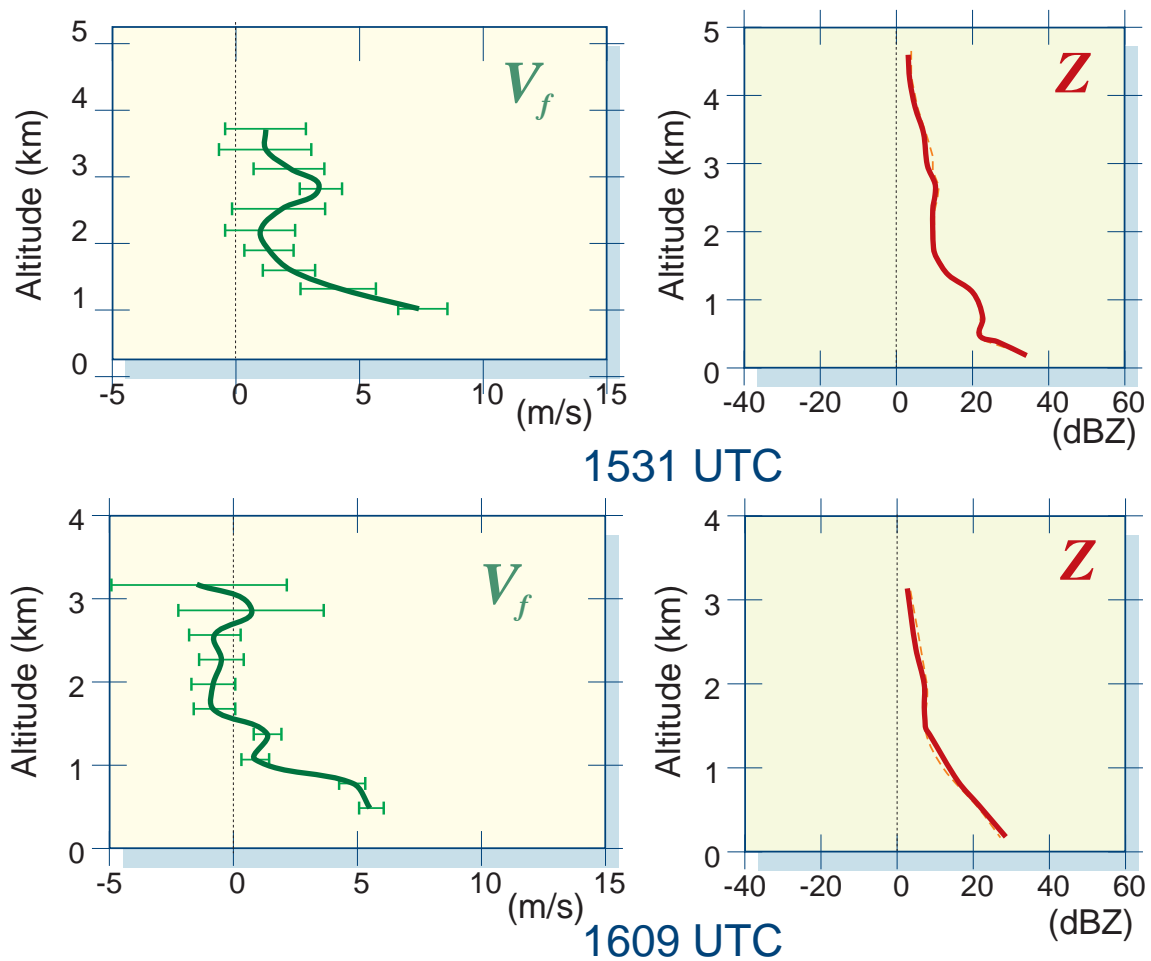mum being 300 m below the 0°C isotherm, it means the 0°C isotherm is at 1050 m altitude. The transition between rain and snow on the terminal fall velocity profile, also corresponding to the 0°C isotherm, can be estimated for $V_f = 3.5$ ms^{-1}, i.e. 900 m, in agreement with the previous estimation.

5.5   Wind field properties

The vertical profiles of the wind components u and v (respectively directed eastward and northward as usual) have been retrieved as well for the purls of main interest performed during the aircraft mission (not shown here, see Scialom et al., 1999). They appear strongly variable with time, due to the fact these winds are characteristic of the location of the sampled area with respect to the front. These winds are in good agreement with the winds provided by the wind sensor onboard the aircraft, about 1.5 km in the present case, and also with the vertical profiles obtained about the purls using the MANDOP analysis. However, a slight discrepancy appears between

MANDOP and DAVAD profiles for purls at 1634 and 1645 UTC, due to poor data coverage in the corresponding areas.

Vertical profiles of the vertical component of the vorticity are displayed Fig. 5.6. The vertical vorticity appears to be mainly positive, i.e. cyclonic, consistent with the existence of a low. The profile of 1732 UTC (bottom panel of Fig. 5.6) obtained within the main active part of the low located in the area where the cloud head rolls around the dry slot evidences a maximum at low levels, below 500 m altitude. This is an absolute maximum, as shown by the comparison with another profile located ouside this active area, that of 1609 UTC (top of Fig. 5.6), which exhibits values about twice smaller. This vorticity maximum could be due to the shear between the cloud head and the dry slot area, as suggested by the strong value of the shearing deformation at 1732 UTC (See fig. 5.9 below).

The vertical profiles of the horizontal divergence, of the stretching deformation, and of the shearing deformation also exhibit strong variations according to their location within the system. Comparison with profiles locally determined using the MANDOP analysis shows that the agreement is better within the area far from the edges (1557 and 1720 UTC) than close to the edges (1645, 1659, 1732 UTC and especially 1625, 1634 UTC).

In the main active part of the low, one observes ascending motions in low layers, as shown by the profile of vertical velocity w (Fig. 5.7). Note that outside this active area, for example at 1634 UTC, the vertical velocities are weak, suggesting quasi-horizontal motions in the northwestern part of the cyclone (top of Fig. 5.7). These observations appear consistent with Lemaître et al (1999) results.

The orientation (Browning and Wexler, 1968) of the axis of deformation (or deformation angle) also provides information on the dynamics of the flows (Fig. 5.8). When the angle is null or 90°, that means that pure stretching deformation occurs. For values of 45 or 135°, pure shearing deformation is present. The profile of the deformation angle at 1732 UTC (Right of Figs. 5.8 and bottom of Fig. 5.9) is close to 15°, evidencing that stretching dominates, contrarily to the northwest area for example at 1609 UTC (Left of Fig. 5.8 and top of Fig. 5.9) where shearing dominates (angle close to 45°).

The effect of these deformations on the horizontal temperature gradient can be estimated following Bluestein (1986), expressing the frontogenetic fonction $\mathcal{F}$ in terms

Figure 5.6: *Profiles of the vertical component of vorticity ζ at two particular times. See Fig. 5.3 for locations and Figs. 5.8 and 5.9 for other properties of the horizontal wind field at the same times.*
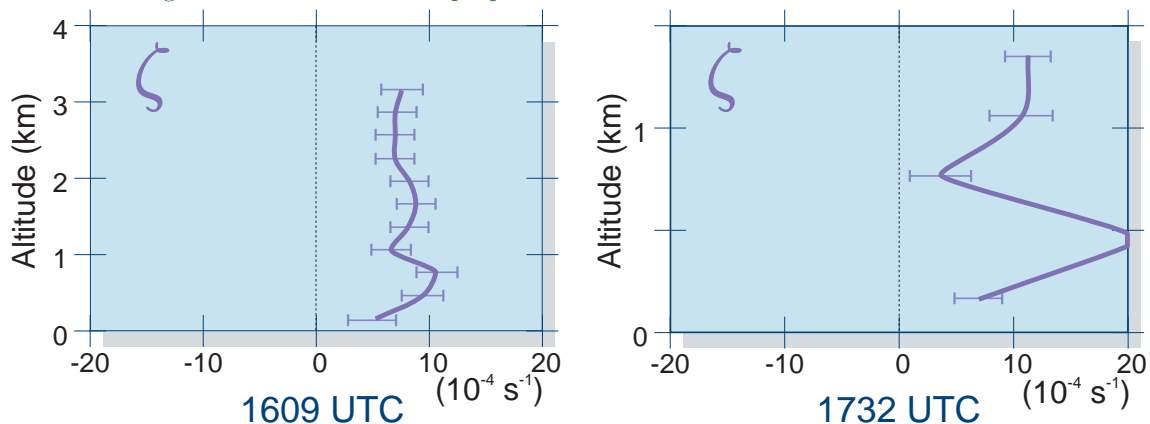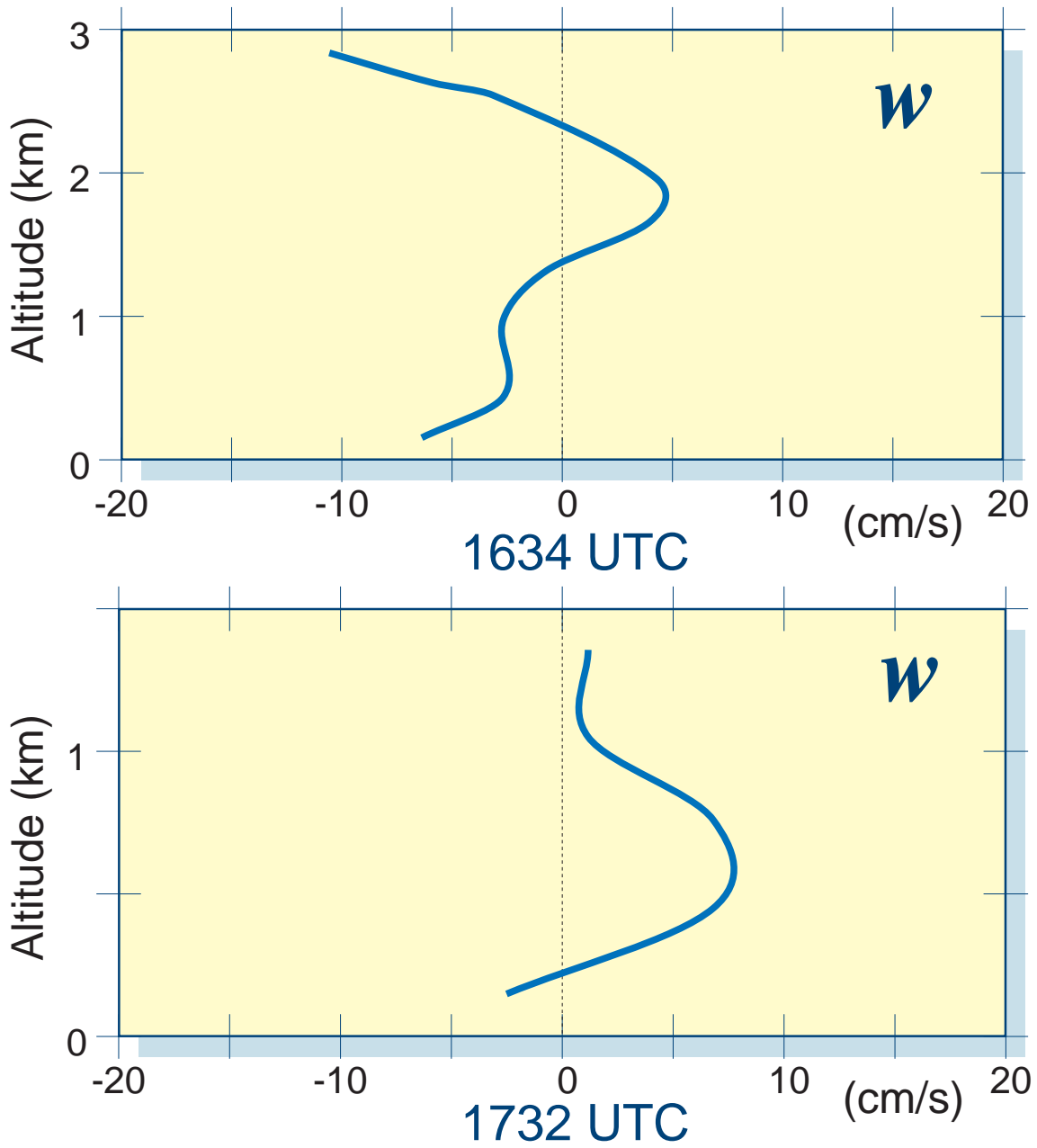
Figure 5.7: *Profiles of the vertical velocity at two particular times. See Fig. 5.3 for locations.*

of these deformations (respectively denoted D_{eT} for its so-called stretching component and D_{eS} for the shearing part) and of divergence D, tilting and diabatic function:

$$\mathcal{F} \;=\; \frac{D}{Dt}\|\boldsymbol{\nabla}\theta\| \;=\; \frac{1}{2}\,\left(\frac{\partial S_\theta}{\partial s_\theta} - \frac{\partial \theta}{\partial z}\frac{\partial w}{\partial s_\theta}\right) \;-\; \frac{1}{2}\,\|\boldsymbol{\nabla}\theta\|\,\left(D - D_{eT}\cos 2\gamma_\theta - D_{eS}\sin 2\gamma_\theta\right)$$

$$(5.3)$$

Figure 5.8: *Profiles of the principal axis of dilatation at two particular times. See Fig. 5.3 for locations and Fig. 5.6 and 5.9 for other properties.*

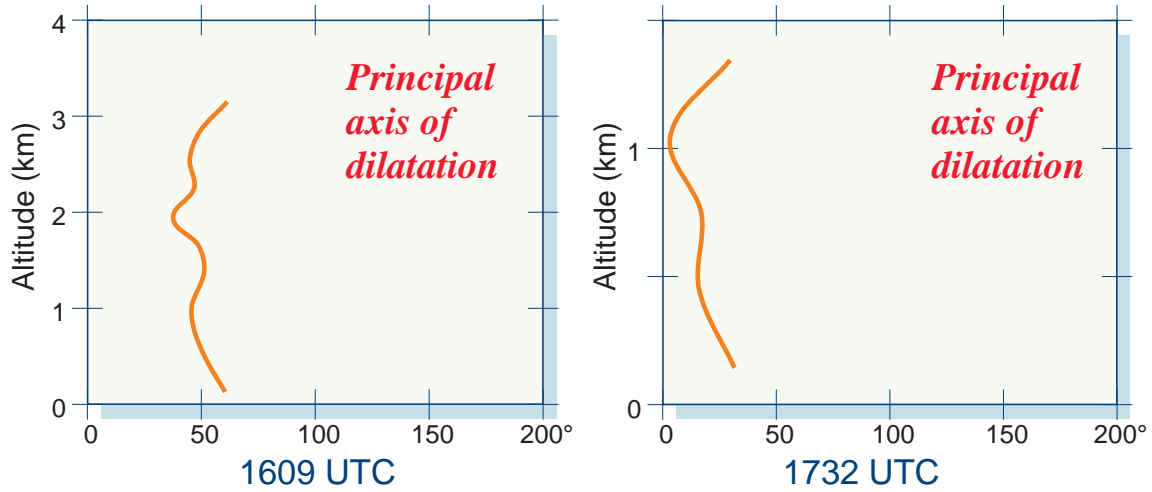where S_θ is the diabatic heat source of θ, the potential temperature, the coordinate s_θ is taken along the local isentrope (iso-θ), w is the vertical velocity and γ_θ is the angle between the principal axis of dilatation and the local isentrope.

Application of equation 5.3 to the present data leads to the conclusion that, in the active part of the cloud head, the observed stretching deformation is frontolytic (the stretching term of $\mathcal{F}$ is indeed -4×10^{-4} $\mathrm{Km}^{-1}\mathrm{s}^{-1}$), and this tends to reduce the horizontal gradient of temperature, whereas on the western part of the cyclone, the observed shearing deformation tends to produce a new baroclinic zone (indeed the shearing term $\mathcal{F}$ is indeed 3×10^{-4} $\mathrm{Km}^{-1}\mathrm{s}^{-1}$). These results seem to be consistent with the temperature pattern retrieved by Lemaître et al (1999) who evidence a relatively uniform field on the eastern side of the cloud head, and a well-defined baroclinic region on its western side.

5.6   Concluding remarks

The DAVAD analysis described previously was aimed at retrieving the wind field and its divergence, deformation components and vertical vorticity within the stratiform area of convective precipitating systems. The analysis takes advantage of the VAD approach which it is derived from, since the data are rearranged in the same scanning geometry (conical), and of the two viewing angles under which the dual-beam antenna samples the convective system. This allows all the derivatives to be retrieved, in particular the vertical vorticity.

Simulations reported in Scialom et al. (1999) have shown that the method was able to retrieve the wind and its first derivatives, including the terminal fall velocity of the hydrometeors with good accuracy. Application to real data extracted from the FASTEX experiment data set was possible in spite of the somewhat poor resolution in azimuth of the P3-42 data. The results are highly consistent. The profiles of the fall velocity of the hydrometeors were obtained for all the processed purls. When they are typical of stratiform precipitation areas, they constitute an a posteriori validation for the whole DAVAD analysis and can be included as input for the models. The DAVAD

technique is the best one to access this particular parameter V_f with some precision, and it is subsequently employed as one of the inputs in the 3-D retrieving techniques such as MANDOP: see Part 6.

The wind field is representative of the area in which it is obtained (Warm Conveyor Belt, Cold Conveyor Belt, cold air) in good agreement with the wind sensor onboard the aircraft, and the corresponding derivative terms are also consistent: the vertical vorticity, cyclonic at the mesoscale, is consistent with the one independently obtained by applying the MANDOP analysis on a data set at the scale of the perturbation. The cyclonic vorticity is maximum at the center of the observed secondary low. Identification of the various flows acting about the secondary low are suggested from the divergence, vertical velocity and deformation profiles, depending on the area considered. The paper was aimed at illustrating the capabilities of the proposed analysis of purls. Only a few selected profiles are presented in this paper. However a systematic application of this analysis on all the purls performed during this IOP has been done and will be provided to the FASTEX database.

Figure 5.9: *Profiles of the components of deformation, respectively stretching D_{eT} and shearing D_{eS}, at two particular times. See Fig. 5.3 for locations and previous figures for other properties.*
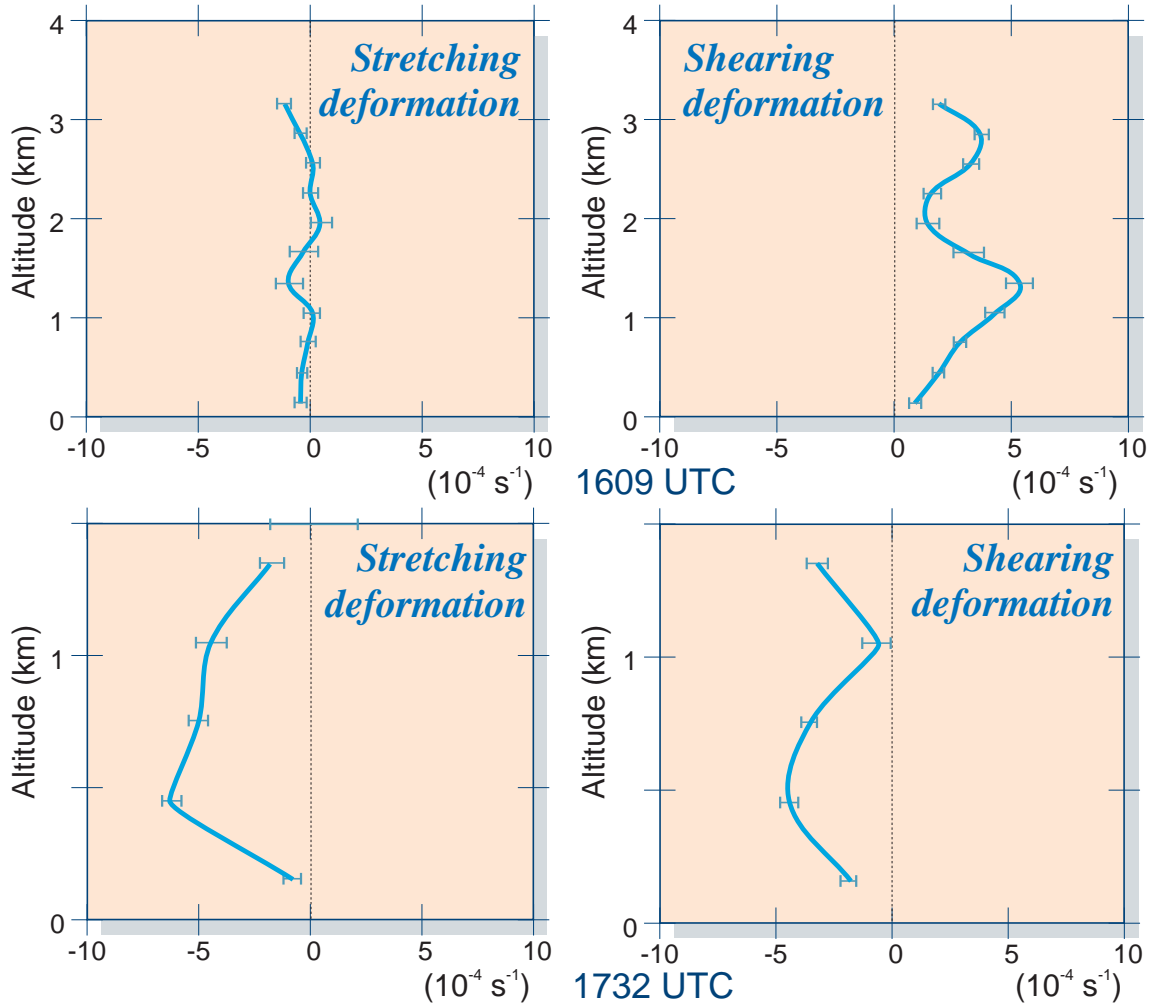
Application to ASTRAIA-ELDORA data set whose resolution is twice better than that of the P3-43 will be also performed for other case studies of the FASTEX experiment.

5.7   References

Alberty, R. L., T. Crum and F. Toepfer, 1991:
The NEXRAD program. Past, present and future. A 1991 perspective.
Preprints, *25th Int. Conf. on Radar Meteorology*, Paris, Amer. Meteor. Soc., 1–8.

Bennetts, D. A. and B. J. Hoskins, 1979:
Conditional symmetric instability: a possible explanation for frontal rainbands.
Quart. J. Roy. Meteor. Soc., **105**, 945–962.

Bennetts, D. A. and J. C. Sharp, 1982:
The relevance of conditional symmetric instability to the prediction of mesoscale frontal rainbands.
Quart. J. Roy. Meteor. Soc., **108**, 595–602.

Browning, K.A., and R. Wexler, 1968:
The determination of kinematic properties of a wind field using Doppler radar.
J. Appl. Meteor., **7**, 105–113.

Bluestein, H. B., 1986:
Fronts and jet streaks: a theoretical perspective.
in *Mesoscale meteorology and forecasting*, American Meteorological Society, Boston, chap. 9, 173–215.

Chong, M. and J. Testud, 1996:
Three-dimensional air circulation in a squall line from airborne dual-beam Doppler radar data: A test of coplane methodology software.
J. Amos. Oceanic. Technol., **13**, 36–53.

Chong, M. and C. Campos, 1996:
Extended overdetermined dual-Doppler formalism in synthesizing airborne Doppler radar data.
J. Amos. Oceanic. Technol., *in press (?!)*.

Dou, X. K., G. Scialom, and Y. Lemaître, 1996:
MANDOP analysis and airborne Doppler radar for mesoscale studies.
Quart. J. Roy. Meteor. Soc., **122**, 1231–1261.

Emanuel, K. A., 1983:
On assessing local conditional symmetric instability from atmospheric soundings.
Mon. Weather Rev., **111**, 2016–2033.

Fischer C. and F. Lalaurette, 1995:
Meso-β circulations in realistic fronts. Part II: frontogenetically forced basic states.
Quart. J. Roy. Meteor. Soc., **121**, 1285–1322.

Frush, C. L., P. H. Hildebrand and C. Walther, 1986:
The NCAR airborne Doppler radar. Part II: System design considerations.
Preprints *23rd Radar Meteorology Conf.*, Snowmass, Amer. Meteor. Soc., 151–154.

Hildebrand, P. H., and C. K. Mueller, 1985:
Evaluation of Meteorological airborne Doppler radar. Part I: Dual-Doppler analyses of air motions.
J. Atmos. Oceanic. Technol., **2**, 362–380.

Hildebrand, P.H., and R. K. Moore, 1990:
Meteorological radar observations from mobile platforms.
Chapt 22a in *Radar in Meteorology*, D. Atlas, Ed., Amer. Meteor. Soc., Boston, 287–315.

Houze, R. A. and A. K. Betts, 1981:
Convection in GATE.
Rev. Geophys. Space Phys., **16**, 541–576.

Joly, A., K.A. Browning, P. Bessemoulin, J.P. Cammas, G. Caniaux, J.P. Chalon, S.A. Clough, R. Dirks, K.A. Emanuel, L. Eymard, R. Gall, T.D. Hewson, P.H. Hildebrand, D. Jorgensen, F. Lalaurette, R.H. Langland, Y. Lemaitre, P. Mascart, J.A. Moore, P.O.G. Persson, F. Roux, M.A. Shapiro, C. Snyder, Z. Toth, and R.M. Wakimoto, 1999:
Overview of the field phase of the Fronts and Atlantic Storm-Track Experiment (FASTEX) project.
Quart. J. Roy. Meteor. Soc., **125**, *submitted.*

Jorgensen, D., P. H. Hildebrand and C. L. Frush, 1983:
Feasibility test of an airborne pulse Doppler radar.
J. Climate Appl. Meteor., **22**, 744–757.

Jorgensen D.P., P. Bessemoulin, S. Clough, and J.A. Moore.
Fastex operations plan, 1996.
Technical Report 5, FASTEX Project Office, Centre National de Recherches Météorologiques, 164pp.

Lemaître, Y., and J. Testud, 1988:
Relevance of conditional symmetric instability in the interpretation of wide cold-frontal rainbands.
Quart. J. Roy. Meteor. Soc., **114**, 259–270.

Lemaître, Y. and G. Scialom, 1992:
Three-dimensional mesoscale circulation within a convectivr post-frontal system. Possible role of conditional symmetric instability for triggering convective motions.
Quarterly J. Royal Meteor. Soc., **118 A**, 71–99.

Lemaître, Y., A. Protat and D. Bouniol, 1999:
Pacific and Atlantic "bomb-like" deepening in mature phase: a comparative study.
Quart. J. Roy. Meteor. Soc., *submitted*.

Protat, A., Y. Lemaître, and G. Scialom, 1997:
Retrieval of kinematic fields using a single-beam airborne Doppler radar performing circular trajectories.
J. Atmos. Oceanic Technol., **14**, 769–791.

Scialom, G., and J. Testud, 1986:
Retrieval of horizontal wind field and mesoscale vertical vorticity in stratiform precipitation by conical scannings with two Doppler radars.
J. Atmos. Oceanic Technol., **3**, (4), 693–703.

Scialom, G. and Y. Lemaître, 1990 :
A new analysis for the retrieval of three-dimensional mesoscale wind fields from multiple Doppler radar.
J. Atmos. Oceanic Technol., **7**, 640–665.

Scialom, G., A. Protat, and Y. Lemaître, 1999 :
Vertical structure of a FASTEX secondary cyclone derived from dual-beam airborne radar data.
Quart. J. Roy. Meteor. Soc., *submitted*.

Testud, J., G. Breger, P. Amayenc, M. Chong, B. Nutten and A. Sauvaget, 1980:
A Doppler radar observation of a cold front. Three dimensional air circulation, related precipitation system and associated wave-like motions.
J. Atmos. Sci., **37**, 78–98.

Mesoscale organization of IOP 12 Cloud System

by
Yvon Lemaître,
Alain Protat,
and Dominique Bouniol

Centre d'étude des Environnements Terrestre et Planétaires, CNRS,
Vélizy, France.

6.1 Synoptic overview of IOP 12

Let us first give an overview of the synoptic context and main characteristics associated with the FASTEX IOP12. A quick-look summary is shown in section 3.15 of Part 3, page 112 of this Report. The whole of February was characterized by a very stable zonal regime. During this month, the wind at 300 mb was on average 10 ms^{-1} stronger than its climatological value (Joly et al. 1999).
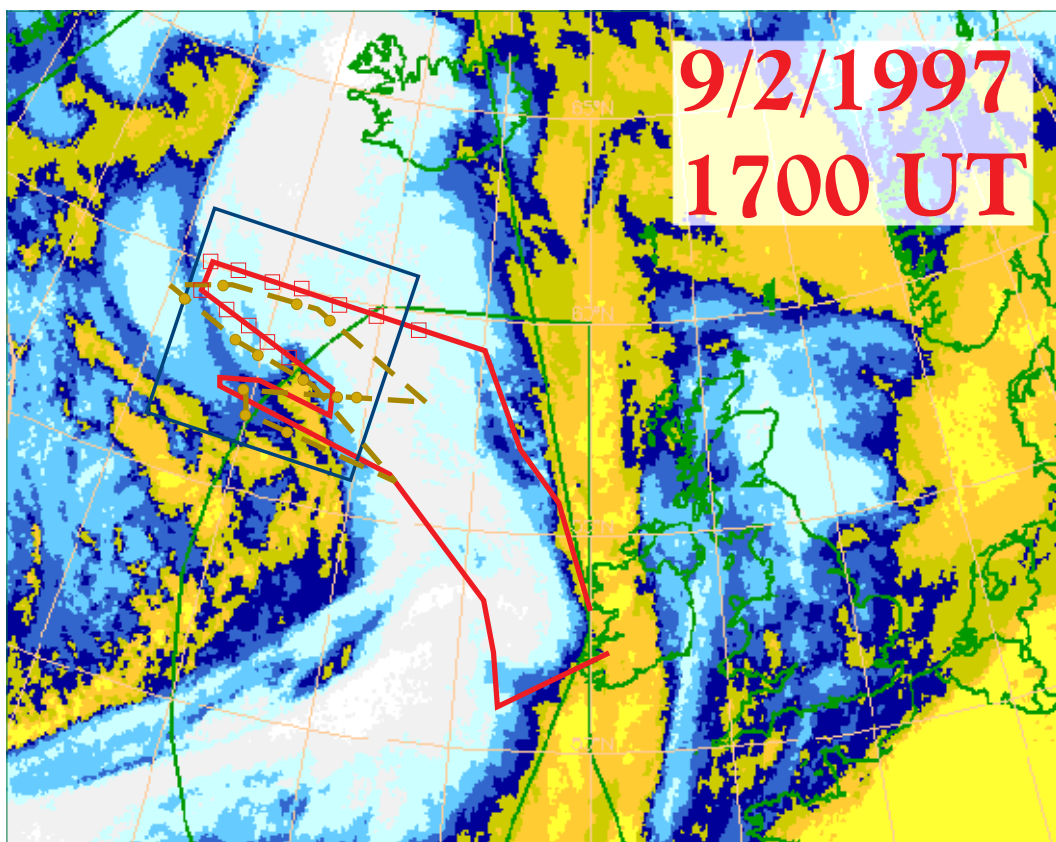
Figure 6.1: *METEOSAT infrared image at 1700UTC. The trajectories of the P3 and C-130 aircraft (red solid and brown dashed lines, respectively) are also displayed in the moving frame relative to the cyclone motion. Boxes correspond to the locations of the regular circular trajectories performed by the P3 aircraft. The mesoscale domain in which the 3D wind and precipitation fields are retrieved is also shown as a large rectangle. Image courtesy of Eumetsat and processed by Météo-France.*

The IOP 12 was conducted on Low 34A, which underwent on 9 February 1997 the most explosive deepening of the period, roughly -54 mbar in 24 hours. This very rapid development is illustrated on the METEOSAT images in the infrared channel shown on Fig. 2.3 in Part 2. Between 06 and 12 UTC, Low 34A moved northeastwards at a fast speed of 40 ms^{-1}. Subsequently, the cyclone deepened very rapidly as it turned to the north just after it crossed the upper-level jet, and tracked towards Iceland, traversing the northwestern corner of the MSA. This Low, which marked the

end of the first most active portion of the zonal regime, was preceded by numerous active systems. It appeared to interact with Low 31 and with the cold air which had been previously advected eastwards by Low 32 (an arctic vortex centered near 62°N, 55°W). Chaigne (1998) also showed, using the potential vorticity inversion technique, that when removing the upper-level feature Low 34A does not develop, which suggests the importance for rapid deepening of a baroclinic interaction process between two independent precursors, one in the lower troposphere and the other at the tropopause.

6.2   Mesoscale measurements collected in the MSA

The documentation of the mesoscale dynamic structure of the cyclone is conducted in the present paper using the MSA facilities. We will focus more precisely at the end of the life cycle of the cyclone, corresponding to the last panel of Fig. 2.3 in Part 2 reproduced here as Fig. 6.1. Among the numerous instruments involved in this experiment, the P3-43 airborne Doppler radar instrumented with a C-band lower fuselage non-Doppler radar and the dual-beam X-band Doppler radar designed at the CETP (mounted on the tail of the aircraft) gathered Doppler informations within this particularly impressive secondary cyclone, using a new sampling strategy defined for FASTEX. An example of raw radar data showing one of the features discussed later in the text is shown on Fig. 6.2.

This strategy consists of a systematic, regular survey (called the "lawnmover" or "systematic survey" pattern) using straight-line flight patterns (called "legs"). The P3 and C-130 aircraft flew parallel legs spaced about 100 km apart, providing a continuous radar coverage and regularly-spaced dropsonde-derived vertical profiles relative to the whole wave cyclone from front to rear (with respect to cyclone motion). The leg length are about 500 km long accross the system and perpendicular to the cyclone motion vector, with at regular interval complete 360°turns. This type of scanning allows for the recovery of vertical profiles of crucial kinematic parameters, such as the terminal fall velocity V_f of hydrometeors, as shown by Protat et al. (1997) and Scialom et al. (1999). The technique employed in this case and the related results are presented in Part 5 on this Report for the same case study.

In the present part, the 3-D wind field is recovered inverting the Doppler measurements collected during the IOP 12 "lawnmover" pattern using the MANDOP technique (Scialom and Lemaître 1990; Dou et al. 1996). The dynamic perturbations (pressure and temperature, essentially) are retrieved under an analytical form, by introducing the analytical form of the 3-D wind field in the non-dissipative and stationary first-order anelastic approximation of the equation of motion (Protat et al. 1998).

6.3   Structure and features of the Cloud System

The purpose of this section is to document the mesoscale dynamics of the secondary cyclone sampled during the IOP 12 of FASTEX. Fig. 6.1 shows the METEOSAT infrared picture at 1700 UTC. It gives the cloud cover associated with the frontal system along which the secondary cyclone develops. Several features are well recognized :

(i)   a well-defined frontal cloud band, generally associated with the synoptic warm conveyor belt (WCB, Harrold 1973),

Figure 6.2: *Example of raw radar data obtained from the lower fuselage radar of the NOAA-P3 aircraft, showing the cloud system around 1600UTC, this image being an average over 20′. These images are available in real time during the flight and they are used to adjust the flight plan when this is needed. On this particular image, the maximum of reflectivity that can be seen near the lower right corner is feature A of Fig. 6.3. Image courtesy of Dave Jorgensen, NOAA/NSSL.*
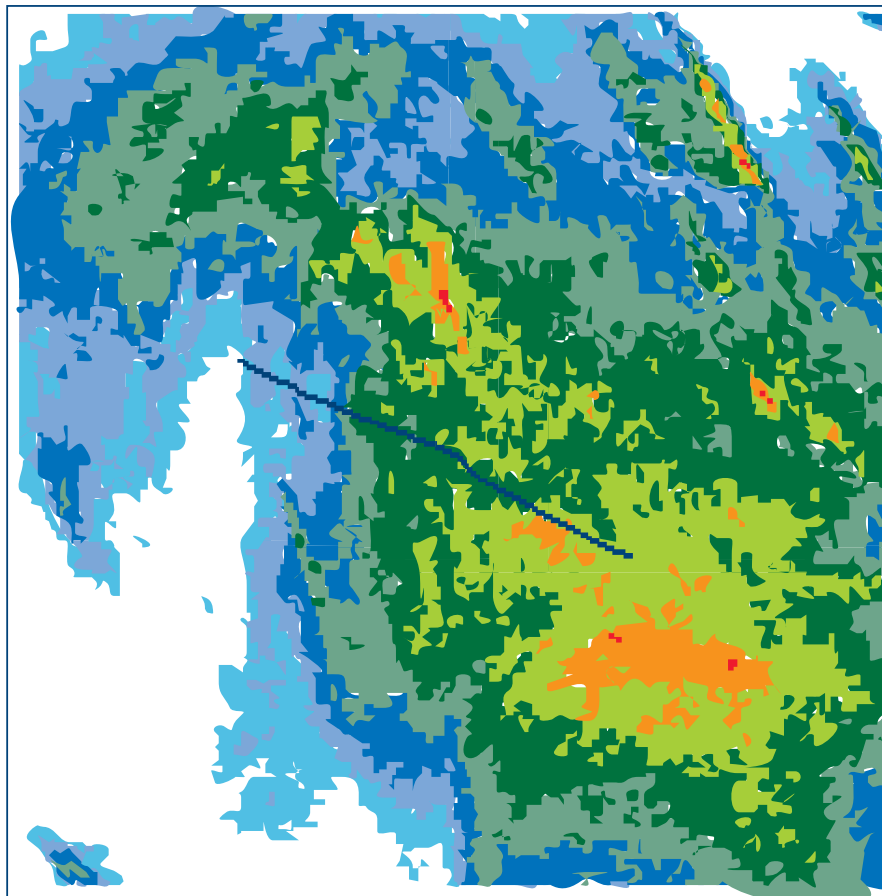
FASTEX P3-LF composite 09 FEB 97 1600UTC
30 sweeps average - 240 km by 240 km - alt. 1.5 km
<22 22 24 26 28 30 32 34 36 38 40 42 44 dBZ

(ii) a well-developed "cloud head" (Bottger et al. 1975) to the northeast of the main baroclinic zone cloud band, the apparition of which is a well-known symptom of cyclogenesis (e. g., Browning and Roberts 1994),

(iii) a dry slot forming between the main baroclinic zone cloud band and the cloud head indicative of a dry intrusion (Reed and Danielsen 1959) of air coming from the upper-troposphere towards the centre of a developing cyclone, and

(iv) the existence of scattered clouds associated with the cold polar air propagating over the sea.

In Fig. 6.1 are also given the trajectories performed by the P3 (solid line) and C-130 (dashed line) aircraft within the secondary cyclone. These trajectories are relative to the cyclone phase speed. The measurements collected by the Doppler and dropsonde facilities along these trajectories allow to retrieve 3-D fields in the mesoscale domain ($430 \times 430 \times 7$ km^3) indicated by the box of Fig. 6.1. Fig. 6.3a is a zooming view of the satellite picture of Fig. 6.1 in the vicinity of this mesoscale domain, with upper clouds contoured. This figure can be compared with the 3-D precipitation field derived from the processing of the tail-radar measurements, which is given in Fig. 6.3b on a horizontal cross-section at the flight altitude (roughly 1.5 km). Superimposed to this horizontal cross-section of precipitation are the trajectory of the P3 aircraft and the flight-level in-situ horizontal wind measurements. On the satellite picture (Fig. 6.3a), several upper cloud features are well identified. Within the edge of the main baroclinic zone cloud band appear three distinct upper level features referred to as I, II, and III, respectively, in Fig. 6.3a. These features are associated with the cold frontal surface (features II and III), and likely with the presence of a warm frontal surface (feature I). The warm frontal feature could result from the ascent of the WCB over a cold conveyor belt, a configuration that is often observed during the life cycle of an occlusion (e. g., Carlson 1980; Neiman and Shapiro 1993; Browning and Roberts 1994; L98).

The cloud head itself, located in the mesoscale domain, is characterized by two main upper cloud regions (with a lesser vertical extent, denoted A and B in Fig. 6.3a). The precipitation field of Fig. 6.3b exhibits a large area of precipitation along the northern part of the domain within the main baroclinic zone cloud band. The cloud head is characterized by two main comma-shaped precipitating areas, separated by a transition region of lighter precipitation. These two comma-shaped regions are closely related to the upper cloud features A and B observed on the satellite picture of Fig. 6.3a. The most intense comma-shaped area wraps around a clear-air region, denoted DS in the following, corresponding to the northernmost part of the dry slot. The southernmost precipitating area (only a part of which is sampled by the Doppler radar, see Fig. 6.3b) is correlated with the southeastern part of the large cloudy area located southwest of the cloud head (Fig. 6.3b).

This comparison between cloud cover and radar-derived precipitation evidences that precipitation is not homogeneously distributed inside the cloud head, but rather distributed *along the border of the cloud head*. This suggests that distinct dynamical characteristics may be acting within the various precipitating features of the cloud head. The in-situ horizontal wind measurements in the ground-relative frame (Fig. 6.3b) confirm the link between the most active part of the cloud head (region A in Fig. 6.3) and the WCB (roughly 35 ms^{-1} at the 1.5 km altitude). They also evidence two different dynamical characteristics, associated respectively with the main baroclinic zone cloud band (strongest winds on the right-side) and with the cloud head (weaker winds on the left side).

Finally, a southwesterly airflow is detected in the dry slot area, which likely corresponds to the well-known dry intrusion of upper-tropospheric air approaching the cyclone center (e. g., Reed and Danielsen 1959; Green et al. 1966; Young et al. 1987).

6.4   3-D kinematics retrieved from the Doppler radar

We now turn to a description of the 3-D kinematic fields derived from the Doppler measurements using the MANDOP technique (Scialom and Lemaître 1990; Dou et
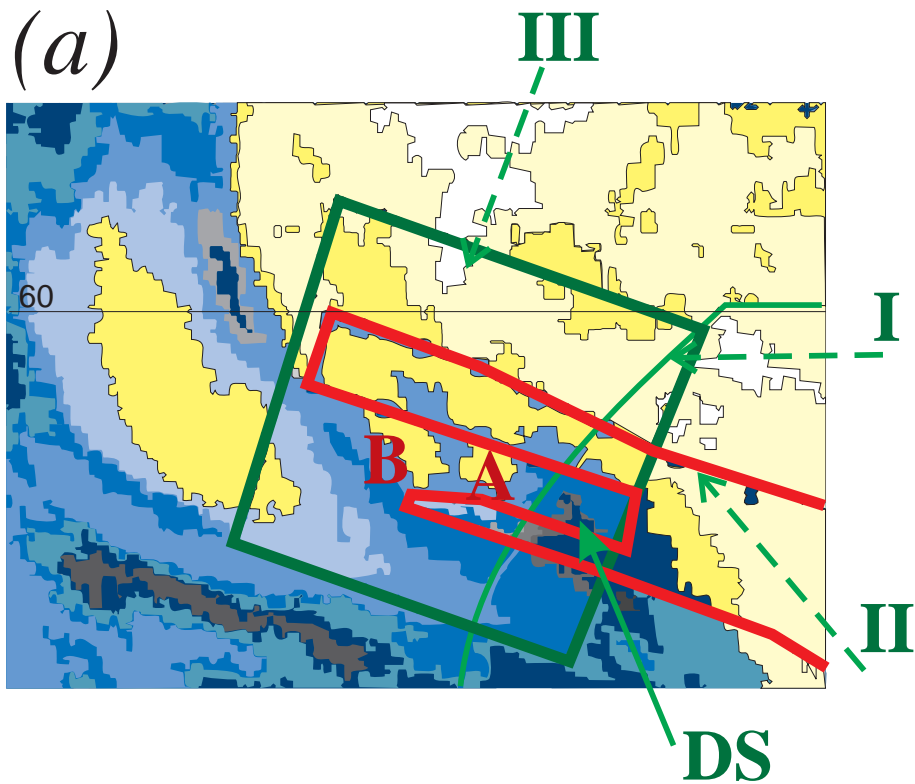
Figure 6.3: *(a) zooming view of Fig. 6.1 in the vicinity of the mesoscale domain (large rectangle), with the upper-clouds contoured and (b) horizontal cross-section of the 3D radar reflectivity field deduced from the tail-radar measurements at the flight-level altitude (1.5 km) within the mesoscale domain of Fig. 6.3a. The respective locations of the features I, II, III, A, B and DS discussed in the text are also given. As usual, brighter shading corresponds to higher clouds (that is, lower brightness temperatures). Arrows in Fig. 6.3 are the in-situ horizontal wind measurements collected at the flight-level altitude (1.5 km).*
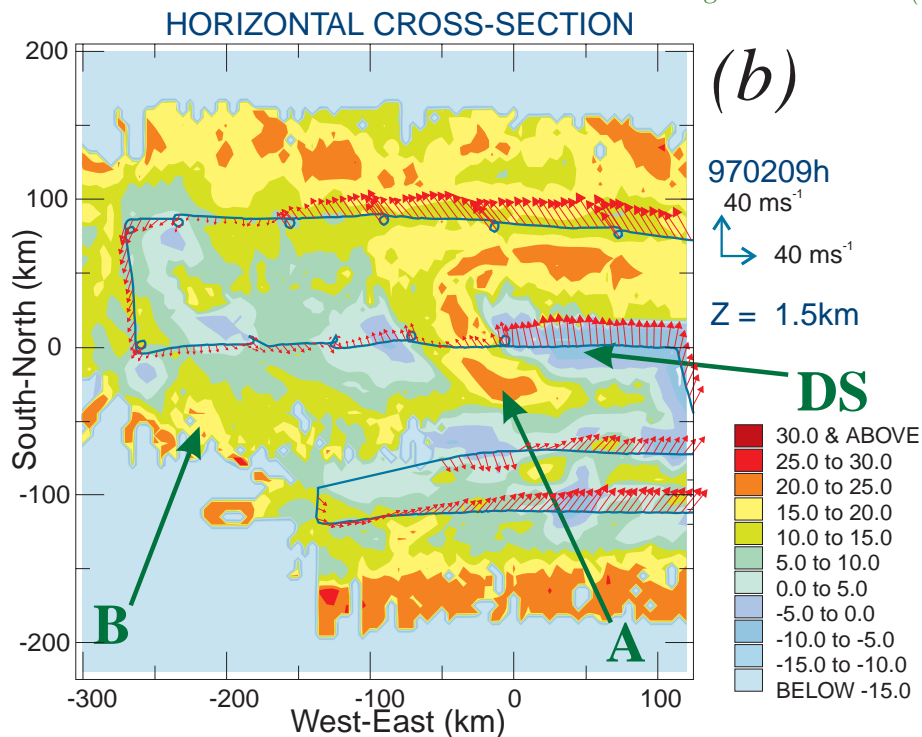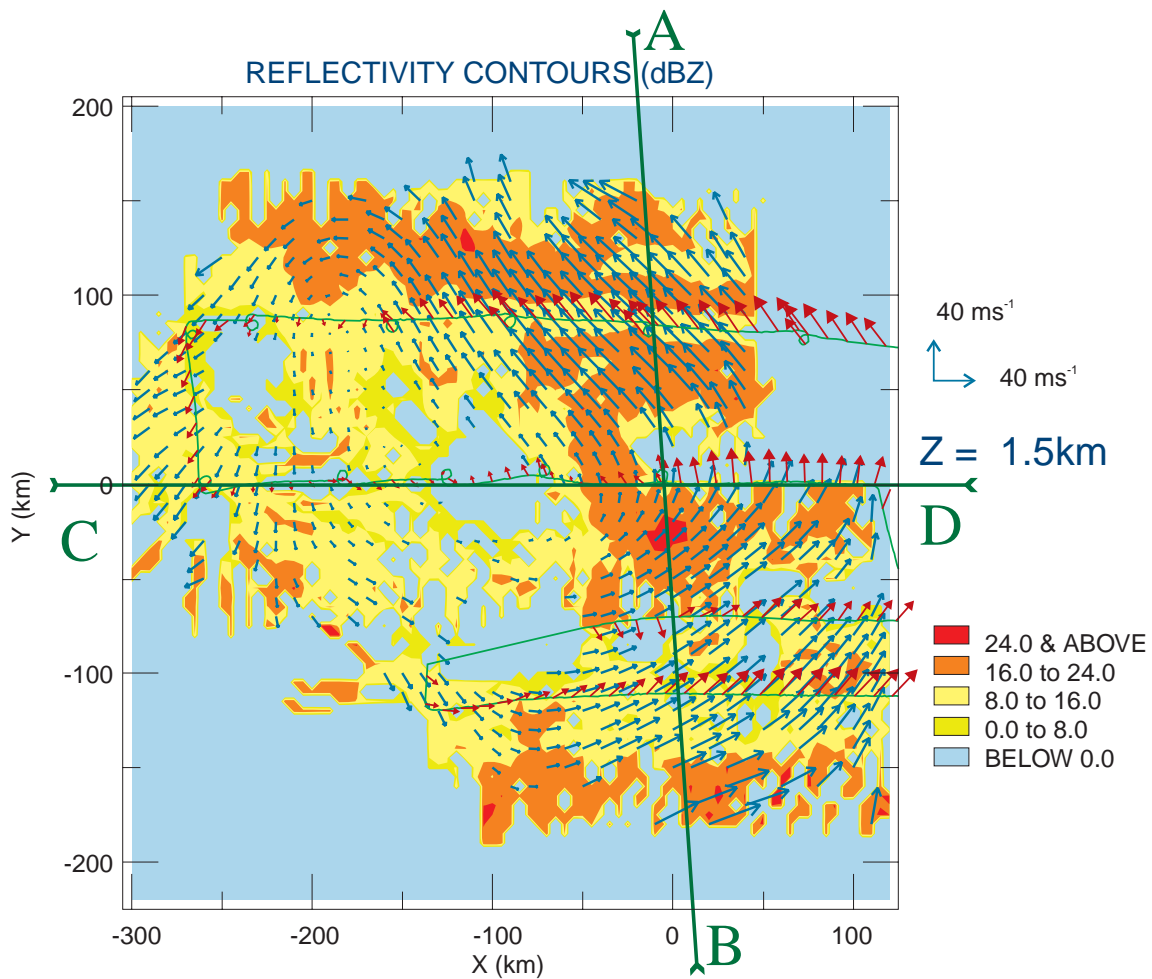
Figure 6.4: *Horizontal cross-section of the 3D radar reflectivity and absolute wind fields at the 1.5-km altitude. Superimposed along the P3-trajectory are the in-situ horizontal wind measurements collected at the flight-level altitude (arrows with solid head). For display purposes, one arrow out of ten is drawn for the in-situ measurements, and one arrow out of two for the retrieved horizontal wind vectors. Also given are the locations in the mesoscale domain of the vertical cross-sections (AB) and (CD) of Fig. 6.6.*

al. 1996). Fig. 6.4 shows the horizontal cross-section of the 3-D precipitation and absolute wind fields at the 1.5-km altitude, with the in-situ measurements of horizontal wind superimposed. First, notice the good agreement between the retrieved and in-situ horizontal winds. The retrieved horizontal wind confirms the existence of the southeasterly flow (WCB) in the region of strong precipitation located in the northeastern part of the domain. It also shows that the region of lighter precipitation corresponds in terms of dynamics to the transition zone between this WCB and the diffluent northeasterly flow located in the western part of the domain. The same 3-D fields are now shown in a frame relative to the cyclone motion and at the 0.5- and 2.5-km altitude (Figs. 6.5a and 6.5b, respectively).

Globally, the same kinematic characteristics are found at both altitudes, except in the northeastern part of the domain, where the easterly relative airflow at the
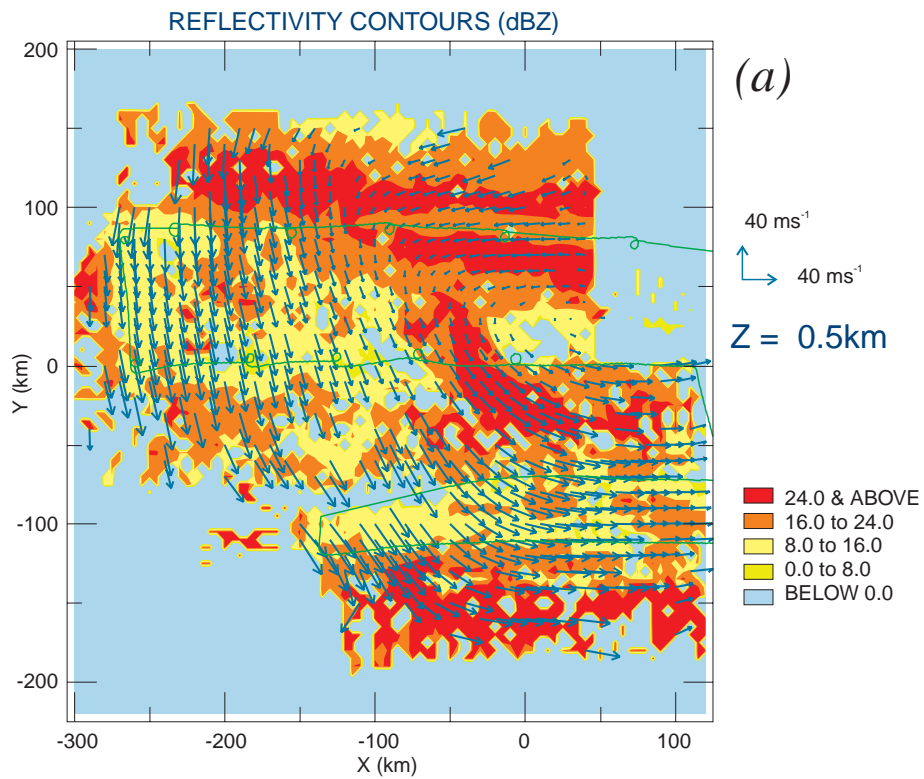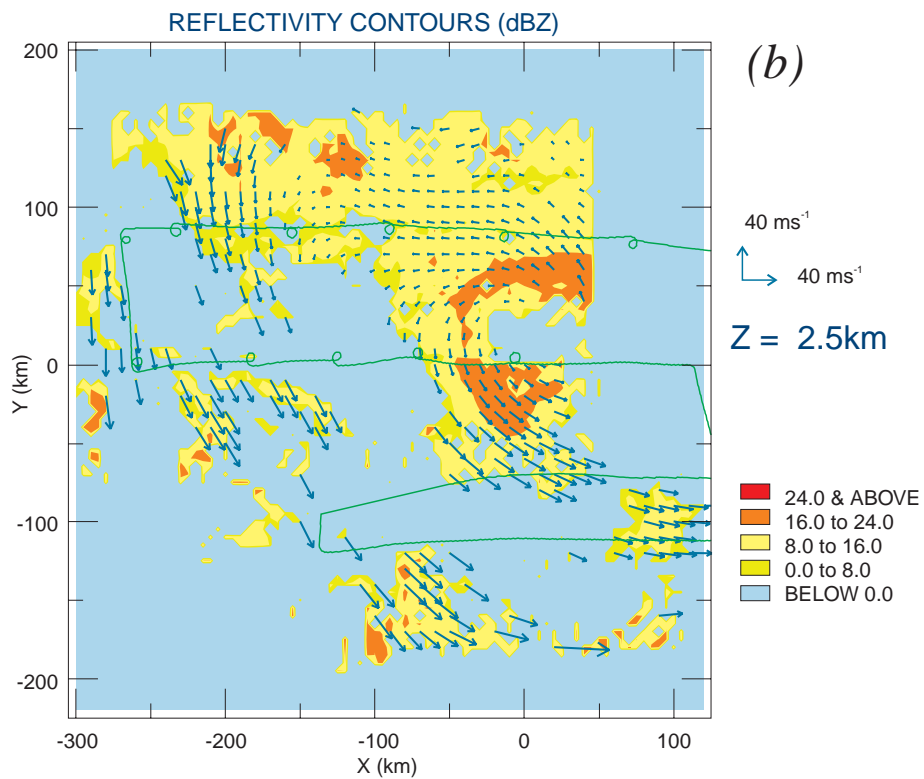
Figure 6.5: *Horizontal cross-section of the 3D radar reflectivity and relative wind fields at the (a)0.5- and (b)-2.5 km altitude.*

2.5-km altitude (corresponding to the WCB) is found to penetrate further west with height, suggesting an overlapping of the northerly flow by the WCB. A more precise inspection of this easterly relative airflow reveals at the 0.5-km altitude (Fig. 6.5a) the existence of two distinct flows that enter in confluence. The southernmost flow corresponds to the lower part of the WCB, while the northernmost flow could be, according to the conceptual scheme proposed by Browning and Roberts (1994, 1996), the signature of a cold conveyor belt. This lower part of the WCB (denoted W2 in the following so as to keep consistency with the notations of Browning and Roberts 1994) appears to wrap around the most active part A (in terms of precipitation) of the cloud head, suggesting that W2 peels off from the base of the WCB to feed the upper part of the cloud head, as first introduced by Young et al. (1987), developed by Young (1989), and diagnosed recently using numerical models (e. g., Browning and Roberts 1994). The importance of this "peeling-off" process will be confirmed observationally in the following using vertical cross sections through the cloud head and air parcel trajectory analysis.

Such a vertical cross-section through the main entities of this cyclone (the cold conveyor belt, the most active part of the cloud head, and the dry slot) is given in Fig. 6.6. It is seen from the radar reflectivity of Fig. 6.6a that the maximum depth of the reflectivity echoes within the whole cloud head (6 km) is associated with its most active part, which is consistent with the upper clouds located here on the satellite picture of Fig. 6.3a. The depth of the convective cells associated with the southeastern part of the large cloudy area located southwest of the could head (Fig. 6.3b) does not exceed 2 km. The precipitating area located on the northernmost part of the domain results from ascending motions initiated at low levels where W2 overlaps the cold conveyor belt.

6.5   Air trajectories

An air parcel trajectory illustrating these ascending motions is given in Fig. 6.7a. It shows that low-level air parcels are advected along the main baroclinic zone cloud band while rising, corresponding to a vertical transport to the northwest of low-level potential energy. Whether this parcel is part of the cold conveyor belt or of W2 cannot be assessed unambiguously, given the horizontal scale resolved by the mesoscale analysis in the present case. This point will be addressed in future works by performing higher-resolution 3-D wind field retrieval in a convective-scale domain focussing on this particular area.

Interestingly, the shape of these rising trajectories (see in particular the projection of the trajectory of Fig. 6.7a onto the horizontal plane) explains the southwestward limit of stronger precipitation associated with this ascending flow. In contrast, precipitation within the most active part A of the cloud head are associated with ascending motions present at higher altitude (above 2.5 km altitude, see Fig. 6.6a). The air parcel trajectory analysis reveals that these motions are fed by air parcels located initially within W2. An air parcel trajectory representative of these motions, given in Fig. 6.7b, shows effectively that the precipitation area A (Fig. 6.3) within the cloud head results from the slantwise ascent of W2, which wraps around the clear-air region DS. The vertical cross-section of Fig. 6.6a also reveals the existence of descending motions in the dry slot area, as expected from previous studies (e. g., Reed and Danielsen 1959; Green et al. 1966; Young et al. 1987). A better 3-D view of this descending flow is shown by the air parcel trajectory given in Fig. 6.7c.

Figure 6.6: *Vertical cross-section through the mesoscale domain of wind along the plane of the cross-section and (a) radar refelctivity along cross-section (AB) of Fig. 6.4, (b) vertical component of vorticity along cross-section (CD) of Fig. 6.4, taken roughly perpandicular to (AB).*
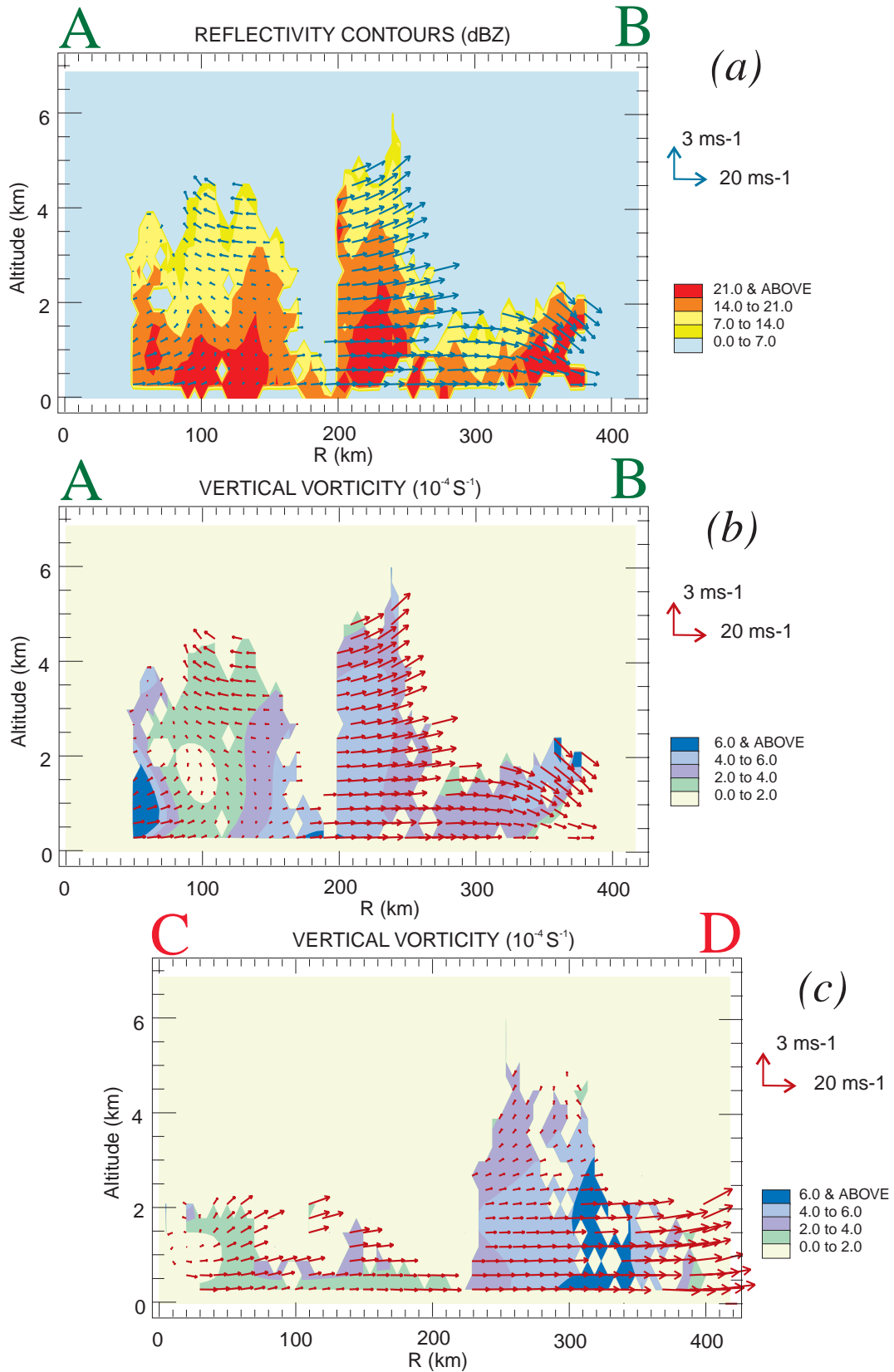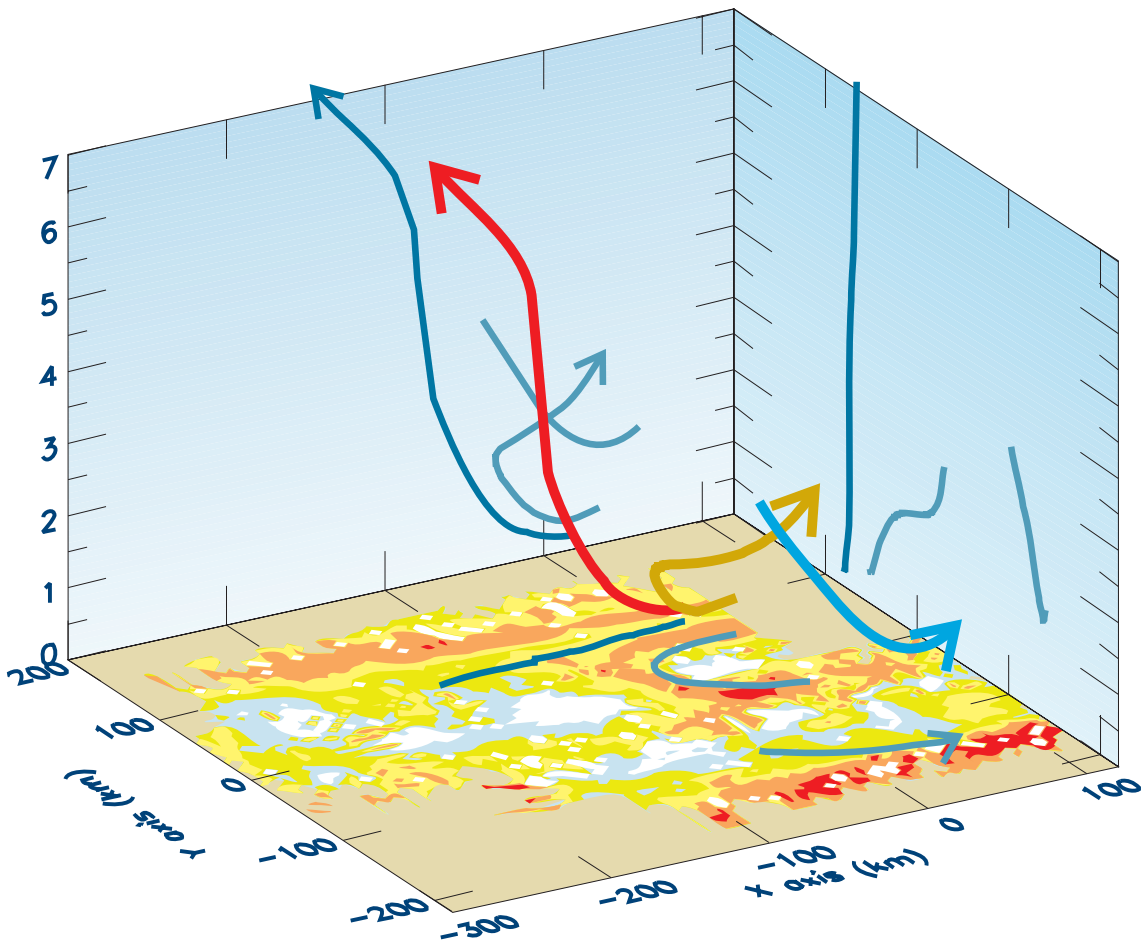
Figure 6.7: *Air parcel trajectories representative of (a) the air rising along the northernmost precipitating area associated with the frontal cloud band (red stream), (b) the W2 airflow wrapping around the most active part of the cloud head (sandy stream, a region of Fig. 6.3c), (c) the southernmost part of the dry intrusion (blue stream).*

Although the second comma-shaped precipitation structure (denoted B in Fig. 6.3) is not well sampled by the Doppler radar, some valuable information can be gained using the air parcel trajectory analysis about the difference in precipitation intensity between B and the region of lighter precipitation located between A and B. It appears indeed that the westernmost air parcel (Fig. 6.8a) rises more vertically than the easternmost one (Fig. 6.8b) although these two regions are fed by the same airflow (see Figs. 6.8a,b). In any case, the parcels associated with the B region seem to originate at low levels rather than at upper levels, which is not a common feature (to our knowledge) found in previous studies. This suggests that this part of the cloud head could result from the release of convective instability during the propagation of the northeasterly flow in the western part of the domain above the warmer ocean (see for instance the recent simulations of Vallis et al. 1997). This aspect will be further studied using convective-scale retrievals of the 3-D dynamic fields.

The vertical component of vorticity (referred to as the "vertical vorticity" in the following) in the same vertical cross-section as Fig. 6.6a (Fig. 6.6b) shows the exis-
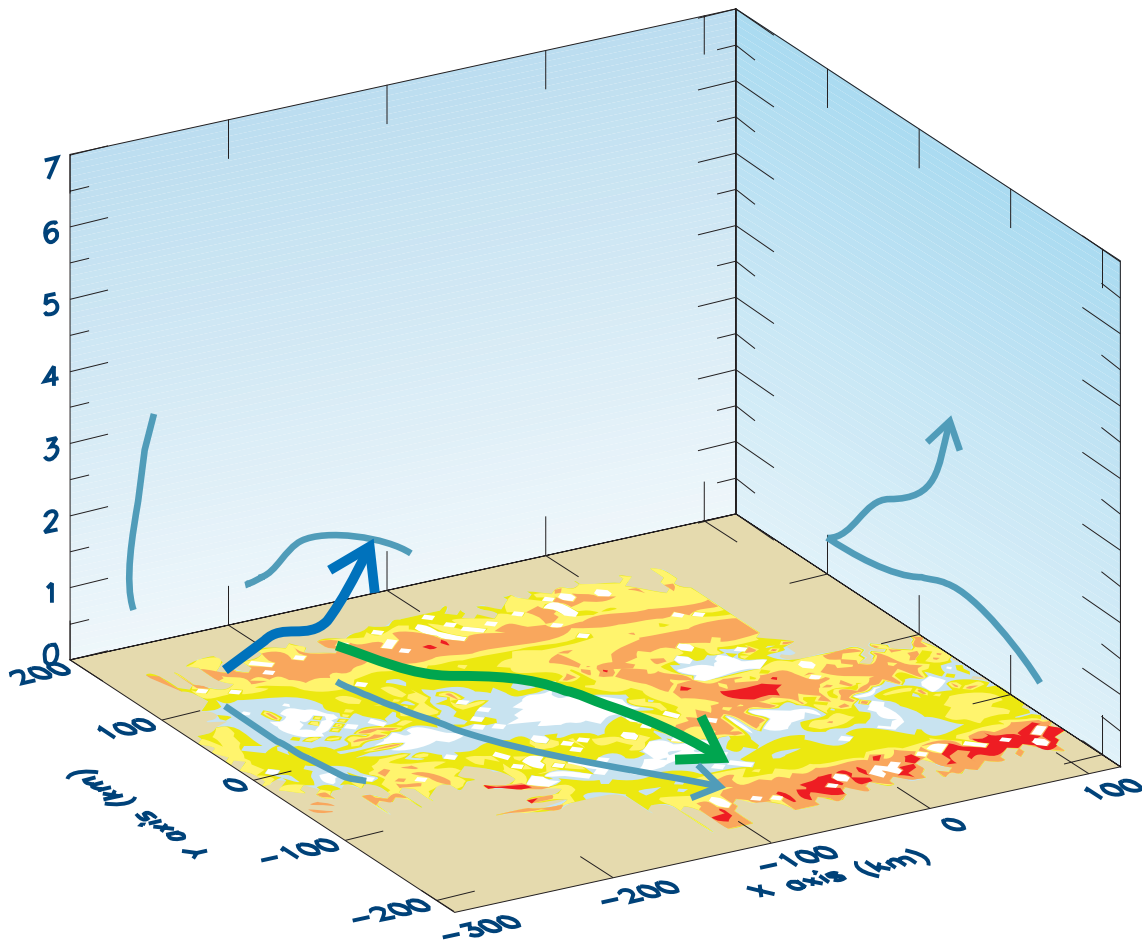
Figure 6.8: *Air parcel trajectory representative of the northerly flow: (a) westernmost trajectory (blue stream), (b) easternmost trajectory (green strem).*

tence of a vertical vorticity maximum in the DS region of the dry slot. This maximum extends vertically up to 3 km, with a peak magnitude of 6×10^{-4} s^{-1}. Another vertical cross-section (given in Fig. 6.6c) taken accross the cloud head, the dry intrusion and the main baroclinic zone cloud band (almost perpendicular to the cross-section of Fig. 6.6b) also indicates the strong link between the vertical vorticity maximum and the dry slot region DS. Unfortunately, the lack of radar targets (precipitating particles) in the upper-levels, and in particular in the dry slot region, does not allow documentation of an upper-level vorticity anomaly and its potential baroclinic interaction with the low-level vorticity anomaly seen in Figs. 6.6bc. This problem will be overcome in the future using analysis methods that combine Doppler radar and dropsonde information so as to access dynamic fields in both regions of clear-air and precipitation (Montmerle and Lemaître 1998; Bouniol et al. 1999).

6.6   Mass fields anomalies

The "virtual cloud" potential temperature and pressure perturbations at the 1.5-km altitude are given in Figs. 6.9a and 6.9b, respectively. Let us recall that these fields are deviations from a reference state that is constant horizontally, as discussed in Protat et al. (1998). Hence, these deviations include both the baroclinic basic state of the atmosphere and all other local horizontal perturbations developing from this basic state (such as warming or cooling associated with upright or slantwise motions). The temperature perturbation field (Fig. 6.9a) reveals a well-defined baroclinic signature from the colder northerly flow (left side of the domain) to the warmer W2, cold conveyor belt, and WCB flows (right side of the domain), with characteristic averaged horizontal temperature gradients of 9 K for 100 km accross the domain. This global baroclinic tendency is found to be modulated in precipitating areas by local diabatic warming, for instance on the southwestern border of the domain. However, it is to be noted that those local effects are likely not well-resolved, due to the fact that small-scale features are filtered out by the analysis for this mesoscale retrieval. Again, the effect of the diabatic processes on the mesoscale circulation will be addressed in a near-future by performing dynamic retrievals at convective-scale in these particular precipitating regions.

The pressure perturbation field (Fig. 6.9b) evidences a local minimum, characterized by mean horizontal gradients of roughly 6 mbar for 100 km. This pressure perturbation minimum is located along the easternmost baroclinic region of Fig. 6.9a, in the particular precipitating region A source of vertical transport to the southeast within the cyclone illustrated in Fig. 6.7b (W2 flow). Since these slantwise transports depend on latent heat release, this indicates that latent heat release likely plays a significant role in the secondary cyclone growth. This seems to support observationally the conclusions of Shutts (1990) deduced from a fine-mesh numerical simulation of a secondary cyclone, according to which the contribution of latent heat release to an explosive development appears to dominate the dry baroclinic instability process.

The location of the low pressure can be compared with the location of the vertical vorticity maximum at mesoscale. For this purpose, a horizontal cross-section of vertical vorticity at the 1.5-km altitude is given in Fig. 6.10. It exhibits a tongue of positive vertical vorticity oriented along the northeastern border of the northerly flow, characterized by two local maxima. The first maximum is located into the region of vertical mass transport to the northwest (described previously, Fig. 6.7a), and the second maximum is associated with the clear-air region DS. Comparison between Figs. 6.9b and 6.10 shows that the low pressure is slightly shifted on the southeastern border of the vertical vorticity core.

Pressure perturbation field at the 1.5-km altitude resulting only from the Coriolis terms (that is, using only accelerations due to the Coriolis and pressure forces in the two horizontal projections of the momentum equations) has been computed. First, let us notice the good agreement between the absolute wind field given in Fig. 6.6 and the "Coriolis-derived" pressure perturbation, with the horizontal wind that follows the pressure isolines, as expected. Comparison between this "Coriolis-derived" pressure perturbation and the retrieved "full" pressure perturbation field of Fig. 6.9b reveals the important contribution of other physical mechanisms than the Coriolis effect in the low pressure formation. It reveals in particular the southeastward shift of the low pressure (between the "full" and "Coriolis-derived" pressure fields). This low pressure lies on the southern border of the DS region, which suggests the importance of non-hydrostatic effects linked to the ascent of W2 and the reascent of the dry intrusion while approaching the cyclone center.

VIRTUAL CLOUD POTENTIAL TEMPERATURE θ^* (K)

(a)

40 ms^{-1}

40 ms^{-1}

Z = 1.5km

	10.0 & ABOVE
	8.0 to 10.0
	6.0 to 8.0
	4.0 to 6.0
	2.0 to 4.0
	0.0 to 2.0
	-2.0 to 0.0
	-4.0 to -2.0
	-6.0 to -4.0
	-8.0 to -6.0
	BELOW -8.0
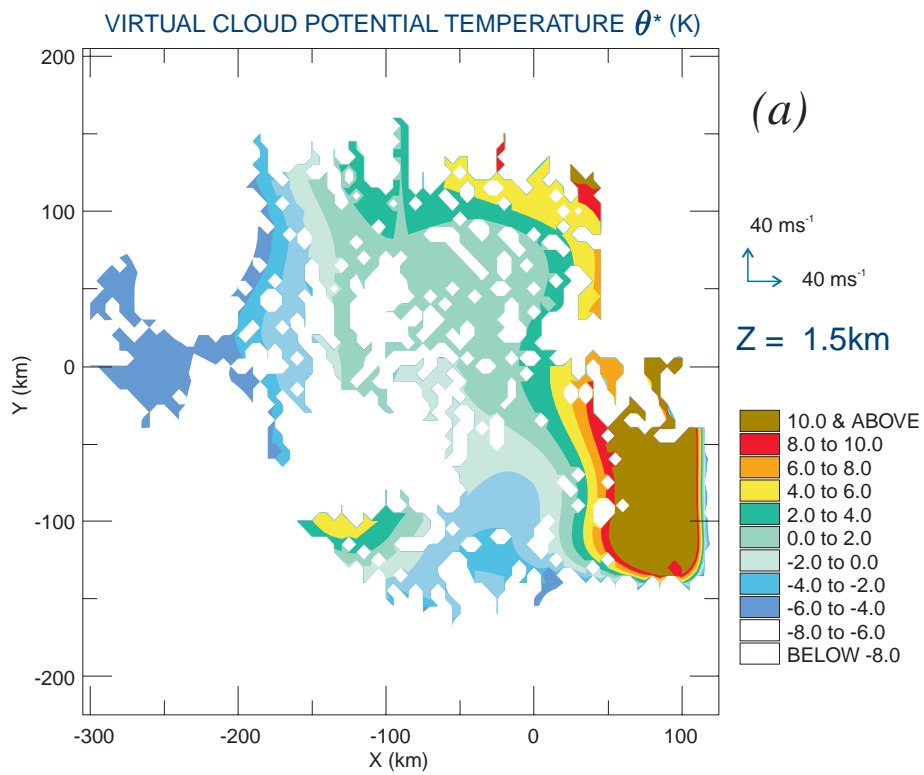
Figure 6.9: *"Virtual cloud" potential temperature (a) and pressure (b) perturbations at the 1.5 km altitude derived from the 3D wind field.*

PRESSURE PERTURBATION p* (mbar)

(b)

40 ms^{-1}

40 ms^{-1}

Z = 1.5km

	10.0 & ABOVE
	8.0 to 10.0
	6.0 to 8.0
	4.0 to 6.0
	2.0 to 4.0
	0.0 to 2.0
	-2.0 to 0.0
	-4.0 to -2.0
	-6.0 to -4.0
	-8.0 to -6.0
	BELOW -8.0
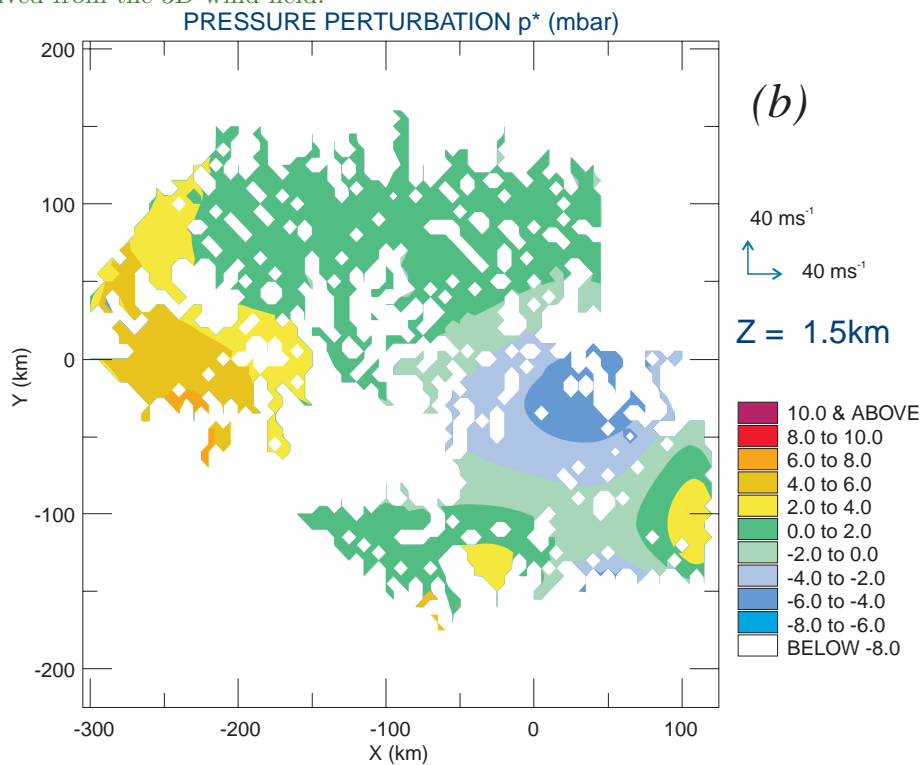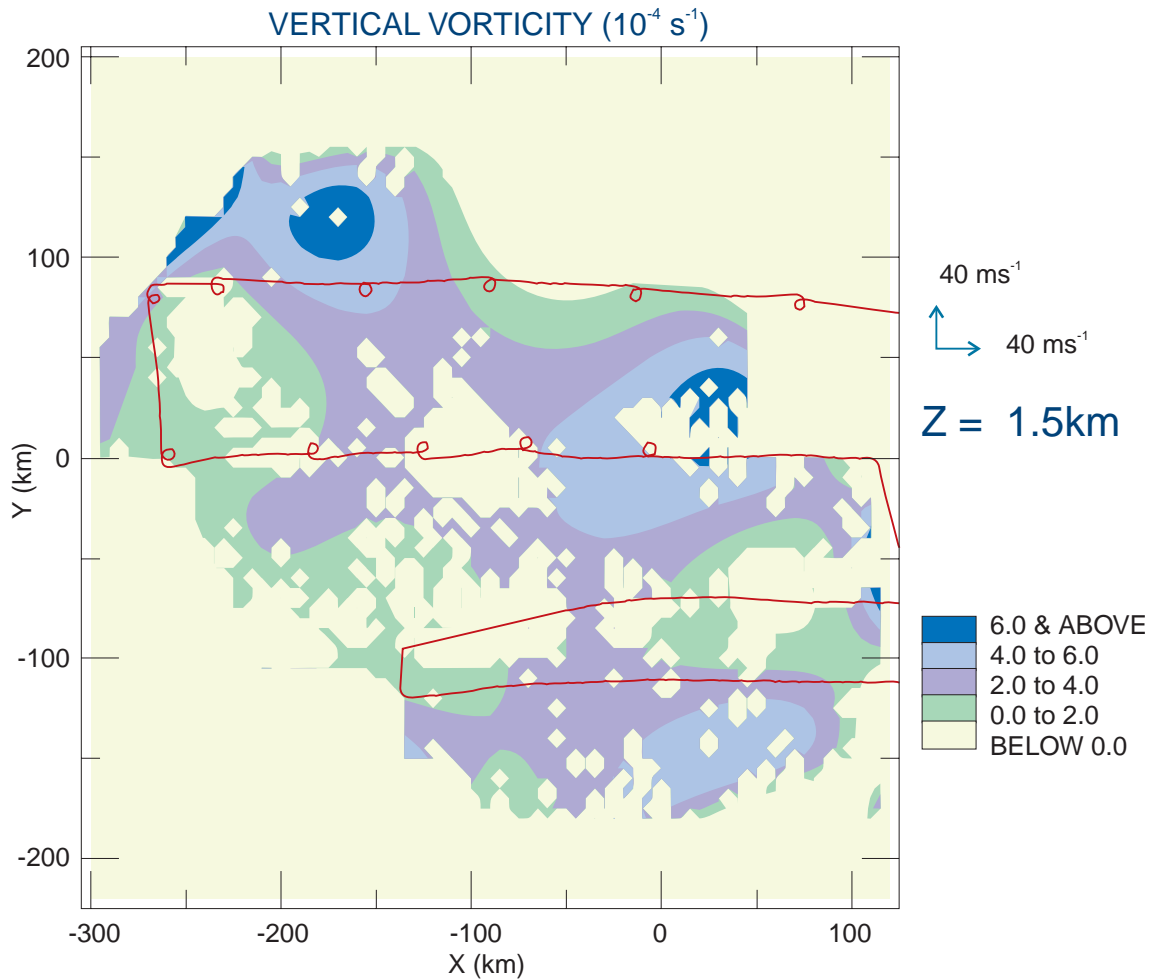
Figure 6.10: *Horizontal cross-section of vertical vorticity at the altitude of 1.5 km.*

6.7   Summary and perspectives

In this paper, the mesoscale dynamics of an explosively deepening secondary cyclone sampled during the field phase of FASTEX (IOP 12) was documented using airborne Doppler radar data. Let us recall that the meteorological interest of this case lies in the presence of well-developed cloud head and dry slot features and of a well-organized line of thunderstorms which highlights the interest to scrutinize the mesoscale dynamic structure of this particular case study. This study illustrates that the sampling strategy defined for FASTEX is suitable for accessing the mesoscale dynamics of the whole core of a cyclone, in addition to the internal structure of each precipitation component of this cyclone (as done more classically).

The main flows responsible for the mesoscale organization of the cyclone have been documented under the assumption of stationarity. First, this study confirms observationally the existence of a warm airflow W2 peeled-off from the base of the WCB and its crucial importance on the development of the most active part of the cloud head (in terms of precipitation), as claimed at broader scale by Browning and

Roberts (1994, 1996). It also evidences the intrusion of a dry airflow approaching the cyclone center. Unfortunately, the lack of radar targets (precipitating particles) in the upper-levels, and in particular in the dry slot region, does not allow documentation of an upper-level vorticity anomaly and its potential baroclinic interaction with the low-level vorticity anomaly.

A cold conveyor belt is found to contribute to the upward mass transport towards the upper part of the main baroclinic zone cloud band. Documentation of the distinct behaviour of the W2 and cold conveyor belt flows that feed distinct precipitating entities of the cyclone was not made possible using the present mesoscale 3-D fields, due to the limited areal coverage of the Doppler observations. These last two problems will be overcome in the near-future by combining Doppler radar data, dropsonde measurements, and numerical model outputs in order to access dynamic fields in both regions of clear-air and precipitation (Montmerle and Lemaître 1998; Bouniol et al. 1999) and to quantify the importance of the large-scale environmental forcing with respect to the mesoscale and convective-scale processes.

In addition, this study evidences a slight shift between the location of the high vertical vorticity core associated with the most active part of the cloud head and the location of the low pressure, suggesting the importance of the non-hydrostatic effects associated with the ascent of the peeled-off W2 flow and with the reascent of the dry intrusion while approaching the cyclone center. A further quantification of these non-hydrostatic processes will be conducted in a future paper by performing convective-scale retrievals in the low pressure area. The dynamical importance of a cold northerly flow which tends to wrap around the low center is also revealed by analysis of the mesoscale fields. It is suggested that the associated precipitating entities are generated by release of convective instability during the propagation of this flow above the warmer ocean. To confirm this aspect, a smaller-scale study of the air-sea interactions in this northerly flow area will be performed.

This paper highlights the high-quality of the IOP12 airborne Doppler dataset. It also shows the need to combine in the near-future airborne Doppler radar and dropsonde measurements in order to access multiscale processes involved in the mature stage of this FASTEX cyclone in both clear-air and precipitating regions and to address the numerous open questions raised by the present mesoscale study. This work is presently under progress (see recent results of Bouniol et al. 1999 concerning the FASTEX IOP16) using an analysis method that permits combination of such measurements (Montmerle and Lemaître 1998). The mesoscale fields analyzed in this paper will be used to initialize mesoscale models (see recent works of Montmerle 1998) in order to diagnose associated microphysical fields and evaluate the importance of microphysical processes in the cyclone organization. This advanced part of the interpretation is included in the *FASTEX Cloud System Study* project, also supported by the European Commission.

6.8   References

Appenzeller, C., 1994 :
  Wave developments on surface fronts and stratospheric intrusions.
  PhD thesis, Swiss Federal Institute of Technology (ETH). Dissertation No 10471, 117pp.

Baehr, C., B. Pouponneau, F. Ayrault, and A. Joly, 1999 :
  Dynamical characterization and summary of the FASTEX cyclogenesis cases.
  Quart. J. Roy. Meteor. Soc., *submitted.*

Bouniol, D., A. Protat, and Y. Lemaître, 1999 :
Mesoscale dynamics of a deepening secondary cyclone (FASTEX IOP16) : Three-dimensional structure retrieved from dropsonde data.
Quart. J. Roy. Meteor. Soc., *submitted.*

Browning, K. A., 1994 :
GEWEX Cloud System Study (GCSS) : Science Plan.
Volume **11**, IGPO Publication Series. 62 pp.

Browning, K. A, and N. M. Roberts, 1994 :
Structure of a frontal cyclone.
Quart. J. Roy. Meteor. Soc., **120**, 1535-1557.

Browning, K. A, and N. M. Roberts, 1996 :
Variation of precipitation structure along a cold front.
Quart. J. Roy. Meteor. Soc., **122**, 1845-1872.

Bond, N. A., and Co-authors, 1997:
The Coastal Observation and Simulation with Topography (COAST) experiment.
Bull. Amer. Meteor. Soc., **78**, (9), 1941-1955.

Bottger, H., M. Eckardt, and U. Katergiannakis, 1975 :
Forecasting extratropical storms with hurricane intensity using satellite information.
J. Appl. Meteorol., **14**, 1259-1265.

Carlson, T. N., 1980 :
Airflow through midlatitude cyclones and the comma cloud pattern.
Mon. Wea. Rev., **108**, 1498-1509.

Chaigne, E., 1998 :
Application de l'inversion du tourbillon potentiel (Aplication of the PV inversion technique).
Master's thesis, Ecole Nationale de la Météorologie, Note de Travail No 618, Toulouse, 86pp.

Dou, X. K., G. Scialom, and Y. Lemaître, 1996:
MANDOP analysis and airborne Doppler radar for mesoscale studies.
Quart. J. Roy. Meteor. Soc., **122**, 1231-1261.

Green, J. S. A., F. H. Ludlam and J. F. R. McIlveen, 1966 :
Isentropic relative-flow analysis and the parcel theory.
Quart. J. Roy. Meteor. Soc., **92**, 210-219.

Harrold, T. W., 1973 :
Mechanisms influencing the distribution of precipitation within baroclinic disturbances.
Quart. J. Roy. Meteor. Soc., **99**, 232-251.

Joly, A., D.Jorgensen, M.A.Shapiro, A.Thorpe, P.Bessemoulin, K.A.Browning, J.P.Cammas, J.P.Chalon, S.A.Clough, K.A.Emanuel, L.Eymard, R.Gall, P.H.Hildebrand, R.H.Langland, Y.Lemaitre, P.Lynch, J.A.Moore, P.O.G.Persson, C.Snyder, R.M.Wakimoto, 1997:
The Fronts and Atlantic Storm-Track Experiment (FASTEX): Scientific Objectives and Experimental Design.
Bull. Amer. Meteor. Soc., **78**, (9), 1917–1940.

Joly, A., K.A. Browning, P. Bessemoulin, J.P. Cammas, G. Caniaux, J.P. Chalon, S.A. Clough, R. Dirks, K.A. Emanuel, L. Eymard, R. Gall, T.D. Hewson, P.H. Hildebrand, D. Jorgensen, F. Lalaurette, R.H. Langland, Y. Lemaitre, P. Mascart, J.A. Moore, P.O.G. Persson, F. Roux, M.A. Shapiro, C. Snyder, Z. Toth, and R.M. Wakimoto, 1999:
Overview of the field phase of the Fronts and Atlantic Storm-Track Experiment (FASTEX) project.
Quart. J. Roy. Meteor. Soc., **125**, *submitted.*

Jorgensen D.P., P. Bessemoulin, S. Clough, and J.A. Moore.
Fastex operations plan, 1996.
Technical Report 5, FASTEX Project Office, Centre National de Recherches Météorologiques, 164pp.

Lemaître, Y., and A. Protat, 1998 :
Dynamics of a "bomb-like" deepening secondary cyclone from airborne Doppler radar.
Quart. J. Roy. Meteor. Soc., *under revision.*

Lemaître, Y., A. Protat and D. Bouniol, 1999:
Pacific and Atlantic "bomb-like" deepening in mature phase: a comparative study.
Quart. J. Roy. Meteor. Soc., *submitted.*

Montmerle, T., and Y. Lemaître, 1998 :
Three-dimensional variational data analysis to retrieve thermodynamical and dynamical fields from various nested measurements.
J. Atmos. Oceanic Technol, **15**, 360-379.

Montmerle, T., 1998 :
Validation et initialisation d'un modèle tridimensionnel méso-échelle non-hydrostatique par des données expérimentales issues de l'expérience TOGA-COARE (Validation and initialization of a 3-D non-hydrostatic mesoscale model using data collected during the TOGA-COARE experiment).
PhD thesis, University Paris 6. Available from the author, 10-12 Avenue de l'Europe, 78140 Vélizy, France.

Neiman, P. J. , and M. A. Shapiro, 1993 :
The life cycle of an extratropical marine cyclone. Part I : Frontal-cyclone evolution and thermodynamic air-sea interaction.
Mon. Wea. Rev., **121**, 2153-2176.

Protat, A., Y. Lemaître, and G. Scialom, 1997:
Retrieval of kinematic fields using a single-beam airborne Doppler radar performing circular trajectories.
J. Atmos. Oceanic Technol., **14**, 769-791.

Protat, A., Y. Lemaître, and G. Scialom, 1998 :
Thermodynamic analytical fields from Doppler radar data by means of the MANDOP analysis.
Quart. J. Roy. Meteor. Soc., **124**, 1633-1669.

Reed, R. J., and E. F. Danielsen, 1959 :
Fronts in the vicinity of the tropopause.
Arch. Meteorol. Geophys. Bioklim., **A11**, 1-17.

Sanders, F., and J. R. Gyakum, 1980 :
Synoptic-dynamic climatology of the 'bomb'.
Mon. Wea. Rev., **108**, 1589-1606.

Scialom, G. and Y. Lemaître, 1990 :
A new analysis for the retrieval of three-dimensional mesoscale wind fields from multiple Doppler radar.
J. Atmos. Oceanic Technol., **7**, 640-665.

Scialom, G., A. Protat, and Y. Lemaître, 1999 :
Vertical structure of a FASTEX secondary cyclone derived from dual-beam airborne radar data.
Quart. J. Roy. Meteor. Soc., *submitted.*

Shutts, G. J., 1990 :
Dynamical aspects of the October storm, 1987 : A study of a successful fine-mesh simulation.
Quart. J. Roy. Meteor. Soc., **116**, 1315-1347.

Vallis, G. K., G. J. Shutts, and M. E. B. Gray, 1997 :
Balanced mesoscale motion and stratified turbulence forced by convection.
Quart. J. Roy. Meteor. Soc., **123**, 1621-1652.

Young, M. V., 1989 :
Investigation of a cyclogenesis event, 26-29 July 1988, using satellite imagery and numerical model diagnostics.
Meteorol. Mag., **118**, 185-196.

Young, M. V., G. A. Monk, and K. A. Browning, 1987 :
Interpretation of satellite imagery of a rapidly deepening cyclone.
Quart. J. Roy. Meteor. Soc., **113**, 1089-1115.

Part 7

Dropsonde observation and modelling experiments in IOP 16: an example of dynamical and microphysical interaction

by

Sidney A. Clough

Joint Centre for Mesoscale Meteorology, United Kingdom Meteorological Office, Reading, United Kingdom.

7.1   An overall assessment of the UKMO C-130 dropsonde data

*T*he FASTEX C-130 dropsonde data are the most comprehensive set of mesoscale sounding data on middle latitude weather systems in existence, and the combination with airborne Doppler radar data provides a powerful and unique resource. They show many structures previously unrecorded across a wide range of frontal wave types.
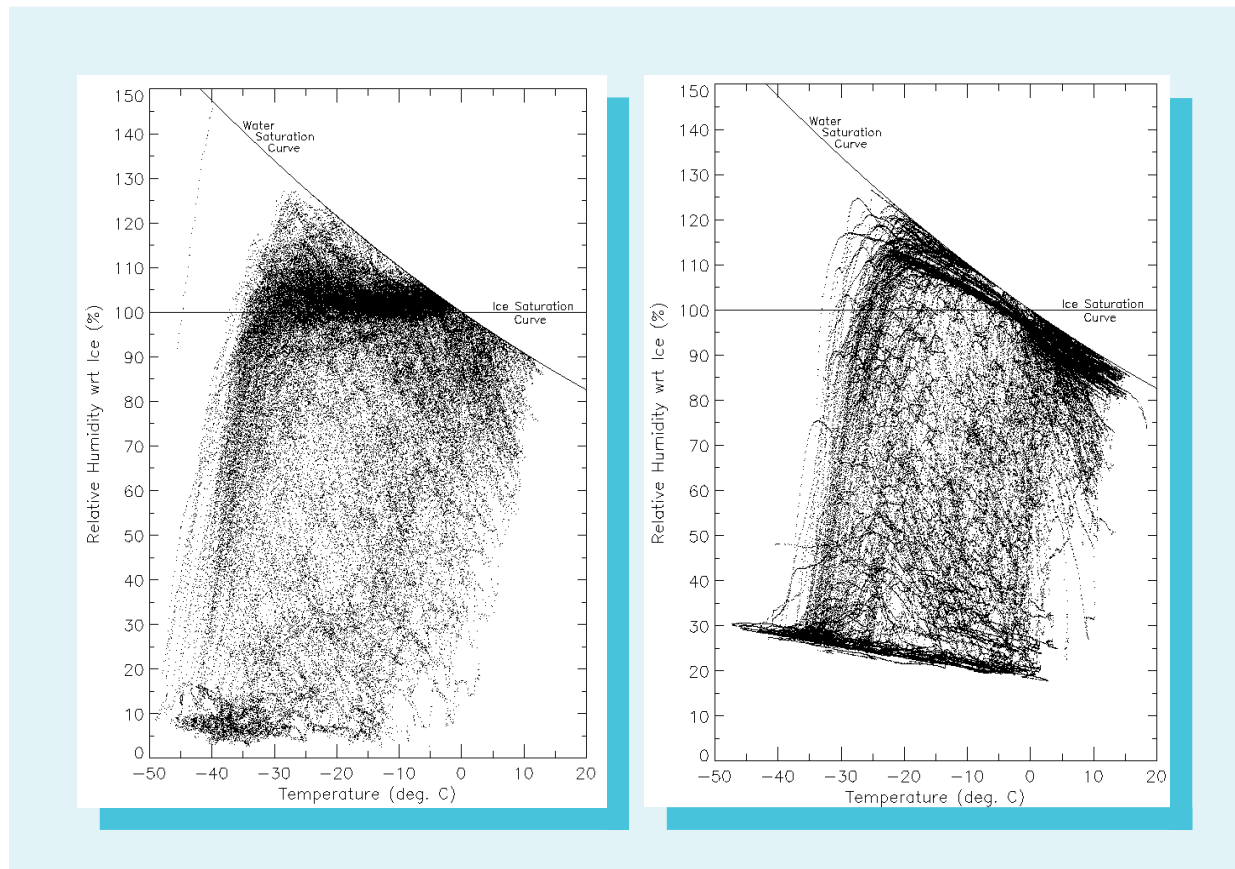
Figure 7.1: *Distribution of all the dropsonde observations taken during the IOP 16 of FASTEX (left panel) and during FRONTS 87 (right panel) in Temperature – Relative Humidity with respect to ice space.*

In particular the data are an improvement on earlier sounding data in two particular respects. Firstly, from IOPs 10 onwards GPS winds are used, which have better resolution and accuracy than the best previously available soundings from LORAN sondes. (GPS wind-finding uses Doppler shift measurements to give instantaneous winds rather than position information time-differenced.)

Secondly, the sondes use the Vaisala unheated humidity sensor which is proving to be a considerable improvement upon the earlier Meteorological Office dropsonde's carbon hygristor. Aside from better response in the dry part of the range it shows indications of a clear quantitative response near ice saturation. Figure 7.1(left) shows a scatter plot of the relative humidity vs temperature for all C130 FASTEX GPS

dropsondes while Figure 7.1(right) presents the equivalent for the Fronts 87 experiment dropsondes (Clough and Testud, 1988). The former show a clear tendency of values to cluster near ice saturation which is not evident in the latter. The clustering behaviour is a natural property to expect of the atmosphere because of operation of the Bergeron-Findeisen process of precipitation growth causes it to relax towards a state of saturation with respect to ice in active weather systems. This appears to occur both because of the evaporation of water droplets but also the sublimation of ice crystals increasing humidity in sub-saturated conditions.

Figure 7.1 is also interesting in that the soundings also show, though in only one event (IOP 16), water saturation being achieved at temperatures as low as $-23°$C in the strong ascent ahead of a deepening low. Since these observations are isolated and not part of a continuously varying pattern, though they occur in several soundings, it seems most likely that they are valid an indicate a significant microphysical feature.

This derived diagram thus represents a very important observational result. Such plots seem likely to prove a useful discriminant of the accuracy of NWP and climate model microphysical parametrization schemes to produce realistic distributions in a range of situations.

One reservation, however, is necessary regarding these observations. There are indications that the humidity near and above ice saturation may be too high. Attempts are currently being made to conduct a comparison between these measurements and other sondes and aircraft to check and perhaps correct the calibration, but to date without success.

7.2 Evidence of dynamical effects driven by sublimation of precipitation in IOP 16

Studies of dropsonde observations from the earlier Anglo-French FRONTS'87 experiment led to theoretical calculations and the proposal of a mechanism by which

Figure 7.2: *METEOSAT composite images showing the devlopment of Low 39A during IOP 16 that shows through the expansion of the cloud head. The images combine, whenever possible, the 3 channels of the METEOSAT radiometer in a way that help materializing the cloud types. Images courtesy of EUMETSAT, processed by the Centre de Météorologie Spatiale of Météo-France.*
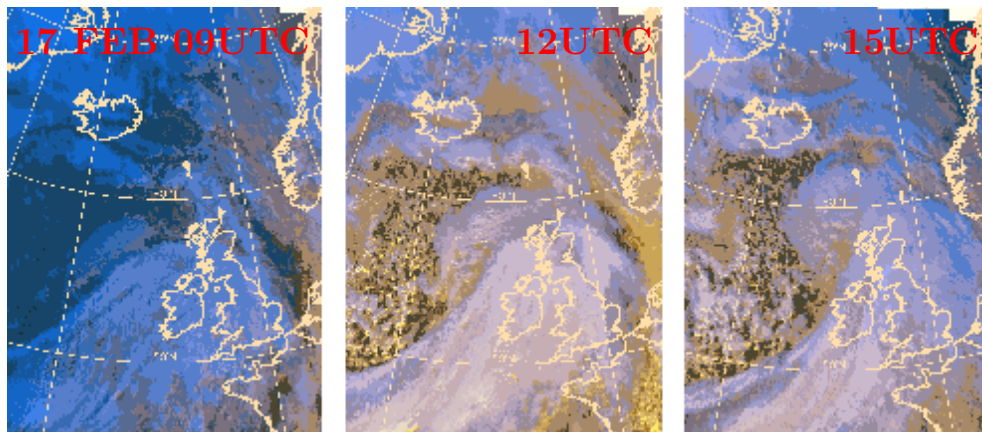
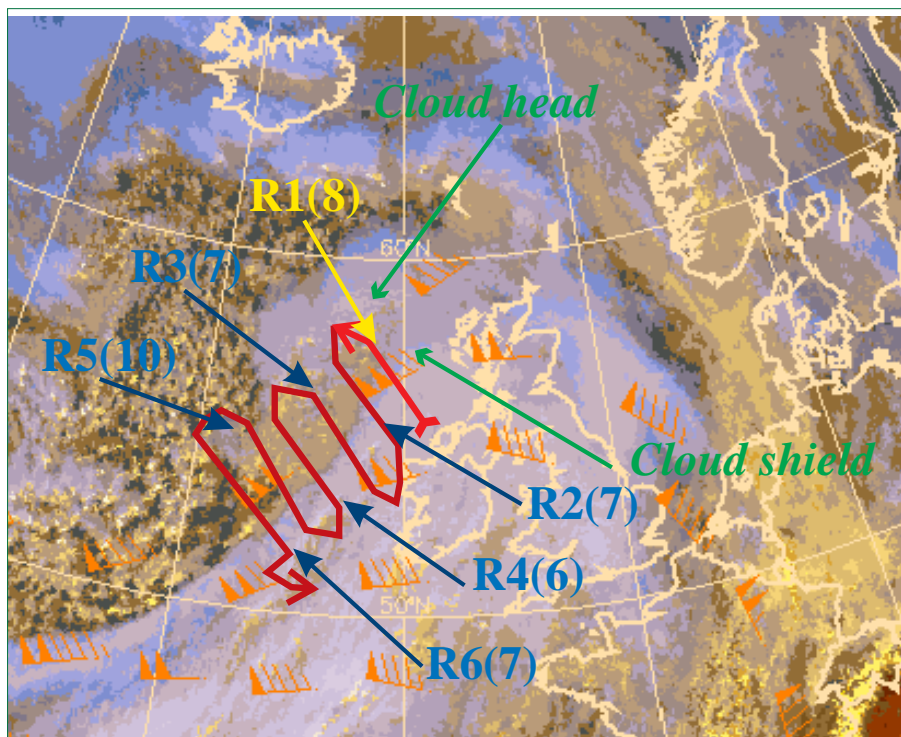Figure 7.3: *METEOSAT composite satellite image similar to Fig. 7.2, but at 12UTC superimposed to the ARPEGE analysis of upper-level wind (orange arrows) showing Low 39A and the jet-stream. The flight plan of the C-130 on 17 February is superimposed. Legs are labelled Rn, the number of dropsondes within each leg is shown in parentheses.*

the sublimation of ice precipitation might lead to descending mesoscale circulations important to the dynamics of weather systems (Clough and Franks, 1991; Thorpe and Clough, 1991). One of the important scientific goals of FASTEX is to confirm and quantitatively refine that hypothesis and investigate the role of precipitation in weather systems and Numerical Weather Prediction (NWP) more generally.

An observational and modelling study has been carried out on one of the events, Intensive Observing Period (IOP) 16, which has led to confirmation of the earlier results and the possibility of more quantitative results for modelling. The results have important implications for understanding the mesoscale structure of frontal waves.

A quick-look summary of IOP 16 is shown in section 3.19 of Part 3, page 116 of this Report. The frontal wave studied in this IOP formed from a weak trough on the main baroclinic zone in the western Atlantic (Fig. 7.2). The rearmost of two troughs, it passed Newfoundland around 06–12UTC on 16th February 1997 and travelled rapidly (30–40 ms^{-1}) across the Atlantic, deepening to form a low pressure centre in the first half of 17th February.

Figure 7.3 shows a satellite image during the flight with dropsonde run locations marked in a system-relative frame. The observations for the first run, highlighted in red, contain particularly interesting symptoms, which are discussed below. This first run crossed the upper cloud shield and the region immediately ahead of the forming cloud head. It can be seen that the upper cloud shield is broken up by the occurrence of bands, which formed in the few hours before the start of observing.
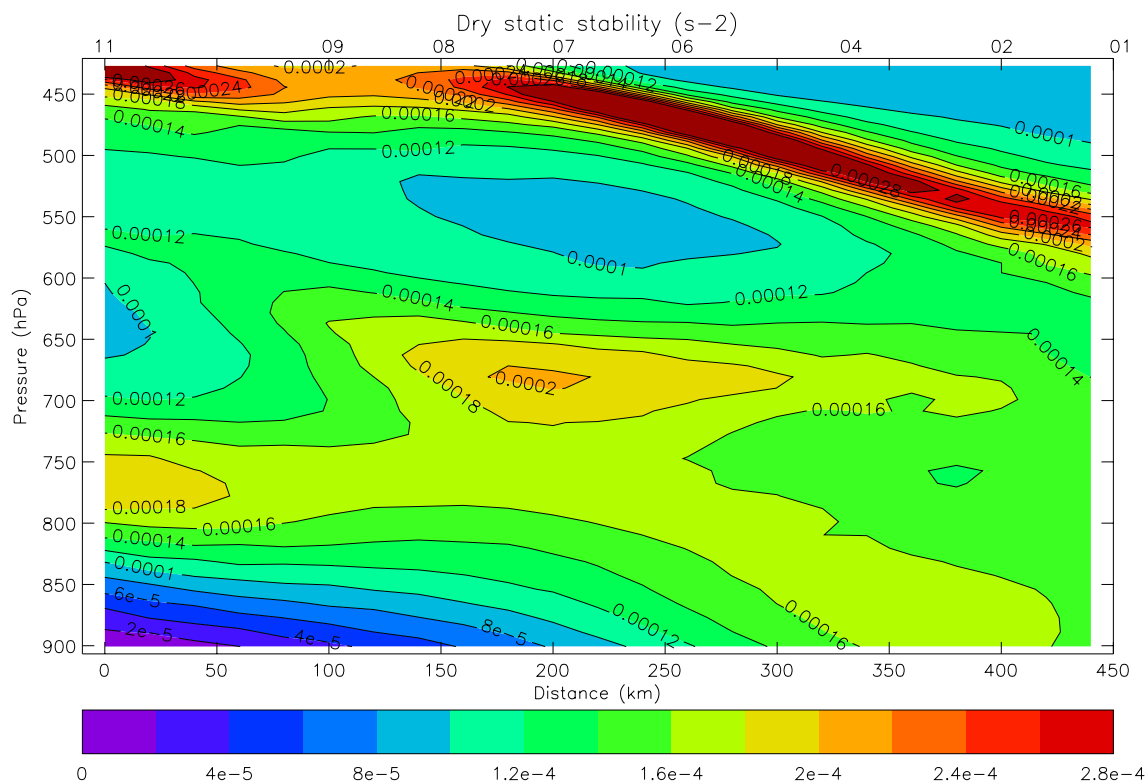
Figure 7.4: *Vertical cross-section of dry static stability N^2 derived from the dropsondes. The plane of the cross-section is shown on Fig. 7.3.*

The flight plan executed in this case is the best example carried out of the systematic survey pattern, which lends itself well to model comparison over a wave domain, and the system is the early stage of a well-forecast wave development. Both of these are well suited to the Cloud System Study project, where the ability to compare observations and models is vital.

Vertical cross-sections have been objectively analysed from individual dropsonde runs to characterise the internal mesoscale structure of the systems observations. The 1.5 s sounding data of basic parameters (temperatures, scalar wind components and humidity) were objectively analysed as 2-dimensional vertical cross-sections for each of the runs as indicated in Figs. 7.3(c) and 7.4 in log-pressure vs distance coordinates using successive correction algorithms developed by Pedder (1993) to produce the cross-section illustrations. It should be noted that the parameters of the analysis have been subjectively defined to maximise the vertical resolution while avoiding a break-up of differentiated features because of the limited horizontal resolution. This was achieved by using 15 s sampling of the data and filtering with a vertical scale of 25 s (corresponding to 250 m) and horizontal scale of twice the mean sounding separation of 50–90 km in the successive correction algorithm. Horizontal distances are shown as the projected distance onto the plane chosen to resolve vector quantities.

Figure 7.4 shows the analysed static stability in the form of the Brunt-Vaisala frequency N^2. The dropsondes used to prepare the cross-section are numbered along the top axis. This clearly shows the presence of a frontal surface, the sloping stable

layer around 500 hPa. A very important feature, however, is the deep layer of weakly stable air beneath the frontal surface. In fact at full data resolution soundings 8, 9 and 11 possess shallow dry adiabatic layers immediately beneath the inversion, a typical symptom of sublimation cooling highlighted by Harris (1977). The extent of the feature is striking, crossing the whole 440 km section and θ_w values from 10 to 13°C, suggesting that it may be formed by a process operating over the system's extent. It is suggested that sublimation from the upper cloud shield makes an important contribution to the presence and amplitude of such a structure.

The cross-frontal flow also shows particularly interesting structure (Fig. 7.5). A shallow layer of strong forward flow coincides with much of the stable zone of the upper front. The pattern in mid-troposphere shows a pair of forward-rearward flow near 500 hPa and another weaker pair at 650–700 hPa, with maxima of relative humidity (not shown) above the peak forward flows. This pattern, of forward descending motion where precipitation is subliming, qualitatively matches that predicted by the Clough-Franks mechanism.

The Clough-Franks mechanism is as follows. Ice crystals sublime very efficiently in sub-saturated environments because of their low fall rate and long residence time, as well as their large effective surface area. The sublimation cools the surrounding air, which descends. Descent increases the subsaturation, which further increases the sublimation until all the precipitation has evaporated. This can occur in a depth scale of a few hundred metres or less. Normally the atmosphere is statically stable and

Figure 7.5: *Vertical cross-section of along-plane wind velocity derived from the dropsondes, in the same plane as Fig. 7.4, shown on Fig. 7.3.*
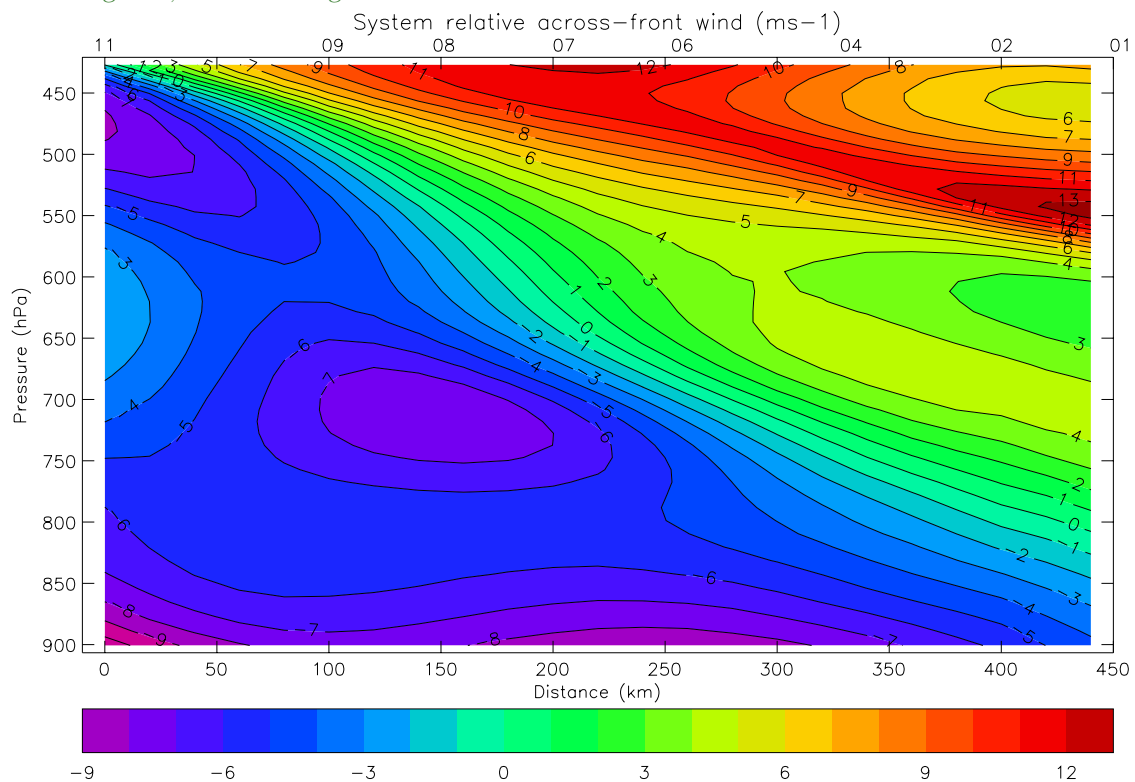
Figure 7.6: *Vertical cross-section of dry static stability N^2 derived from the Unified Model reference simulation, to be compared to Fig. 7.4.*

so descent can only occur in sloping trajectories towards the warm air mass, though Harris (1977) demonstrated that static instability can also be caused by sublimation of intense precipitation. The depth and strength of this circulation are sensitive to the microphysical parameters and so are significant to accurate prediction of weather system structure. For practical NWP and climate simulation sublimation raises some difficulty because of the high vertical resolution necessary to simulate the atmospheric behaviour accurately, which is as yet not well achieved in practice.

The overall forward flow in the warm sector aloft is associated with the anticyclonic flow into the ridge strengthening downstream of the main latent heating zone near the low centre. This probably corresponds to the reduction of potential vorticity above and downstream of the level of maximum heating. The local maximum in the frontal surface corresponds to a direct circulation driven by local sublimation cooling, and the fact that the maximum coincides with the lower part of the saturated region is consistent with moist adiabatic descent occurring where precipitation is sufficient to support it. The layer is shallow because the available precipitation sublimes efficiently but is insufficient to support a deep layer of descent, hence the structure degenerates into finer scales because of the moisture distribution.

7.3 Model results: quantitative assessment of the impact of sublimation

The event was simulated with the UK Meteorological Office's Unified Model, using versions with both conventional forecast resolution and mesoscale resolution. The models were initialised at 21UTC on 16th February and integrated to 12UTC on 17th February. Although it was a comparatively short integration period, significant mesoscale structure was evolved even by the time of the first run at 06UTC.

The forecast model, the Limited Area Model (LAM), had resolution 50 km and 19 levels and produced a good forecast used to plan the observations. Despite this the model failed to reproduce the above front and associated circulation, presumably because the vertical resolution was insufficient to simulate the sublimation accurately.

Figure 7.6 shows a cross-section of the static stability located near run 1 in a mesoscale model simulation. Compared to Fig. 7.4 it reproduces qualitatively well the upper front and reduced stability beneath the front. Figure 7.7 shows the corresponding cross-frontal wind component, which may be compared to Fig. 7.5. A forward flow occurs in the frontal surface, which corresponds to the circulation inferred from the observed structure. Figure 7.8 shows the actual descent in the model, thus confirming the applicability of the assumption made in analysing the observations that the forward horizontal flow does in fact correspond to descent.

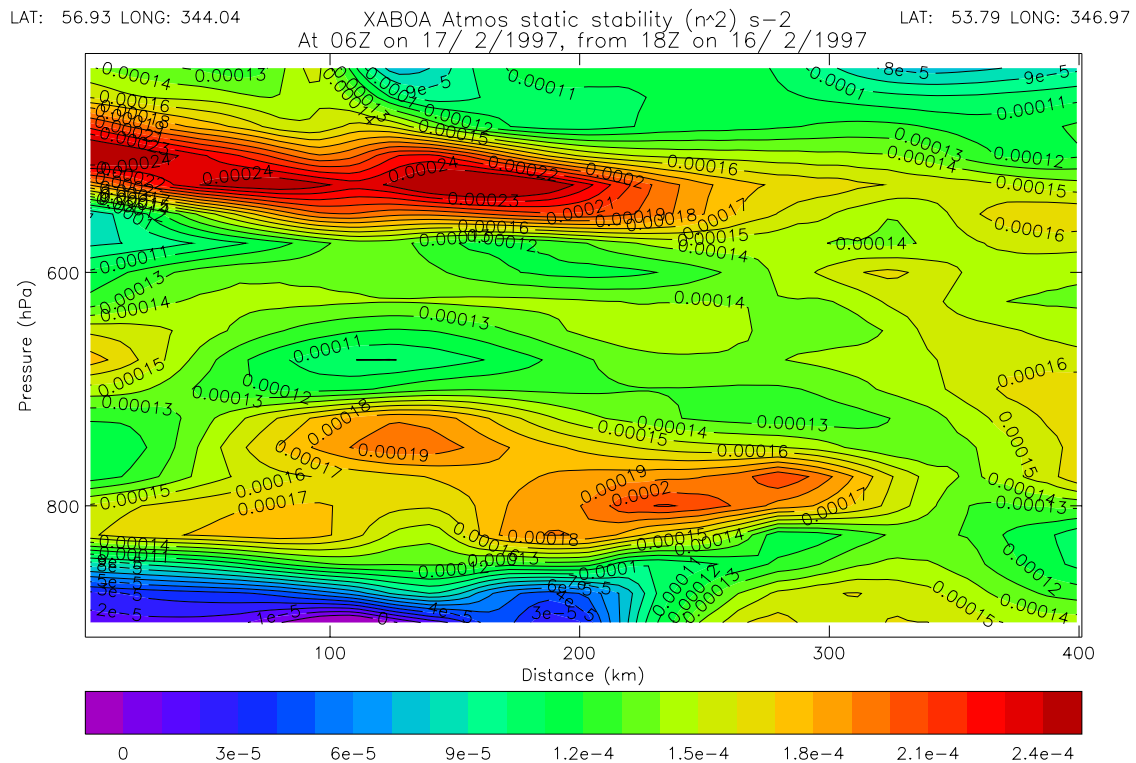Figure 7.7: *Vertical cross-section of dry static stability N^2 derived from the Unified Model reference simulation to be compared to Fig. 7.5.*
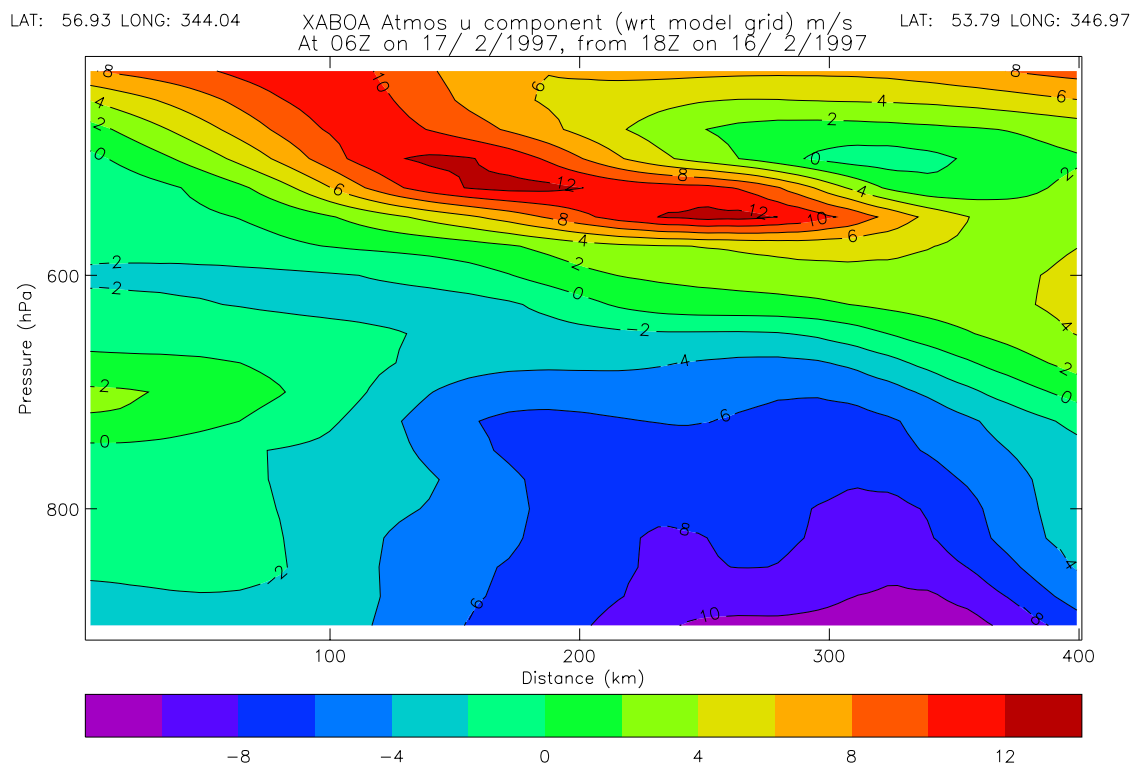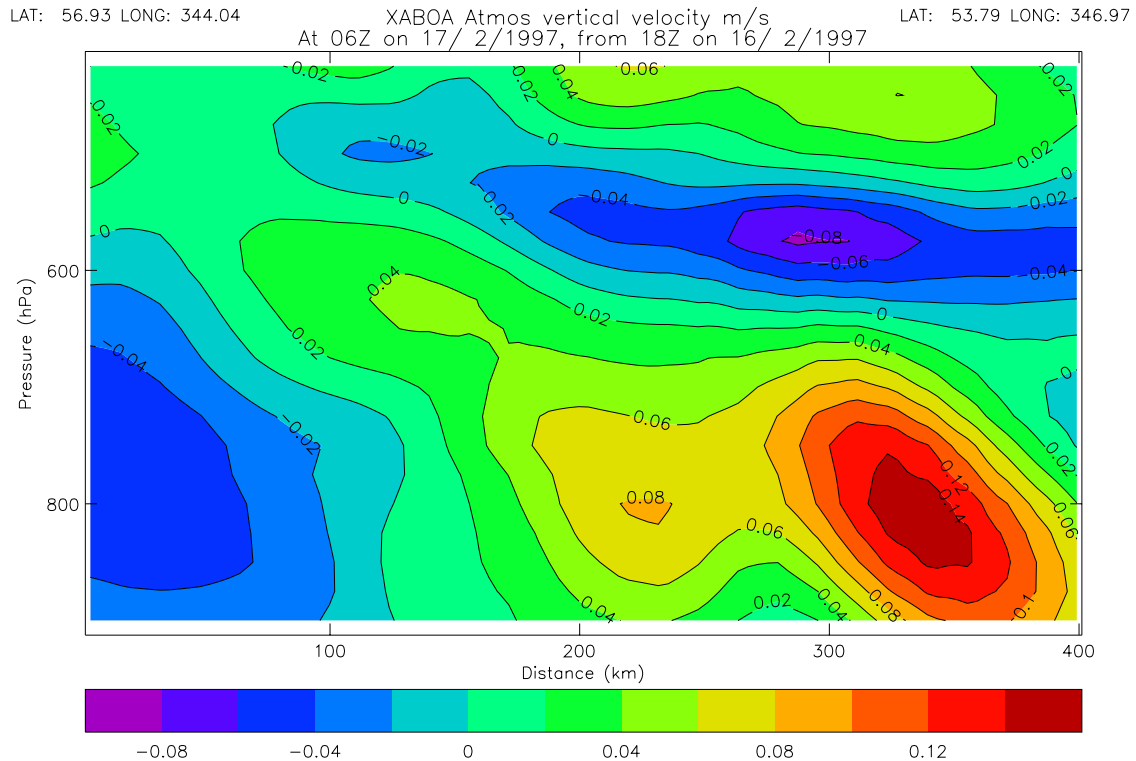
Figure 7.8: *Vertical cross-section of vertical velocity w derived from the Unified Model reference simulation, which, together with the wind shown on Fig. 7.7, materializes the cross-frontal circulation, in particular the descent of the upper-level front.*

In the model environment more information is available than in the dropsonde observations because complete 3-dimensional fields are available, including ascent/descent and potential vorticity.

Thus the link between the circulation and stability has been confirmed by omitting from a model simulation the sublimation cooling. This modifies both the stability and flow in the predicted manner, weakening the observed signatures. Figure 7.9 shows the vertical velocity from this integration, which also confirms numerically an aspect of the Clough-Franks mechanism, that the sublimation mechanism acts primarily to amplify descent for which forcing may be already present, through the shallow depth scale permitted by the presence of ice precipitation.

7.4   Concluding remarks

The integrations have also shown a strong interaction between the sublimation and the potential vorticity. A region of low potential vorticity (PV) is normally associated with the upper part of the diabatically heated region of a frontal wave. In the presence of sublimation in the numerical model, however, the low PV is amplified to strongly negative values, the circumstances in which symmetric instability or conditional symmetric instability (SI or CSI) is present.
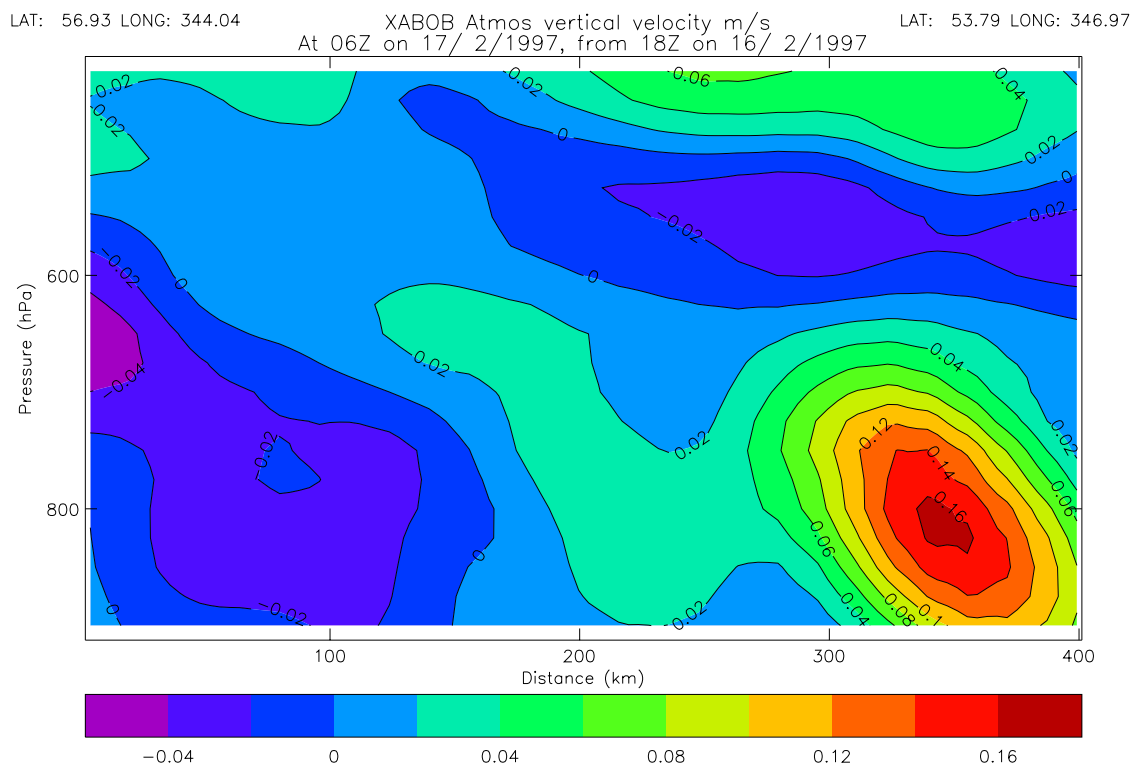
Figure 7.9: *Vertical cross-section of vertical velocity w derived from the Unified Model simulation without sublimation. Compared to Fig. 7.8, this figure shows the quantitative impact of Clough-Franks mechanism.*

This result strongly suggests that the combination of sublimation and negative potential vorticity is associated with the occurrence of strong mesoscale circulations and probably the formation of broad mesoscale cloud and precipitation bands.

It is hoped in future work to combine analyses of Doppler radar cloud-mesoscale motions and aircraft microphysical and other data in order to test existing models and to develop more sophisticated parametrizations of mesoscale processes associated with cloud and precipitation on the basis of this and other cases.

7.5 References

Clough and J. Testud, 1988: The FRONTS-87 Experiment and Mesoscale Frontal Dynamics Project. WMO Bulletin, **37**, 276–281.

Clough S.A. and R.A.A. Franks, 1991: The evaporation of frontal and other stratiform precipitation. *Quart. J. Roy. Meteor. Soc.*, **117**, 1057–1080.

Harris F.I., 1977: The effects of evaporation at the base of ice precipitation layers: theory and radar observations. *J. Atmos. Sci.*, **34**, 651–672.

Pedder M.A., 1993: Interpolation and filtering of spatial observations using successive corrections and Gaussian filters. *Mon. Wea. Rev.*, **121**, *(10),* 2889–2902.

Thorpe, A.J. and S.A. Clough, 1991: Mesoscale dynamics of cold fronts - Part I : structures described by dropsoundings in Fronts 87. *Quart. J. Roy. Meteor. Soc.*, **117**, 903–941.

4D-VAR assimilation of FASTEX radiosonde and dropsonde data in IOP 17: towards a reference analysis of FASTEX data

by

Gerald Desroziers[*], Béatrice Pouponneau[*],
Jean-Noel Thépaut[*], Marta Janisková[**]
and Fabrice Veersé[*].

[*]*Météo-France, URA CNRS 1357, Groupe d'Etude de l'Atmosphère Météorologique, Toulouse, France,*
[**]*Slovak HydroMeteorological Institute, Bratislava, Slovakia.*

8.1   Introduction

ne of the main objectives of the FASTEX experiment was to improve the description of the complete life-cycle of a number of cyclones in the Northern Atlantic ocean (Joly et al., 1997). This observation set especially included a large number of additional vertical profiles performed by land-based sounding sites or ships, but also provided by dropsondes launched by aircraft. Some of the dropsonde legs designed to sample some particular features of a developing or mature cyclone can be vertically and horizontally interpolated in a vertical cross-section. Such an approach has for example already been applied by Thorpe and Clough (1991), or Browning et al. (1995) in order to present the mesoscale structures of a number of cyclones observed during FRONTS 87 and FRONTS 92 experiments. Other authors, like Shapiro and Hastings (1973) or Keyser and Shapiro (1986) also used temporal vertical cross-sections , with profiles performed at a single site, in order to recover lower and upper structures associated with fronts.

Figure 8.1: *Dates and times of the soundings performed during IOP 17, between 09 UTC 17 February and 03 UTC 20 February, by the FASTEX land-based sites, the four FASTEX ships, the two ASAP vessels inside the FASTEX zone during this period, a NSF Lear 36 flight, three NOAA Gulfstream IV flights and a UKMO C130 flight.*
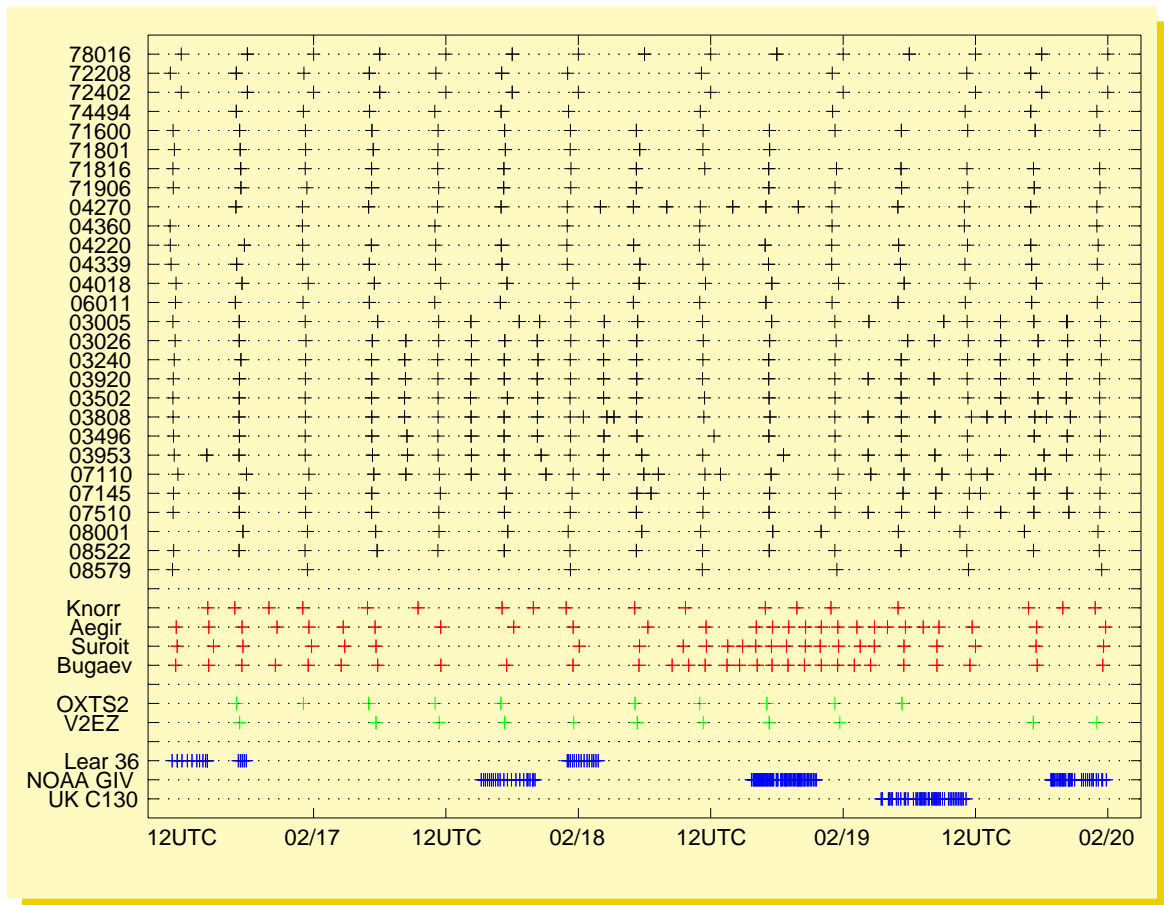
Another approach is to add such particular data collected during an experiment to the conventional dataset and to use an assimilation scheme in order to recover the complete 3-dimensional structures associated with the observed cyclones. This strategy has for example been followed by Browning et al. (1996), using the UK Meteorological Office (UKMO) assimilation scheme with FRONTS 92 dropsondes.

Our objective is to perform a complete analysis of the FASTEX cases, or at least of a number of them, since these 3D composite views of the observed systems are required for diagnostic studies, model initialization but also for the evaluation of adaptive observations as it has been settled during FASTEX (Bergot 1999). Because attention has been paid during FASTEX to disseminate the different vertical profiles in TEMP format on the Global Telecommunications System (GTS), some national weather services were able to include them in their operational analyses in real time. This has been done for example at Météo-France, in order to improve the quality of the short range forecasts and subsequently to ease the control of the operations during the field phase of the FASTEX project. However, this first set of analyses produced by the French meteorological service and included in the Data Base according to the work programme can be improved. Indeed, a significant further step can be taken by employing a 4D-VAR formulation. This 4D-VAR analysis tool is now under development at Météo-France and its present formulation is described in Janisková et al. (1999 , hereafter called *Jan 99*).

The aim of this part of the FASTEX report is to present an application of the 4D-VAR assimilation scheme to the cyclone observed during the Intensive Observation Period 17 (IOP 17), using the whole set of FASTEX soundings collected during this IOP. In the following section, one first describes this FASTEX observation dataset and some elements on the evolution of the system. The 4D-VAR set up and the methodology followed in this study are presented in section 8.2. Subsequent analyses are presented and discussed in section 8.3 and 8.4 and final conclusions and perspectives are given in section 8.5. Further results can be found in Desroziers et al., 1999.

8.2 Experiments settings and design, choice of case

8.2.1 4D-VAR setting

Here, one focusses on the way some particular FASTEX datasets are used by this analysis scheme, rather than the technique itself, which is summarized in the Short Note 8.1. According to the tests presented in *Jan 99*, the incremental 4D-VAR setting will be here fixed to the one that gave sensible results: in all the following 4D-VAR experiments, one uses three updates of the trajectory and the reduced set of simplified physics, presented in *Jan 99*, is made active only in the last minimization of the cost function specified in this variational procedure. Up to 70 iterations are used for the whole analysis, with 25 adiabatic iterations in the first two minimizations and 20 iterations with the reduced simplified physical parametrizations in the last minimization. This parametrization set includes the computation of vertical turbulent diffusion, orographic gravity waves and stratiform precipitation but excludes radiation and deep convection. A 6-hour assimilation period is used, centred on synoptic times, with a surface analysis performed at the end of the filtered variational analysis of the upper fields.

The ARPEGE French forecast model (Courtier et al. 1991) is used to give the trajectory. This spectral model is based on a stretched geometry (Schmidt 1977;

Short Note 8.1:
Some details of the 4D-VAR data assimilation

by M. Janisková, F. Veersé and J.N. Thépaut

8.1.1 The incremental 4D-VAR formulation

The standard formulation of 4D-Var (Le Dimet and Talagrand, 1986) consists in determining the model trajectory which best fits the observations over a given time period $[t_0, t_f]$ and a background field (a priori estimate) at time t_0, by minimizing the cost function:

$$\mathcal{J}(\mathbf{x}(t_0))$$
$$= \mathcal{J}^b(\mathbf{x}(t_0)) + \mathcal{J}^o(\mathbf{x}(t_0)) \qquad \text{(SN8.1.1)}$$
$$= \frac{1}{2} \left[\mathbf{x}(t_0) - \mathbf{x}^b(t_0) \right]^T \mathbf{B}^{-1} \left[\mathbf{x}(t_0) - \mathbf{x}^b(t_0) \right]$$
$$+ \frac{1}{2} \sum_{i=0}^{n} \left[H_i \mathbf{x}(t_i) - \mathbf{y}_i^o \right]^T \mathbf{R}_i^{-1} \left[H_i \mathbf{x}(t_i) - \mathbf{y}_i^o \right]$$

where:

- $\mathbf{x}(t_0)$ is the initial state of the model;

- $\mathcal{J}^b(\mathbf{x}(t_0))$ is the background cost function, that is the distance at the initial time t_0 of the model state to the background field $\mathbf{x}^b(t_0)$. The latter, which usually results from a forecast valid at the initial time t_0, is an a priori estimate of the optimal initial condition and essentially summarizes the past information of the atmosphere;

- $\mathbf{B}$ is the covariance matrix of background error;

- $\mathcal{J}^o(\mathbf{x}(t_0))$ is the distance of the model to the observations over the time period;

- $\mathbf{y}_i^o$ is the observation vector at time t_i;

- H_i is the observation operator at time t_i. It allows the computation of the model-equivalent observations from the model state $\mathbf{x}(t_i)$ at this time;

- $\mathbf{x}(t_i) = M(t_i, t_0)\mathbf{x}(t_0)$ is the model state at time t_i;

- $\mathbf{R}_i$ is the observation error covariance matrix at time t_i, which accounts for measurement and representativeness errors.

In the incremental formulation (Courtier *et al.*, 1994; Ide *et al.*, 1997; Laroche and Gauthier, 1998; Veersé and Thépaut, 1998) the model and the observation operators H_i are linearized and a "simplified" correction $\delta\mathbf{w}(t_0)$ to the initial condition is determined, instead of the full system SN8.1.1, by minimizing the following quadratic cost function:

$$\mathcal{J}(\delta\mathbf{w}(t_0))$$
$$= \frac{1}{2} \left[\delta\mathbf{w}(t_0) + \mathbf{w}^g(t_0) - \mathbf{w}^b(t_0) \right]^T \mathbf{B}_{(w)}^{-1}$$
$$\left[\delta\mathbf{w}(t_0) + \mathbf{w}^g(t_0) - \mathbf{w}^b(t_0) \right] \qquad \text{(SN8.1.2)}$$
$$+ \frac{1}{2} \sum_{i=0}^{n} \left[\mathbf{G}_i \delta\mathbf{w}(t_i) - \mathbf{d}_i \right]^T \mathbf{R}_i^{-1} \left[\mathbf{G}_i \delta\mathbf{w}(t_i) - \mathbf{d}_i \right]$$

where

- $\mathbf{d}_i = \mathbf{y}_i^o - H_i \mathbf{x}^g(t_i)$ are the innovation vectors, $\mathbf{x}^g(t_i)$ being the model state at time t_i issued from the first-guess field $\mathbf{x}^g(t_0)$ (initially equal to the background field $\mathbf{x}^b(t_0)$);

- $\mathbf{w}^g(t_0) = S\mathbf{x}^g(t_0)$ and $\mathbf{w}^b(t_0) = S\mathbf{x}^b(t_0)$ are the simplified first-guess and background field respectively;

- S is the (possibly nonlinear) simplification operator;

- $\mathbf{B}_{(w)}^{-1}$ is the inverse of the background error covariance matrix in the simplified space;

- $\mathbf{G}_i$ is the simplified linearized observation operator;

- $\delta\mathbf{w}(t_i) = \mathbf{L}(t_i, t_0)\delta\mathbf{w}(t_0)$ is the simplified increment at time t_i, $\mathbf{L}$ being the simplified tangent linear model.

The first-guess field $\mathbf{x}^g(t_0)$ is then updated:

$$\mathbf{x}^{gnew}(t_0) = \mathbf{x}^{gold}(t_0) + (\mathbf{S}')^{-I} \delta\mathbf{w}(t_0) \qquad \text{(SN8.1.3)}$$

where $(\mathbf{S}')^{-I}$ is the generalized inverse of the linearized simplification operator.

The whole process (minimization of the quadratic incremental cost function and updating of the first-guess) is then repeated a number of times to account for the nonlinearities in the model and in the observation operators (this is the so-called "outer loop" of the incremental 4D-Var process).

8.1.2 Description of the system

The operational model at Météo-France is part of the ARPEGE/IFS system developed jointly with ECMWF. It is a global spectral model with a terrain-following pressure-based hybrid vertical coordinate η (Simmons and Burridge, 1981). On the horizontal the prognostic variables and the orography are discretized using triangular truncated series of spherical harmonics.

A specificity of the ARPEGE model is the use of a conformal transformation of the η surfaces to obtain an increased resolution on a geographical zone of interest (Courtier and Geleyn, 1988; Hardiker, 1997). Such an irregular (hereafter denoted *stretched*) grid leads to some difficulties regarding the specification of the background error covariances (Desroziers *et al.*, 1995) and may require an adequate modeling of representativeness errors (Desroziers *et al.*, 1997). As a first step it has been decided to compute the analysis increments on a regular *unstretched* grid in the present incremental 4D-Var data assimilation system. The innovation vectors $\mathbf{d}_i$ are computed using a model at triangular truncation T95, with 27 hybrid vertical levels and a stretching coefficient equal to 3.5 (as defined in Courtier and Geleyn, 1988). The minimizations of the quadratic incremental cost functions are performed at truncation T63, with the same vertical levels but on a reduced unstretched Gaussian grid (Naughton *et al.*, 1996). This configuration is denoted in short by T95L27C3.5/T63L27C1.0. An option is included in the system for initializing the updated first-guess fields using an incremental digital filter (Lynch *et al.*, 1997).

As stated in the introduction, the incremental approach allows for an improvement of the simplified tangent linear model $\mathbf{L}$ by introducing some physical parametrizations progressively. A complete set of simplified physical parametrizations has been developed (Janisková *et al.*, 1998) including a simplified computation of radiation, vertical turbulent diffusion, orographic gravity waves, deep convection and stratiform precipitation fluxes. The simplifications aim at having the parametrization schemes as much differentiable as possible, while remaining as close as possible to the full physical parametrizations of the complete forecast model. This approach should ensure a correct direction of the physical tendencies even if the intensities of the physical processes are different. This is supposed to be sufficient for transporting adequately the perturbation $\delta\mathbf{w}$ in time.

After some trials the following configuration was established for the experiments reported in this part, with three passes in the outer loop. 25 iterations of the limited-memory quasi-Newton algorithm are used in the first two minimizations, using the simplified adiabatic model. Then 20 iterations are used for the last minimization with either the adiabatic, or simplified physics models. As stated above, the digital filters are used only after the last update, to initialize the final upper-air variational analysed fields. The background term $\mathcal{J}^b$ used in the 4D-Var experiments is identical to the one used in the French operational 3D-Var scheme (Thépaut *et al.*, 1998). It is based on a generalized linear balance operator. The specified structure functions are multivariate, non separable and latitude dependent (Bouttier *et al.*, 1997), as used in the operational suite. The minimization itself is performed using a limited-memory quasi-Newton code from INRIA (Gilbert and Lemaréchal, 1989).

Courtier and Geleyn 1988). In these experiments, the model is used with a T95 spectral truncation on the stretched sphere and a stretching factor 3.5, that provides a roughly $L = 180$ km resolution near Newfoundland and a $L = 70$ km resolution near Ireland, using the $L = (4\pi)^{1/2}a/(N+1)$ formula proposed by Laprise (1992), where N stands for the spectral resolution and a for the earth radius.

On the other part, the successive minimizations, around the different trajectories with this stretched model, are performed using a non-stretched tangent linear model and its adjoint with a $N = 63$ spectral truncation, corresponding to an uniform $L = 370$ km resolution using the previous formula again. In the vertical, both the model for the trajectory and the tangent linear model for the inner minimizations are used with the same 27 η-levels.

8.2.2   Choice of case

One focusses on the system associated with IOP 17, which occurred between 17 February and 20 February and has shown one of the strongest deepening rate observed in FASTEX. It has also been one of the best documented case of the experiment, indeed, of the history of meteorology to date. A quick-look summary of IOP 17 is shown in section 3.21 of Part 3, page 118 of this Report.

A detailed synoptic-dynamic overview of IOP 17 is proposed by Cammas et al. (1999). Using a manipulation of initial conditions through potential vorticity, Arbo-

Figure 8.2: *(a) background field, wind speed at 18 UTC 18 February and at 250 hPa (contours in solid lines every 5 m/s and only for values above 50 m/s), superimposed on potential vorticity on the 310 K isentropic surface (contours in dashed lines every 1 PV unit and for values more than 1 PV unit; values between 1 and 3 PV units are shaded); (b) 4D-VAR analysis using only the soundings given by the FASTEX ships (circles with the symbol × inside) and ASAP ships (circles with the symbol + inside); (c) 4D-VAR analysis using only the conventional data; (d) 4D-VAR analysis using both conventional data and FASTEX ship soundings; (e) 3D-VAR analysis using only the soundings closest to the synoptic analysis time; (f) 4D-VAR analysis using the same observations as (e).*
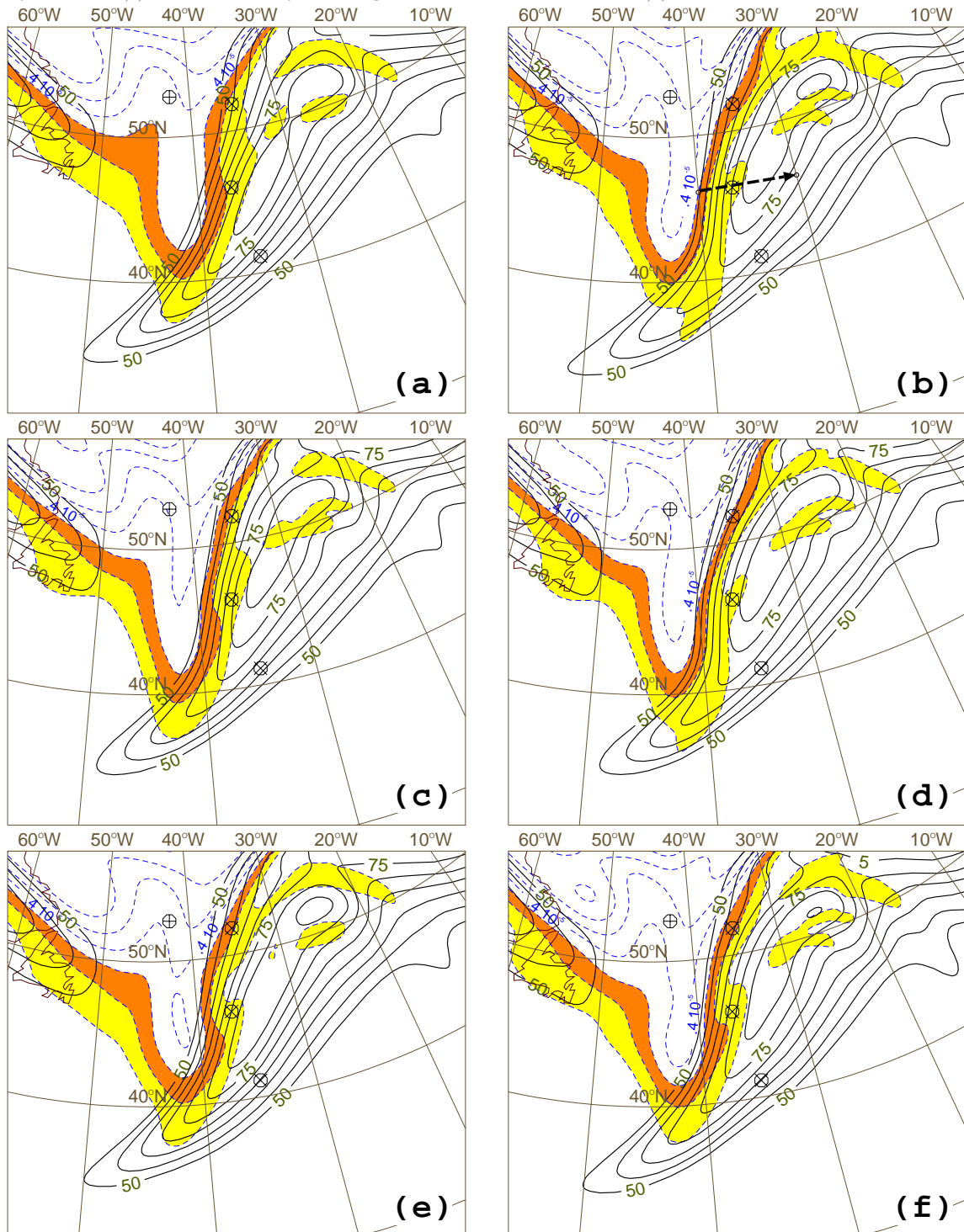
gast and Joly (1998) have also shown in a direct way the triggering features in the initial conditions.

Here, the goal is to exploit fully the available profiles and turn them into a set of reference fields. The present study concentrates on the mature stage of the system and investigate the ability of the FASTEX observing network and of the assimilation scheme to recover some realistic structures of the developed cyclone, and in particular the organization of the humidity field, directly related to the cloud system.

Figure 8.1 indicates the set of soundings performed during IOP 17, by land-based upper-air stations, FASTEX ships, ASAP ships and aircraft having launched drop-sondes. Land-based upper-air stations all around the North-Atlantic basin performed soundings at 06 UTC and 18 UTC and a number of UK, French, and Irish stations also made soundings at 03 UTC, 09 UTC, 15 UTC and 21 UTC, from 00 UTC 19 February until 00 UTC 20 February, during the mature stage of the system. From figure 8.1, it also appears that three of the FASTEX ships, namely the Ægir, Suroit and Victor Bugaev, performed up to 1.5-hourly radio-soundings from 09 UTC 18 February to 12 UTC 19 February. The fourth FASTEX ship, the US research vessel Knorr, was taking part during this period to a parallel experiment in the Labrador Sea.

On 18 February, it appears that the three FASTEX ships were quite well located with respect to the developing low. Two ASAP ships, with WMO station Ids OXTS2 and V2EZ, also performed additional soundings at 06 UTC and 18 UTC during that period, the last ship V2EZ being also located close to the system. At that time, the cyclone has developed a cloud band associated with the cold front and a well formed cloud head above the surface low. The system has also been sampled by a NOAA Gulfstream-IV flight from St-John's to Shannon, between 1541 UTC and 2134 UTC 18 February with 54 launched dropsondes. Around 18 UTC, this aircraft jet passed just above the French Suroit vessel.

Twelve hours later, at 06 UTC 19 February, the low was even deeper and the cloud head was associated with a bent-back warm front and a dry zone entering between this back-bent front and the cold front. At that time, the UKMO C130 aircraft performed a flight, from 0327 UTC to 1109 UTC 19 February with 44 dropsondes, in order to observe the mesoscale structures within this region.

Here, most of the soundings found in the FASTEX Data Base are used. However for some flights, as the NOAA Gulfstream-IV flight, providing dropsondes with a very high horizontal density (up to 20-30 km), a data selection of these dropsondes has been performed, since some preliminary tests with FRONTS 92 dropsondes (Browning et al., 1995) and an incremental 3D-VAR scheme showed that a problem of representativeness error could occur with a too coarse analysis increment (Desroziers et al., 1997).

All the FASTEX vertical profiles are also available in the central archive with a very high vertical resolution. However for the time being, only the TEMP format versions of these profiles have been used, due to the largely coarser vertical resolution of the analysis compared to the high resolution FASTEX soundings. An intermediate way to handle these high resolution profiles would be to compute averaged profiles that could be better compared to their model equivalents in the vertical.

Among the advantages of using 4D-VAR, one of them is to enable the use of the observations at their true dates and times. This is particularly important, since it allows the use of all the vertical profiles performed with a high cadence by the FASTEX ships but also dropsondes given by long duration flights, with launching time departures up to 3 hours.

Figure 8.3: *(a) background field, θ_w at 18 UTC 18 February and at 950 hPa (shaded contours every 1°C and only from 280°K to 284°K) superimposed to the vertical velocity at 600 hPa (contours in thin lines every 2 Pa/s, upward velocity dashed), and to mean sea level pressure (contours every 5 hPa in thick solid lines); (b) 4D-VAR analysis of the same fields as (a), the only observations being the soundings from the FASTEX ships (circles with the symbol × inside) and ASAP ships (circles with the symbol + inside).*
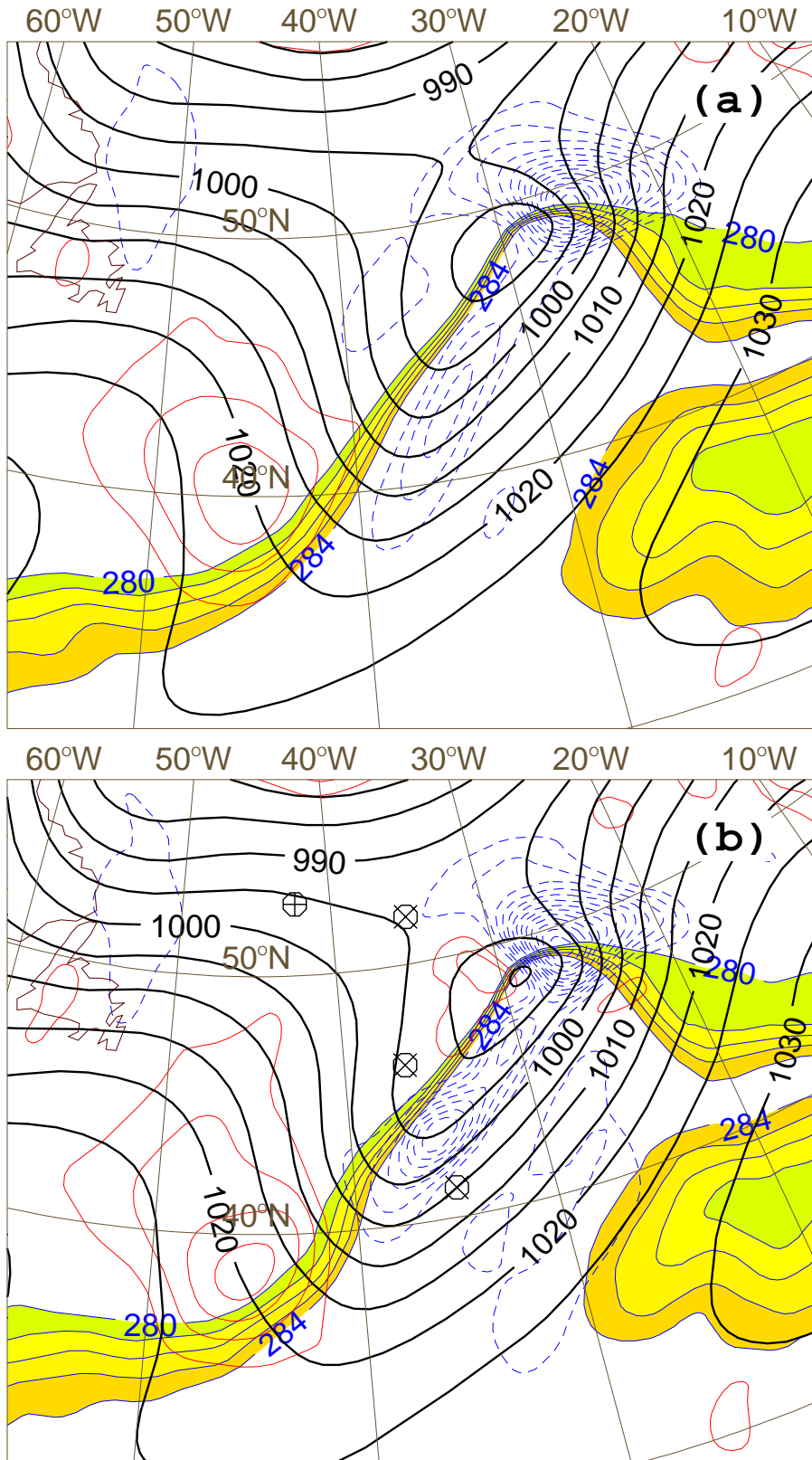
8.3   Analyses at 18 UTC 18 February 1997

In this section, one investigates the impact of the FASTEX data on the final analyses, but also the role of the assimilation scheme used to produce these analyses. In order to document these points, different analyses are presented at 18 UTC 18 February, at the time when FASTEX ships started their intensive soundings (Fig. 8.1) and corresponding also to the mid-flight time of the St John' s–Shannon NOAA Gulfstream-IV flight. All these analyses are performed with the same background (or first guess) field, the one provided by a preliminary incremental 3D-VAR assimilation using the operational observation files as in *Jan 99*.

Figure 8.2.a presents the structure of the jet at 250 hPa, as given by this background at 18 UTC 18 February. At this time, the jet stream had split in two jet streaks (Cammas et al., 1999): the outflow jet (not shown in Fig. 8.2) and another one, which will be referred to as the polar jet, with an entrance region near 40°N - 40°W and a maximum value of about 80 m/s. Three of the FASTEX vessels were then located along the 35°W meridian (from north to south, one founds the Ægir, Suroit and Victor Bugaev vessels) and the German ASAP V2EZ was also located close to the cyclonic side of the jet.

A 4D-VAR analysis using only the soundings associated with these ships has been performed (the soundings from the FASTEX vessel Knorr and the Danish ASAP OXTS2 have also been included, but at that time their positions were far from this area of interest). We can observe that the resulting analysis for the wind velocity (Fig. 8.2.b) is different from the background one: the jet streak structure of this polar jet is reinforced, with the maximum values around 80 m/s pushed north-eastward. Also, this part of the jet now presents a more curved shape on its cyclonic side. The main point to be noted is that this characteristic curved flow appears to better fit the cyclonic curvature of the sharp edge of high altitude clouds found along the jet axis.

A 4D-VAR analysis, still based on the same background, has also been produced but using only the conventional data and excluding the previous FASTEX ship soundings. Figure 8.2.c shows that the increase of cyclonic curvature of the polar jet brought by the FASTEX ships is also suggested when using only these conventional data. Finally, a 4D-VAR analysis with both sets of data gives a representation of the jet very close to the one obtained with only the FASTEX ships (Fig. 8.2.d).

Figure 8.2 also shows the structure of the potential vorticity field on the 310 K isentropic surface. According to what has been observed on the wind field, the analysis using only the FASTEX ship soundings (Fig. 8.2.b) appears to be more different from the background representation (Fig.8.2.a) than the analysis using the conventional observations (Fig. 8.2.c): the amplitude of the potential vorticity anomaly on the south-west part of the polar jet streak is increased; this is consistent with the above-mentioned change of the jet structure in the south-west entrance region (near 41N-41W).

In order to evaluate the impact of the intensive soundings performed by the FASTEX ships during this 6-hour assimilation period, a 3D-VAR analysis has been produced at 18 UTC, using only the FASTEX soundings closest to this synoptic time. The retrieved wind and potential vorticity analyses (Fig. 8.2.e) show far less differences with the background representations than the previous analyses obtained with 4D-VAR and all the profiles available in the 6-hour period. However, a 4D-VAR analysis including only the same subset of FASTEX ship soundings (Fig.8.2.f) appears to be closer to the one obtained with all the profiles: the maximum values of the polar jet streak are moved north-eastward and the characteristic curvature of the jet entrance

Figure 8.4: *(a) vertical and temporal cross-section of the meridional component of the wind (contours every 5 m/s), at the Suroit vessel location (46.1N-36.6W) and between 15 UTC and 21 UTC 18 February; the time has been reversed and the data have been interpolated by a spline algorithm; (b) same as (a) but for the background equivalent; (c) same as (a) and (b) but for the 4D-Var analysis with only the FASTEX ship soundings; (d), (e) and (f) respectively same as (a), (b) and (c) but for relative humidity (contours every 10 % RH).*
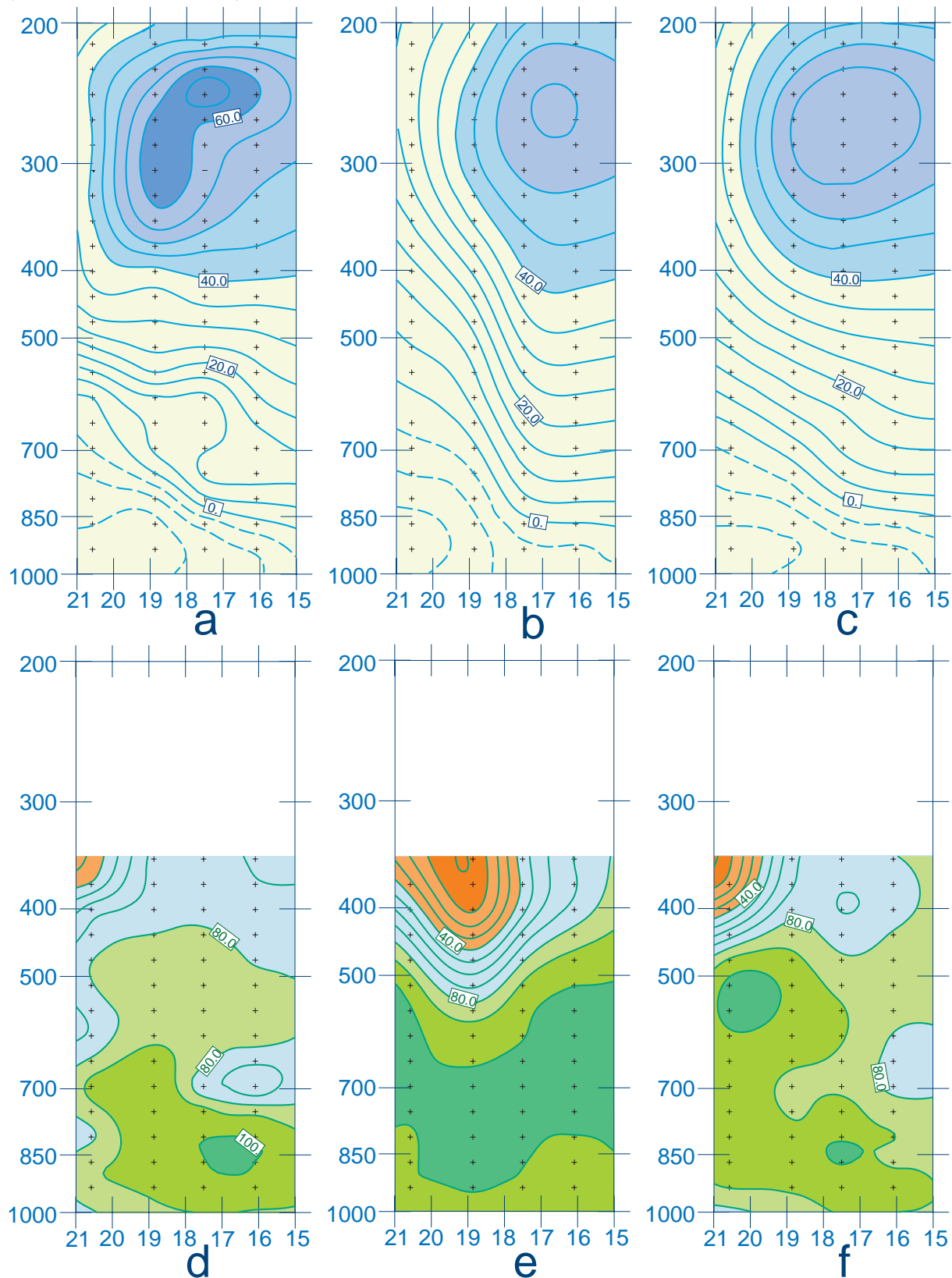
is suggested with a reinforcement of the potential vorticity anomaly. This indicates a clear improvement of 4D-VAR over 3D-VAR for this case, that can be likely related to the use of implicit dynamical structure functions by the 4D-VAR formulation, as isotropic and less realistic structure functions are used in the 3D-VAR formulation (Thépaut et al. 1996).

From a dynamical point of view, the increase of the jet curvature found near 42°N-42°W in the 4D-VAR analyses (Figs.8.2.b and d, particularly) should be associated with a dipole of mid-tropospheric descent and ascent, due to ageostrophic motions along the jet flow, with confluence and diffluence areas, respectively located upstream and downstream of this flow inflection (Keyser and Shapiro 1986). The descending vertical velocities, associated with this secondary circulation, should also reinforce the downward branch of the direct transverse ageostrophic circulation at the entrance of the jet streak axis (43°N-38°W/52°N-22°W).

The differences at low levels between the background field (Fig.8.3.a) and the 4D-VAR analysis using only the FASTEX ship soundings (Fig.8.3.b) seem to be consistent with the above-mentioned dynamical processes. These differences show a displacement and a reinforcement in the analysis of the downward velocities at 600 hPa, south-west of the PV anomaly axis (38N-45W), which is in agreement with the water-vapour image (not shown). The expected increase of upward velocities west of the latter PV anomaly axis is also found. One has to note that these likely dynamical modifications, due to ageostrophic adjustment, are a direct and positive consequence of the use of the temporal dimension in 4D-VAR.

A striking point is also the appearance of a frontal wave, quite clear in the θ_w field at 950 hPa, in the surface trough south-west of the main cyclone. This frontal wave can be observed in the measurements made by the Victor Bugaev vessel (not shown) as mentioned in Cammas *al.* (1999). The surface cyclogenesis associated with the frontal wave might be related to the reinforcement of ageostrophic vertical motions, inducing a coupling between an area of initial strong vorticity at low levels and the circulation associated with the upper PV anomaly shown in Fig. 8.2.b (Hoskins et al. 1985).

The high cadence FASTEX ship soundings performed in a meteorological active region actually makes up an unique dataset. A way to investigate how 4D-VAR handles this dataset is to look at what happens in time at a particular ship location. Figure 8.4.a shows the temporal evolution of the meridional component of the wind above the Suroit location (46.1°N-36.6°W).

The observations associated with the four soundings performed by this ship during the 6-hour assimilation period are analyzed with a spline algorithm (Desroziers and Lafore 1993). In order to filter observation and representativeness errors, a smoothing is applied, the amplitude of this smoothing being determined by an objective cross-validation method (Wahba 1980).

This figure shows that the Suroit vessel was very nicely located during this 6-hour period, since it sampled the jet structure with a characteristic sharp gradient on its cyclonic side. The background equivalent evaluations at the same time and location can also be interpolated by the previous spline algorithm, but with no additional smoothing in this case (Fig. 8.4.b). The resulting cross-section presents large differences: the maximum value of the wind is lower and the cyclonic gradient is also less important, the whole upper wind structure being too early in time in the background; the lower structure is also quite different with a too steep slope in the gradient associated with the system cold front. Figure 8.4.c presents the corresponding vertical
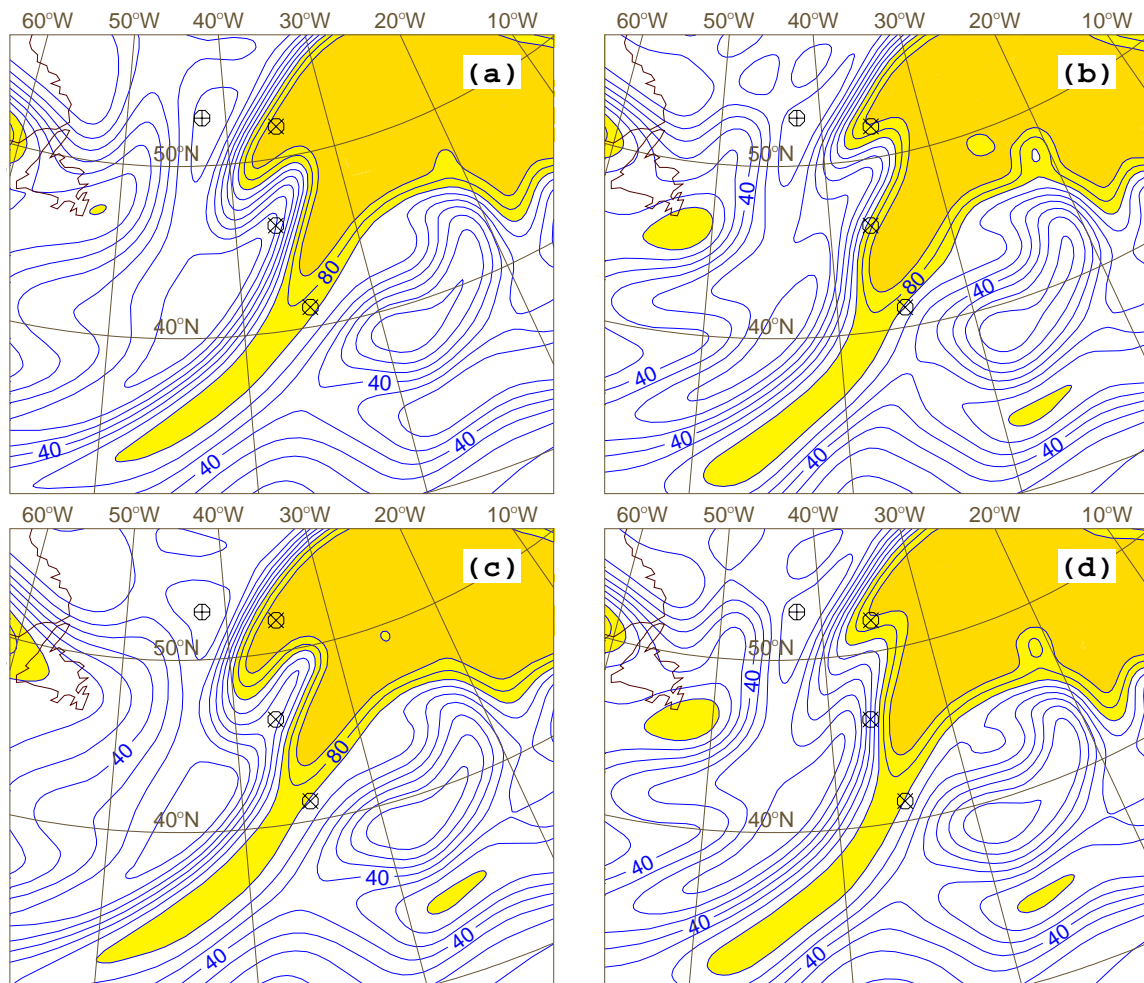
Figure 8.5: *(a) background field, relative humidity at 18 UTC 18 February and at 350 hPa (contours every 10 % RH); (b) 4D-VAR analysis using only the soundings given by the FASTEX ships (circles with the symbol × inside) and the ASAP ships (circles with the symbol + inside); (c) 3D-VAR analysis using only the soundings closest to the analysis time; (d) 4D-VAR analysis using the same restricted set of soundings as (c).*

cross-section for the 4D-VAR analysis with only the FASTEX ship soundings. This representation is much closer to the observed values: the cyclonic upper gradient of the wind is better described and the lower structure is also modified. Of course, the small details found in the observations are not retrieved but one has to keep in mind that this incremental assimilation is performed with an only T 63 tangent linear model.

The same vertical and temporal cross-sections at the Suroit location can be produced for the observation (Fig. 8.4.d), background (Fig. 8.4.e) and analysis (Fig. 8.4.f) representations of relative humidity. According to Cammas et al. (1999), the values less than 70 % RH at 400 hPa and at 21 UTC, found in Fig.8.4.d, are associated with the upper level dry air intrusion on the cyclonic side of the jet stream. The values of humidity less than 70 % RH at 700 hPa and at 16 UTC are related

to the low level part of this dry intrusion. The values more than 80 % RH below 400 hPa correspond with the above-mentioned cloud head structure associated with the system. Figure 8.4.e shows that the humidity background cross-section is quite different from the observed one: one can especially note that accordingly to the wind representation, the upper level dry air intrusion on the cyclonic side of the jet, is too early in time in the background description. This deviation between observation and background is however strikingly corrected in the final analysis (Fig. 8.4.f): the latter upper level dry air intrusion is moved backward in time and the low level dry intrusion is also suggested.

The comparison of the humidity field representations at 350 hPa, given by the different experiments (Figs. 8.5) also shows that, as for the jet description, the differences in these representations are associated with the use of a 3D or 4D-VAR analysis scheme: with the same subset of FASTEX ship soundings synchronous with synoptic time, 4D-VAR produces a description of the humidity (Fig. 8.5.d) that is much more in agreement with the vertical and temporal cross-section shown in Fig. 8.4.d, than the one obtained with 3D-VAR (Fig. 8.5.c). However, the use of the whole set of FASTEX soundings available during the 6-hour assimilation period still brings a refinement of this description (Figs. 8.5.b): the strong gradient zone in the humidity field associated with the clouds is pushed westward of the Suroit location, in agreement with the vertical cross-section found in Fig. 8.4.f. This description of the humidity field also better fits the water-vapour image.

8.4 Analysis at 06 UTC 19 February 1997

Starting from the same 3D-VAR background used to produce the previous assimilation experiments at 18 UTC 18 February, two 4D-VAR analysis cycles have been performed from 18 UTC 18 February to 06 UTC 19 February, using different datasets: a first one has been produced with the data normally available operationally with the addition of the soundings made during that period by the land-based sites around the Atlantic basin plus the profiles provided by the FASTEX and ASAP ships (experiment called A hereafter), and a second one obtained by adding the dropsondes launched by the NOAA Gulfstream-IV and the UKMO C130 during this time to the previous dataset (experiment called B hereafter).

Figures 8.6.c and d present the 4D-VAR analysis at 06 UTC 19 February resulting from the last experiment B, that is to say using all the FASTEX soundings, including the UKMO C130 dropsondes, added to the operational dataset. As mentioned above, these dropsondes were launched during a long duration and system-relative flight which makes difficult the use of the corresponding observations in an intermittent analysis scheme with an unique analysis time such as 3D-VAR: in that sense, the 4D-VAR formulation simplifies the use of such asynchronous data. The background humidity field used for this assimilation depicts the global structure of the cloud head associated with the mature cyclone (Fig. 8.6.a), with homogeneous values everywhere higher than 70 % RH. On the opposite, the retrieved analysis (Fig. 8.6.c) shows a clear tongue of dry air on the 310 K isentropic surface, just west of the UKMO C130 flight. This is in better agreement with the composite water-vapour image at 06 UTC 19 February (not shown), which shows this darker and then dryer area on the west part of the flight. This dry air intrusion, north of the main intrusion associated with the "polar jet" is likely related to the subsidence zone at the entrance of the "outflow jet" (Cammas et al. 1999). Moreover, the analyzed potential vorticity field

Figure 8.6: *(a) background field, relative humidity at 06 UTC 19 February on the 310 K isentropic surface (contours every 10 % RH) in experiment B with all FASTEX observations; (b) same as (a) but for potential vorticity (contours every .5 PV unit and between 1 and 4 PV units); the different legs of the UKMO C130 flight are also indicated and the dashed one corresponds to the cross-sections shown in Fig. 8.7; the dashed line AB indicates the location of the cross-sections presented in Fig. 8.8; (c) and (d) respectively same as (a) and (b), but for the the 4D-Var analysis B with all FASTEX observations; (e) and (f) respectively same as (a) and (b), but for the 4D-Var analysis A with all FASTEX observations but without the dropsonde data.*
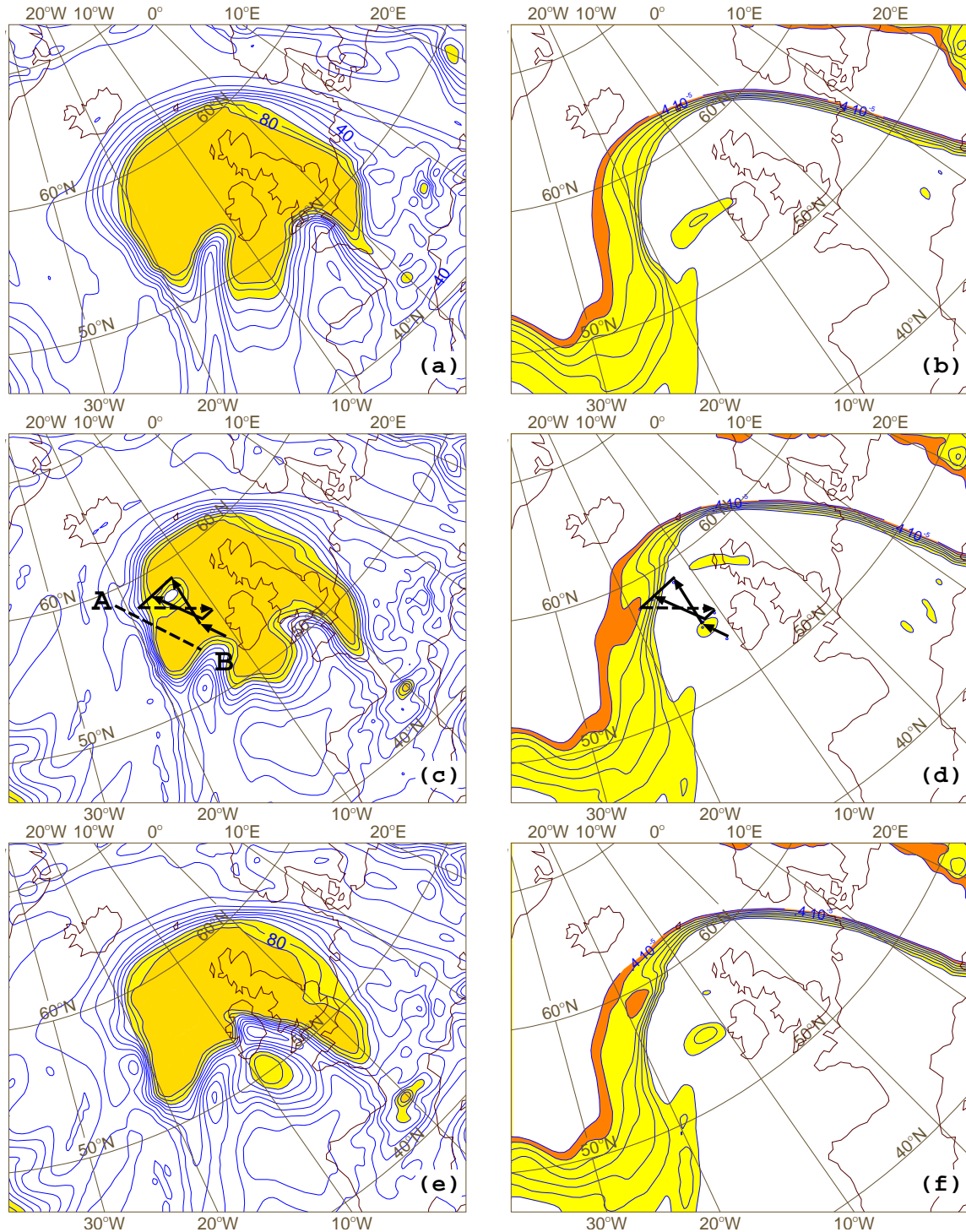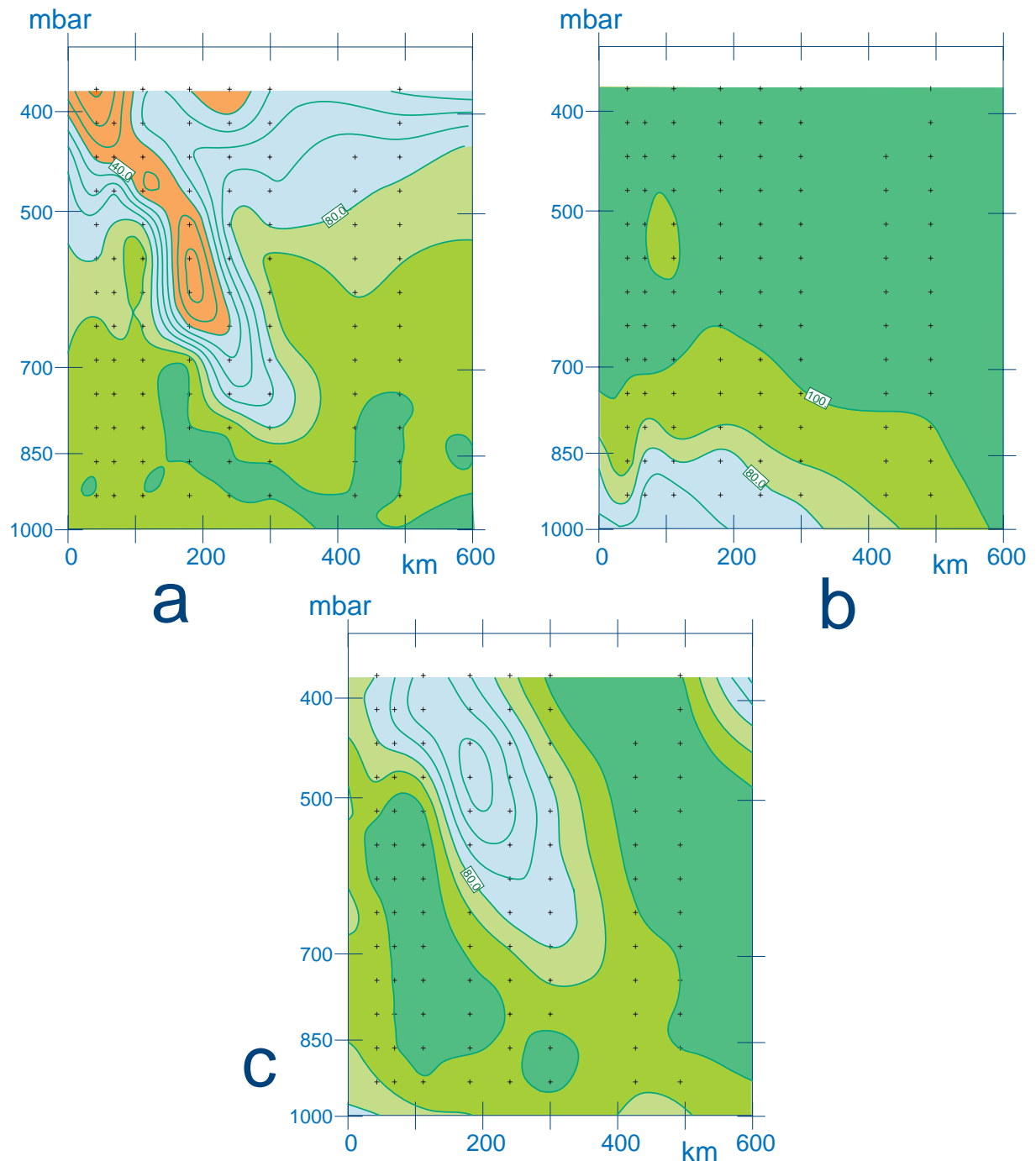
Figure 8.7: (a) vertical cross-section of relative humidity (contours every 10 % RH) along the UKMO C130 leg defined in Fig. 8.6; (b) same as (a) but for the background field; (c) same as (a) and (b) but for the 4D-Var analysis B including all FASTEX observations.

on the 310 K isentropic surface (Fig. 8.6.d) also presents a singularity just west of the dropsonde leg, that suggests a downward and north-eastward dry air intrusion (note that this potential anomaly is also missing in the corresponding background field found in Fig. 8.6.b). On the other hand, Figures 8.6.e and 8.6.f present the corresponding representations of the humidity and potential vorticity fields for the 4D-VAR experiment A, that is to say with no dropsonde data: they do not show the dry air intrusion, which proves that the UKMO C130 dropsondes contain an essential information not found in other observations and that this information is correctly treated by the 4D-VAR scheme.

The comparison of the observation, background and analysis descriptions along one of UKMO C130 leg (see Fig. 8.6.b for its position) confirms the correct use of the dropsonde data by the 4D-VAR analysis . In agreement with the previous horizontal views, the vertical cross-section through the background relative humidity field (Fig. 8.7.b) only presents very high values except in the lower levels. On the opposite, the vertical cross-section through the observations (Fig. 8.7.a) lets appear a narrow and tilted dry air intrusion with values everywhere less than 80 % RH. The retrieved analysis cross-section (Fig. 8.7.c) consistently depicts this dry air intrusion with in particular a good agreement in the slope of this tongue of dry air. However, the scale of this intrusion appears broader in the analysis than in the observations and the mimimum values are also larger, but one has again to keep in mind the coarse resolution of the analysis increment.

The description by the analysis of the dry intrusion structure is confirmed by the vertical cross-section presented in Fig. 8.8.a and located south-westward of the UKMO C130 flight in the dry zone appearing very clearly on the 310 K isentropic surface in Fig. 8.6.c (the position of this cross-section is also indicated in this figure). Figure 8.8.b also shows that this dry air entrance is associated with clear downward vertical velocities in this area. Moreover, these downward vertical velocities are completely absent in the background representation (Fig. 8.8.c), which proves that the whole correction to this background is dynamically consistent.

8.5   Conclusion

We have presented a case study of the use of FASTEX additional soundings in the 4D-VAR analysis formulation, including simplified and regular physical parametrizations described in the first part of this paper. The results are found to be extremely encouraging, since this 4D-VAR analysis scheme appears to handle the FASTEX dataset consistently. The 4D-VAR formulation especially provides a natural and beneficial framework to deal with the high cadence soundings performed by the FASTEX ships: the background used in the variational procedure is modified accordingly to the observations performed by the ships. Even with the same limited dataset of observations synchronous with synoptic time, 4D-VAR provides a better analysis than 3D-VAR.

There is also a clear impact of the FASTEX observations, containing an information that is not present in the operational dataset. This is particularly evident in the case of the system-relative UKMO C130 flight which brings an essential information on fine structures of humidity and therefore of the cloud system associated with the low, but also of dynamical fields such as vertical velocity or potential vorticity.

This application of 4D-VAR to the dense FASTEX network is also considered particularly promising as these first analyses have been obtained with a low resolution

Figure 8.8: *(a) vertical cross-section along the dashed line AB in Fig. 8.6 of relative humidity in the 4D-Var analysis B including all FASTEX observations (contours every 10 % RH); (b) same as (a) but for vertical velocity w (contours every 1 Pa/s); (c) same as (b), that is w, but in the initial background field.*
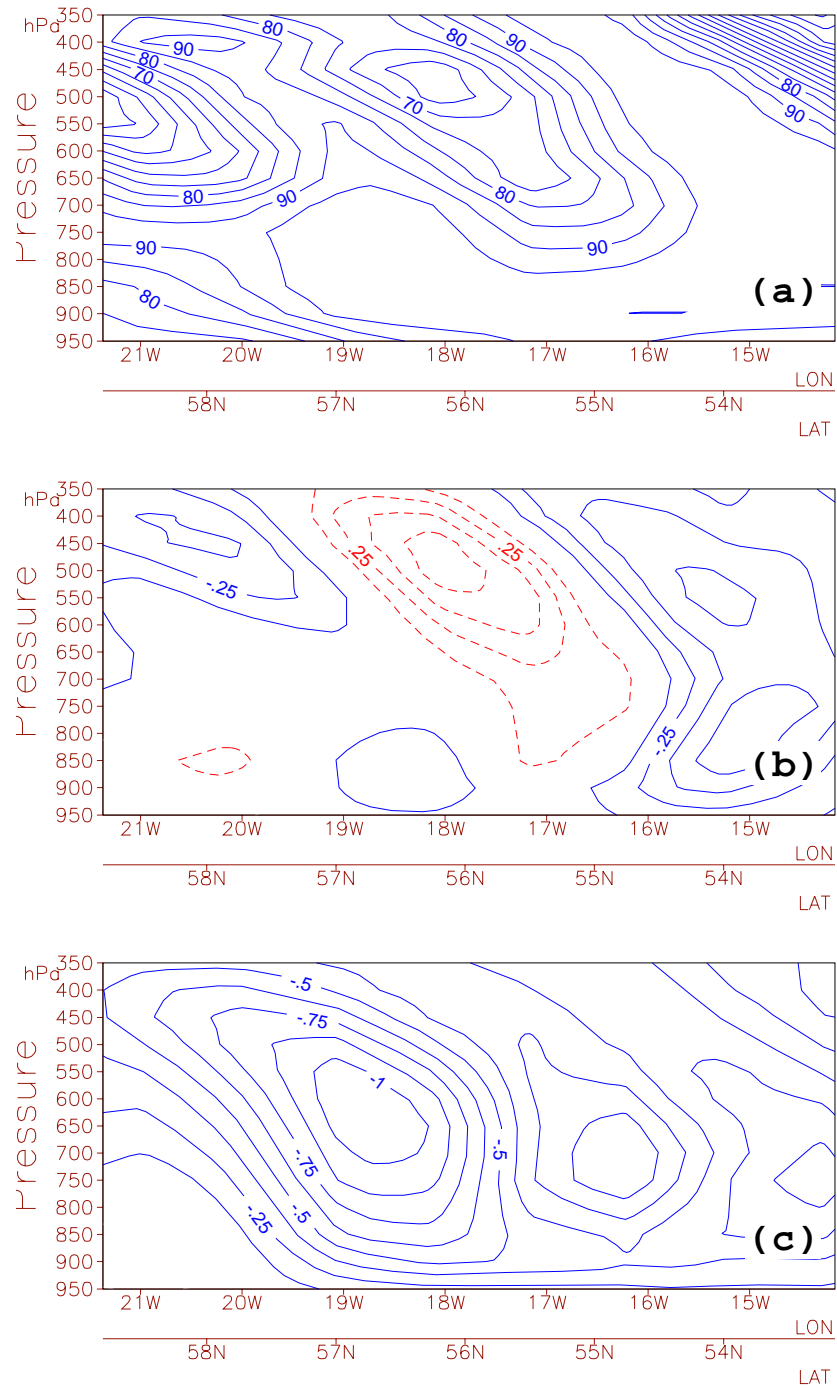
tangent linear model. However, the comparison to the high resolution FASTEX observations show that some sub-structures or strong gradient regions are mis-represented in the analysis. This suggests that there is still a scope to improve this preliminary set of analyses by increasing the resolution of the increments.

Another point of potential improvement is to increase the length of the assimilation period: according to what is known on 4D-VAR, this should still improve the way the increments between observations and background are spread in space and time.

In this part, the different analyses have been validated by looking at the proximity of the final analysis to an unused subset of FASTEX observations. This has been possible in region where these observations were dense, as in vertical cross-sections respectively sampled in time and space by ship soundings and by dropsondes. In Desroziers et al. (1999), the way the analysis came closer to a FASTEX subset of observations deliberately withdrawn from the assimilation, such as a NOAA Gulf-stream-IV flight is also shown. This need of an objective procedure to estimate the quality of an analysis is obvious and crucial in the scope of the re-analysis project of a field experiment such as FASTEX.

Acknowledgements

8.6   References

Arbogast Ph. and A. Joly, 1998:
Precursor identification of a cyclogenesis.
Comptes Rendus de l'Académie des Sciences, **326**, 227–230.

Bergot T., 1999:
Adaptive observations during FASTEX: a systematic survey of upstream flights.
Quart. J. Roy. Meteor. Soc., *submitted*.

Bouttier, F., J. Derber and M. Fisher, 1997:
The 1997 revision of the J_b term in 3D/4D-Var.
ECMWF Tech. Memo., **238,** ECMWF Reading, 54 pp.

K.A. Browning, 1990:
Organization of clouds and precipitation in extratropical cyclones.
In *Extratropical cyclones: the Erik Palmén Memorial Volume*, pages 129–153. C.W. Newton and E.O. Holopainen, eds American Society.

K.A. Browning, S.P. Ballard, and C.S.A. Davitt, 1996:
High resolution analysis of frontal fracture.
Mon. Wea. Rev., **125**, 1212–1230.

K.A. Browning, S.A. Clough, C.S. Davitt, and N.M. Roberts, 1995:
Observations of the mesoscale sub-structure in the cold air of a developing frontal cyclone.
Quart. J. Roy. Meteor. Soc., **121**, 1229–1254.

J.P. Cammas, B. Pouponneau, G. Desroziers, and P. Santurette, 1999:
Initiation, trigerring and development phases of the FASTEX cyclone IOP 17: Synoptic and dynamic overview.
Quart. J. Roy. Meteor. Soc., *submitted*.

P. Courtier and J.-F. Geleyn, 1988:
A global numerical weather model with variable resolution: application to the shallow-water equations.
Mon. Wea. Rev., **114**, 1321–1346.

P. Courtier, C. Freydier, J.-F. Geleyn, F. Rabier, and M. Rochas, 1991:
The Arpege project at Météo-France.

In *Proceedings of the ECMWF Workshop on Numerical methods in atmospheric models*, pages 193–231, Reading.
9-13 September.

Courtier, P., J.-N. Thépaut and A. Hollingsworth, 1994:
A strategy for the operational implementation of 4D-Var, using an incremental approach.
Q. J. R. Meteorol. Soc., **120,** 1367–1387.

G. Desroziers and J. P. Lafore, 1993:
A coordinate transformation for objective frontal analysis.
Mon. Wea. Rev., **121**, 1531–1553.

Desroziers, G., V. Mathiot, F. Orain, and P. Bernardet, 1995:
Estimation locale des covariances d'erreurs de prévision d'un modèle spectral sur la sphère: Application au modèle à résolution variable ARPEGE.
Technical Report 34, CNRM/GMME, available from Météo-France.

G. Desroziers, B. Nechad, W. Sadiki, and J.-N. Thépaut.
Analyse variationnelle du réseau de dropsondes de l'expérience FRONTS 92: application du 3D-Var Arpège et discussion de l'erreur due à la formulation incrémentale de l'analyse à partir d'une maquette 1D-Var sur le cercle.
Technical Report 53, CNRM, 1997.

Desroziers, G., B. Pouponneau, J.N. Thépaut, M. Janisková, and F. Veersé, 1999:
Four dimensional variational analyses of FASTEX situations. part II: use of additional observations.
Quart. J. Roy. Meteor. Soc., **125**, *submitted*.

Gilbert, J.-Ch. and C Lemaréchal, 1989:
Some numerical experiments with variable storage quasi-Newton algorithms.
Mathematical Programming, **B 25,** 407–435.

Hardiker, V., 1997:
A Global Numerical Weather Prediction Model with Variable Resolution.
Mon. Wea. Rev., **125,** 59–73.

B.J. Hoskins, M.E. McIntyre, and A.W. Robertson, 1985.
On the use and significance of isentropic potential vorticity maps.
Quart. J. Roy. Meteor. Soc., **111**, 877–946.

Ide, K., P. Courtier, M. Ghil and A.C. Lorenc, 1997:
Unified Notation for Data Assimilation: Operational, Sequential and Variational.
J. Meteor. Soc. Japan, **75-1B,** 181–189.

Janisková, M., J.-N. Thépaut and J.-F. Geleyn, 1998:
Simplified and regular physical parametrizations for incremental four-dimensional variational assimilation.
Mon. Wea. Rev., *in press*.

M. Janisková, F. Veersé, J.-N. Thépaut, G. Desroziers, and B. Pouponneau, 1999:
Four dimensional variational analyses of FASTEX situations - Part I: Impact of a simplified physical package in the assimilating model.
Quart. J. Roy. Meteor. Soc., *submitted*.

G. Jaubert, C. Piriou, M.L. Scot, A. Petitpa, and J.A. Moore, 1999.
The FASTEX experiment Data Archive.
Quart. J. Roy. Meteor. Soc., *submitted*.

Joly, A., D.Jorgensen, M.A.Shapiro, A.Thorpe, P.Bessemoulin, K.A.Browning, J.P.Cammas, J.P.Chalon, S.A.Clough, K.A.Emanuel, L.Eymard, R.Gall, P.H.Hildebrand, R.H.Langland, Y.Lemaitre, P.Lynch, J.A.Moore, P.O.G.Persson, C.Snyder, R.M.Wakimoto, 1997:
The Fronts and Atlantic Storm-Track Experiment (FASTEX): Scientific Objectives and Experimental Design.
Bull. Amer. Meteor. Soc., **78**, (9), 1917–1940.

Joly, A., K.A. Browning, P. Bessemoulin, J.P. Cammas, G. Caniaux, J.P. Chalon, S.A. Clough, R. Dirks, K.A. Emanuel, L. Eymard, R. Gall, T.D. Hewson, P.H. Hildebrand, D. Jorgensen, F. Lalaurette, R.H. Langland, Y. Lemaitre, P. Mascart, J.A. Moore, P.O.G. Persson, F. Roux, M.A. Shapiro, C. Snyder, Z. Toth, and R.M. Wakimoto, 1999:
Overview of the field phase of the Fronts and Atlantic Storm-Track Experiment (FASTEX) project.
Quart. J. Roy. Meteor. Soc., **125**, *submitted*.

D. Keyser and M.A. Shapiro, 1986:
A review of the structure and dynamics of upper-level frontal zones.
Mon. Wea. Rev., **114**, 452–499.

R. Laprise, 1992:
The resolution of global spectral models.
BAMS, **73**, *(9)*, 1453–1454.

Laroche, S. and P. Gauthier, 1998:
A validation of the incremental variational data assimilation in a two-dimensional turbulent flow.
Tellus, *in press*.

Le Dimet, F.-X. and O Talagrand, 1986:
Variational algorithms for analysis and assimilation of meteorological observations: theoretical

aspects.
Tellus, **38 A,** 97–110.

Lynch, P., D. Giard and V. Ivanovici, 1997:
Improving the Efficiency of a Digital Filtering Scheme for Diabatic Initialization.
Mon. Wea. Rev., **125,** 1976–1982.

M.P. Moine and F. Roux.
Dynamic and thermodynamic structure of the mid-latitude cyclone observed on 19 february 1997 during FASTEX.
In *Proceedings of the Conference on Cloud Physics*, Washington, 1998.
17-21 August.

Naughton, M., P. Courtier and W. Bourke, 1996:
Representation errors in various grid and spectral truncations for a symmetric feature on a sphere.
Q. J. R. Meteorol. Soc., **122,** 253–265.

C. Pires, R. Vautard, and O. Talagrand, 1996:
On extending the limits of variational assimilation in nonlinear chaotic systems.
Tellus, **48A**, 96–121.

F. Schmidt, 1977:
Variable fine mesh in spectral global model.
Beitr. Phys. Atmos., **50**, 211–217.

M.A. Shapiro and J.T. Hastings, 1973:
Objective cross-section analyses by Hermite polynomial interpolation on isentropic surfaces.
J. Appl. Meteor., **12**, 753–762.

Simmons, A. and D. Burridge, 1981:
An energy and angular momentum conserving vertical finite difference scheme and hybrid vertical coordinates.
Mon. Wea. Rev., **109,** 758–766.

J.-N. Thépaut, P. Alary, P. Caille, V. Cassé, J.-F. Geleyn, P. Moll, J. Pailleux, J.-M. Piriou, D. Puech , and F. Taillefer.
The operational global data assimilation system at météo-france.
In *Proceedings of HIRLAM 4 Workshop on Variational Analysis in Limited Area Models*, pages 25–31, Toulouse, 1998.

J.-N. Thépaut, P. Courtier, G. Belaud, and G. Lemaître, 1996:
Dynamical structure functions in a four-dimensional variational assimilation: A case study.
Quart. J. Roy. Meteor. Soc., **122**, 535–561.

A.J. Thorpe and S.A. Clough, 1991:
Mesoscale dynamics of cold fronts: structures described by dropsoundings in FRONTS 87.
Quart. J. Roy. Meteor. Soc., **117**, 903–941.

Veersé, F. and J.-N. Thépaut, 1998:
Multiple-truncation incremental approach for four-dimensional variational data assimilation.
Q. J. R. Meteorol. Soc., **124,** 1889–1908.

G. Wahba, D.R. Johnson, F. Gao, and J. Gong, 1995:
Adaptative tuning of numerical weather prediction models: randomized GCV in three- and four-dimensional data assimilation.
Mon. Wea. Rev., **123**, 3358–3369.

G. Wahba and J. Wendelberger, 1980:
Some new mathematical methods for variational objective analysis using splines and cross validation.
Mon. Wea. Rev., **108**, 1122–1143.

Part 9

Publications

9.1 Project documents

• Joly A. and F. Lalaurette, 1991:
Une proposition pour une expérience FRONTS 9x.
Centre National de Recherches Météorologiques, FASTEX Project Office, Tech. Report, 42pp.

• Joly, A. and A.J. Thorpe, 1995.
The Fronts and Atlantic Storm-Track Experiment (FASTEX), proposal to the Environment and Climate Programme. April 1996.

• Joly , A., Y. Lemaître, S. Clough, K. Commins, F.H. Sigurdsson, 1997.
The Fronts and Atlantic Storm-Track Experiment (FASTEX), first interim report. *European Commission*, ENV4-CT96-032, 61pp.

• Jorgensen D. and A. Joly, 1995:
FASTEX field programme, Operations overview.
Centre National de Recherches Météorologiques, FASTEX Project Office, Tech. Report, 55pp.

• Jorgensen D., P. Bessemoulin, S. Clough and J.A. Moore, 1996a:
FASTEX Operations Plan.
Centre National de Recherches Météorologiques, FASTEX Project Office, Tech. Report, 164pp.

• Thorpe A.J. and M.A. Shapiro, 1995:
FASTEX, Fronts and Atlantic Storm Tracks Experiment. The Science Plan.
Centre National de Recherches Météorologiques, FASTEX Project Office, Tech. Report, 25pp.

9.2 Articles published in refereed journals

• Arbogast, P., 1998:
Sensitivity to potential vorticity.
Quart. J. Roy. Meteor. Soc., **124**, 1605–1615.

• Arbogast, P. and A. Joly, 1998:
Potential vorticity inversion of a two-dimensional steady flow: application to symmetric instability.
Quart. J. Roy. Meteor. Soc., **124**, 317–339.

• Arbogast, Ph. and A. Joly, 1998:
Identification des précurseurs d'une cyclogenèse.
Compte-Rendus à l'Académie des Sciences, Sciences de la Terre et des planètes, **326**, 227–230.

• Bergot, T., G. Hello, A. Joly, and S. Malardel, 1999:
Adaptive observations: a feasability study.
Mon. Wea. Rev., **127**, (5), 743–765.

• Fischer, C., A. Joly, and F. Lalaurette, 1998:
Error growth and kalman filtering within an idealized baroclinic flow.
Tellus, **50A**, (5), 596–615.

• Horanyi A. et A. Joly, 1996. Some aspects of the sensitivity of idealized frontal waves. *Beitr. Phys. Atmos.*, **69**, (4), 517–533.

•Joly, A., D. Jorgensen, M.A. Shapiro, A.J. Thorpe, P. Bessemoulin, K.A. Browning, J.P. Cammas, J.P. Chalon, S.A. Clough, K.A. Emanuel, L. Eymard, R. Gall, P.H. Hildebrand, R.H. Langland, Y. Lemaitre, P. Lynch, J.A. Moore, P.O.G. Persson, C. Snyder, R.M. Wakimoto, 1997: The Fronts and Atlantic Storm-Track Experiment (FASTEX): Scientific Objectives and Experimental Design. *Bull. Amer. Soc.*, **78**, (9), 1917–1940.

•Lebouar, E, M Petitdidier, and Y. Lemaître, 1998.
Retrieval of ageostrophic wind from a radiosounding network and a single ST radar *Quart. J. Roy. Met. Soc.*, **124**, *in press.*

•Malardel S., A.J. Thorpe et A. Joly, 1996.
Consequence of the Geostrophic Momentum Approximation on barotropic instability. *J. Atmos. Sci.,* **54**, (1), 104–112.

•Pouponneau, B., F. Ayrault, T. Bergot, and A. Joly, 1999:
The impact of aircraft data on an atlantic cyclone analysed in terms of sensitivities and trajectories.
Weather and Forecasting, **14**, (1), 67–83.

•Rivals, H., J.P. Cammas, and I.A. Renfrew, 1998:
Secondary cyclogenesis: the initiation of a frontal wave observed over the eastern atlantic.
Quart. J. Roy. Meteor. Soc., **124**, 243–267.

•Olafsson, H., 1998:
Different predictions by two NWP models of the surface pressure field northeast of iceland.
Meteorological Applications, **5**, 253–261.

•Snyder, C. and A. Joly, 1998:
Development of perturbations within growing baroclinic waves.
Quart. J. Roy. Meteor. Soc., **124**, 1961–1983.

9.3   Recently submitted articles

•Baehr, Ch., B. Pouponneau, F. Ayrault, and A. Joly, 1999:
Dynamical characterization and summary of the FASTEX cyclogenesis cases.
Quart. J. Roy. Meteor. Soc., **125**, *submitted.*

•Bergot, T., 1999:
Adaptive observations during FASTEX: a systematic survey of the impact of upstream flights.
Quart. J. Roy. Meteor. Soc., **125**, *submitted.*

•Bouniol, D., A. Protat, and Y. Lemaître, 1999:
Mesoscale dynamics of a deepening secondary cyclone (FASTEX IOP 16): three-dimensional structure retrieved from dropsonde data.
Quart. J. Roy. Meteor. Soc., **125**, *submitted.*

•Browning, K.A. and N.M. Roberts, 1999:
Mesoscale analysis of arc rainbands in a dry slot.
Quart. J. Roy. Meteor. Soc., **125**, *submitted.*

•Cammas, J.P., B. Pouponneau, G. Desroziers, P. Santurette, A. Joly, Ph. Arbogast, I. Mallet, G. Caniaux, P. Mascart, and M. Shapiro, 1999:

Initiation, triggering and development phases of the FASTEX cyclone (IOP 17): synoptic and dynamic overview.
Quart. J. Roy. Meteor. Soc., **125**, *submitted.*

•Chaboureau, J.P. and A.J. Thorpe, 1999:
Frontogenesis and the development of secondary wave cyclones in FASTEX.
Quart. J. Roy. Meteor. Soc., **125**, *accepted.*

•Chaigne, E. and Ph. Arbogast, 1999:
PV inversion: a multi FASTEX case perspective.
Quart. J. Roy. Meteor. Soc., **125**, *submitted.*

•Clough, S.A., H.W. Lean, N.M. Roberts, and R.M. Forbes, 1999:
Observations and model simulations of the FASTEX IOP 16 frontal wave – effects of sublimation.
Quart. J. Roy. Meteor. Soc., **125**, *submitted.*

•Desroziers, G., B. Pouponneau, J.N. Thépaut, M. Janisková, and F. Veersé, 1999:
Four dimensional variational analyses of FASTEX situations. part II: use of additional observations.
Quart. J. Roy. Meteor. Soc., **125**, *submitted.*

•Eymard, L., G. Caniaux, H. Dupuis, L. Prieur, H. Giordani, R. Troadec, and D. Bourras, 1999:
Surface fluxes in the North-Atlantic Current during the CATCH/FASTEX experiment.
Quart. J. Roy. Meteor. Soc., **125**, *submitted.*

•Janisková, M., F. Veersé, J.N. Thépaut, G. Desroziers, and B. Pouponneau, 1999:
Four dimensional variational analyses of FASTEX situations. part I: impact of a simplified physical package in the assimilating model.
Quart. J. Roy. Meteor. Soc., **125**, *submitted.*

•Jaubert, G., C. Piriou, S.M. Loehrer, A. Petitpa, and J.A. Moore, 1999:
The FASTEX experiment data archive.
Quart. J. Roy. Meteor. Soc., **125**, *submitted.*

•Joly, A., K.A. Browning, P. Bessemoulin, J.P. Cammas, G. Caniaux, J.P. Chalon, S.A. Clough, R. Dirks, K.A. Emanuel, L. Eymard, R. Gall, T.D. Hewson, P.H. Hildebrand, D. Jorgensen, F. Lalaurette, R.H. Langland, Y. Lemaitre, P. Mascart, J.A. Moore, P.O.G. Persson, F. Roux, M.A. Shapiro, C. Snyder, Z. Toth, and R.M. Wakimoto, 1999:
Overview of the field phase of the Fronts and Atlantic Storm-Track Experiment (FASTEX) project.
Quart. J. Roy. Meteor. Soc., **125**, *submitted.*

•Lemaître, Y., and A. Protat, 1998 :
Dynamics of a "bomb-like" deepening secondary cyclone from airborne Doppler radar.
Quart. J. Roy. Meteor. Soc., *under revision.*

•Lemaître, Y., A. Protat and D. Bouniol, 1999:
Pacific and Atlantic "bomb-like" deepenings in mature phase: a comparative study. *Quart. J. Roy. Meteor. Soc.*, **125**, *submitted.*

•Malardel, S. and Ph. Arbogast, 1999:
Upstream and downstream development induced by vorticity anomalies: detection in FASTEX IOPs.
Quart. J. Roy. Meteor. Soc., **125**, *submitted.*

•Mallet, I., Ph. Arbogast, Ch. Baehr, J.P. Cammas, and P. Mascart, 1999:
Effects of a low level precursor and frontal stability on cyclogenesis during FASTEX IOP17.
Quart. J. Roy. Meteor. Soc., **125**, *submitted.*

•Mallet, I., J.P. Cammas, P. Mascart, and P. Bechtold, 1999:
Effects of cloud diabatic heating on the FASTEX cyclone (IOP 17) early development.
Quart. J. Roy. Meteor. Soc., **125**, *submitted.*

•Montani, A., A.J. Thorpe, R. Buizza, and P. Unden, 1999:
Forecast skill of the ECMWF model using targeted observations during FASTEX.
Quart. J. Roy. Meteor. Soc., **125**, *submitted.*

•Santurette, P., F. Lalaurette, Y. Bachimont, and G. Hello, 1999:
A review of forecast during fastex: an overview and some météo-france highlight.
Quart. J. Roy. Meteor. Soc., **125**, *submitted.*

•Scialom, G., A. Protat, and Y. Lemaître, 1999:
Vertical structure of a FASTEX secondary cyclone derived from dual-beam airborne radar data.
Quart. J. Roy. Meteor. Soc., **125**, *submitted.*

9.4   Other publications

•Amstrup, B. and X.-Y. Huang, 1998:
Impact of the additional FASTEX radiosonde observations on the HIRLAM data assimilation and forecasting system.
Technical Report 38, HIRLAM Technical Reports, Dublin, Ireland.

•Arbogast Ph., 1998.
L'inversion du tourbillon potentiel: méthodologie, application à l'étude des interactions non-linéaires dans la formation des dépressions météorologiques.
Thèse de l'Université Paul Sabatier, soutenue le 11 décembre 1998, 227pp.

•Ayrault, F., 1998:
Environnement, structure et évolution des dépressions météorologiques: réalité climatologique et modèles types.
PhD thesis, Doctorat de Université P. Sabatier, Toulouse.
328pp.

•Chaigne, E., 1998:
Application de l'inversion du tourbillon potentiel.
Master's thesis, Ecole Nationale de la Météorologie, Note de Travail n 618, Toulouse, 86pp.

•Clough, S.A., H.W. Lean, N.M. Roberts, H. Birkett, J.P. Chaboureau, R. Dixon, M. Griffiths, T.D. Hewson, and A. Montani, 1998:
A JCMM overview of FASTEX IOPS.
Technical Report 81, Joint Centre for Mesoscale Meteorology, Reading, UK.

•Fourrié, N., 1997:
Analyse dynamique de cyclogenèses sur l'Atlantique Nord au moyen d'observations satellitaires TOVS dans le cadre de la campagne FASTEX.
Master's thesis, D.E.A. Université P. et M. Curie, Méthodes Physiques en Télédétection, Paris VI.

•Joly , A., Y. Lemaître, S. Clough, K. Commins, P. Lynch, F.H. Sigurdsson, J.P. Cammas,1998.
The Fronts and Atlantic Storm-Track Experiment (FASTEX).
Proceedings, *European Climate Science Conference*, Vienna, 19–23 Oct. 1998, 12pp.

•Lebouar E., 1997:
Etude des circulations agéostrophiques entre la basse et la haute troposphère. Leur role dans la formation des ondulations frontales observées pendant l'expérience FRONTS'87.
Doctorat de l'Université Paris VI, Paris, 4 décembre 1997.

FASTEX (continued): the FASTEX Cloud System Study

by
Alain Joly[*],
Alan J. Thorpe[**],

[*]*Météo-France, URA CNRS 1357, Groupe d'Etude de l'Atmosphère Météorologique, Toulouse, France,*
[**]*Department of Meteorology, University of Reading, Reading, United Kingdom.*

10.1   General conclusion

ASTEX is a research programme focused on one weather phenomena, mid-latitude cyclogenesis, but addressing several of their aspects. This programme has begun by gathering new data on cyclones, both climatologically and from special direct observations. The major deliverables of the first part of the FASTEX programme presented in this Report were:

- to achieve a two-month Atlanticwise field experiment involving many facilities including dedicated ships and aircraft spread from one side of the ocean to the other,

- to coordinate the actions from these platforms in such a way that the *same* weather systems were observed at several stages of their life-cycle,

- to collect and organize the data obtained during the field experiment into a Data Base with a wide access,

- to include in this Data Base series of objective analyses making use of the special data obtained during the field experiment.

The field phase has taken place in January and February 1997. Its logistically extremely ambitious objectives have been successfully reached: about 10 cyclones have been tracked at various stages of their life-cycle and about the same number of fully developed cloud systems have been sampled by a combination of in-situ and Doppler radar observations. Partial coverage of nearly as many cases has also been performed.

Extremely interesting data for other objectives has been gathered, such as the surface fluxes observed in extreme conditions of wind and sea state (Eymard et al., 1999: see Short Note 2.2 in Part 2).

The data base has been opened to the *whole* of the scientific community via INTERNET a few weeks after the end of the field operations and is close to be completed. A CD-ROM dissemination is planned to take place within the next few months.

This Data Base is, by far, the most important legacy of the project. It is a truly unique source of information on cyclogenesis. It hosts more than 400 h of research aircraft in-situ data, hundred thousands of surface ship and commercial aircraft messages, 90 000 globallly analyzed fields. Its most important asset are its 10 300 high resolution sounding profiles, including 1 600 from ships and 1 300 from dropsondes, many of them in usually barely observed areas, spread all along the storm-track: this alone puts this Data Base at the level of the most ambitious weather observing projects to date, such as TOGA-COARE. But that is not all. This exceptional source of in-situ data is complemented by 25 000 images and 4 000 processed satellite products as well as a growing number of wind profiles within the clouds obtained from the airborne Doppler radar (following the technique shown in Part 5).

Scientists from several fields and from anywhere working on or interested by the problem of mid-latitude weather systems are strongly encouraged to use this Data Base.

The groups involved in FASTEX have issued reports and submitted a series of article containing their first results (see Part 9). These results have been discussed at the FASTEX workshop in Toulouse, at the end of April 1998. It is planned to publish them in a special issue of the *Quarterly Journal of the Royal Meteorological Society* during the autumn 1999.

10.2   Some results from FASTEX

It is possible to mention briefly here results that directly relate to the initial scientific objectives, some of them being illustrated by this report.

It is worth to recall that a completely new standard of description of cyclones has been reached. The arrays of sondes can be exploited on their own and they reveal the structure of precursor structures within their environment (examples are shown in Part 2), but they can also be incorporated into coherent four-dimensional datasets (as in Part 8). Both detailed and broad features of the cyclone cloud system can be displayed in terms of 3D-wind field and precipitating areas (reflectivity) from within

Figure 10.1: *Example of systematic study of the dynamical properties of the FASTEX cases. The cases have been set into a common frame of reference using automatic tracking within the analyses. They have then been separated between perturbation and environment using a time-filter. The graphic shows a number of properties of the environment at the time of the first detection of each case. The mainframe highlight the influence of baroclinicity and deformation, but the presence of pre-existing structures, such as bands of potential vorticity P has also been examined. While the presence of such a structure does not seem to discriminate these cases (implying that the related instability is a possible but not dominant mechanism), the views put forward by Bishop and Thorpe (1994) on the role of deformation seems to have an influence. From Baehr et al. (1999).*
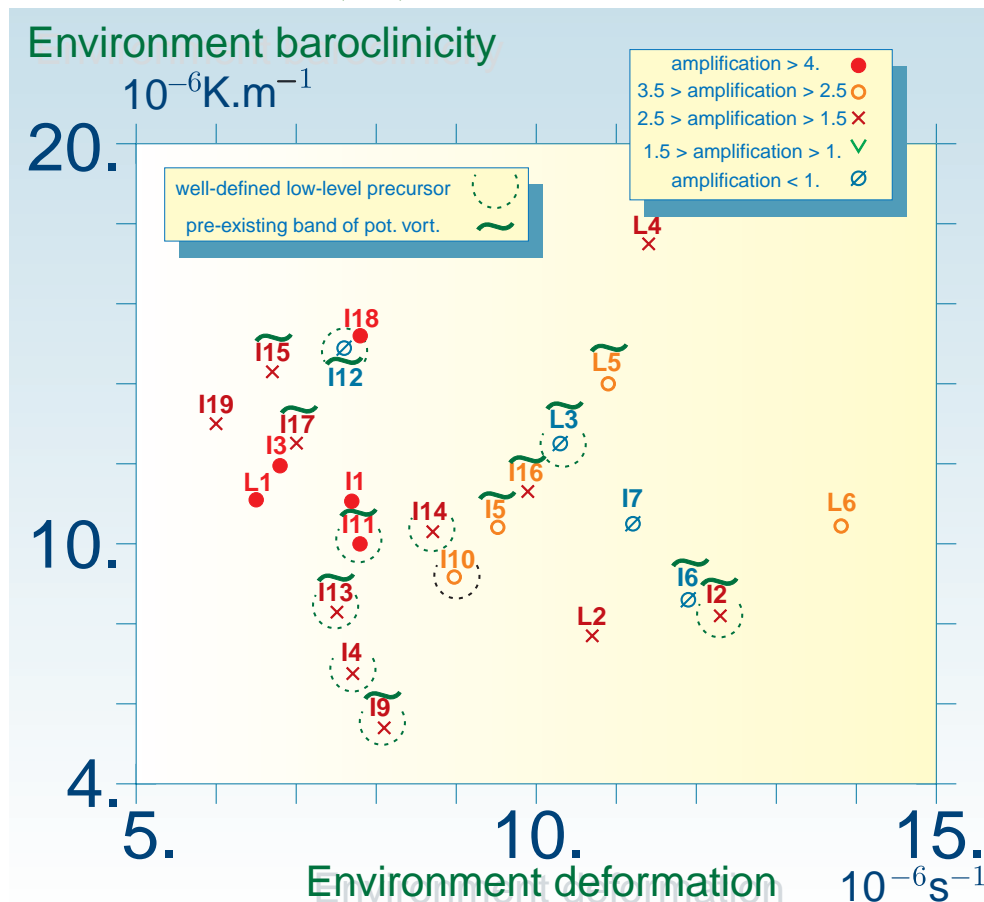
by the airborne Doppler radars (Part 6) and from above using satellite data (DMSP for example: its data is included in the Data Base, see Part 4). Although it is going to take some time to exploit it, this is a radical change with respect to the previous situation, where only few legs were describing — in very great details, it is true — a very small portion of the system.

The vertical distribution of precipitations within a very active cyclone has been observed by the Doppler radars (Part 5) and reveals significant horizontal variability. The transition from snow or ice particles to rain can be quite sudden and, a few hundred kilometers from there, become smooth and extending over a deep layer. Profiles of terminal fall velocity also bear the signs of the presence of large, rapidly falling ice crystals at about 3 km height, while generally small crystals are present.

One of the most interesting results can be inferred from the distribution of saturation given by the dropsondes deployed by the UK Met Office group (Part 7). These distributions are extremelly interesting because they give access to the scale of the cloud system as a whole and are precise enough to deduce information on the droplets. The simplest growth mechanism of ice crystals, sublimation, appears to dominate in these clouds, close to saturation with respect to ice. However, the sondes enable to spot areas of saturation with respect to water at extremely cold temperature, meaning at high level. This indicates the presence of powerful ascent zones. Such areas are not exceptional and the next step is obviously to study their geographical distribution. The presence of water in upper-bands of the cloud system is a challenging modelling problem if it turns out to influence the average budget.

Consider now the other obectives:

- the air-sea measurements of Eymard *et al.* (1999) reveal that the current generation of parameterizations of turbulence underestimate the fluxes in the presence of strong winds; as a result, the wind velocity is overestimated by models as it was indeed apparent in the forecasts used during the operations. Few of the expected areas of wind larger than 30 m.s^{-1} actually showed up. Given that most of the Earth surface is actually a sea surface, it is clear that these measurements, obtained in difficult conditions, exploring a new part of parameter space will have an important impact in future generations of climate and coupled models.

- the first assessments of the impact of adaptive observations are becoming available; on average, the impact is currently modest, but generally positive. It is of the order of magnitude of a major change in a numerical weather prediction system. This result has been obtained by several groups (Météo-France, ECMWF, NRL and NCEP, the last two in the USA: these results will all be in the special issue of the *Quarterly Journal*). However, that is not the goal. The goal is to significantly improve the practical predictability on specific events, not on average. Bergot (1999) shows that the adaptive observations are efficient when the quality when the quality of the initial guess field is bad and threatens the subsequent forecast. The theoretical result of Fischer et al. (1998) also demonstrates that the choice of assimilating system is critical to the impact of the observations.

- FASTEX has been a good opportunity to revisit our knowledge of the basic properties of cyclones. Using the recent re-analysis from ECMWF, Ayrault (1998) has constructed a new set of cyclone paradigms that are enterely quantitative. Their structure is described by fields and their frequency and spatial distribution is also known. This work shows that the transformation of a weak wave into a major storm is a single-mechanism process which is statistically independent of

the initial formation of the wave. The genesis of a new wave can, on the other hand, involve several different mechanisms. Some of them have not been studied so far (see Short Note 1.5 for a summary). Baehr et al. (1999) have checked that these "new" types are present in the FASTEX sample, so that they can be studied both theoretically and with observations.

- Chaboureau and Thorpe (1999) verify, in a number of FASTEX cases, that the early stages of the formation of a cyclone are controlled by the larger scale properties such as the deformation. This is a complex time-dependent stability problem that has been studied theoretically only recently (Bishop and Thorpe, 1994) but is clearly very important. This is confirmed in the more systematic but less detailed study of Baehr et al. (1999) (Fig. 10.1).

- Arbogast and Joly (1998), Arbogast (1998) and Mallet et al. (1999) have also clearly and directly established the essential role of cyclone precursors. They truly determine the existence of many a storm, and they do that in ways that can be much more complex than anticipated by Sutcliffe (1947) and Petterssen and Smebye (1971) on poorly documented case studies. The full scale observation system set up for FASTEX that never left cyclones out of areas of increased observations combined to new analysis tools such as the inversion of potential vorticity has allowed, for the first time, the actual and unambiguous, step by step breakdown description of the generation of a new north-Atlantic cyclone (see Short Note 2.3 for an example). In the case of Low 41 (see section 3.21), for example, a low-level to low-level interaction at a distance has been revealed by using several inversion-like techniques.

Apart from a number of historical papers mentioned also in Part 1, the articles cited here are listed in the project bibliography (Part 9).

Very few studies have been undertaken, so far, that attempts to exploit the full FASTEX sample of cases. the detailed studies, on the other hand, have addressed a few of the cases. Many more results can still be expected.

10.3   About other benefits

This short section attempts to bring out the benefits of the FASTEX project beyond the normal contributions to the progress of science, such as the publications listed in Part 9, or the ability of the project to provide its deliverables.

Consider first the small world of atmospheric scientists. FASTEX has been successfully designed and implemented by a small group of European scientists. It benefited, of course, from the scientific and technical input from our more experienced colleagues from the other side of the Atlantic, as well as from the most remarkable professionalism of their aircraft and instrument teams. Indeed, FASTEX would not have been possible without their strong support. Yet, it remains that the initiative came from Europeans, that the project was attractive enough for our american and canadian colleagues to find an interest in it and that, roughly speaking, things turned out to keep very close to the very first plans. The backbone of the coordination structure required for the project in Shannon, most notably the weather forecast and a number of data communication lines has been organised, set-up and run successfully by European groups. Most large scale experimental projects are initiated by the american community, so that the situation created by FASTEX is exceptional enough to be noted.
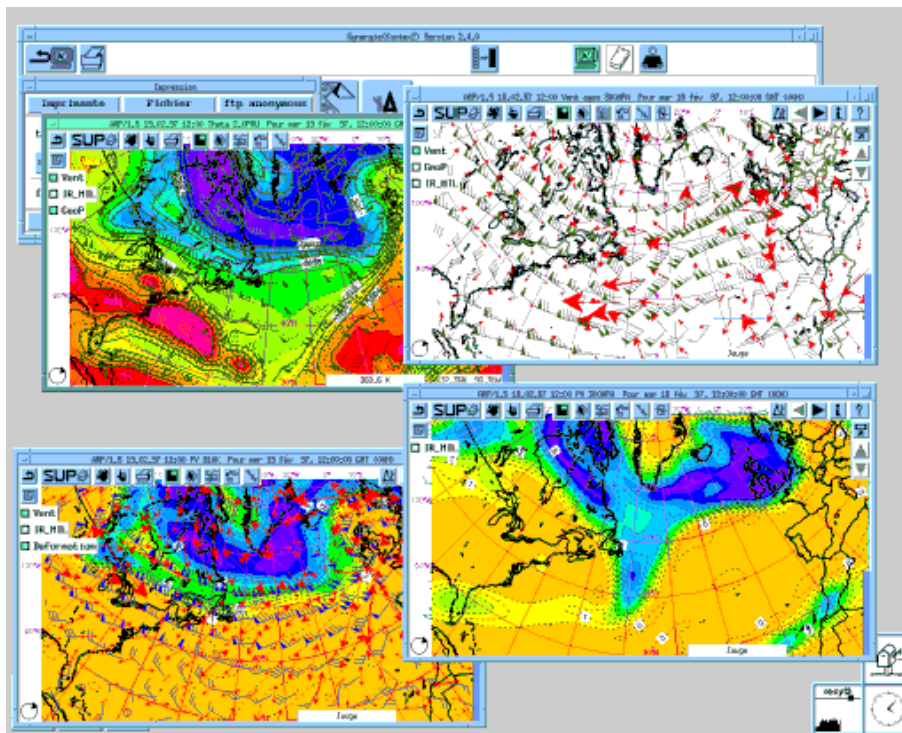
Figure 10.2: *Running FASTEX implied that forecasters and scientists speak the same language and discuss the weather in a similar framework. It has been chosen, at Météo-France, to modify the operational weather display system SYNERGIE rather than use a research display terminal, so that this common framework is now employed operationally. The figure shows a SYNERGIE session with some of the products that are now employed daily but were typical of the research world in 1994: the thermal and height distribution on the $P = 2$ PVU potential vorticity surface (the dynamical tropopause) (top left), direct display of the ageostrophic velocity (top right) contributed by the Laboratoire d'Aérologie (a University laboratory), the deformation field (bottom left), both of them enabling a much better analysis of the wind field and potential vorticity P on pressure p or isentropic θ surfaces.*

It is also worth noting that, in terms of know-how, european scientists have shown, during the FASTEX operations, that they were able to run in a proper way such large facilities as the several ships in mid-ocean and the jet as well as the turboprop aircraft. One can then but note that the next natural step, here, would be for the european community as a whole to coordinate the renewal of its observing platforms in such a way that FASTEX-like programmes can be mastered in Europe from A to Z: compared to FASTEX, this requires more independence in the access to, typically, long range aircraft.

As shown clearly by Parts 5 and 6, the french group from the Centre d'étude des Environnements Terrestre et Planétaires fully masters the airborne Doppler radar technology, from both the side of the instrument (the dual beam antennas of both the P3 and the Electra have been developed by this group) and its data processing.

Beyond the running of the ships and aircraft, the most expensive component of FASTEX has to do with the many radiosondes and dropsondes needed. Most of them by far successfully used the recent GPS technology, and most of them have

been produced by the European company VAISALA and its american subsidiary of the same name. One of the dropsonde type employed has been developed by NCAR in the USA, but the other one is the result of close cooperation between the UK Met Office and VAISALA all along the planning phase of FASTEX. The last tests and adjusments took place during the first flights of the Met Office C-130 under maximum pressure but finally gave access to new standards, as shown in Part 7 of the Report.

Beyond the small world of atmospheric scientists, there is the slightly larger world of operational weather forecast, the products of which have an obvious impact on the public at large.

In this area, there are one or things worth mentioning. The forecast component of the Shannon Operations Centre required, by design, many people from the different groups (from Canada, France, Ireland and the United Kingdom). In most groups, some kind of rotation of the people have been organized. As a result, FASTEX can be seen as a successful training action that allowed a number of operational forecasters to:

- interact directly with scientists working on the same weather systems as the forecasters, but sometimes with quite different approaches,

- interact directly with forecasters from the other groups,

- discover and use the forecasting tools from the other groups, that often implement the vision that different services have of operational forecast.

In this instance, the Canadian contribution has been most noted and appreciated in the sense that it is the system for which the control of the forecast suite by the forecasters is the most effectively implemented. It should be repeated here that the forecast group as a whole has been most efficient and that the daily meetings between forecasters offered a very nice example of active and effective international collaboration.

In order to fully appreciate the meaning of this training action, one must have in mind that the "conceptual world" of the scientists has been evolving considerably this past decade (this is summarized in section 1.2 in Part 1 of this Report) and it is through actions similar to this one that the best of these ideas become to be employed beyond research. It is our belief that these new concepts are useful for interpreting rapidly and properly a given situation, the evolution of which is, nowadays, given by model simulations. The work of forecasters is now a typical decision taking process based on the assessment of the numerical products available.

Along the same line, it has been chosen, at Météo-France, to modify the operational display system SYNERGIE with these concepts in mind, rather than bring a research tool and train the forecasters on it. As a result, the training in question has happened in Shannon, but instead of returning to an environment from which dynamical concepts are largely absent, the forecasters have found, on their operational terminal, the same environment as in Shannon and these dynamical concepts are becoming more and more popular, as they are found actually useful. This is the case, in particular, in winter. The monitoring of storms for the benefit of our countries has been, in this respect, improved on the same (short) time scale as the part of the FASTEX programme detailed here.

Another benefit of FASTEX has been the extensive use of the ensemble prediction provided by the European Centre for Medium-Range Weather Forecast for the medium-range outlook in Shannon. It has been shown, in particular, that the seven-day prediction of the weather regime is effective. The success, here, must, ob-

viously, be credited to ECMWF, but FASTEX has allowed a significant number of people to realize the effective jump that has been made in this area.

On a time scale that goes beyond that of this report, but much shorter than that of climatic research, the most serious possibility of direct economical benefit lies with the potential of adaptive observation to secure the forecast of extremely rapid cyclogenesis events, something that even the most recent models and data assimilation techniques still do not offer (as has been seen these last two winters). At this stage, it is not fully clear what form will take the operational implementation of adaptive observation. There are several possibilities:

- it can be used to improve the control of active remote sensing instruments, or to perform a more clever thinning of the data provided by passive instruments,

- it can lead to the development of a truly adaptive component of the observing system, based either on ships and aircraft of opportunity (but employed very differently from the current practice) or on remotely controlled "sondes", although this sounds a bit like science fiction, at least for european budgets,

- it can also, and more realistically, help improving existing data assimilation algorithm, since these do not, currently, make direct use of the yet computable predictability informations required to adapt the observing system.

The benefit to operational forecast of these ideas can safely be expected to be within the next five years.

10.4   The FASTEX Cloud System Study project

This section now returns to the more familiar small world of research. Indeed, the scientific benefits of the FASTEX data set are only just beginning to be collected. A significant effort is put into several of the scientific objectives listed in Part 1, such as, for example, predictability.

However, this Report is concluded by focusing again on those objectives relating to the cloud systems, their evolution and structure.

10.4.1   Overview

The FASTEX-Cloud System Study (FASTEX-CSS) aims at producing a complete life-cycle description and understanding of the FASTEX cloud-cyclone system. The aim of FASTEX-CSS is to exploit the FASTEX data to describe, in as complete a way as possible, the cloud systems associated with cyclones, their initiation, evolution and the role of the synoptic environment in that development.

Based on these results FASTEX-CSS will provide a multiscale synthesis of the cloud-cyclone system enabling tuning of cloud parameterization and validation of climate models.

A set of reference cloud classification during the life-cycle of frontal waves will be produced.

There will be an intercomparison of mesoscale numerical models of FASTEX cyclones, exploiting sophisticated cloud physics representation.

This will allow the validation of regional and cloud-scale models of the cyclone/cloud system. In addition a set of reference FASTEX simulations suitable for parameterization tuning (cloud and marine boundary layer structure) will be produced which

will lead to an improved cloud physics parameterization scheme for such clouds for use in climate models.

The FASTEX-Cloud System Study Project is funded by the European Commission under the contract ENV4-CT97-0625.

10.4.2 Project components

Initiation and evolution of cloud systems

(i). Using the MANDOPAS scheme, both radar and dropsonde data are now being used to cover both clear air and precipitation regions at the Centre des Environnements Terrestre et Planétaires from CNRS, concentrating on IOP 12 and IOP 16. The long-term aim is to retrieve microphysical fields.

(ii). The Irish Met Service is involved in the analysis of ozone ascents from Valentia and the HIRLAM model will be used once 4D var system is in place.

(iii). The cloud field classification is being developed at the Laboratoire d'Aérologie in Toulouse in collaboration with the Laboratoire de Météorologie Dynamique. The 3I method is being used based on a pattern recognition technique.

(iv). The UK Met-Office is extending to theta surfaces its iterative successive correction method to analyse dropsonde data from IOP 16. The ice sublimation hypothesis discussed in Part 7 is being developed using the static stability field. This approach also aims at integrating with Doppler radar data.

(v). DNMI works on slantwise convection in IOP 11 at 00Z on 6 February 1997. These experiments are going to 0.2°× 0.1°resolution in future.

Figure 10.3: *A preliminary result from FASTEX-CSS: direct comparison between a high-resolution global model simulation of IOP 16 (left panel) (for a summary of IOP 16, see section 3.19, page 116) and the brightness temperature measured by the METEOSAT satellite (right panel). The simulated brightness temperature is the outgoing infra-red flux produced by the radiative scheme of ARPEGE. It combines the profiles of temperature, humidity and the diagnosed cloudiness. The model is Météo-France ARPEGE, run at T213, C=3.5, which means that the resolution is equivalent to T740, and with 41 levels. The image is obtained after a 24 h simulation. Images provided by Ph. Lopez, Météo-France GAME.*
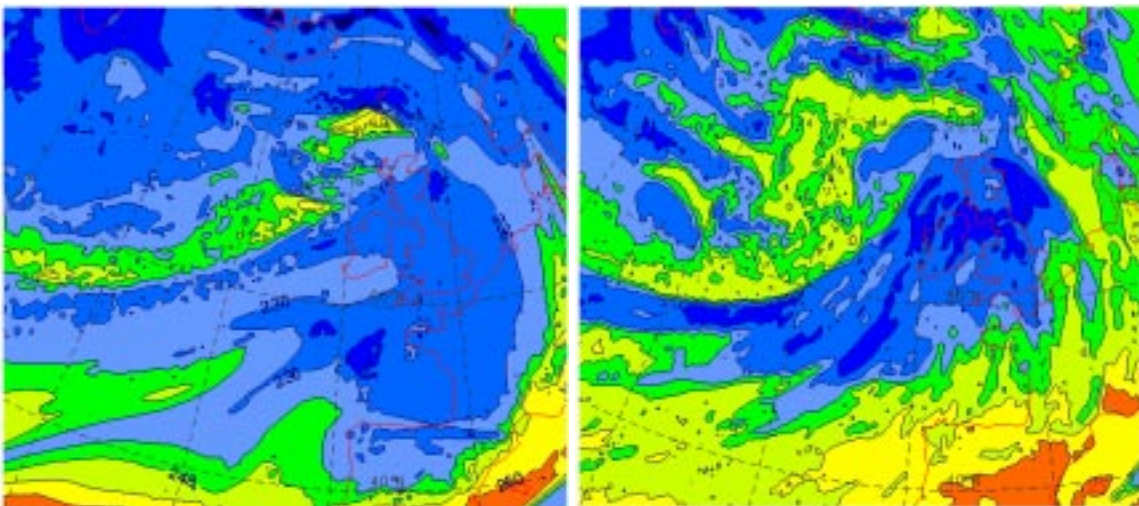
Mesoscale modelling

(i). The mesoscale model intercomparison project is taking shape (Fig. 10.3). It is coordinated by Philippe Lopez, from Météo-France/GAME. Such mesoscale simulations are needed for: tuning the free parameters of the cloud schemes, validation, intercomparison, and to compare with SSM/I and radar and dropsonde data. Three cases are IOPs 11, 16 and 17. GAME will provide 4D-VAR re-analysed data by the end of January (first case) and February (second case) at 80 km resolution in GRIB format. Models will run at 10 km and output a variety of quantities. Models that would be involved are: the UK Unified Model, HIRLAM and MESO-NH (Météo-France and CNRS non-hydrostatic model).

There is a potential for extending this intercomparison to the GCSS Working Group 3 (stratiform clouds).

(ii). The Irish Met Service will perform extended sensitivity tests for various IOPs to parameterization schemes for clouds and surface layer processes.

(iii). DNMI investigates the evolution of the boundary layer within a cold-air outbreak part of IOP 17.

(iv). UPS/LA will use the MESO-NH model for IOPs 11, 16 and 17. This model has 3 cloud ice variables.

Multi-scale synthesis

(i). The Reading group had been looking at the 3 cloud heads of IOP 16 and the attendent transverse circulations. Analysis of dropsonde data on θ_w has been performed. In IOP 16 there was evidence of SCAPE (Slantwise CAPE) but little CAPE (Convective Available Potential Energy).

(ii). The Reading group also plans to use the extended energy concept to examine the dynamical role of regions of reduced static stability in triggering cyclogenesis. An important quantity to be output from the mesoscale model intercomparison component is (diabatic) heating which is important for this dynamical study.

(iii). The Iceland Met Institute concentrates on the IOP 8 Greenland wave case and other cases that have their development influenced by Greenland.

These research tasks develop one or two aspects only of the scientific topics that can be addressed with the FASTEX data. This Report, it is hoped, will be a useful landmark in the course of the long-term FASTEX programme, but, as the above lines are meant to suggest there is still a large potential to derive from the data collected during the field phase of FASTEX.

While the climate-related results will ultimately join, as a modest contribution, the many process studies that are still needed to monitor, understand and forecast the dynamics of climate, the daily use by the national weather services involved in FASTEX will sooner turn and is already turning the ideas and tools mentioned in this Report into actual contributions to improving the difficult forecast of strong winds and/or strong rains over Europe associated with cyclogenesis.

FASTEX project contacts:

The FASTEX World Wide Web home page and Data Base:
http://www.cnrm.meteo.fr/fastex/

FASTEX Project Manager:
Dr. Alain JOLY,
Météo-France, CNRM/GMME,
42, avenue G. Coriolis,
F-31057 Toulouse cedex 1, France
e-mail: alain.joly@meteo.fr
fax: +33 5 61 07 96 26

Appendix A
List of acronyms

Table A.1: *List of Abbreviations/Acronyms*

ACARS	Aircraft Automated Reporting System
AES	Atmospheric Environment service
AMDAR	Automated Meteorological DAta Relay
ARGOS	Argos is a satellite-based location and data collection system dedicated to monitoring and protecting the environment
ARPEGE	Action de Recherche Petite Echelle Grand Echelle
ASAP	Atmospheric Sounding Automated Program
ASCII	American Standard Code for Information Interchange
AVISO	Archiving, Validation and Interpretation of Satellite Oceanographic data
BUFR	Binary Universal Format (GTS data format)
CD-ROM	Compact Disc - Read Only Memory
CERSAT	Centre ERS d'Archivage et de Traitement
CETP	Centre de l'Environnement Terrestre et Planetaire
CLS	Collect and Locaton per Satellite
CMM	Centre de Météorologie Marine
CMS	Centre de Météorologie Spatiale
CNES	Centre d'études Spatiales
CNRM	Météo-France's Centre National de Recherches Météorologique
CNRS/LA	Centre National de la Recherche Scientifique/Laboratoire d'Aérologie
COST	Coopération Scientifique et Technique (European cooperation in the field of scientific and technical research
CSG	Core Steering Group
DMI	Danish Meteorologic Institut
DMS	Database Management System
DMSP	Defense Meteorological Satellite Program
ECMWF	European Center for Medium Range Weather Forecasts
EGOS	European Group of Oceanic Stations
ERS	European Space Agency's environmental satellite
ETL	NOAA's Environmental Technology Laboratory
FASTEX	Fronts and Atlantic Storm-Track Experiment
FCA	FASTEX Central Data Archive
FDA	FASTEX Data Archive
FTP	File Transfer Protocol
GDC	NOAA's Global Drifter Center
GMEI	CNRM's Groupe de MEtéorologie Instrumentale
GOES	Geostationary Operational Environmental Satellites
GRIB	Gridded Met information - Binary
GPS	Global Positioning Systm
GTS	Global Telecommunications System
HIRLAM	Hi-Resolution Limited Area Model
HRPT	High Resolution Picture Transmission
IcMS	Icelandic Meteorological Service
IFREMER	Institut Français de Recherche pour l'Exploitation de la Mer
IFS	ECMWF's Integrated Forecast System
INM	Instituto National de Meteorologia (Spanish Weather Service)
INMG	(Portuguese Weather Service)
INSU	Institut des Sciences de l'Univers
IOP	Intensive Observational Period
IR	InfraRed
IrMS	Irish Meteorological Service
JCMM	Joint Center for Mesoscale Meteorology
JOSS	Joint Office for Science Support
KNMI	Meteorological Service of the Netherlands
NCAR	National Center of Atmospheric Research
NESDIS	National Environmental Satellite Data and Information Service
NOAA	National Oceanic and Atmospheric Administration
NPS	US-Navy's Naval Postgraduate School
NSSL	NOAA's National Severe Storms Laboratory
NWS	NOAA's National Weather Service
PERL	Standard 2-minute 360°turn
PI	Pricipal Investigator
PYREX	PYRenean EXperiment
QC	Quality Control
QCF	Quality Control Format
RAF	NCAR's Research Aviation Facility
SCEM	Météo-France's Service Central d'Exploitation Météorologique
SSMI	Special Sensor Microwave Imager
SVP	Lagrangian surface drifter
TOVS	TIROS Operational Vertical Sounder
UCAR	University Corporation for Atmospheric Research
UK	United Kingdom
UKMO	United Kingdom Meteorological Office
USA	United States of America
USAF	USA's Air Force
USGS	US Geographical Service
VIS	VISible
WMO	World Meteorological Organisation
WV	Water Vapor
WWW	World Wide Web